Alma Mater Studiorum – Università di Bologna

DOTTORATO DI RICERCA IN

Ingegneria Chimica dell'Ambiente e della Sicurezza

Ciclo XXVI

Settore Concorsuale di afferenza: 09/D3 – Impianti e processi industriali chimici

Settore Scientifico disciplinare: ING-IND/25 – Impianti Chimici

ANALISI E MODELLAZIONE DI SISTEMI DI TRATTAMENTO FUMI DERIVANTI DA PROCESSI DI TERMOVALORIZZAZIONE

-

ANALYSIS AND MODELLING OF THE PERFORMANCE OF TECHNOLOGIES FOR FLUE GAS TREATMENT IN WASTE-TO-ENERGY PROCESSES

Presentata da: Daniele Guglielmi

Coordinatore Dottorato

Prof.ssa Ing. Serena Bandini

Relatore

Prof. Ing. Valerio Cozzani

Correlatore

Ing. Giacomo Antonioni

Esame finale anno 2014

Table of contents

1 Abstract

Waste management has been representing an important issue in last years. Among the solutions provided by legislators, thermal treatment with energy recovery plays a significant role in waste management, showing an increased importance in Europe in the last ten years. Indeed, municipal solid waste incineration (MSWI) permits to stabilize and reduce the volume of solid residues for landfilling and to recover energy, further allowing a reduction of coal and oil consumption for power production. However, one of the main issues related to waste combustion is the generation of air contaminants, which have to be efficiently removed. Particular attention has to be paid to acid gases, mainly hydrogen chloride and sulfur oxides, due to their impact on the environment and on human health.

The aim of the present study was the prediction and optimization of the acid gas removal efficiency of dry systems for flue-gas treatment. In fact, in these processes a large amount of reactants is required to comply with the emission limits and, consequently, plenty of solid hazardous residues may be formed if the system is not properly operated.

In the first part of the study, a general description of the technologies for flue gas treatment in waste-to-energy incineration plants is provided. Particular attention was paid to dry treatment systems, due to the growing interest in their application to MSW incinerators. The analysis focused on the two-stage dry treatment systems, which were extensively investigated because of their enhanced acid gas removal efficiencies. These systems consist of two stages where a powdered sorbent is injected into the flue gas. As the reaction products are solids, a particulate control device, usually a fabric filter, is present in each stage. A wide industrial interest was shown in recent years for a configuration with the injection of solid calcium hydroxide (hydrated lime) in the first stage, while in the second stage removal is obtained by reaction with sodium bicarbonate (which is more effective but also more expensive than calcium hydroxide). A literature review of reactions of these solid sorbents with HCl and SO_2 in MSWI treatment system conditions is proposed in Section 3.

In the second part of the study (Section 4), an operational model was proposed to estimate the acid gas removal efficiency of a two-stage dry treatment system. The model was based on available literature data. HCl and SO_2 conversions were expressed as a function of the ratio of reactant flow rate to its stoichiometric rate. The parameters in the correlation can be defined from literature data or from plant data. The model was implemented in a software for process simulation to describe both design and process conditions of an existing MSWI (Section 5). The recycle rate of solid products and unreacted calcium hydroxide in the first stage were taken into account. Simulations were carried out with the aim of optimizing both reactant feed rates and amounts of solid wastes formed in the acid gas removal process. The model was then adapted to simulate the performance of the reference plant when using the same reactant in both stages. The considered alternatives were a double stage with calcium hydroxide and a system with bicarbonate in both stages.

The third part of the work concerned the development of a fundamental predictive model for the description of acid gas sorption in filter cakes through their governing equations (Section 6). Solid-state diffusion through the product layer and chemical reaction rate were taken into account, since they have been identified as the rate controlling steps during the removal process in the simulated conditions. The model was validated reproducing literature data (Section 7) and was then implemented to predict acid gas removal in the case-study analyzed (Section 8). In order to further validate the model and to apply it to different plants, a

laboratory apparatus (described in Section 9) was designed to evaluate the model parameters in different process conditions.

2 General introduction

Waste management issue

Nowadays waste management represents one of the main issues in our society. The European Community has been dealing with this problem and laid down some basic principles for protection of human health without harming the environment. Indeed, according to the Waste Framework Directive (Directive 2008/98/EC on waste), Member States shall ensure that waste management is carried out without risk to water, air, soil, plants or animals, without causing a nuisance through noise or odors, and without adversely affecting the countryside or places of special interest. The legislator set a hierarchy of solutions for waste management that Member States shall take (shown in Figure 2.1). These measures, listed in order of priority, are:

- *prevention*, which means measures, taken before a material has become waste, that reduce:
  - the quantity of waste, through the re-use of products or the extension of their life span;
  - the negative impacts of waste on the environment and human health;
  - the content of harmful substances in materials and products;
- *preparing for re-use*, which means checking, cleaning or repairing recovery operations realized in order to prepare wastes so that they can be re-used without any other pre-processing;
- *recycling*, which means any recovery operation by which waste materials are reprocessed into products, materials or substances whether for the original or other purposes, including the reprocessing of organic material; energy recovery and the reprocessing into materials used as fuels or for backfilling operations are not considered as recycling;
- *other recovery*, e.g. energy recovery;
- *disposal*, which means any operation which is not recovery.

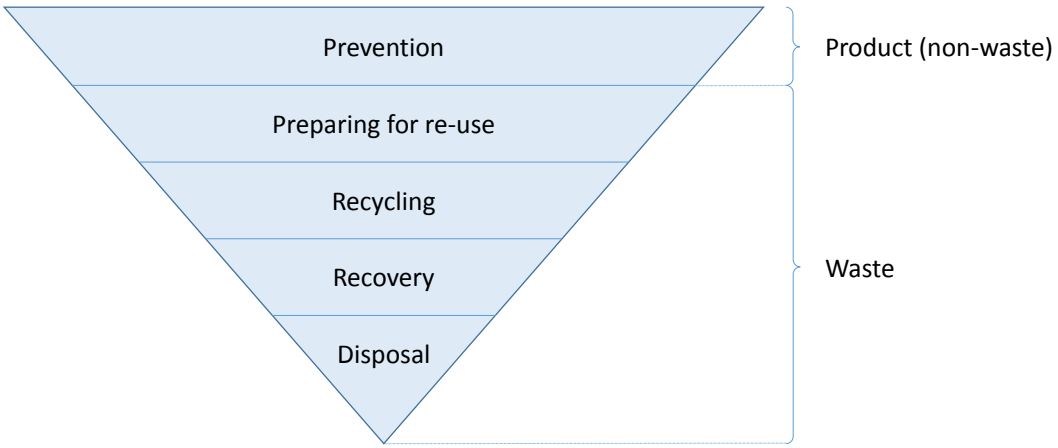

Figure 2.1 - Waste management hierarchy established by Directive 2008/98/EC on waste (Waste Framework Directive).

According to this hierarchy, prevention, preparing for re-use and recycling should be preferred to energy recovery from waste, making incineration a controversial topic. Indeed, while it is preferable to reduce waste material production or re-use the waste into the process, this is not always technically or economically realistic (Baukal Jr., 2003).

Statistic data provided by Eurostat (2013) show that prevention measures permitted to stop the growing of municipal waste production in Europe and to keep it constant during the last decade, as reported in Appendix A. Despite the fact that waste production has not decreased, a continuous reduction has been observed for landfilling disposal since firsts 2000's. This trend was made achievable by an enhanced use of other waste treatment processes, i.e. composting and digestion, material recycling and incineration.

In particular, energy recovery from municipal solid waste (MSW) incineration has rapidly increased in Europe in the last ten years, reaching in 2011 a production of 16354 thousand tonnes of oil equivalent (Eurostat, 2013). In the period 2001-2011, an increase of energy production from MSW incineration has been recorded in all of Member States and especially in Italy, where a fourfold increase has been shown (as reported in Appendix A). Moreover, according to Niessen (2010), a continuing role of incineration should be expected in the future due to increasing concern over waste in landfills (for leachate, odor and greenhouse gas generation), and increases in the energy value.

Waste-to-energy incineration plants

Waste incineration consists in the oxidation of the combustible materials contained in the waste. It permits to treat a very wide range of wastes, which present a highly heterogeneous composition (as shown in Appendix B). Energy production is possible recovering the heat of flue gases produced during incineration. Combustion process starts when the substances contained in the waste are exposed to oxygen and the temperature reaches the ignition value. In these conditions, the gas phase can burn releasing energy. If the calorific value of waste is high enough, combustion is self-supporting, otherwise the addition of other fuels is required.

Despite the great variability of incineration sector, some main class are identified in the reference document on the best available techniques for waste incineration (WI BREF, 2006):

- *Mixed municipal waste incineration*, where mixed and untreated household wastes are mainly treated, even though sometimes industrial wastes or sewage sludge are added.
- *Pretreated waste incineration*, where treated wastes have been selectively collected or prepared; refuse derived fuel (RDF) incinerators are a sub-sector.
- *Hazardous waste incineration* includes incineration on industrial sites and at merchant plants, which usually treat very heterogeneous wastes.
- *Sewage sludge incineration*, where sewage sludge is incinerated separately from other wastes.
- *Clinical waste incineration*, which is dedicated for the treatment of clinical wastes.

Raw flue gas composition (i.e. after the boiler and before the treatment system) is presented in Appendix E for main incineration sectors.

Incineration sector has undergone rapid technological development over the last decades. In particular, substantial improvements were achieved in reducing emissions to air from W-t-E plants, where current techniques permitted to limit costs maintaining, or improving, environmental performance (WI BREF, 2006). These permitted a rapid development of incineration sector, as demonstrated by the increased energy production from municipal waste incineration shown in Appendix A. This trend has been justified by a series of advantages offered by thermal treatment plants. In fact, waste incineration permits to stabilize the solid residues for landfilling through volume reduction, detoxification (particularly important for carcinogens, pathologically contaminated materials and toxic organic compounds) and sanitation (through the destruction

of pathogenic organisms) (Niessen, 2010). Indeed, incineration forms oxides or glassy sintered residues that are insoluble, avoiding leaching phenomena. On an environmental point of view, waste management impact can be mitigated incinerating organic materials that leach from landfills or create odor nuisances. Moreover, the greenhouse effect of the CO_2 generated in incinerating solid waste is substantially less than that of the methane and CO_2 generated in landfilling operations[1]. In addition, energy recovery allows reducing the consumption of coal and oil for power production with significantly less emission of air pollutants per kilowatt produced due to the strict requirements applicable to municipal refuse incinerators. Furthermore, very high energy recovery efficiencies can be achieved in CHP plants, reaching 80 % in some cases (WI BREF, 2006).

In contrast, incineration presents some disadvantages. It is an expensive processing step in waste management, both in initial investment and in operation. Other issues are posed by the variability in waste composition, waste-handling problems, high maintenance requirements, and equipment unreliability. Particular concern is present about the potential environmental impacts given by air emissions (mainly sulfur dioxide, hydrogen chloride, carbon monoxide, nitrogen oxides, polycyclic aromatic hydrocarbons and fly ash), waterborne emissions (blowdown from wet-scrubbers and wastewater from residue quenching are highly acidic and may contain heavy metals and high levels of dissolved solids), and residue disposal (fly ash and bottom ash). Another important problem associated to incinerators is the public sector reaction: high concern (and possibly hostility) is generally expressed by the public, from environmental associations and regulatory agencies (Niessen, 2010). Moreover, controlling the combustion process could be very difficult because of changes in waste composition related to seasonal variations in municipal waste or product changes in industrial waste. In fact, flue-gas treatment systems have to operate in a wide range of conditions and high performance expected in design conditions could not be achieved if the process is not promptly regulated.

Consequently, the increased use of Waste-to-Energy processes in last years has heightened the need for efficient treatment systems. Indeed, a growing interest in environmental impact has been shown by legislators, which set more restrictive emission limit values from W-t-E plants and requested to minimize the environmental impact (Directive 2010/75/EU on industrial emissions). In particular, air pollutant emissions from incineration facilities have become subject of public concern and regulatory examination (main legislative references are summarized in Appendix C). In fact, because of the award for air emission limitations, the capital cost for flue-gas treatment system is more than 35% of the total investment in many plants (Niessen, 2010). For these reasons, a wide industrial interest was shown in analyzing the relationships between the quantity and characteristics of air pollutant emissions and the operating conditions and design of air-pollution-control (APC) devices.

Flue gas pollutants

Several air contaminants are generated by waste combustion. A first category is formed by inorganic particulate matter, which is mainly inert ash (primarily composed of silicon, aluminum, calcium, iron and oxygen). However, also heavy metals may be present in this fraction (Niessen, 2010). This kind of pollutants can be removed from flue gas through particulate control devices, such as cyclones, inertial collectors,

[1] According to Niessen 2010, the atmospheric warming impact from landfilling is from 45 to 115 times that of incineration alternatives.

electrostatic precipitators, and fabric filters. Main particulate control devices adopted in waste incinerators and corresponding removal efficiencies are reported in Appendix F.

A second group of pollutants includes products of incomplete combustion of the waste. These compounds include carbonaceous soot and char, carbon monoxide, hydrocarbons, and halogen compounds, such as polychlorinated and polybrominated dibenzo furans (PCDF, PBDF), dibenzo p-dioxins (PCDD, PBDD), and polychlorinated biphenyls (PCB). This class of contaminants shall be minimized through an accurate control of combustion process conditions, and eventually further removed in the air pollution control devices (e.g., through activated carbons).

A particular class is represented by nitrogen oxides (NO_x), whose emission is related to both the combustion process and fuel chemistry. Indeed, in combustion processes, nitrogen oxides arise through reaction of nitrogen and oxygen from the combustion air (thermal generation) and through oxidation of nitrogen bound in the fuel (fuel nitrogen generation). NO_x formation can be reduced by controlling operating conditions in the combustor and by means of reduction technologies: Selective Non-Catalytic Reduction (SNCR) and Selective Catalytic Reduction (SCR).

Finally, there are several pollutants directly related to fuel chemistry, which are generated by release and/or reaction of elements in the fuel. These are sulfur oxides, halogens and hydrogen halides (mostly hydrogen chloride, HCl), and other trace elements. The removal of these compounds was analyzed in the present study, as an increased interest was expressed in their impact on the environment and on human health.

Sulfur oxides (SO_x) are produced by combusting any material containing sulfur. Even though the main source of SO_x emission is fossil-fuel combustion for electric power generation (Cooper and Alley, 2010), also municipal waste contains sulfur, which form SO_x during incineration. SO_x cause human health problems (especially in combination with inhalable particulate matter), damage to fauna and flora, formation of acid mists, and corrosion of materials (Cooper and Alley, 2010). During combustion, mainly SO_2 is produced, but some SO_3 is also formed. Both SO_2 and SO_3, when come into contact with water, can hydrolyze forming acids (mainly sulfuric acid), which can have detrimental effects on environment. As water vapor is present in the flue gas, the temperature in the treatment system and in the stack should be keep safely above the sulfuric acid dew point to prevent corrosion phenomena (Niessen, 2010).

Hydrogen halides, being strong acids, represent another important class of fuel gas contaminants. In fact, as shown in Appendix B, halogens are important constituents of waste and acid gases are formed in combustion environment, where hydrogen is in considerable excess. Chlorine is generally the most important halide in waste, although fluorine, bromine, iodine and their acids can be more problematic in APC systems. Chlorine is contained in waste charged to the furnace in significant amount both as inorganic salts (e.g., sodium chloride) and as organic compounds. During combustion, organic chlorine is converted, almost quantitatively, to hydrogen chloride (Niessen, 2010) and about 35–40% of the HCl generated is absorbed by alkaline constituents of the ash (Na_2O, CaO, etc). Indeed, hydrogen chloride is usually formed in higher concentration than sulfur dioxide in MSW incineration plants. HCl presents very serious potential health effects: inhalation of vapors may cause pulmonary edema, circulatory collapse, damage to upper respiratory tract, coughing, difficulty breathing and choking (Air Liquide, 2011). HCl is severely irritating and corrosive to the eyes, mucous membranes and upper respiratory tract, and contact with liquid can cause severe burns of skin and eyes. For these reasons, HCl emission limit value laid down by European legislation on industrial emissions (see Appendix C) is set to 10 mg/Nm^3 as daily average, which is one fifth of the limit set for SO_2.

Flue gas treatment systems

Hydrogen halides and sulfur oxides shall be removed from flue gases by means of air-pollution-control devices. Wet systems, such as scrubbers and absorbers, are consolidated technologies and are included among the Best Available Techniques (BAT). However, they present the disadvantage of producing wastewater streams that require further treatment due to high acidity, presence of heavy metals and high levels of dissolved solids. An increasingly applied alternative system is based on the Dry Sorbent Injection (DSI), described in Section 3.1. This technology shows significant reductions in the emission of acid gases with modest capital and operating costs and minor layout impact (Niessen, 2010). DSI processes are based on injection of dry powdered calcium-based sorbents (calcium hydroxide, calcium carbonate or calcium oxide), or sodium-base alkali (carbonate or bicarbonate) into the flue gas with subsequent collection in particulate control devices. The solid alkaline reactant neutralizes HCl, HF, SO_2, and other acid gases. However, several processes are involved in dry injection and process control could be problematical. Indeed, many parameters affect the removal efficiencies, including the system temperature, the physical and chemical form of the sorbent, and the flue gas composition. Many studies have focused on reactions between acid gases and solid sorbents (main results and approaches are reported in Section 3) with the aim of optimizing acidic compounds neutralization in Waste-to-Energy facilities. However, laboratory results obtained by different authors are hardly applicable to real treatment systems, where many phenomena affect the acid gas removal and specific data are required for an effective description.

3 State of the art

The increased interest in waste incineration has heightened the need for more efficient air pollution control systems. Therefore, a review of gas purification technologies is presented in this study. In particular, the Best Available Techniques applicable for HCl and SO_2 removal have been investigated (Section 3.1), while the treatment systems for other flue gas pollutants are discussed in Appendix E. The two-stage dry treatment system emerged as one of the most promising techniques for acid gas removal in MSW incinerators. Therefore, this technology is analyzed in Section 3.2, while modeling of gas-solid reactions is discussed in Section 3.3. Particular attention has been paid to reaction of hydrogen chloride with solid sorbents (mainly calcium hydroxide and sodium bicarbonate), analyzing the models proposed in literature and the effect of other flue gas components on HCl removal (Section 3.4).

3.1 Technologies for acid gas removal from flue gases

Several processes were proposed for acid gas removal from MSWI flue gas. These systems are generally based on the use of alkaline reagents and the coverage of gas purification technologies that are applicable in HCl and SO_2 removal has been investigated considerably (Cooper and Alley, 2010). However, three main categories can be identified for flue-gas cleaning processes:

- wet processes, which consist in removing acid gases by means of water or a washing solution containing the reagent (e.g. sodium hydroxide solution)
- semi-wet processes, also called semi-dry. In these systems the sorption agent is an aqueous solution or suspension; when it is brought into contact with the hot flue gases, water evaporates so the reaction products are dry
- dry processes, where a dry sorption agent (e.g. calcium salts, sodium bicarbonate) is injected into the flue-gas flow and the reaction products are dry salts

Wet systems

Main design of scrubbers used in wet flue-gas cleaning processes are (WI BREF, 2006):

- jet scrubbers
- rotation scrubbers
- venturi scrubbers
- dry tower scrubbers
- spray scrubbers
- packed tower scrubbers.

A typical configuration consists in two stages with upstream de-dusting. Usually water is injected in the first stage, producing a strongly acidic solution (typically, pH is lower than one). HCl and HF are mainly removed in the first stage and the effluent is recycled with a small addition of fresh water. A second stage is required to remove sulfur dioxide. In this stage, SO_2 removal is achieved by means of neutral or alkaline solution (generally with pH 6 - 7), obtained adding NaOH, $Ca(OH)_2$, or $CaCO_3$, which permit the further absorption of HCl and HF. When calcium based sorbents are used, corresponding sulfate, carbonates and fluorides can

form water-insoluble residues and may be removed to reduce the risk of encrustation within the system. Some residues, as gypsum, can be recovered. Conversely, products formed from NaOH solutions are water-soluble. Figure 3.1 shows a typical two-stage wet scrubbing system. However, the number of scrubbing stages varies between 1 and 4, usually with multiple stages incorporated in a vessel (WI BREF, 2006).

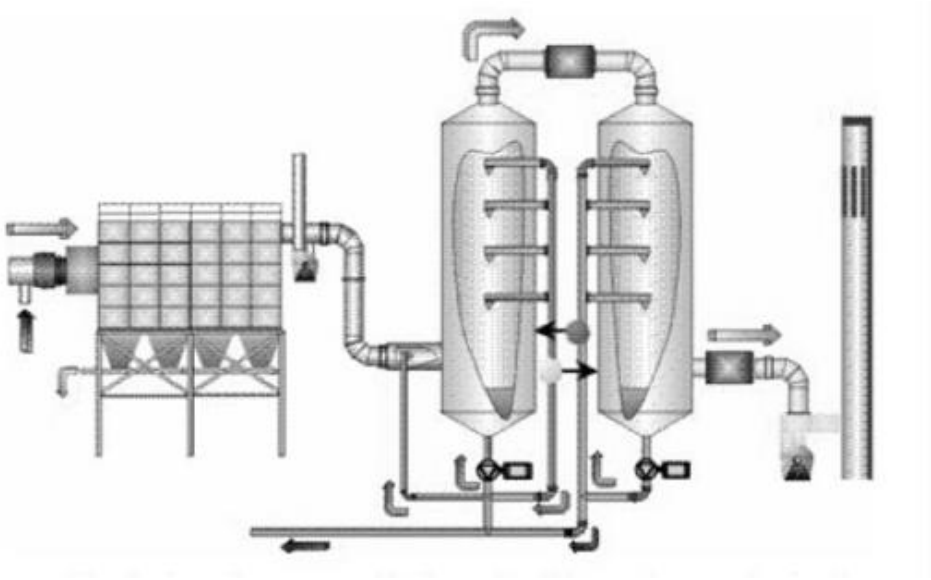

Figure 3.1 - Typical two-stage wet scrubber with upstream de-dusting (WI BREF, 2006).

One of the main issues related to wet scrubbers is wastewater. Indeed, to guarantee elevated scrubbing efficiencies, a portion of the scrubbing solution must be removed from the system. The wastewater is highly acidic and can contain heavy metals (a special attention is required by mercury, which is present mainly as $HgCl_2$) and high levels of dissolved solids. Therefore, it must be subjected to special treatments, i.e. neutralization and precipitation of heavy metals.

Dry and semi-dry systems

Treatment systems based on the Dry Sorbent Injection (DSI) are increasingly applied to avoid the problems related to the treatment of wastewater streams produced by wet systems. Dry sorbent injection involves the injection of dry, powdered sorbents, e.g. limestone, calcium hydroxide, or sodium-base alkali (carbonate or bicarbonate) into the flue gas. Unreacted sorbent and solid products are then collected by means of particulate control device (Appendix F). Alkaline sorbents neutralize HCl, HF, SO_2, and other acid gases. When additives, e.g. activated carbon, are injected with the solid sorbents, also high-molecular-weight organic matter (such as dioxins, furans, and polynuclear hydrocarbons) and heavy metals (mainly Hg and Cd) are removed from the flue gas. Because of the high performance given by dry systems, they are increasingly applied in existing plants, permitting to achieve significant reductions in the emission of acid gases with modest capital and operating costs and minor layout impact (Niessen, 2010).

The control of a dry system is difficult because of the complex processes involved in the acid gas removal with solid sorbents. Main parameters include the chemical form of the additive and the temperature. The most common sorbents are calcium-based alkali. Indeed, even though sodium-based systems show higher performance, the calcium alkalis are preferred due to the lack of field data for sodium-based sorbents and their higher cost (Niessen, 2010). A solution used to limit the overdose of calcium-based sorbents is the

recirculation of the solids separated by the particulate control device, which permits to reduce the required stoichiometric ratio and the corresponding amount of solid residues.

Dry injection systems are classified in three categories according to the temperature range: high-temperature furnace injection (HTFI), moderate-temperature duct injection (MTDI), and low-temperature duct injection (LTDI). In HTFI processes, limestone or lime are usually used as sorbent and are injected into the combustor at 760 - 1100 °C. However, this system is mainly used for SO_2 control, since the equilibrium for the HCl neutralization is not favorable at high temperatures (Niessen, 2010). In MTDI and LTDI systems the sorbent injection is made at a reactor (often a Venturi constriction) located after the economizer and ahead of the particulate control system. The temperature in this section is in the range 200 - 315 °C for MTDI and at about 150 °C for LTDI, while the residence time ahead of the particulate control device is usually of 1-2 s, which are generally sufficient to guarantee an adequate HCl and SO_2 removal. When a fabric filter is used for particulate control, the gas–solid reactions proceed within the cake of solids accumulated on the filtering surface, giving better removal efficiencies. According to Niessen (2010), lower-temperature processes provide the best performance with overall removal efficiencies from 80 % to 90 % for HCl and from 40 % to 50 % for SO_2.

A similar solution that permits to avoid wastewater streams is given by semi-wet (or semi-dry) processes. The sorbent is fed as suspension or solution into the hot flue-gas stream, where the water of the injected spray evaporates (WI BREF, 2006). Therefore, reaction products are solid and a de-dusting system (illustrated in Appendix F) is needed for their removal. The lower amount of water with respect to wet systems permits to avoid the formation of visible plumes at the emission stack.

3.2 Two-stage dry treatment systems

One of the main drawbacks of dry treatment systems for acid gas removal is the considerable production of solid residues. According to Astrup (2008), solid residues from modern Waste-to-Energy facilities constitute the primary emission route to the surrounding environment. Indeed, even though bottom ashes are generated in larger amounts, solid products originated from flue gas cleaning have the main pollution potential.

Therefore, an accurate control of the system is required and individuation of optimal operating conditions is crucial to avoid high sorbent consumption. A further improvement is given by the use of two-stage processes. These solutions permit to reduce the total flow rate of solid reactants because of the non-linearity between acid gas conversion and solid sorbent flow rate (Antonioni et al., 2011), as shown in Figure 3.2. Indeed, to obtain overall conversions near to 100 %, it is necessary to increase substantially the sorbent flow rate if only one stage is available.

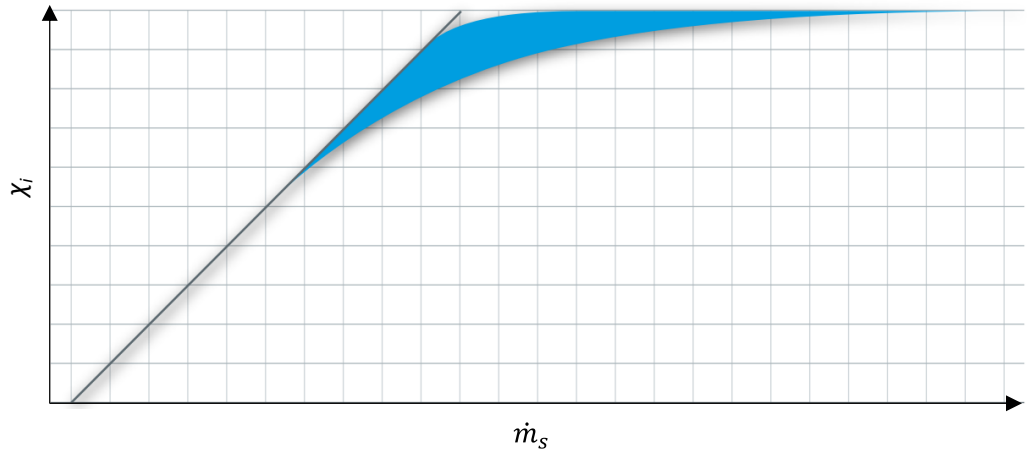

Figure 3.2 - Typical range of acid gas conversions (χ_i) vs. sorbent mass flow rate ($\dot{m}_s$).

The two-stage dry treatment of flue gas is an emerging process that combines two among the Best Available Technologies for acid gas cleaning (WI BREF, 2006). A typical configuration adopted in several Italian waste-to-energy plants, consists in injecting granulated calcium hydroxide (slaked or hydrated lime) in the first stage of the process, while in the second stage sodium hydrogen carbonate (bicarbonate) is used. This system permits to take advantage of the low cost of $Ca(OH)_2$, which is used for a first reduction of acid gas concentrations, and the high efficiency of $NaHCO_3$. In fact, the latter is more expensive, but permits to reach low acid gas emissions with lower stoichiometric excesses. Indeed, as reported by Verdone and De Filippis (2004), bicarbonate is more effective than calcium based sorbents in the typical temperature range of dry treatment systems. Another advantage of this process is that fly ash is almost completely removed in the first stage with calcic solid products, so the residual sodium chemicals produced in the second stage can be recovered and recycled, decreasing landfill cost for final waste and reducing the quantity of final waste (Brivio, 2007).

Figure 3.3 shows a schematization of the two-stage dry treatment system considered in the present study. Each stage is composed of a reactor, where solid sorbent is mixed with the flue gas, followed by a fabric filter. The fabric filter has the double function of removing solid particles (i.e. fly ash and solid reaction products) and creating a cake of partially unreacted particles, which allows increasing of the acid gases neutralization efficiencies.

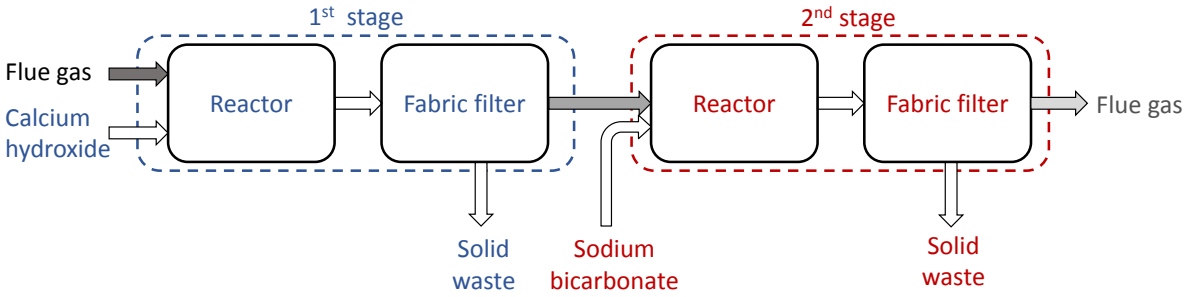

Figure 3.3 - Schematization of a two-stage dry treatment system. In this example, solid particles of calcium hydroxide are injected in the first stage, while granulated sodium bicarbonate is used as solid sorbent in the second stage.

Thus, the acid gas removal begins in the reactor and proceeds in the cake of particles deposited on the bags of the fabric filter. According to Bodénan and Deniard (2003), the reactions of calcium hydroxide with hydrogen chloride, sulfur dioxide and hydrogen fluoride are:

$$Ca(OH)_2 + 2HCl \rightarrow CaCl_2 + 2H_2O \quad (3.1)$$

$$Ca(OH)_2 + 2HF \rightarrow CaF_2 + 2H_2O \quad (3.2)$$

$$Ca(OH)_2 + SO_2 + ½O_2 \rightarrow CaSO_4 + H_2O \quad (3.3)$$

Since this dry treatment occurs after a combustion process, it is crucial to take into account the carbonation reaction:

$$Ca(OH)_2 + CO_2 \rightarrow CaCO_3 + H_2O \quad (3.4)$$

Indeed, carbon dioxide is a weak acid and reacts with calcium hydroxide (Chin et al., 2005). Moreover, being CO_2 concentration orders of magnitude higher than those of other acid gases, the consumption of calcium hydroxide could be substantial.

In the second stage, the flue gas cleaning is performed with sodium bicarbonate. As bicarbonate is a non-corrosive, non-irritant and non-toxic powder, it can be handled easily and safely. This flue gas cleaning technique, proposed by Solvay, is known as Neutrec process. It is based on the use of granulated sodium bicarbonate, and its high efficiencies in flue gas cleaning allows the respect of the emission limit values for waste incineration in a wide range of operating conditions. As low stoichiometric excesses are used, recirculation of solid residues is not required.

Granulated sodium bicarbonate, stored in a silo, is break into small particles in a grinder and then injected in a contact reactor, where an adequate mixing between the reagent and the flue gas is achieved (a minimum residence time of 2 seconds before the filter is guaranteed). Grinding permits to increase the contact surface area of the sorbent, producing bicarbonate particles with a $d_{90} < 35$ µm (a typical granulometric distribution of ground sodium bicarbonate is shown in Figure 3.4).

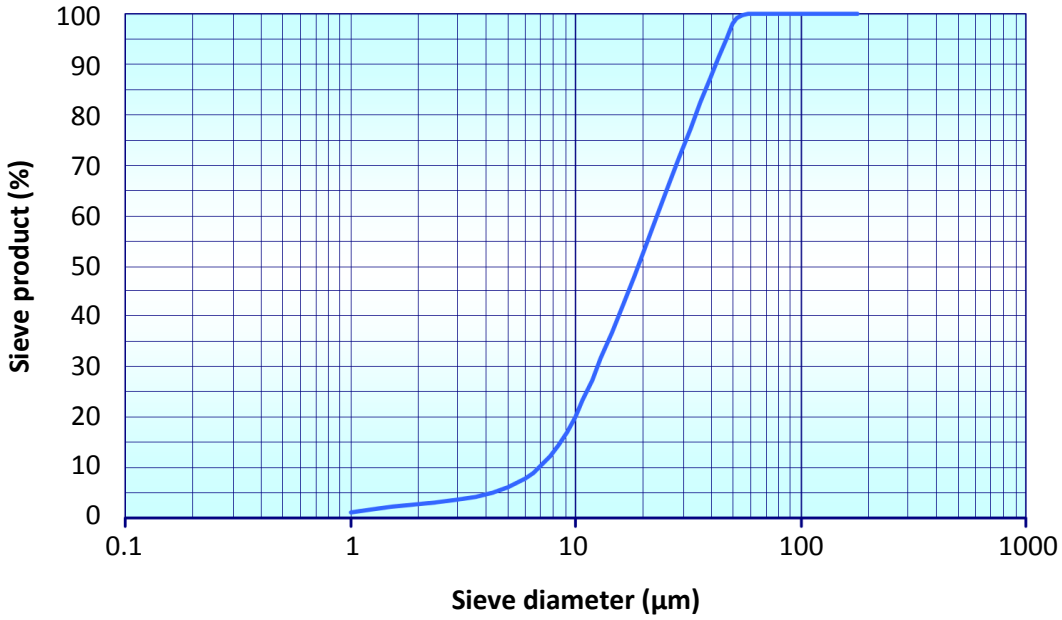

Figure 3.4 - Granulometry of ground sodium bicarbonate (adapted from Solvay, 2005).

When sodium bicarbonate is exposed to hot flue-gases (typically at temperature in the range 150-200 °C) undergoes to thermal activation according to the following reaction:

$$2NaHCO_3\ (s) \rightarrow Na_2CO_3\ (s) + CO_2\ (g) + H_2O\ (g) \qquad 3.5$$

The release of carbon dioxide and water vapor creates a porous structure, increasing the surface area available for acidic compounds removal and hence the neutralization performance of the process (Solvay, 2012). The effect of this process is clearly shown by Figure 3.5, where the smooth surface of sodium bicarbonate is compared with the porous structure of sodium carbonate formed by the thermal activation.

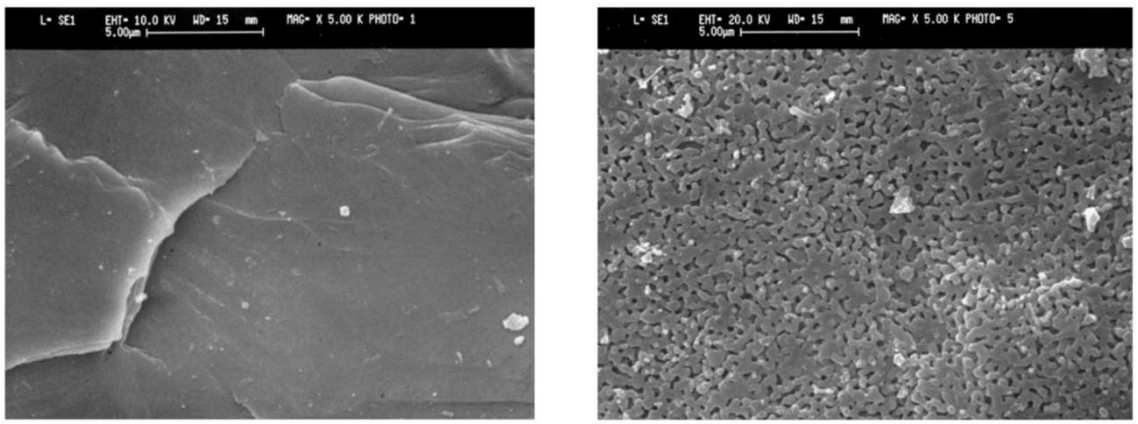

Figure 3.5 - Sodium bicarbonate before thermal activation (on the left side) and porous structure of sodium carbonate formed by the release of carbon dioxide and water vapor (on the right) (Solvay, 2012).

Formation of gaseous products has the further advantage of reducing the weight of solid products. According to the stoichiometry of reaction 3.5[2], the weight loss is 37 % with respect to sodium bicarbonate.

[2] Molecular masses of the solid compounds are reported in Appendix D.

The bicarbonate decomposition is almost instantaneous, so the acid neutralization reactions begin as soon as bicarbonate is injected within the flue gas, according to the following reactions:

$$Na_2CO_3 + 2HCl \rightarrow 2NaCl + CO_2 + H_2O \quad 3.6$$

$$Na_2CO_3 + 2HF \rightarrow 2NaF + CO_2 + H_2O \quad 3.7$$

$$Na_2CO_3 + SO_2 + ½O_2 \rightarrow Na_2SO_4 + CO_2 \quad 3.8$$

As the dust removal is performed by a fabric filter, the sodium carbonate forms a homogeneous layer on the filtrating surface. This cake allows the increase of the acid gases neutralization efficiencies, complying with the strictest emission limits and reducing bicarbonate consumption.

However, due to the relatively scarce industrial experience presents on this two-stage technology, there is still a lack of knowledge about efficiencies and yields of flue gas treatment stages (Yassin et al., 2007). Thus, in order to operate the process on the safe side, solid reactants are often fed in high excess causing relevant amounts of unreacted solids to be present in the solid waste stream recovered from fabric filters. Therefore, a description of the governing phenomena is of great interest in order to predict and optimize the acid gas removal efficiency in dry systems. The following section reports some of the main models for gas-solid reactions, which were then implemented and adapted to simulate the acid gas removal in the analyzed cases and to estimate the optimal operating conditions.

3.3 Mathematical models of gas-solid reactions

3.3.1 Gas-solid reactions

Reactions between gases and solids have been extensively studied because of the major role played in industrial processes. As described in Sections 3.1 and 3.2, solid sorbents are of great interest also in environmental control, and typical examples of gas-solid reactions include the neutralization of acid gases produced by the incineration of municipal solid waste by means of powdered sorbents.

Szekely et al. (1976) presented a general description of gas-solid reactions, showing that most of these systems exhibit certain general trends regarding the effects of particle size and temperature on the overall rate of reaction. These authors showed that certain general trends are exhibited on reaction between a gas and a porous solid. Figure 3.6 shows a plot of the rate of reaction against the reciprocal of the absolute temperature. It portrays that at low temperatures the overall rate tends to be controlled by chemical kinetics through an exponential function of the reciprocal temperature. In contrast, diffusion tends to be rate controlling at high temperatures. At intermediate conditions, both diffusion and chemical kinetics have to be taken into account.

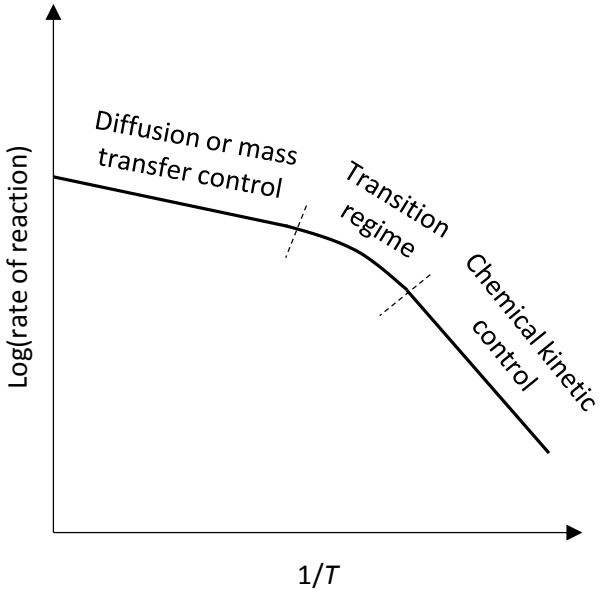

Figure 3.6 - The effect of temperature on the overall reaction rate (adapted from Szekely et al., 1976).

In the specific case of neutralization of acid gases with porous solid sorbents, changes in porosity occur due to differences in the density of the solid reactant and product. In fact, in contrast to heterogeneous catalysis, the consumption of the solid reactant and the formation of the solid product render structural changes crucial for the discussed systems. Several models were developed to describe the changes in the particle structure and to relate the overall reaction rate to mass transfer and kinetic phenomena, and hence to process conditions (e.g., temperature). Main mathematical models for gas-solid reactions are presented in the following sections.

3.3.2 Shrinking-core model

In many gas-solid reactions encountered in chemical processes, solid products are formed. These systems may be described by the general equation:

$$A(g) + bB(s) = cC(g) + dD(s) \qquad 3.9$$

The overall volume of solid may increase or decrease depending on the ratio of solid product density to that of the solid reactant.

Yagi and Kunii developed in 1955 the shrinking core model for spherical particles of unchanging size, which describes gas-solid reactions in which a solid product is formed (Levenspiel, 1998). A sketch portraying the assumptions made in the derivation of the shrinking core model is shown in Figure 3.7. Three steps occur in series during the reaction:

1. Diffusion of gaseous reactant through the film surrounding the particle to the surface of the solid.
2. Penetration and diffusion through the product layer to the surface of the unreacted core.
3. Reaction of gaseous reactant with solid at unreacted core surface.

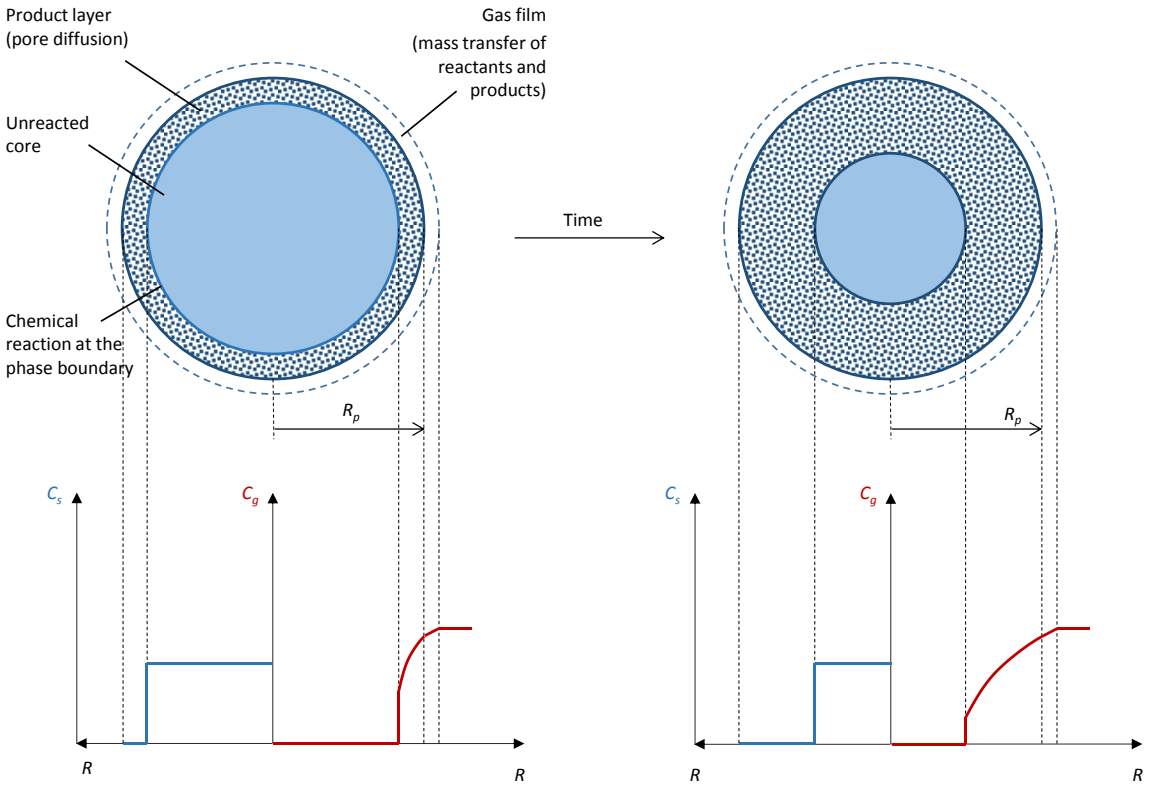

Figure 3.7 - Schematic representation of a reacting particle of unchanging size according to the shrinking core model. Reaction takes place only at the surface of the unreacted core, which shrinks in size during reaction. Blue line illustrates the sorbent concentration, while the red line represents the profile of gaseous reagent concentration.

If gaseous products are formed, two additional steps have to be taken into account:

4. Diffusion of gaseous products through the product layer to the exterior surface of the solid.
5. Diffusion of gaseous products through the gas film back into the bulk of fluid.

If one resistance is much great than others, it is possible to consider only the rate-controlling step. Otherwise, the conversion equation has to consider the combined effect of the different resistances.

3.3.3 Grain model

The shrinking core model has certain drawbacks, mainly the inability to represent a diffuse reaction interface. This is the general case for the reaction of porous solids, where there is a gradual change in the degree of conversion throughout the particle. Under these conditions, in contrast to nonporous solids, the reaction within the partially reacted zone occurs simultaneously with diffusion of gaseous reactants in this zone. In order to describe the case of distributed reaction in porous particles, Szekely et al. (1976) proposed the *grain model*, which is a generalization of previous distributed models. Figure 3.8 shows the schematization of a porous particle sketched according to the grain model. The particle is assumed spherical and made up of spherical grains of equal size[3]. Then, individual grains react according to a shrinking core model. Thus, the grain model scheme incorporates physically measurable properties of the reacting solid (e.g., grain size distribution and porosity).

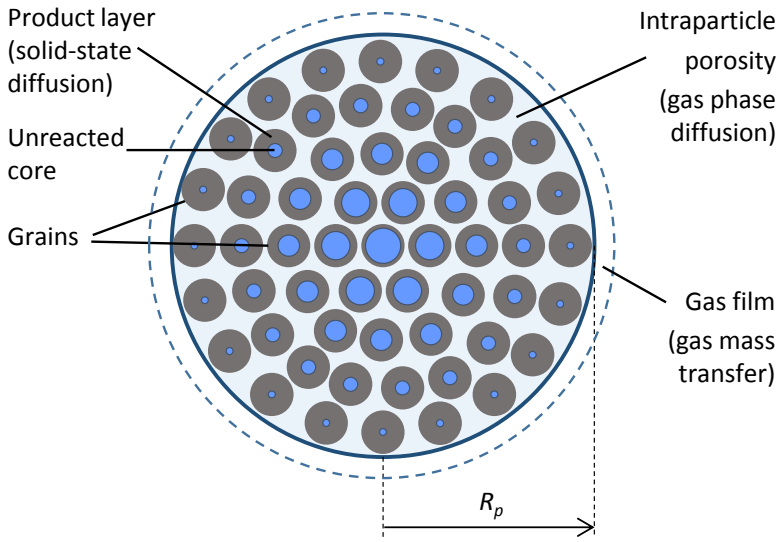

Figure 3.8 - Sketch of a particle according to the grain model, where R_p is the radius of the porous particle.

Accordingly, the reaction between the porous solid and a gas includes the following steps:

1. external mass transport of gaseous reactant from the bulk fluid to the surface of the porous solid;
2. diffusion of the reactant gases within the particle porosity;
3. chemical reaction of the grains according to the shrinking core model, including adsorption of the reactant and desorption of the gaseous products;
4. diffusion of the product through the porous solid;
5. mass transfer of the gaseous product into the bulk gas stream.

Depending on the relative rates of external mass transfer, pore diffusion and chemical kinetics of the grains, the model can represent different cases. In the general case, when diffusion and chemical reaction occur simultaneously throughout the solid, a diffuse reaction front is present. When chemical reaction controls the overall progress of the reaction, the model represents the asymptotic behavior corresponding to spatially uniform reaction. Conversely, when intraparticle diffusion mass transfer is controlling, there is a shrinking core behavior, which was discussed in Section 3.3.2.

[3] According to Szekely et al. (1976), the model permits to describe pellets with the shape of a sphere, a long cylinder, or a flat plate, made up of individual grains, which again could be spheres, long cylinders, or flat plates. However, to simplify the description of the phenomena, both particle and grains were assumed spherical.

3.4 HCl neutralization with solid sorbents

Many studies have focused on the reaction between hydrogen chloride and solid sorbents, in order to find the optimal conditions (e.g. temperature and sorbent properties) for acid gas removal in dry scrubbing processes. Main aims are the increase of HCl removal efficiency and the complete utilization of sorbent particles to optimize the economical conduction of the system.

Several investigations were undertaken with the aim of studying the kinetics and the mechanisms of hydrogen chloride reactions with calcium hydroxide and calcium carbonate. Weinell et al. (1992) investigated HCl binding from a gas stream on porous particles of calcium hydroxide in a laboratory fixed bed reactor. This study was conducted over a large temperature range (60-1000 °C), founding that the removal capacity of calcium hydroxide shows a peak in the range 500-600 °C and below 150 °C. In these ranges, $Ca(OH)_2$ showed an almost complete conversion to $CaCl_2$ according to the reaction:

$$Ca(OH)_2 + 2HCl \rightarrow CaCl_2 + H_2O \qquad 3.10$$

Weinell et al. (1992) studied the causes of the maximum conversion of calcium hydroxide particles. They found that a 10-fold variation of the particle size had little or no influence. Therefore, authors concluded that the conversion limitation was not caused by the block of the outer pores of the particles. Conversely, water content and temperature affected considerably the final conversion of the sorbent, as shown in Figure 3.9. Indeed, in the low-temperature range the complete consumption of calcium hydroxide was possible only if water was present. This behavior was explained by the authors through the formation of a partially liquid product phase, which at low temperatures and high water concentrations could break up the crystal lattice of the solid and expose a larger fraction of the sorbent for the reaction.

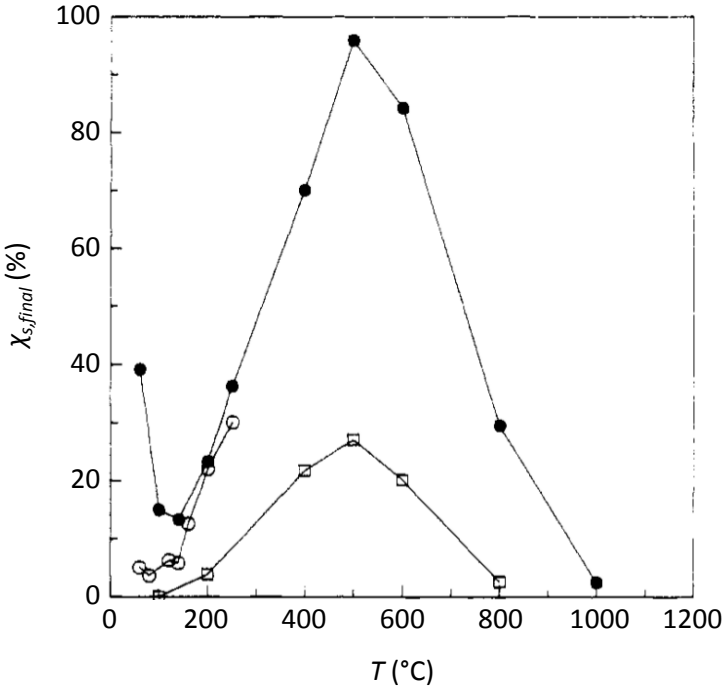

Figure 3.9 - Final solid sorbent conversions observed by Weinell et al. (1992) after 20 min with gas containing 1000 ppm of HCl. Black and white dots correspond to the final conversions of calcium hydroxide particles with S_{BET} = 12.1 m^2/g and a mean size of 2.1 µm, which were exposed to a gas flow with 5 % and 0 % of water respectively. White squares refer to limestone particles exposed to a gas stream with 5 % of water.

Another important evidence reported by Weinell et al. (1992) is that the kinetics of HCl removal is governed by diffusion in the solid phase according to the unreacted grain-core model. This parameter has been calculated from experimental data for the temperature range 80 - 250 °C and corresponding values are reported in Figure 3.10.

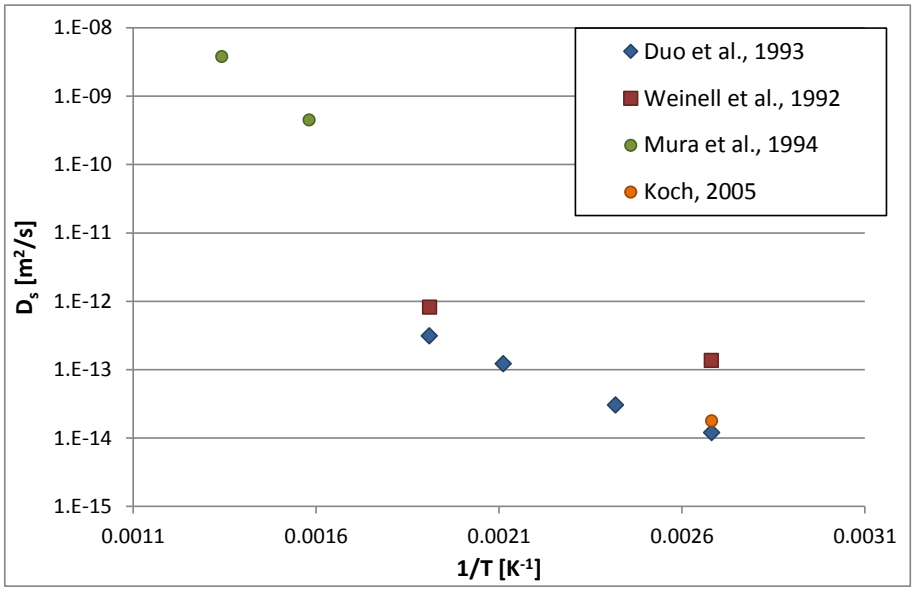

Figure 3.10 – Solid-state diffusion coefficients of HCl in $CaCl_2$ reported by different authors.

Duo et al. (1993) proposed a mathematical model based on Weinell's data to simulate the acid gas removal from flue-gases in dry systems where gas-solid separation is achieved injecting $Ca(OH)_2$ particles ahead of a fabric filter. In their model, main kinetic parameters taken into account were the solid-state diffusivity through the product layer (corresponding literature values are reported in Figure 3.10) and the reaction rate constant (reported in Figure 3.11).

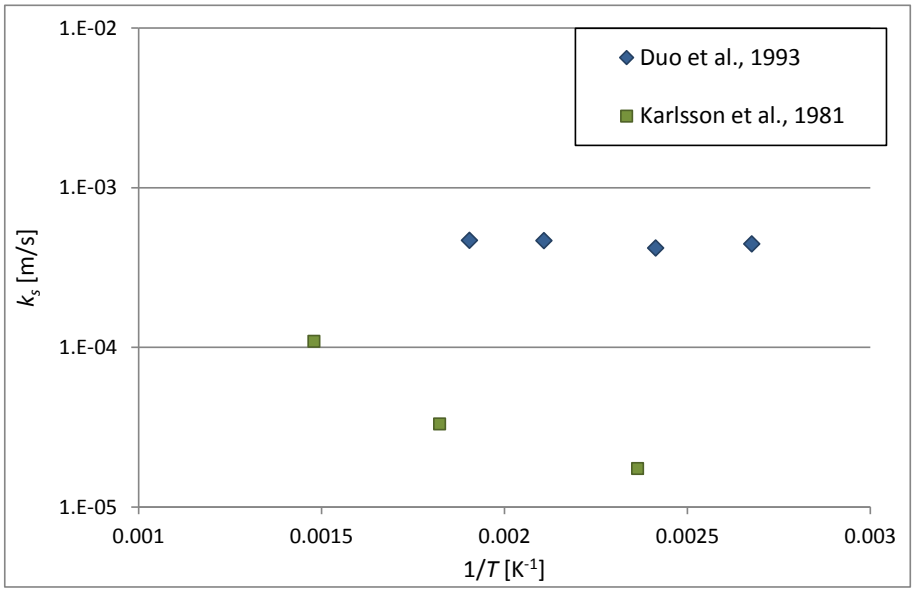

Figure 3.11 - Kinetic constant of the reaction between HCl and $Ca(OH)_2$ reported by Duo et al., 1993 (in blue) and by Karlsson et al., 1981 (in green).

The application of the model to the description of HCl removal through injection of solid $Ca(OH)_2$ led to the conclusion that solid state diffusion through the product layer is the controlling step in the range of

temperature between 100 - 250 °C, confirming the conclusions of Weinell et al. (1992). Indeed, the interpolation of the values found by Duo et al. (1993) for reaction rate constant and solid-state diffusivity through Arrhenius correlations, expressed by

$$k_s = A_{k_s} \cdot \exp\left(-\frac{E_{a,k_s}}{R \cdot T}\right)$$

and

$$D_s = A_{D_s} \cdot \exp\left(-\frac{E_{a,D_s}}{R \cdot T}\right)$$

led to the following values of the fitting parameters:

$$A_{k_s} = 5.659 \cdot 10^{-4}\ \frac{m}{s}$$

$$E_{a,k_s} = 863\ \frac{J}{mol}$$

$$A_{D_s} = 9.813 \cdot 10^{-10}\ \frac{m^2}{s}$$

$$E_{a,D_s} = 35321\ \frac{J}{mol}$$

The activation energy for kinetic constant is significantly lower than that for diffusion coefficient. Therefore, Duo et al. (1993) stated that the overall reaction rate is governed by chemical reaction at higher temperatures and by diffusion at lower temperatures.

Several researchers studied sodium-based sorbents for acid gas neutralization. Fellows and Pilat (1990) used a fixed-bed reactor with sorbent particles of decomposed $NaHCO_3$ and spherical glass beads to study the reaction:

$$Na_2CO_3 + 2HCl \rightarrow 2NaCl + CO_2 + H_2O$$

They studied the HCl neutralization process in different experimental conditions (i.e. gas flow rate, particle diameter, temperature, and inlet HCl concentration). Temperature resulted one of the most important parameters, as shown in Figure 3.12, which illustrates the results of the runs carried out from 225 °F (107 °C) to 550 °F (288 °C).

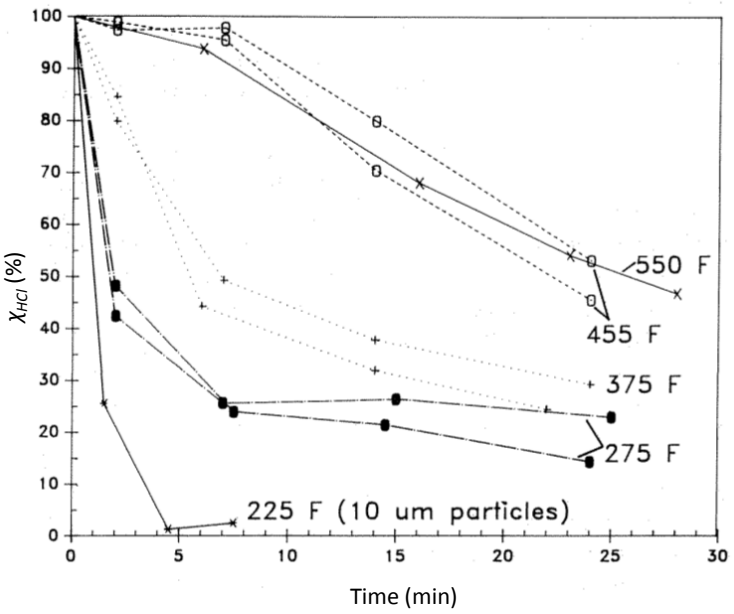

Figure 3.12 - HCl removal efficiency measured by Fellows and Pilat (1990) with $NaHCO_3$ particles of 45 µm (excepts the results at 225 °F, which was obtained with particles of 10 µm).

Fellows and Pilat (1990) analyzed also the effect of particle diameters on HCl collection efficiency. The results showed that particles of $NaHCO_3$ with a reference diameter of 45 µm and 163 µm (and a similar BET surface area) have similar behaviors, while results obtained with particles of 10 µm were probably unreliable because of the difficulty in dispersing the particles to obtain a homogeneous mixture in the fixed bed. Finally, the variation of HCl concentration in the gas flow (tested in the range between 402 and 760 ppm) had a negligible effect on removal efficiencies.

Similar experiments were carried out by Verdone and De Filippis (2006), which used a fixed bed multilayer reactor to investigate the HCl removal efficiency of sodium carbonate. Temperature resulted the most important parameter, showing a maximum of the removal efficiency in the range 400-500 °C. Conversely, HCl concentration and gas humidity had almost no effect on the overall reaction rate. Also sorbent particle size resulted to have negligible influence on the neutralization efficiency. The authors applied the model proposed by Duo et al. (1993) to describe their experimental results. The application of the grain model demonstrated that a first order reaction with respect to HCl concentration was suitable to fit the experimental data. In their conditions, HCl removal rate resulted to be controlled by both chemical reaction (in the first stages of the process) and solid-state diffusion through the product layer (when the reaction further proceeded). Corresponding Arrhenius parameters were assessed for the range 200 – 400 °C:

$$k_s = 169.9 \cdot \exp\left(-\frac{62281}{R \cdot T}\right)$$

$$D_s = 6.88 \cdot 10^{-8} \cdot \exp\left(-\frac{56530}{R \cdot T}\right)$$

The same authors proposed an analysis of the thermodynamic behavior of sodium and calcium based sorbents (Verdone and De Filippis, 2004). Their simulations were performed considering typical conditions of flue gas produced by waste incineration. Accordingly, the compounds taken into account were N_2, H_2O, CO_2, HCl, SO_2, NO and NO_2, while the solid sorbents simulated were $NaHCO_3$, Na_2CO_3, NaOH, $Ca(OH)_2$, CaO and $CaCO_3$. The results of their simulations indicated that sodium based sorbents are more efficient than

calcium based sorbent in the analyzed temperature range (i.e. 100 - 600 °C). Indeed, calcium based sorbent effectiveness was limited to SO_2 neutralization, while the applicability to HCl removal was limited to temperatures lower than 150 °C. Another result shown by simulations was the capability of sodium based sorbent to slightly reduce NO_x concentration.

4 Operational model description

4.1 Introduction

Emission into atmosphere of acid gases from waste-to-energy incineration plants is one of the main issues posed by waste disposal through thermal treatment. In particular, hydrogen chloride (HCl) and sulfur dioxide (SO_2) have to be removed because of their relevant concentration in flue gas and the high potential impact on the environment (as discussed in Section 2). Several technologies are available for the neutralization of these acidic compounds from flue gases produced by waste incineration (Section 3). Among the Best Available Techniques for acid gas cleaning (discussed in Appendix E), the two-stage dry treatment system described in Section 3.2 is increasingly applied because it allows complying with the restrictive limits of current legislation on pollutants emissions (illustrated in Appendix C). However, operational costs related to this technology could be notable if the treatment system is not well operated. Indeed, dry systems require a higher excess of sorbent than wet technologies and solid reactants are often fed in high excess (as described in Section 3.1) causing relevant amounts of unreacted solids in the solid waste streams recovered from fabric filters. For this reason, an optimization of the management of the flue-gas treatment systems is crucial. Therefore, several authors investigated reactions between acid gases and solid sorbents establishing a correlation between acid gas removal efficiencies and process conditions.

Two main approaches emerged from literature review. Some authors (e.g. Jannelli and Minutillo, 2007) proposed a simplified description of the flue gas cleaning system where the calibration was based on design data (mass flow rates, waste composition and plant components) of a specific incineration power plant.

Another approach consists in modeling the mass transfer and kinetic phenomena governing the gas-solid reactions. This method is described in Section 6. However, the adaptation of results obtained through laboratory tests to process conditions could be very problematical, as several parameters affect the analyzed reactions.

Therefore, a first activity consisted in analyzing operating data of an existing waste-to-energy incineration plant (described in Appendix G) to find which process parameters have to be taken into account. The development of a simplified correlation permitted to link the acid gas removal efficiencies measured in the analyzed case-study to corresponding process conditions. The proposed correlation was initially validated with literature data (Section 4.2) and adapted to describe process conditions (Sections 4.3 and 4.4). This procedure permitted the calibration of the model with operating data, with the aim of identifying the optimal process conditions that allow minimizing the operating costs (Section 5).

The case-study considered in the following sections consists in a two-stage dry treatment system adopted in an Italian waste-to-energy plant. The solid sorbents are granulated calcium hydroxide in the first stage of the process, and sodium hydrogen carbonate (bicarbonate) in the second stage. Main reactions involved in acid gas removal in the two stages were identified according to literature evidences reported in Section 3. Corresponding reaction sets are listed in Table 4.1.

Table 4.1 - Chemical reactions that take place in the first and second stages of the analyzed case-study.

First stage: calcium hydroxide	
$Ca(OH)_2 + 2HCl \rightarrow CaCl_2 + 2H_2O$	4.1
$Ca(OH)_2 + 2HF \rightarrow CaF_2 + 2H_2O$	4.2
$Ca(OH)_2 + SO_2 + ½O_2 \rightarrow CaSO_4 + H_2O$	4.3
$Ca(OH)_2 + CO_2 \rightarrow CaCO_3 + H_2O$	4.4
Second stage: sodium bicarbonate	
$2NaHCO_3 \rightarrow Na_2CO_3 + CO_2 + H_2O$	4.5
$Na_2CO_3 + 2HCl \rightarrow 2NaCl + CO_2 + H_2O$	4.6
$Na_2CO_3 + 2HF \rightarrow 2NaF + CO_2 + H_2O$	4.7
$Na_2CO_3 + SO_2 + ½O_2 \rightarrow Na_2SO_4 + CO_2$	4.8

4.2 Conversion function

Dry treatment systems for acid gas removal require higher stoichiometric excesses of sorbent than wet and semi-wet technologies, causing a great production of solid waste if not properly operated. Thus, an empirical model was developed in order to allow an optimization of the two-stage acid gas abatement process of the analyzed plant (described in Appendix G). The aim is the assessment of solid sorbent feed rates that optimize the operating conditions, i.e. reducing operating costs without affecting the overall acid gas removal efficiencies of the system.

By definition, the conversion of the *i*th acid gas (i.e. hydrogen chloride, sulfur dioxide or hydrogen fluoride) is:

$$\chi_{i,s} = \frac{\dot{n}_{i,in} - \dot{n}_{i,out}}{\dot{n}_{i,in}} \qquad 4.9$$

where $\dot{n}_{i,in}$ and $\dot{n}_{i,out}$ are the molar flow rates of the *i*th compound which respectively enters and exits the stage where the solid sorbent *s* (i.e. calcium hydroxide or sodium bicarbonate) is injected.

The model proposed in the present study is based on a simplified correlation that links acid gas conversion to the solid reactant feed rate:

$$\chi_{i,s} = \frac{{rs_s}^{a_{i,s}} - rs_s}{{rs_s}^{a_{i,s}} - 1} \qquad 4.10$$

where rs_s is the ratio of the actual feed rate of solid sorbent *s* to its stoichiometric rate (i.e. the flow rate required to completely convert all of the acid compounds, see Appendix I for details)[4]; $a_{i,s}$ are adjustable parameters that have to be determined for each neutralization reaction listed in Table 4.1 (Antonioni et al., 2013). It can be observed that the higher is the value of $a_{i,s}$ for a given value of rs_s, the higher is the removal efficiency $\chi_{i,s}$.

Thus, the conversion of each reaction is a function only of a single fitting parameter that will take into account all the physical phenomena and operating conditions actually involved in the heterogeneous reactions taking place in the reference stage (e.g. temperature, contact time, sorbent properties, etc.). Therefore, the model needs to be tuned with specific plant data in order to properly predict the process operating performance.

The correlation function (Eq. 4.10) was verified by checking its capability to reproduce literature data. Dots in Figure 4.1 represent the Neutrec data shown by Brivio (2007), where the conversion of hydrogen chloride and sulfur dioxide are plotted as a function of sodium bicarbonate flow rate (expressed as ratio to stoichiometric flow rate). A non-linear regression resulted in a coefficient of determination R^2 equal to 0.9997 for HCl and to 0.9998 for SO_2. Thus, the results showed a very good agreement between the proposed correlation and literature data, suggesting that Eq. 4.10 is suitable to describe the acid gas conversions as a function of dry sorbent feed rates.

[4] The limit of $\chi_{i,s}(rs_s)$ as rs_s approaches 1, is:

$$\lim_{rs_s \to 1} \chi_{i,s}(rs_s) = 1 - \frac{1}{a_{i,s}}$$

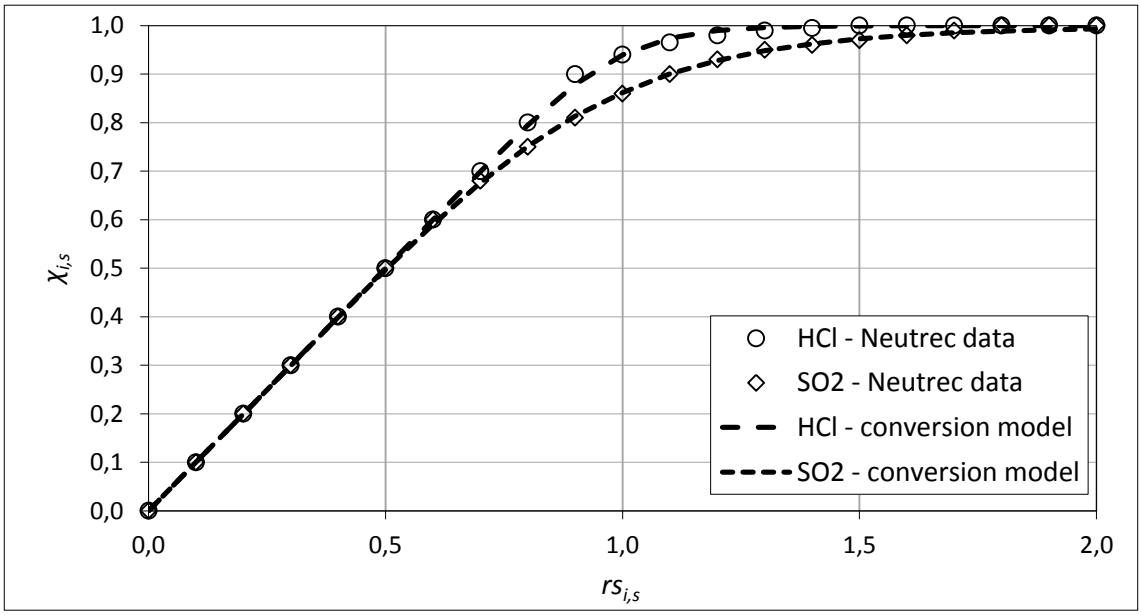

Figure 4.1 – Hydrogen chloride and sulfur dioxide conversions as a function of sodium bicarbonate feed rate (expressed as ratio between the actual feed rate and the stoichiometric flow rate required to completely convert the *i*th acid gas); dots represent literature data (Brivio, 2007) while dashed lines were obtained through the proposed correlation (Eq. 4.10).

Even though reactions between calcium hydroxide and acid gases could follow different reaction mechanisms, since all are heterogeneous non-catalytic gas-solid reactions, it is reasonable to assume that the overall conversion may have the same trend with respect to the excess of calcium hydroxide. Thus, the functional form expressed by Eq. 4.10 was adopted for all the neutralization reactions involved in the analyzed system.

4.3 Carbonation reaction

Competitive reactions have to be considered in order to calculate the feed rate of solid reactant available for the neutralization of the *i*th acid gas. With regard to the first stage, beside reactions for acid gas removal, the carbonation reaction (reaction 4.4 in Table 4.1) takes place (Chin et al., 2005). Carbon dioxide is a weak acid, but reaction with calcium hydroxide is considerable because CO_2 concentration is orders of magnitude higher than concentrations of other acid gases produced during waste combustion. This reaction does not affect significantly the carbon dioxide concentration, but it consumes a considerable amount of calcium hydroxide, which is then not directly available for the reactions with the acid gases. However, as reported by several authors (e.g. Mura and Lallai, 1994, Chin et al., 2005), the calcium carbonate produced through reaction 4.4, can neutralize in turn HCl:

$$CaCO_3 + 2HCl \rightarrow CaCl_2 + CO_2 + H_2O \qquad 4.11$$

In order to consider this reaction[5], the overall conversion of CO_2 in the first stage can be calculated through the amount of $CaCO_3$ in the solid residues produced in the first stage, which is available among design data (Section 5.1.1). However, in order to estimate CO_2 conversion in other conditions (i.e. different sorbent feed rates and CO_2 fraction), a first-order reaction with respect to $Ca(OH)_2$ and CO_2 concentrations was assumed. As the residence time of the sorbent in the filter cake is much longer than that in the entrainment duct (Duo et al., 1993), the equation for carbon dioxide conversion was written only for the layer of particles deposited on filter bags, leading to the following equation:

$$\chi_{CO_2} = \frac{\nu_{CO_2} \cdot \dot{\xi}}{\dot{n}_{CO_2,in}} = \frac{\nu_{CO_2} \cdot k \cdot c_{CO_2} \cdot c_{Ca(OH)_2} \cdot V}{\dot{n}_{CO_2,in}} \qquad 4.12$$

where *k* represents an overall kinetic constant and *V* is the filter cake volume. The ratio of CO_2 concentration to its incoming flow rate, can be expressed as a function of CO_2 conversion in the first stage and flue gas volumetric flow rate *Q*:

$$\frac{c_{CO_2}}{\dot{n}_{CO_2,in}} = \frac{1 - \chi_{CO_2}}{Q} \qquad 4.13$$

By substituting Eq. 4.13 in Eq. 4.12, the expression for carbon dioxide conversion is obtained:

$$\chi_{CO_2} = \frac{k' \cdot \left(1 - \chi_{CO_2}\right) \cdot m_{Ca(OH)_2}}{Q} \qquad 4.14$$

Considering that $\chi_{CO2} \ll 1$ and the fact that the amount of calcium hydroxide in the filter cake is proportional to its feed rate, Eq. 4.14 leads to:

$$\chi_{CO_2} = k'' \cdot \frac{\dot{m}_{Ca(OH)_2,in}}{Q} \qquad 4.15$$

where the inverse proportionality between CO_2 conversion and flue gas flow rate *Q* is due to the variation in contact time, which decreases when *Q* increases.

[5] It should be noticed that reaction 4.11 could be obtained through a linear combination of reactions 4.1 and 4.4.

The proportionality constant *k''* can be determined from design data, which are indicated in the following expression with the symbol *:

$$k'' = \chi_{CO_2}{}^{*} \cdot \frac{Q^{*}}{\dot{m}_{Ca(OH)_2,in}{}^{*}} \qquad 4.16$$

The corresponding fraction of calcium hydroxide consumed by carbonation reaction was subtracted from the total inlet rate to obtain the solid reactant available for the removal of HCl, SO_2 and HF.

4.4 Maximum sorbent conversion

Another adjustment to the correlation is required to take into account the maximum conversion of the sorbent, $\chi_{s,max}$, when it is applied to calcium hydroxide reactions. This phenomenon was observed by several authors (e.g. Weinell et al., 1992, and Chisholm and Rochelle, 1999). To include this limitation in the model, rs_s has been replaced in the Eq. 4.10 by an effective rs_s^*:

$$rs_s^* = rs_s \cdot \chi_{s,max} \qquad 4.17$$

With this correction, when the solid reactant is in defect (i.e. values of rs_s lower than 1), the maximum acid gas conversion expressed by Eq. 4.10 is limited to the corresponding sorbent conversion. For calcium hydroxide, $\chi_{s,max}$ strongly depends on process conditions (e.g. relative humidity, acid gas concentrations, initial fraction of voids of the calcium hydroxide particles). On the basis of literature (Chin et al., 2005) and process data, this limit was set to 80%.

For sodium bicarbonate, the value of $\chi_{s,max}$ can be assumed equal to 100% due to the high fraction of voids (Fellows and Pilat, 1990) produced during the thermal activation (reaction 4.5) compared to the increase of volume given by the formation of solid products according to reactions 4.6 - 4.8 (Verdone and De Filippis, 2004). This assumption is confirmed by the data showed by Brivio (2007), where the conversion of bicarbonate is almost complete when fed in stoichiometric defect. Thus no correction was required to Eq. 4.10.[6]

[6] A more precise estimation can be made taking into account the fraction of sodium bicarbonate that does not form carbonate; nevertheless, in the typical condition of the considered flue-gas treatment system, the decomposition (Eq. 4.5) can be assumed as complete, as reported by Brivio, 2007.

4.5 Calculation of model parameters

The adjustable parameters $a_{i,s}$ of correlation 4.10 have to be determined through literature data (Antonioni et al., 2011) or process data (Antonioni et al., 2012, 2013) for each neutralization reaction taking place in the treatment system. When a single couple of values rs_s and $\chi_{i,s}$ is available (e.g. design conditions of Section 5.1.1), the model parameter can be calculated solving Eq. 4.10 for $a_{i,s}$:

$$a_{i,s} = \frac{\ln\left(\frac{rs_s - \chi_{i,s}}{1 - \chi_{i,s}}\right)}{\ln(rs_s)} \qquad 4.18$$

For sodium bicarbonate, sets of values of conversion vs. stoichiometric rate are available for both HCl and SO_2 removal (shown in Figure 4.1). Therefore, the parameters can be calculated through a non-linear regressions, obtaining $a_{HCl,NaHCO3}$ equal to 16.6 and $a_{SO2,NaHCO3}$ equal to 7.3. However, as the fitting parameters take into account all the system properties (e.g. equipment volume and sorbent characteristic), they need to be assessed with specific data of the described system, as reported in Section 5.1 (where also competitive reactions were considered in the calculation of rs_s).

5 Results and discussions – Operational model

5.1 Analyzed case-study

5.1.1 Description of the flue gas treatment section

The operational model proposed in Section 4 was used to describe the reaction systems that take place at operating conditions in the flue gas treatment section of an existing waste-to-energy plant (a complete description of the plant is reported in Appendix G).

The flue gas cleaning section is aimed at the removal of the typical pollutants produced in a MSWI: fly ash, acid gases (HCl, HF, SO_2), heavy metals (mainly mercury), dioxins and furans, nitrogen oxides. The process flow diagram of this section is reported in Figure 5.1.

A first treatment for the reduction of nitrogen oxides is performed in the post-combustion chamber (not shown in Figure 5.1) with an ammonia solution, and then the flue gas (stream 1) flows into a first reactor where a dry sorption with calcium hydroxide takes place. The reactions involved in this process, aimed to acid gas removal from flue gas, are reported in Table 4.1. Activated carbon is also injected in this stage in order to remove heavy metals (i.e. mercury), dioxins and furans. The stream from the reactor is then fed to a fabric filter where the reactions continue on the filter cake and where the solid products of the reactions (calcium solid waste, CSW, unreacted calcium hydroxide and partially saturated activated carbons) are removed from the flue gas stream. Part of the solids removed by the filter (stream 9) can be recycled to the reactor feed (stream 11), since they can still contain a non-negligible amount of unreacted calcium hydroxide.

In the second stage of the process, a further reactor is present followed by a fabric filter, in order to complete the removal of acid gases through their reactions with sodium bicarbonate according to the Neutrec process (Verdone and De Filippis, 2004). Bicarbonate decomposes to carbonate (reaction 4.5 in Table 4.1) through an almost instantaneous and complete process at temperatures above 130°C (Brivio, 2007). Carbonate than reacts with the acid gases (reactions 4.6-4.8). In the second stage there is no recycle, since sodium bicarbonate is much more efficient than calcium hydroxide and requires a lower stoichiometric excess of sorbent over acid gases. Actually, in the exhaust solid stream leaving the second-stage fabric filter mainly sodium-based salts (or sodium solid waste, SSW) can be found.

The flue gas treatment is completed by a selective catalytic reduction (SCR) of nitrogen oxides where an ammonia solution is fed into a catalytic reactor provided with a honeycomb support for the metal base oxide catalyst with the aim of complying the final emission limit for NO_x. This equipment item will not be considered in the present study and thus is not shown in Figure 5.1.

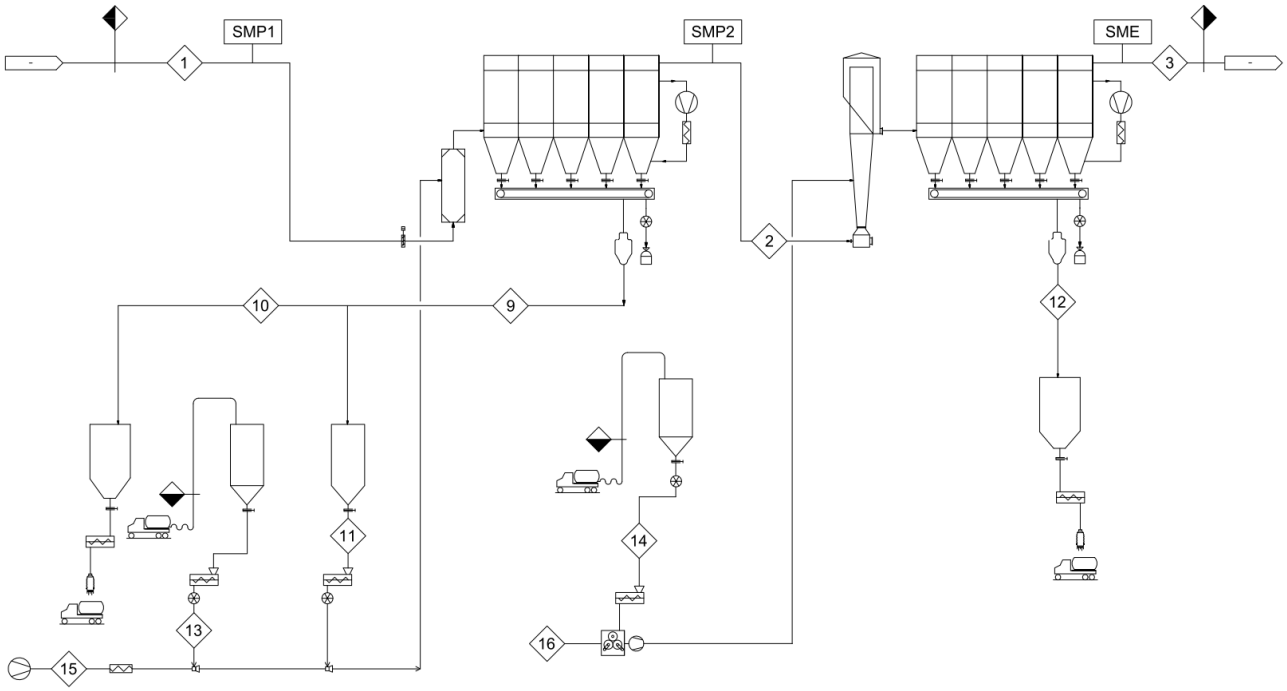

Figure 5.1 - Process flow diagram of the acid gas removal section.

5.1.2 Design conditions

In the flue gas treatment section of a MSWI the actual flue gas flow rate and its temperature change due to the operating conditions of the grid burner, that in turn are governed by the steam requirement set for the energy generation. Moreover, during normal operations, the concentrations of the pollutants are continuously varying due to the heterogeneous composition of the waste feed (as shown in Appendix B). Thus, reference values for the inlet stream based on the maximum energy production (see Appendix G) and on a typical waste composition (Villani et al., 2011) are required as design data. Data reported in the first column of Table 5.1 are part of the reference data assumed for the design of the plant under analysis. These data were considered as the starting point for the analysis of the acid gas removal process and for the calibration of the operational model presented in Section 4.

Table 5.1 - Design data.

		Inlet stream (Stream 1, Figure 5.1)	Outlet stream (Stream 3, Figure 5.1)	1st stage conversion χ_1	2nd stage conversion χ_2	Overall conversion χ
Flow rate	Nm^3/h	110,000	113,400			
H_2O	vol%	12.0	11.7			
O_2	vol%	8.0	8.4			
CO_2	vol%	8.5	8.2	0.004		
HCl	mg/Nm^3 [a]	800.0	2.0	0.700	0.992	0.998
HF	mg/Nm^3 [a]	10.0	0.5	0.700	0.833	0.950
SO_2	mg/Nm^3 [a]	200.0	5.0	0.300	0.964	0.975

[a] dry gas, 11 vol% O_2;
[b] for HF and SO_2 minimum required conversions are reported; actually higher conversions are usually achieved.

The main design information required for the flue gas treatment section are the flow-rate of the flue gas, the initial pollutant concentrations and their maximum allowable concentrations at the emission stack. Usually a reduction factor is applied to the emission limits of the most critical pollutant in order to define the design outlet concentrations. In the reference plant considered, the output design values reported in the second column of Table 5.1 for acid gases were obtained considering a reduction factor of five for HCl concentration, being hydrogen chloride the most critical pollutant due to its higher inlet concentration and to its lower emission limit with respect to other acid gases[7]. Hydrogen halides are in general more reactive to alkaline sorbents than sulfur dioxide (Chisholm and Rochelle, 1999), accordingly in the first stage a design conversion value of 70 % was assumed for hydrogen chloride and hydrogen fluoride. In the second stage, since the outlet concentration is known, the design value assumed for HCl conversion (see Table 5.1) was calculated by means of Eq. 5.1 where the overall conversion χ can be calculated from the flow rates and the concentrations assumed at the inlet stream and at the emission stack:

$$\chi_2 = \frac{\chi - \chi_1}{1 - \chi_1} \qquad 5.1$$

where χ is the overall conversion, χ_1 is the first-stage conversion and χ_2 is the second stage conversion. The first stage conversion, χ_1, was the independent variable considered in process simulations (Section 5.5).

[7] Directive 2010/75/EU on industrial emissions sets the daily average emission limit values for HCl to 10 mg/Nm^3 (see Appendix C for further details).

The second-stage design conversion value for HCl reported in Table 5.1 (99.2 %), obtained from the design value assumed for first stage conversion (70 %), is in good agreement with literature data, since sodium bicarbonate has typically a higher efficiency than calcium hydroxide in acid gases removal (Verdone and De Filippis, 2004).

Design reference values for the fresh feed rates of calcium hydroxide and of sodium bicarbonate are 313 kg/h and 142 kg/h respectively. These values were provided in the design phase on the basis of the first and second stage reference conversions reported in Table 5.1.

Concentration of fly ash in the incoming flue-gas is 3000 mg/Nm^3, which corresponds to a fraction in the solids separated by the fabric filter in the first stage of about 50 %. The filtration efficiency of the first stage is reported to be 99.7 %.

In design conditions, the recycle ratio is set to 0.8, intended as the ratio of recycled solid flow rate (stream 11 in Figure 5.1) to the total solid products rate leaving the first-stage fabric filter (stream 9).

The outgoing concentration for SO_2 and its conversion in both stages were as well provided in design data on the basis of the reference feed rates reported above.

The concentration of carbon dioxide decreases in the first stage because of reaction 4.4 (carbonation). In order to properly quantify its variation, also reaction 4.11 (where CO_2 is a product) and dilution (due to air for pneumatic transportation of sorbent particles, stream 15, and air entrainment) have to be taken into account. As the overall variation of CO_2 concentration in flue gas is negligible with respect to other acid gas, a more precise estimation can be obtained through the amount of calcium carbonate formed in the first stage. Indeed CO_2 concentration is orders of magnitude higher than those of other gaseous pollutants and in design conditions the amount of $CaCO_3$ in the solid residues (stream 10) is about 30 % of calcic solid products. According to reaction 4.4, the corresponding CO_2 decrease in the first stage is 0.4 % (reported in the third column in Table 5.1).

5.1.3 Operating conditions

Operating data of the two-stage acid gas abatement process for a period of 13 days were obtained on the basis of the monitoring system of the plant analyzed (Appendix G). With reference to Figure 5.1, operating variables of stream 1 were measured before the first stage at the sampling port 1 (SMP1), then in the intermediate stream between the two stages (SMP2). Finally, according to the requirements of Italian law (D.Lgs. 11-5-2005 n. 133), the operating variables at the emission stack (SME), through which flue gases are emitted into atmosphere, were recorded.

The following data were obtained:

- continuous measurement of the main process variables: total volumetric flow rate (at standard conditions), temperature, pressure, oxygen concentration, humidity;
- continuous measurement of the concentration of macropollutants: dusts, nitrogen oxides, acid gases, carbon monoxide, total organic carbon and ammonia;
- continuous measurement of mercury concentration;
- automatic sampling at given time intervals of dioxins and furans;
- semi-automatic periodic sampling of heavy metals and other organic micropollutants.

Most important measured data are reported as daily averages in Figure 5.2 - Figure 5.7, while the complete sets of data are reported in Appendix H.

Figure 5.2 and Figure 5.3 show respectively the measured values of hydrogen chloride and sulfur dioxide concentrations at the three sampling points. Figure 5.4 reports the flow rates of fresh calcium hydroxide, of recycled solids (1^{st} stage) and of bicarbonate feed (2^{nd} stage). The concentrations of carbon dioxide, water vapor and oxygen measured in SMP1 are reported in Figure 5.5, while the overall volumetric flow rate (at standard conditions) and the temperature of the flue gases measured in SMP1 are reported in Figure 5.6 and Figure 5.7 respectively.

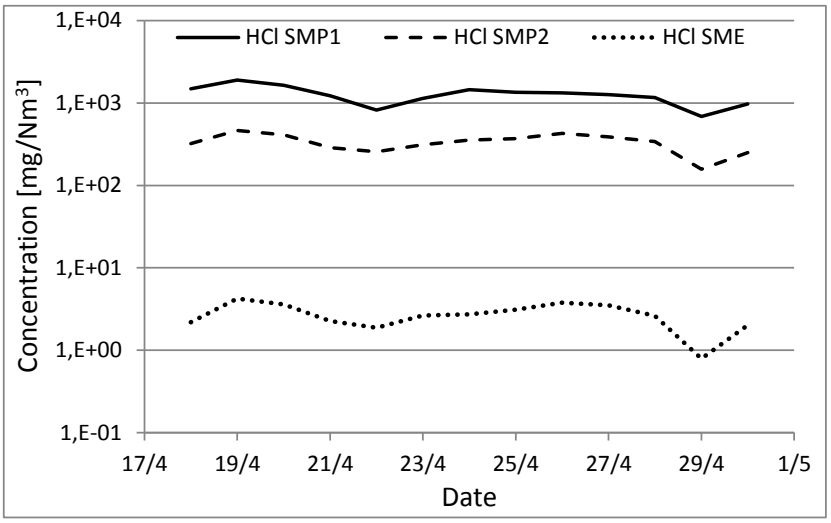

Figure 5.2 - Operational data: daily averages of hydrogen chloride concentration in SMP1 (solid line), SMP2 (dashed line) and SME (dotted line).

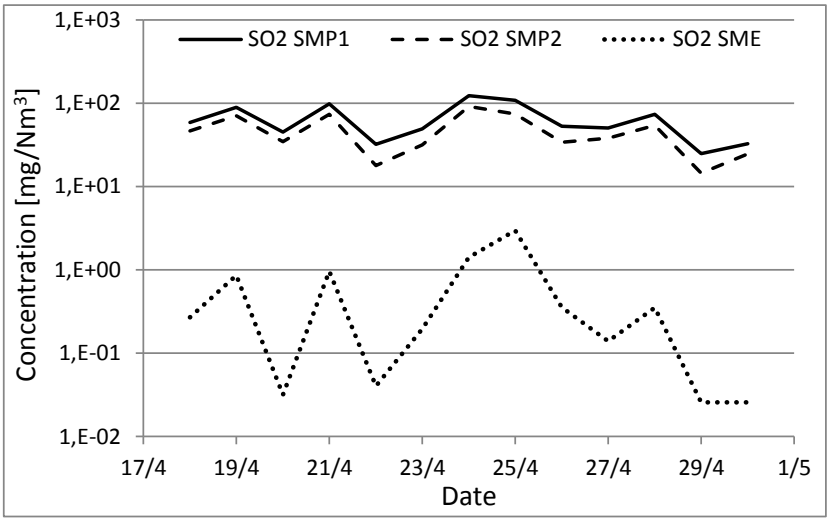

Figure 5.3 - Operational data: daily averages of sulfur dioxide concentration in SMP1 (solid line), SMP2 (dashed line) and SME (dotted line).

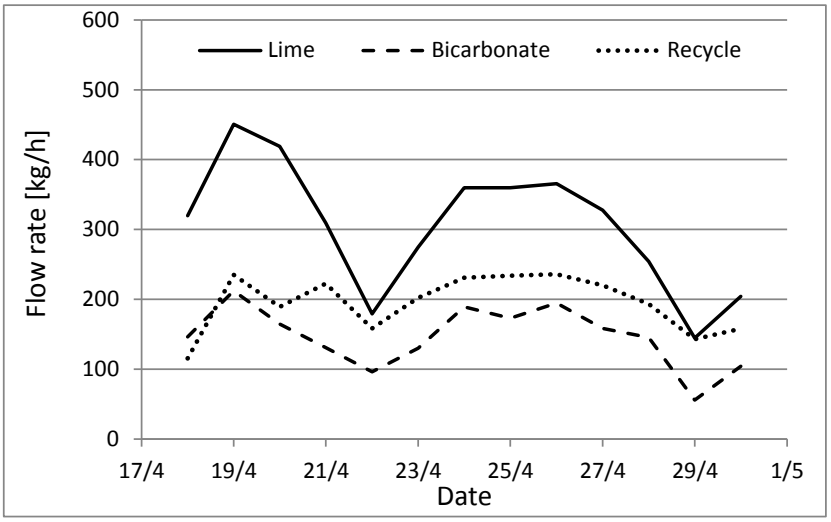

Figure 5.4 - Operational data: daily averages of fresh calcium hydroxide flow rate in the first stage (solid line), recycled solid flow rate in the first stage (dotted line) and bicarbonate flow rate in the second stage (dashed line).

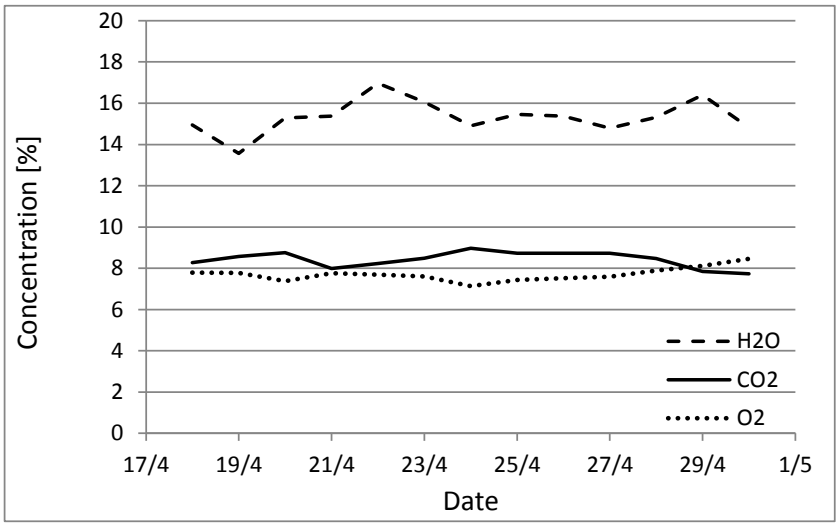

Figure 5.5 - Operational data: daily averages of carbon dioxide (solid line), water vapor (dashed line) and oxygen (dotted line) concentration measured in SMP1.

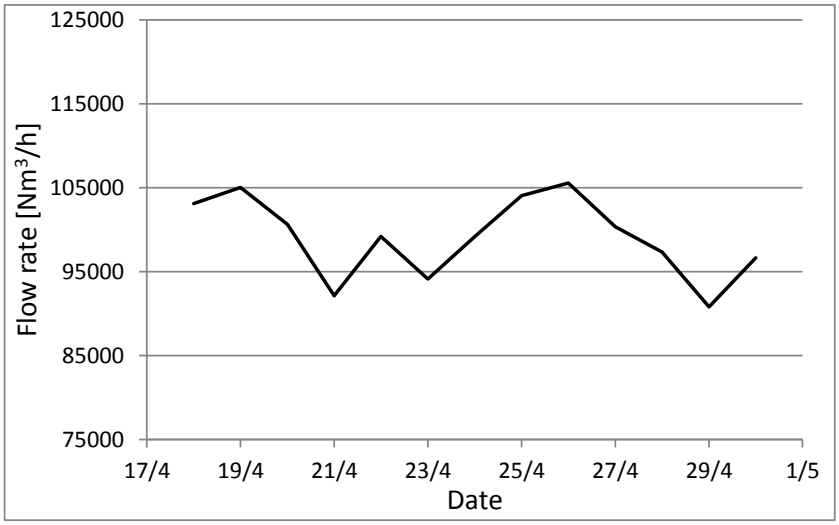

Figure 5.6 - Operational data: daily averages of volumetric flow rate (at standard conditions) of flue gas in SMP1.

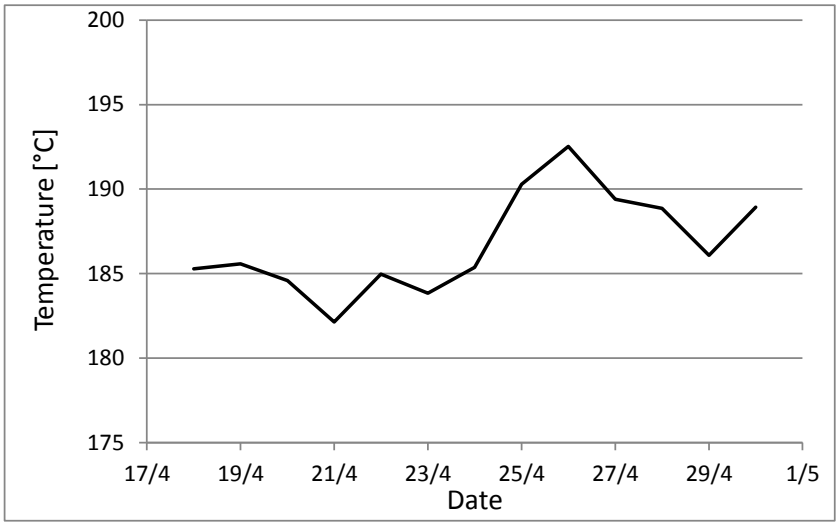

Figure 5.7 - Operational data: daily averages of flue gas temperature in SMP1.

The control system of the acid gas removal process is a hybrid feedback-feedforward system, where the controlled variables are the desired conversion in the first stage and the concentration of hydrogen chloride in the flue gases leaving the second stage (set to 2 mg/Nm^3). The manipulated variables are the fresh calcium hydroxide flow rate and the bicarbonate rate for the first and the second stage respectively, while the recycle rate is operated manually. Usually the active loops are those of the hydrogen chloride, but an override system is present to limit the SO_2 concentration in the flue gases leaving the second stage of the process.

As shown in Figure 5.2, the HCl inlet concentration is continuously varying (ranging from 690 to 1905 mg/Nm^3 as daily average), thus the manipulated variables change accordingly to the control system logic (solid, dashed and dotted lines in Figure 5.4) to obtain the desired set-point concentrations (dashed and dotted lines in Figure 5.2).

5.1.4 Operating costs

An economic optimization of operating conditions is possible starting from the flow rates and compositions of all the streams, using process simulations to assess the system performance. The unit costs reported in Table 5.2 were considered for the solid sorbents and the disposal of the products. The table reports the costs of raw materials (calcium hydroxide and sodium bicarbonate) on the Italian market (€ 2012) as obtained by operating company and the costs of the disposal of solid products (calcium salts and sodium salts for the first and the second stage respectively) paid per metric ton. Cost of equipment and other operational costs were not taken into account in the optimization carried out, since they do not significantly depend on reactants feed rates.

Table 5.2 - Cost of solid reactants and of solid waste disposal.

Material	**Stream (see Figure 5.1)**	**Cost ($€_{2012}$/t)**
Calcium hydroxide	13	80
Sodium bicarbonate	14	240
Calcium solid waste (CSW)	10	200
Sodium solid waste (SSW)	12	200

5.2 Model calibration

The parameters of the operational model (Section 4) were calculated on the basis of a complete set of process data (Section 5.1.3) in order to describe and optimize the analyzed plant (described in Appendix G). As operating conditions were continuously changing, rs_s and $\chi_{i,s}$ varied accordingly (shown by dots in Figure 5.8 as daily average for hydrogen chloride).

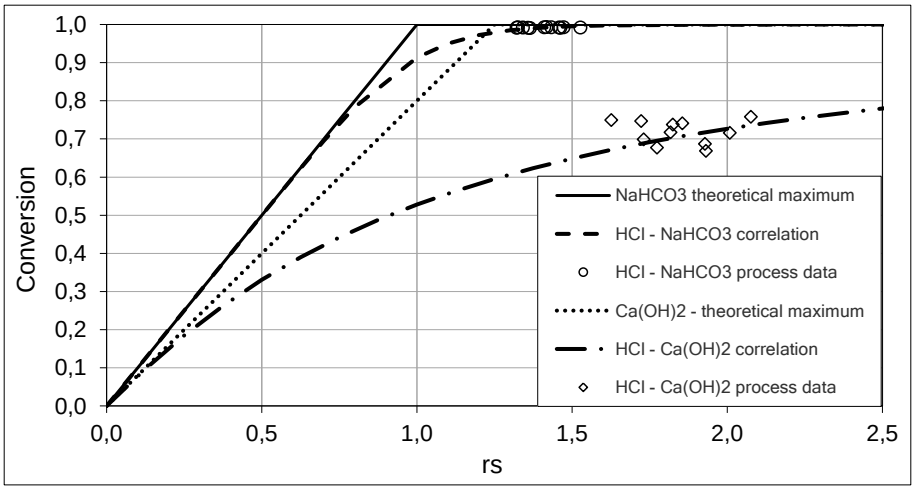

Figure 5.8 - Daily averaged HCl conversion in the first and second stages of the reference plant and corresponding correlations; dots represent process data for the reference plant as daily averages, while lines represent trends calculated through the operational model.

In the first stage, values of $rs_{Ca(OH)2}$ were calculated taking into account the carbonation reaction (Section 4.3), the maximum conversion of calcium hydroxide (Section 4.4) and unreacted sorbent injected with the recycled solids. Nevertheless, in the analyzed plant (Appendix G) the composition of separated solids is not measured, so it was calculated accordingly to acid gas conversions and taking into account inert solids. The latter is mostly fly ashes, and its flow rate[8] was calculated assuming that the concentration in flue gas was constant during the entire analyzed period and equal to the design value[9], while flue-gas flow rates were measured (corresponding values are shown in Figure 5.6).

The parameters $a_{i,s}$ were determined from daily averaged values of $\chi_{i,s}$ and rs_s through non-linear regressions (according to Section 4.5). The values obtained for both solid reactants are reported in Table 5.3 for HCl and

[8] For the sake of simplicity (see stoichiometry of reactions 4.1-4.4 of Table 4.1), flow rates of solid streams that enter and exit the reaction stage were expressed on a molar basis.

[9] The molar fraction of fly ash, x_{FA}, in inlet and outlet solid streams (and consequently in the recycled stream) is the same and can be easily calculated for the inlet stream:

$$x_{FA} = \frac{Q \cdot c_{FA}}{\dot{n}_{Ca(OH)_2,fr} + Q \cdot c_{FA}}$$

where Q is the flue-gas volumetric flow rate (in Nm^3/h), c_{FA} is the fly ash concentration in flue-gas entering the first stage (in mol/m^3) and $\dot{n}_{Ca(OH)_2,fr}$ is the molar flow rate of fresh calcium hydroxide injected into the system (in mol/h).
Design data provides the concentration of fly ash in flue gas in mass (i.e. 3000 mg/Nm^3). To convert this value in molar concentration, the average molar mass is required. An estimation was made assuming that fly ash is made only from its main components: SiO_2, CaO and Al_2O_3. Maintaining the proportions between mass fractions (Rémond et al., 2002), their percentage results to be respectively 50%, 30% and 20%. Accordingly, the average molar mass is:

$$\bar{M}_{FA} = \frac{m_{FA}}{n_{FA}} = \frac{m_{SiO_2} + m_{CaO} + m_{Al_2O_3}}{n_{SiO_2} + n_{CaO} + n_{Al_2O_3}} = \frac{m_{SiO_2} + m_{CaO} + m_{Al_2O_3}}{\frac{m_{SiO_2}}{M_{SiO_2}} + \frac{m_{CaO}}{M_{CaO}} + \frac{m_{Al_2O_3}}{M_{Al_2O_3}}} = 64\ \frac{g}{mol}$$

SO_2. The resulting conversion curves obtained from the operating conditions are plotted in Figure 5.8. The correlation between the correlation and the real process data is not as good as when literature data were considered, as evident from the comparison between Figure 4.1 and Figure 5.8. However, the agreement between model results and operating data can be considered sufficient, taking into account the uncertainties and the extreme variability of real plant data.

Table 5.3 - Values calculated for model parameters $a_{i,s}$ using process data.

	$Ca(OH)_2$	**$NaHCO_3$**
HCl	2.29	11.6
SO_2	1.27	12.3

Since process data for hydrogen fluoride concentrations at exit of first and second stages (sampling points SMP2 and SME in Figure 5.1) were often under the detection limit, its parameters (i.e. $a_{HF,Ca(OH)2}$ and $a_{HF,NaHCO3}$) were assumed to be equal to those calculated for hydrogen chloride.

5.3 Implementation of the model

Correlations for acid gas conversion (discussed in Section 4) were implemented within the Aspen Hysys software (Aspen HYSYS, 2009) to simulate the two-stage process described in Section 5.1.1. The process flow diagram (Figure 5.1) was described using blocks representing the different unit operations, obtaining the schematization reported in Figure 5.9.

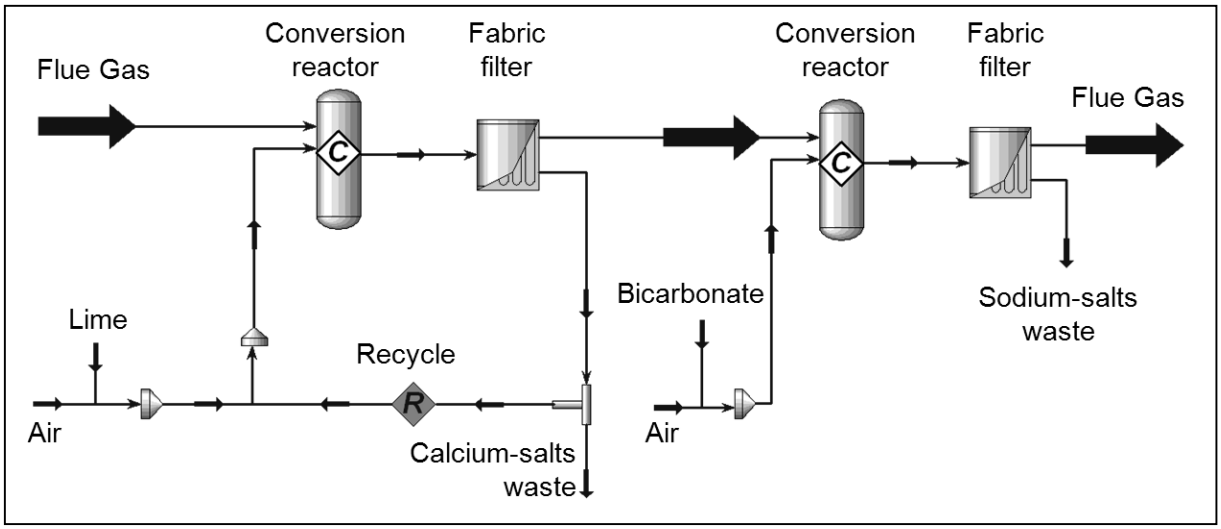

Figure 5.9 - Schematization of the two-stage process considered for the implementation of the operational model within Aspen Hysys.

In the numerical implementation, for the sake of simplicity, the combined effect of the reactor and the filter cake on acid gas removal was associated to the *Conversion reactor*. This type of reactor requires the definition of the conversion for each reaction showed in Table 4.1. The default correlation available in Aspen HYSYS is reported in Eq. 5.2, which relates the conversion *C* with temperature *T*:

$$C = C_0 + C_1 \cdot T + C_2 \cdot T^2 \qquad 5.2$$

The considered reactions do not produce significant thermal effects because the amount of reactive substances is considerably lower than the total flow. Therefore, the temperature is approximately constant and the coefficients C_1 and C_2 were set to zero. Dependency of coefficient C_0 on process conditions was expressed by means of user defined functions according to Eq. 4.16 for CO_2 conversion and to 4.10 for other acid gases (i.e. HCl, HF and SO_2), making use of the $a_{i,s}$ parameters reported in Table 5.3 and including the contribution of the fabric filters to the overall conversion. Indeed, in the simulation model, the units labeled *Fabric filter* act only as ideal separators (gas-solid separation was assumed complete). Due to the features of the model implemented, this assumption does not have any effect on the results of the simulations.

As shown in Figure 5.9, the software allowed the simulation of solid products recycle in the first stage, where the tool labeled *Recycle* permits to input the recirculation ratio or the recycled flow rate. In the implementation fly ash was not taken into account, so recycle stream in the first stage was considered as formed only by calcium solid waste (CSW): unreacted $Ca(OH)_2$ and calcic products (i.e. $CaCl_2$, CaF_2, $CaSO_4$ and $CaCO_3$).

The simulation software requires as input the properties of the flue gas that enters in the treatment system. The information required is flow rate, acid gas (HCl, HF and SO_2) concentrations and volumetric fractions of CO_2, O_2 and H_2O (nitrogen concentration is calculated accordingly). Solid sorbent feed rates have to be set in

the properties of streams *Lime* (i.e. calcium hydroxide) and *Bicarbonate*, while streams labeled *Air* include the volumetric flow rate of air for pneumatic transportation of solid sorbents (i.e. streams 15 and 16 of Figure 5.1) and they are used in order to simulate also air entrained in the system due to its slightly negative pressure.

Once set inlet streams and model parameters, the software computes flow rate and composition of intermediate and outgoing streams (both gaseous and solid).

5.4 Validation with average process data

The model was initially applied to describe average process data in order to verify the model implementation through the comparison between measured concentration at the stack (SME) and the values calculated through the simulation software. The average flue gas input concentrations are illustrated in Table 5.4, while Table 5.5 shows the solid reactants feed rates measured during the analyzed time interval. These data were used as an input to the model. The model parameters set in the process simulations are those listed in Table 5.3. In order to take into account the air used for pneumatic transportation of solid powders and the air entrainment into the system in model simulations, the total flow rate of the outlet stream was set equal to the value measured at the emission stack (SME sampling point in Figure 5.1).

Table 5.4 - Flue gas conditions (average measured during the entire analyzed period and calculated through the model).

		Inlet stream (stream 1, Figure 5.1)	Outlet stream (stream 3, Figure 5.1)	
		Process data	Process data	Model data
Flow rate	Nm^3/h	99,096	107,821	107,821
H_2O	vol%	15.33	14.92	14.17
O_2	vol%	7.70	8.78	8.77
CO_2	vol%	8.43	7.99	7.75
HCl	mg/Nm^3 [a]	1262.62	2.72	2.94
HF	mg/Nm^3 [a]	8.30	0.00	0.02
SO_2	mg/Nm^3 [a]	64.59	0.59	0.31
[a] dry gas, 11 vol% O_2.				

Table 5.5 - Feed rates of solid reactants (average process conditions).

	Stream No. (Figure 5.1)	Feed rates (kg/h)
Calcium hydroxide	13	298
Recycle	11	98[10]
Sodium bicarbonate	14	144

The results obtained from the above input values and assumptions are shown in the last column of Table 5.4. The comparison between the measured values and the data calculated from the model data, reported as values averaged on the 13 days of operation, shows that a good agreement is present. In particular, it should be remarked that the average HCl measured concentration (2.72 mg/Nm^3) well corresponds to the value calculated through the operational model (2.94 mg/Nm^3). Also the concentrations of the other gaseous species are similar, although the abatement of SO_2 is slightly overestimated.

[10] The measured values of the recycled flow rate (Figure 5.4) were corrected deducting the fraction of fly ash (FA) to consider only Ca-salts (CSW) and unreacted lime:

$$\dot{n}_{CSW,rec} = \dot{n}_{rec,measured} \cdot \left(1 - x_{FA,rec}\right)$$

5.5 Optimization of process conditions

5.5.1 Optimization of sorbents feed rates

A first set of simulations was dedicated to analyze the dependency of the second stage feed rate as function of the first stage conversion keeping constant the overall conversion (see also Eq. 5.1). The conditions of incoming flue gas (stream 1 of Figure 5.1) were considered constant at their average value measured during the 13 days of operation considered (first column of Table 5.4).

Simulations were carried out by varying calcium hydroxide feed rate (stream 13) and varying consequently acid gas conversions in the first stage. The total recycle rate was kept constant at its average value (reported in Table 5.5). However, the recycle stream composition changes according to the stoichiometry of the reactions and to the amount of fly ash (whose concentration in flue gas was fixed to the design value of 3000 mg/Nm^3). So acid gas concentrations in stream 2 could be calculated through Eqs. 4.10 and 4.16, taking into account all the reactions involving calcium hydroxide and dilution due to air entrainment.

The bicarbonate feed rate was adjusted in order to keep constant the concentration of hydrogen chloride emission at 2.94 mg/Nm^3, thus also the overall conversion is kept constant. This value corresponds to the calculated concentration of HCl emissions from the plant stack, reported in the last column of Table 5.4. Thus, this choice also assures that emission concentrations of all acid gases are well below the emission limits, being hydrogen chloride the most critical pollutant in typical process conditions (as discussed in Section 5.1).

A series of simulation were carried out varying the independent variable (in this case, calcium hydroxide feed rate in the first stage) and calculating accordingly the dependent variables (e.g. acid gas conversions and bicarbonate feed rate). In Figure 5.10 solid sorbents feed rates (calcium hydroxide, sodium bicarbonate and their sum) are shown as a function of HCl conversion in the first stage for the same acid gas being removed[11], being hydrogen chloride conversion $\chi_{HCl,Ca(OH)2}$ the controlled variable in the control system). The figure clearly evidences that a minimum in the total reactants feed rate can be obtained when operating with a first stage conversion between 50 % and 60 % (thus not very far from the average measured first-stage conversion obtained from the available operating data).

[11] This plot was created with the tool *DataBook* of Aspen Hysys. This instrument permits to carry out a series of simulation varying the independent variable (in this case, HCl conversion in the first stage) and calculating the depend variables (i.e. calcium hydroxide, bicarbonate and total solid reactants feed rates) accordingly.

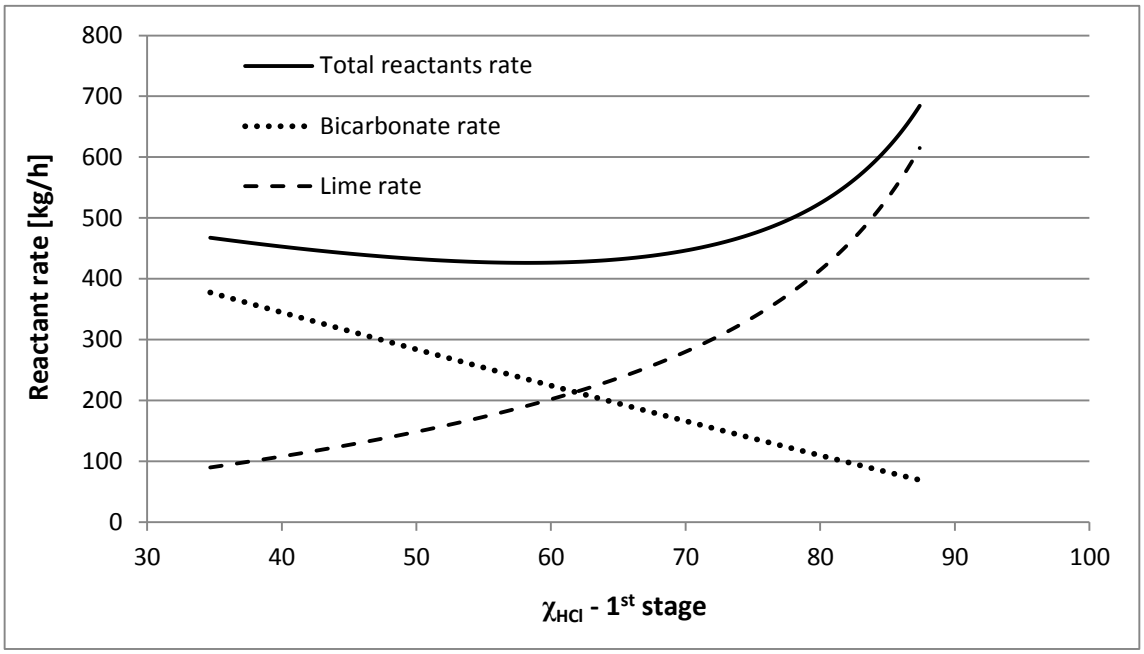

Figure 5.10 - Calcium hydroxide, bicarbonate and total solid reactants feed rates as a function of HCl conversion in the first stage.

5.5.2 Economic optimization

Average operational conditions

As calcium hydroxide and sodium bicarbonate have different unit costs (as reported in Table 5.2), an economic optimization was performed considering the costs of injected sorbents (streams 13 and 14 in Figure 5.1). Also disposal costs were included in the evaluation (streams 10 and 12 of Figure 5.1). Indeed, even though unit cost of solid waste disposal is the same for both stages (as shown in Table 5.2), the weight of calcium and sodium salts produced removing the same amount of acid gas is different (according to reactions illustrated in Table 4.1). Thus, the overall operating cost of the process was calculated considering the average conditions of incoming flue gas (where the concentration of hydrogen chloride is 1260 mg/Nm^3).

In order to find economic optimal operating conditions, a series of simulations were carried out following the same procedure described in Section 5.5.1 and calculating the cost associated to sorbent feed rates and to solid products disposal. Cost variation with respect to average conditions is reported in Figure 5.11 as a function of the HCl conversion obtained in the first stage. The figure evidences that a minimum is present in the operating costs when first stage conversion is of about 60 %. The minimum corresponds to an economic saving of about 7 % in the operating costs considered. Clearly enough, uncertainties may affect this calculation, in particular concerning the influence of the consumptions of calcium hydroxide due to carbonation (reaction 4.4).

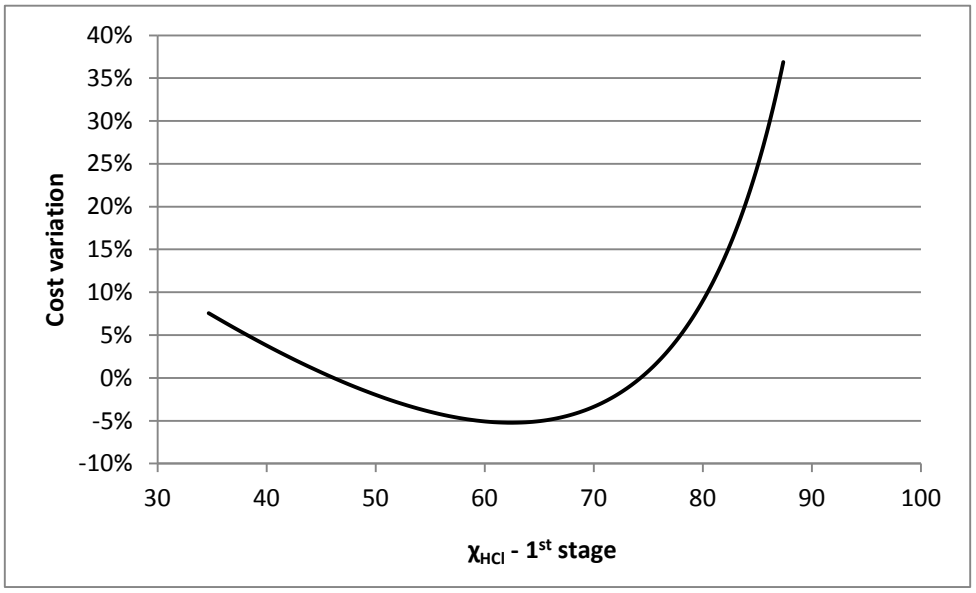

Figure 5.11 - Variation of operating costs (%) with respect to design conditions as a function of first stage hydrogen chloride conversion.

In order to assess the influence of the conversion value assumed for CO_2 in the carbonation reaction on the operating costs, simulations were carried out changing the reference value of the carbon dioxide conversion (χ_{CO2}^* in Eq. 4.16). Model runs were carried out assuming CO_2 conversion values of 0.2 % and of 0.6 % (which correspond to ±50 % variations around the design value of 0.4 % reported in Table 5.1 and assumed in the standard simulations). The operating costs resulted in variations as high as 10 %, evidencing the strong influence of this reaction on the operating costs of the process.

Daily conditions

Since the HCl inlet concentration can vary significantly in a MSWI, a second set of simulations was carried out to evaluate the sorbent feed rates that optimize the operational costs for different conditions of the incoming flue gas (corresponding to the average conditions measured in some representative days). In Table 5.6 the measured conditions of the flue gas entering the treatment system (stream 1 of Figure 5.1) are reported for some selected days, with the corresponding calcium hydroxide and recycled solids feed rates (1st stage) and bicarbonate feed rate (2nd stage).

Table 5.6 - Daily averaged conditions of streams 1, 13, 11 and 14 (with reference to Figure 5.1) in three days; acid gas concentrations are referred to dry gas and standardized at 11 % oxygen in flue gas.

Day	Flow rate	HCl	SO_2	HF	CO_2	O_2	H_2O	$Ca(OH)_2$	Recycle	$NaHCO_3$
-	SMP1	SMP1	SMP1	SMP1	SMP1	SMP1	SMP1	Stream 13	Stream 11	Stream 14
-	Nm^3/h	mg/Nm^3	mg/Nm^3	mg/Nm^3	%	%	%	kg/h	kg/h	kg/h
1	90,805	688	24.9	4.3	7.8	8.1	16.4	144.8	142.8	55.7
2	100,367	1266	50.6	8.9	8.7	7.6	14.8	327.6	220.1	158.5
3	105,044	1905	89.4	14.3	8.6	7.8	13.6	450.6	235.2	212.2

All simulations were carried out setting HCl concentration at the emission stack at a value of 2.94 mg/Nm^3. Results reported in Figure 5.12 show that the removal costs clearly increase with the concentration of hydrogen chloride in the flue gas entering the treatment system (daily averaged values are reported in the third column of Table 5.6). However, for each considered day, a minimum in overall costs is always present for a first stage conversion of between 60 % and 65 %. Actual costs (white dots in Figure 5.12) can be estimated to have been between 3 % and 8 % higher with respect to the calculated optimal conditions (black dots in the figure).

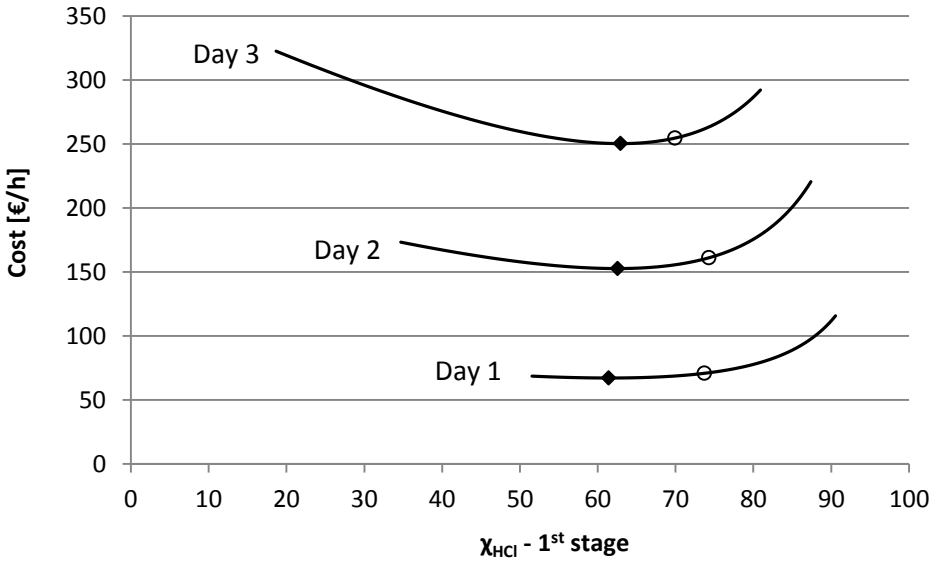

Figure 5.12 - Solid lines represent operating costs for acid gas removal with current configuration as a function of first stage HCl conversion in some selected days (whose corresponding conditions are reported in Table 5.6); white dots denote daily average conditions, while black dots represent the cost minimum.

For the higher values of HCl inlet concentrations considered it is important to operate the first stage within this range, as outside it the costs rapidly increase, as shown in Figure 5.12. Conversely, in the lower range of inlet HCl concentrations considered (i.e. the lowest line in Figure 5.12), keeping the conversion of the first stage below 70 % is sufficient to minimize the operating costs of the acid gas removal section.

5.6 Simulation of alternative configurations

The model was then applied in order to simulate the performance of the plant if different configurations of the treatment system were adopted. The considered cases consist of injecting the same reactant (i.e. only calcium hydroxide or only sodium bicarbonate) in both stages. The simulations were aimed to the prediction of the performance of the analyzed plant (Appendix G) when only the injected sorbent is changed, therefore without additional capital costs related to modifications of the plant configuration.

The first simulated alternative was a two-stage system where solid particles of calcium hydroxide are injected in both reactors. Operating conditions measured during Day 2 (shown in Table 5.6) were selected as reference point for the flue gas inlet composition, since it is representative of the average inlet concentration. Simulation results show that using this configuration (second bar of Figure 5.13), operating costs would be definitely higher than current configuration (first bar, corresponding to the minimum operating cost estimated in Section 5.5.2) to reach the same HCl concentration at the stack. This is due to the very low emission limit set in the analyzed plant, where an overall removal efficiency higher than 99.7 % is required for hydrogen chloride, making a low efficient sorbent unsuitable for the second stage. However, for flue gas with high HCl content, the fraction of $Ca(OH)_2$ that forms $CaCO_3$ reacting with CO_2 could decrease because of reaction 4.11: this effect is not taken into account by the present model and could determine a slightly better performance of the $Ca(OH)_2$. Also the use of calcium hydroxide with high surface area could be of interest because the expected maximum conversion (discussed in Section 4.4) is higher, thus reducing reactant and disposal costs for the calcic stage.

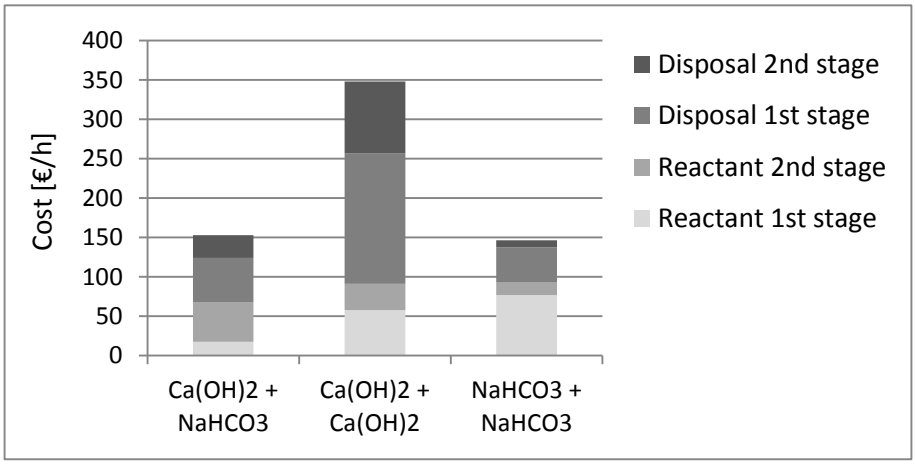

Figure 5.13 - Minimum operating costs with current configuration (1st bar), two stages with calcium hydroxide (2nd bar) and bicarbonate-bicarbonate system (3rd bar); inlet flue gas conditions refer to Day 2 of Table 5.6.

The second alternative was referred to a bicarbonate - bicarbonate systems (in this case, the recycle rate in the first stage was set to zero, as the high single-pass conversion efficiency of $NaHCO_3$ and low stoichiometric excess required make a recycle worthless). Simulation results (illustrated in the third column of Figure 5.13) indicate that it would be possible to achieve a slight reduction of operating costs with respect to the actual condition, but the difference is so low that this conclusion could be affected by uncertainties, especially due to the assumption that the model parameters are constant outside the calibration range. However, the benefits expected injecting sodium bicarbonate in both stages are more significant when the HCl concentration in the flue gas is higher, as shown in Figure 5.14 by the comparison with current configuration.

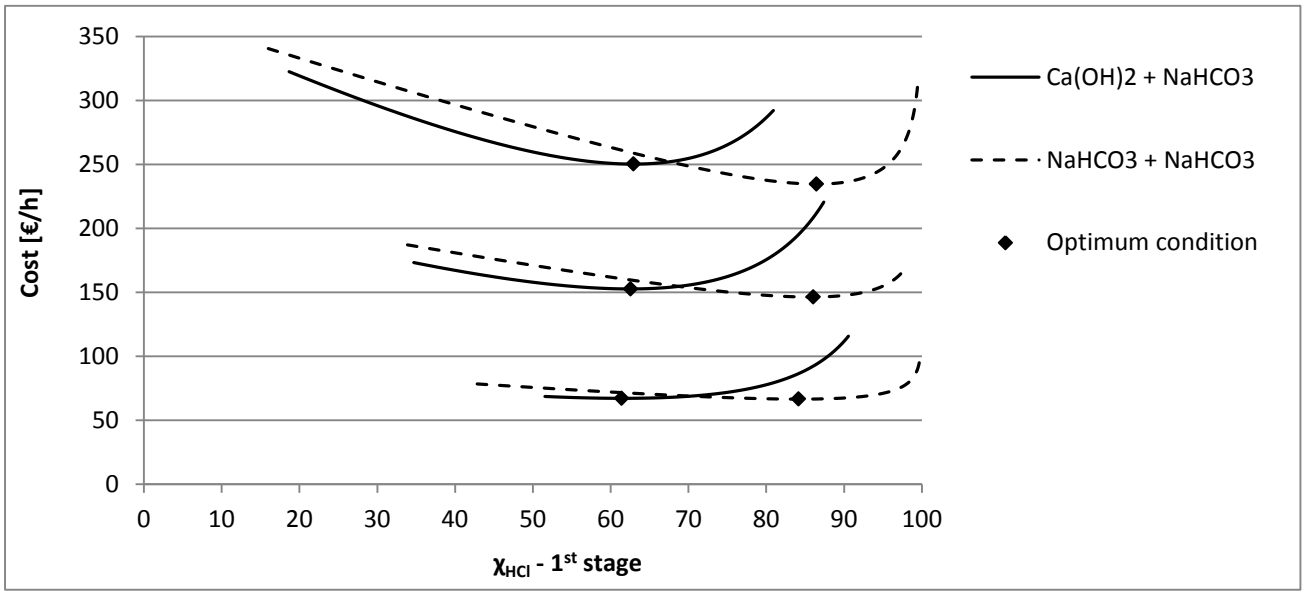

Figure 5.14 - Dashed lines represent operating costs for acid gas removal expected injecting sodium bicarbonate in both stages as a function of first stage HCl conversion in some selected days, compared with solid lines which represent the costs with current configuration (already shown in Figure 5.12).

The distribution of reactants and disposal cost (Figure 5.13) shows that when calcium hydroxide is the only reactant, disposal costs are about 75 % of the total operating costs. In fact, considerable amounts of unreacted $Ca(OH)_2$ and $CaCO_3$ present in solid waste. Calcium hydroxide could be reduced using an higher recycle rate, which would decrease also operating costs of the existing plant (operating with calcium hydroxide and bicarbonate), possibly lowering costs below the process with bicarbonate injected in both stages.

6 Fundamental model

6.1 Introduction

An operational model based on a simplified description of the acid gas removal process was presented in Section 4. Its implementation permitted to identify the optimal operating conditions in the analyzed case-study. However, the model needs operational data of the specific plant for the calibration and it is not predictive. Thus, a fundamental approach was adopted in order to establish a correlation between acid gas removal efficiencies and process conditions. It consisted in modeling the mass transfer and kinetics phenomena that characterize gas-solid reactions. However, acid gas neutralization with sorbent particles is a complex process, which results from the superimposition of different effects, such as flow through a porous fixed bed of particles, diffusion in the particle pores and reaction with the sorbent, where also equilibrium thermodynamics plays an important role in the outcome.

Many investigations (e.g. Weinell et al., 1992; Chisholm and Rochelle, 1999; Verdone and De Filippis, 2006) were undertaken to study the kinetics and the mechanisms of the reactions between acid gases and solid sorbents. Therefore, the fundamental model was developed and validated on the basis of these literature results and then adapted to predict the acid gas removal in typical operating conditions of dry treatment processes. In particular, hydrogen chloride neutralization was considered, as its concentration is much higher than that of other acid gases in the analyzed conditions. Accordingly, the first aim of the model was the description of the HCl removal in the design conditions of the analyzed flue gas treatment system (described in Section 5.1.2), where calcium hydroxide and sodium bicarbonate are used as solid sorbents and injected upstream to fabric filters. The modeling of the system is presented in Section 6.2, while the mass transport and kinetics phenomena involved in the process are presented in the next sections. In Section 6.3, the differential mass balance equation was written for the gaseous phase flowing through a layer of porous particles, where the acid gas reacts with the solid sorbent. Section 6.4 reports the modeling of a sorbent particle reacting with HCl. The model implementation was finally verified through the comparison of the mass balances of the solid sorbent and the acid gas (described Appendix N).

6.2 Modelled system

A fundamental model was developed to simulate the acid gas removal occurring in in a dry treatment system where a solid sorbent in injected in a reactor upstream to a fabric filter, as shown in Figure 6.1.

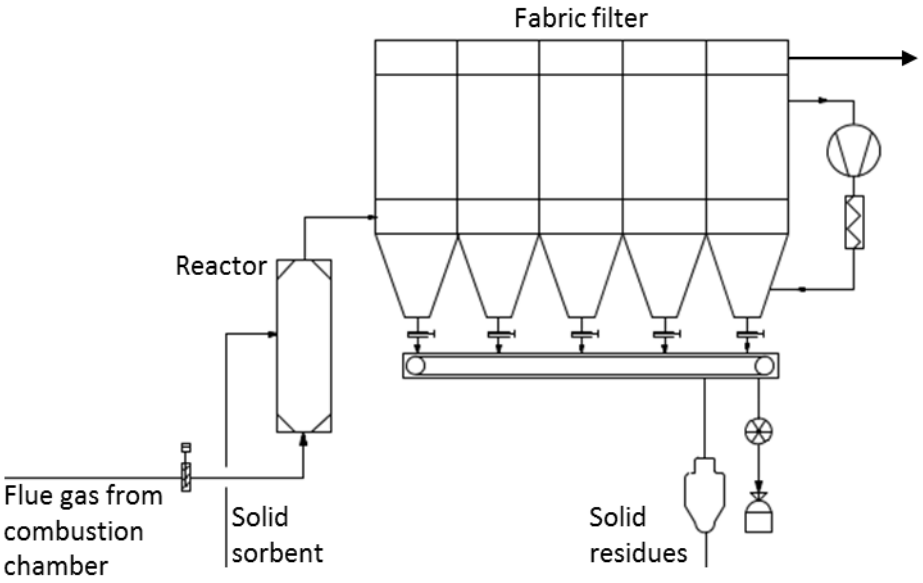

Figure 6.1 - Schematization of the system analyzed.

Acid gas removal takes place in both reactor and fabric filter. However, according to Duo et al. (1993), much of the gas-solid reaction is expected to happen in the cake of solid particles deposited on the filter bags. This assumption derives from the fact that in dry treatment systems the residence time of the sorbent particles in the filter cake is much longer than that in the entrainment duct. Thus, the acid gas removal was initially assumed to take place only in the filter cake, which was described as a fixed bed of porous particles where the gaseous phase flows and reacts with the stationary phase, as shown in Figure 6.2.

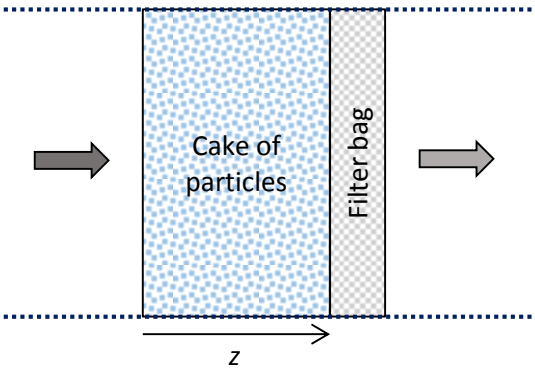

Figure 6.2 - Representation of the filter cake; *z* represents the length coordinate along the flue gas direction.

The corresponding mass balance equation was written with only two independent variables, the time *t* and the axial coordinate along the bed thickness *z*. Indeed, the properties can be assumed homogenous in the direction perpendicular to gas flow (i.e. they are constant in a given cross section). This assumption was justified by great difference between the length of a bag (which is of the order of meters) and the thickness of the cake (only of some millimeters). Therefore, border effects could be neglected. Furthermore, cross

sections can be approximated equal to each other neglecting the variation due to different radial position, because the thickness of the layer of particles is much lower than the filter bag diameter[12].

Modeling presented in Section 6.3 refers to a fixed bed with constant thickness. Indeed, even though the cake builds up continuously, the system was firstly described as a fixed boundary problem, and then extended to consider the movement of the cake boundary.

According to these assumptions, the governing differential equation for one-dimensional convection and diffusion can be written as:

$$\rho \cdot \frac{\partial \phi}{\partial t} = -\frac{d}{dx}(\rho \cdot u \cdot \phi) + \frac{d}{dx}\left(\Gamma \cdot \frac{d\phi}{dx}\right) + S \qquad 6.1$$

where

- $\rho \cdot \frac{\partial \phi}{\partial t}$ is the accumulation term
- $\frac{d}{dx}(\rho \cdot u \cdot \phi)$ is the convection term
- $\frac{d}{dx}\left(\Gamma \cdot \frac{d\phi}{dx}\right)$ is the diffusion (or axial dispersion) term
- S is the source term

The system can be considered isothermal because the neutralization reactions do not produce significant thermal effects (the amount of reactive substances is considerably lower than the total flow). Therefore, gas properties (including density) were assumed constant.

In the analyzed case, the dependent variable ϕ represents the acid gas concentration and the source term is related to the chemical reaction with the sorbent. Therefore, the description of sorbent particle structure is required in order to calculate the reaction rate in each section of the fixed bed. The diffusion of gas component in the particle porosity and sorbent consumption have to be taken into account, thus the single particle behavior was described through the grain model, which was illustrated in Section 3.3.3. The implementation of the grain model is reported in Section 6.4.

The following description of the model was written in a general form, where a single gas-solid reaction is considered. Neutralization reactions described in Section 3.2 can be represented in the general form:

$$A(g) + bB(s) \leftrightarrow pP(g) + qQ(s) \qquad 6.2$$

where *A* is the acid gas to be removed (i.e. HCl), *B* the solid sorbent (i.e. $Ca(OH)_2$ or $NaHCO_3$), and *P* and *Q* the gaseous and solid products respectively. In agreement with Duo et al. (1993), it was assumed that both the forward and reverse reactions are first order with respect to the gas concentration. Thus, the reaction rate per unit area of surface was expressed as follows:

$$r_A'' = k_s \cdot C_A - k_{-s} \cdot C_P = k_s \cdot [C_A - (k_{-s}/k_s) \cdot C_P] \qquad 6.3$$

where:

[12] In the considered fabric filters, the diameter of the bags was 130 mm, while a typical range for the cake thickness was 2-4 mm.

- k_s is the rate constant of reaction 6.2
- k_{-s} is the reverse reaction rate constant
- C_A is the concentration of the reactant gas *A* at the reaction surface
- C_P is the concentration of the product gas *P* at the reaction surface

At equilibrium, $k_s \cdot C_A = k_{-s} \cdot C_P$, thus:

$$\frac{k_{-s}}{k_s} = \frac{C_{A,eq}}{C_{P,eq}} \tag{6.4}$$

where subscripts *eq* is used to indicate the equilibrium state.

In HCl neutralization reactions (reactions 3.1 and 3.6 in Section 3.2), the gas products are H_2O and CO_2, which are present in combustion flue gases in great excess respect to HCl. In this case, it can be assumed that

$$C_P = C_{P,eq} \tag{6.5}$$

Inserting Eqs. 6.4 and 6.5 into Eq. 6.3 leads to:

$$r_A'' = k_s \cdot \left(C_A - C_{A,eq}\right) \tag{6.6}$$

The value of $C_{A,eq}$ is a function of temperature and can be calculated from the equilibrium constant. However, in the following section the temperature was assumed constant (the influence of the heat of adsorption and reaction was neglected).

6.3 Modelling of a packed bed

6.3.1 Mass balance equation

Governing equation in the filter cake

Filter cake is described as a chemical reactor of length *L* through which the fluid was flowing at a constant velocity u_0[13] mixing axially with a dispersion coefficient D_z [14]. The axial dispersion coefficient includes the contributions of the molecular diffusion and of the non-homogeneity of the flow, the latter often called *eddy diffusion* (Guiochon et al., 2006).

The general form of the partial differential mass balance equation expressed by Eq. 6.1 was adapted to describe the filter cake (represented in Figure 6.2). The mass balance with corresponding initial and boundary conditions were expressed by the following system:

$$\varepsilon \cdot \frac{\partial C}{\partial t} = -u_0 \cdot \frac{\partial C}{\partial z} + \varepsilon \cdot D_z \cdot \frac{\partial^2 C}{\partial z^2} - r_{vb} \qquad 6.7$$

$$C(z, t = 0) = 0 \qquad 6.8$$

$$C(z = 0, t) = C_0 \qquad 6.9$$

$$\left.\frac{\partial C}{\partial z}\right|_{z=L} = 0 \qquad 6.10$$

where

- C is the concentration of reactant gas[15]
- ε is the interparticle void fraction of the filter cake
- r_{vb} is the reaction rate for a unit volume of packed bed
- C_0 is the concentration of the reactant gas at the beginning of the filter cake (z = 0) [16]

The reaction term was expressed as follows:

$$r_{vb} = k_{glob} \cdot \left(C - C_{eq}\right) \qquad 6.11$$

where k_{glob} is an overall reaction rate constant (expressed in s^{-1}), which depends on the kinetics of the sorbent particles. In Section 6.4, the grain model was adopted to relate the term k_{glob} to the main kinetic parameters and to particle conversion.

[13] The gas velocity through the layer of particles could be assumed constant as the variation of acid gas concentration did not affect significantly the volumetric flow rate of the gas phase.
[14] The axial dispersion coefficient was considered constant (it did not depend on acid gas concentration because of its low concentration in the gas mixture).
[15] *C* is the concentration in the interparticle voids of the filter cake, while C_A in Section 6.2 is the concentration at the reacting surface, which depends also on transport phenomena inside the particle.
[16] C_0 can be lower than the concentration of the reactant gas entering the system (C_{in}) because of diffusion in the filter cake. The explanation of this phenomenon is reported in Appendix J.

Variable scaled in dimensionless form

The following dimensionless variables were defined:

- $x = \frac{z}{L}$
- $\tau = \frac{t}{t_c}$
- $y = \frac{C - C_{eq}}{C_{in} - C_{eq}}$

where the characteristic time t_c was taken equal to the mean time of passage:

$$t_c = \frac{L}{u_0}$$

Rewriting Eqs. 6.7 - 6.10 in dimensionless form, the following system was obtained:

$$\varepsilon \cdot \frac{\partial y}{\partial \tau} = -\frac{\partial y}{\partial x} + \frac{1}{Pe} \cdot \frac{\partial^2 y}{\partial x^2} - Da \cdot y \qquad 6.12$$

$$y(x, \tau = 0) = 0 \qquad 6.13$$

$$y(x = 0, \tau) = y_0 \qquad 6.14$$

$$\left.\frac{\partial y}{\partial x}\right|_{x=1,\tau} = 0 \qquad 6.15$$

where y_0 is the dimensionless concentration at the beginning of the filter cake:

$$y_0 = \frac{C_0 - C_{eq}}{C_{in} - C_{eq}} \qquad 6.16$$

It should be noticed that the Eq. 6.12 does not depend on the concentration of the reactant gas entering the system C_{in}. This is due to the assumption of first order reaction with respect to the reactant gas concentration.

From the dimensionless formulation, two dimensionless groups emerged. *Pe* is the axial Peclet number, defined as follows:

$$Pe = \frac{u_0 \cdot L}{\varepsilon \cdot D_z} \qquad 6.17$$

while *Da* is the Damköhler number:

$$Da = k_{glob} \cdot \frac{L}{u_0} \qquad 6.18$$

Peclet number (*Pe*) is a dimensionless group generally defined as $Pe = \frac{u \cdot x}{D_m}$, where *x* is a characteristic length, *u* the mobile phase velocity, and D_m the molecular diffusivity. The definition assumed in this document refers to a flux through a porous bed, where mobile phase velocity is expressed by the ratio of superficial velocity u_0 to the void volume fraction of the bed ε, and axial dispersion coefficient D_z is used instead of molecular diffusivity.

The *Damköhler number* (*Da*) is a dimensionless number that gives a quick assessment of the degree of conversion that can be achieved in continuous-flow reactors. Usually, when Damköhler number is less than

0.1, a conversion of less than 10 % is expected, while values of *Da* greater than 10 usually give conversions of more than 90 % (Fogler, 2006). Indeed, the Damköhler number represents the ratio of the chemical reaction rate to the mass transfer rate[17]:

$$Da = \frac{\text{reaction rate}}{\text{mass transfer rate}}$$

[17] The reaction rate depends on the reaction order. For an irreversible chemical reaction *A* → *B* of *nth* order, the reaction rate is

$$r_A = k \cdot {C_A}^n \cdot V$$

where *k* is the kinetics reaction rate constant, C_A is the concentration of the reactant *A*, and *V* is the reactor volume. When convective transport is the controlling regime, the flow rate can be expressed by the equation:

$$F_A = \dot{V} \cdot C_A$$

where $\dot{V}$ is the volumetric flow rate of the fluid at the reactor entrance. Defining the mean residence time as:

$$\tau = \frac{V}{\dot{V}}$$

the Damköhler number for a convective flow system with a first order irreversible reaction is defined as:

$$Da = k \cdot \tau$$

which corresponds to the expression derived from the dimensionless form of the mass balance equation.

6.3.2 Analysis of the initial transient

In order to verify the importance of the accumulation term of Eq. 6.12, the partial differential equation was solved in the initial stage of the process, i.e. during the initial transient. The assumption adopted for solving the mass balance was that the sorbent consumption is negligible during this interval; therefore, the value of *Da* number was constant.

The solution was obtained through the Matlab® tool *pdepe*. It permits to solve Partial Differential Equations (PDE) of the form:

$$c\left(x,\tau,y,\frac{\partial y}{\partial x}\right)\cdot\frac{\partial y}{\partial \tau}=x^{-m}\cdot\frac{\partial}{\partial x}\left(x^{m}\cdot f\left(x,\tau,y,\frac{\partial y}{\partial x}\right)\right)+s\left(x,\tau,y,\frac{\partial y}{\partial x}\right) \qquad 6.19$$

where

- $x \in [a,b]$ — *x* is the space variable, and the interval [*a*,*b*] must be finite with $a \geq 0$
- $\tau \in [\tau_0,\tau_f]$ — τ is the time variable
- $m = 0,1,2$ — *m* is a parameter corresponding to the symmetry of the problem, which can be slab (*m* = 0), cylindrical (*m* = 1), or spherical (*m* = 2).
- $c \geq 0$

The problem should have for any $x \in [a,b]$ an initial condition of the form:

$$y(x,\tau_0)=y_0(x)$$

and the boundary conditions for any $\tau \geq \tau_0$ have to be expressed as:

$$p\big(a,\tau,y(a,\tau)\big)+q(a,\tau)\cdot f\big(a,\tau,y(a,\tau),y_x(a,\tau)\big)=0$$

$$p\big(b,\tau,y(b,\tau)\big)+q(b,\tau)\cdot f\big(b,\tau,y(b,\tau),y_x(b,\tau)\big)=0$$

From the comparison of Eq. 6.19 and Eq. 6.12, solver parameters were set as follow:

- $m=0$
- $a=0$
- $b=1$
- $c=\varepsilon$
- $f=-y+\frac{1}{Pe}\cdot\frac{dy}{dx}$
- $s=-Da\cdot y$
- $y_0(x)=0$
- $p(a)=y-y_0$ [18]
- $q(a)=0$
- $p(b)=Pe\cdot y$
- $q(b)=Pe$

[18] y_0 was calculated according to the Eq. 11.13.

A typical plot of the solution of Eq. 6.12 is shown in Figure 6.3, where the concentration profile was obtained setting $\varepsilon = 0.6$, $Pe = 1$ and $Da = 1$.

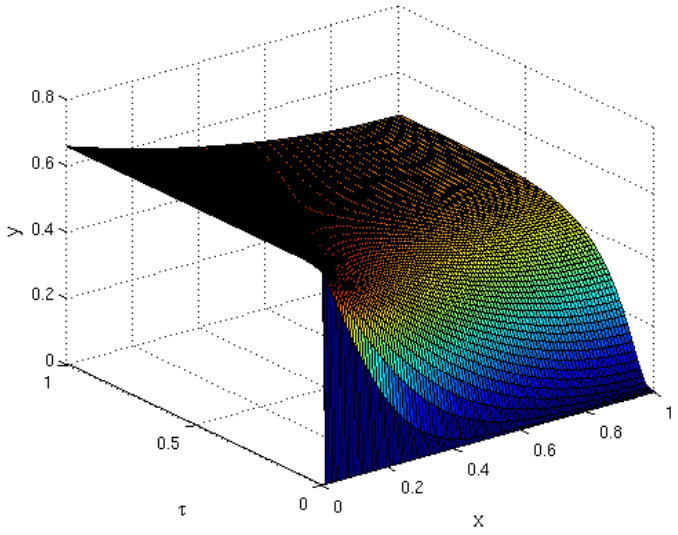

Figure 6.3 - Solution $y(\tau,x)$ of Eq. 6.12 calculated with the Matlab tool *pdepe* for $\varepsilon = 0.6$, $Pe = 1$ and $Da = 1$.

The corresponding profile of dimensionless concentration y at the exit of the system ($x = 1$), illustrated in Figure 6.4, represents the breakthrough curve for HCl removal in the packed bed. As expected, after an initial transient related to the propagation of the HCl front within the bed, the concentration increases reaching a pseudo steady state condition, which is verified until the effect of the sorbent consumption causes a decrease of the overall reaction rate and a corresponding increase of the HCl at the exit section of the bed.

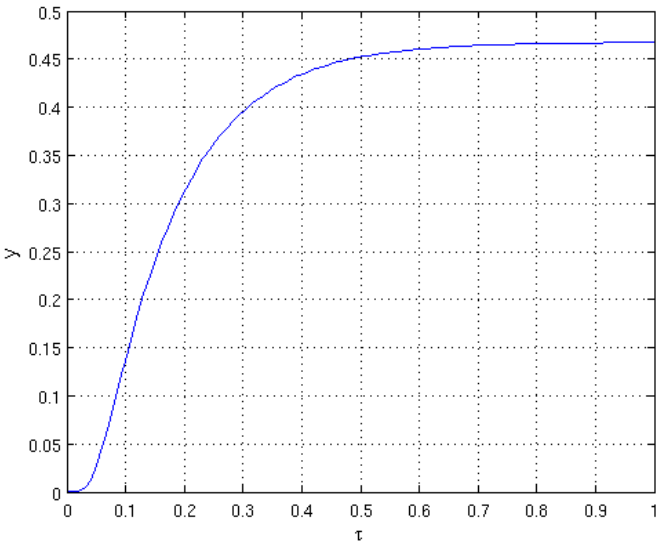

Figure 6.4 - Solution at exit section ($x = 1$) for $\varepsilon = 0.6$, $Pe = 1$ and $Da = 1$.

Discussion about the assumptions on negligible accumulation term

In Figure 6.5 the solution of the partial differential mass balance equation (Eq. 6.12) at $\tau = 1$ is plotted against the analytical solution of the steady state mass balance found in Appendix J. The comparison shows that the solution of the partial differential mass balance at $\tau = 1$ (i.e. at $t = t_c$, taken equal to the time of passage of the mobile phase) already reached a stationary condition.

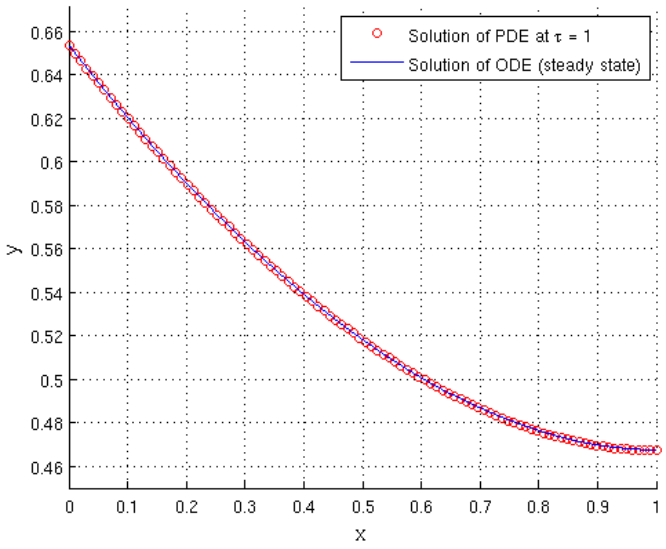

Figure 6.5 - Numerical solution of the partial differential mass balance equation at $\tau = 1$ (red circles) vs. analytical solution of the ODE representing the mass balance at steady state (blue line).

In the analyzed case, i.e. gas flowing through a fixed bed, the steady-state assumption for the gas composition is reasonable because the residence time of the gas in the layer of particles is several orders of magnitude less than the time needed to obtain a significant conversion of the particles. This means that the variation of the *Da* number, which depends on sorbent conversion (according to the grain model), is negligible in the initial transient. However, this approximation has to be validated using *Pe* and *Da* numbers calculated for the specific simulated cases and verifying that the difference between $Da(\tau=0)$ and $Da(\tau=1)$ is negligible.

However, in order to describe the entire process, where the *Da* number unevenly changes because of the concentration profile in the layer of particles, it is more suitable to use a numerical method, which permits to be more easily adapted for modeling of moving boundary problems. Furthermore, the PDE solution calculated in the present section was achieved setting the left-hand boundary condition through Eq. 11.13, i.e. $y(x=0)=y_0(Pe,Da)$. However, this equation was determined assuming that *Pe* and *Da* are uniform in the reaction section, which is not verified when the sorbent conversion becomes significant. The numerical method used to solve this problem is described in Section 6.3.3.

6.3.3 Modeling of convective-diffusive steady mass transfer

The mass balance equation given by Eq. 6.12 was solved with a numerical method which permits to define both *Pe* and *Da* numbers as a function of the axial position *x*. This requirement is due to the uneven conversion of solid sorbent caused by the concentration profile of the gaseous reactant within the layer of particles. Indeed, particles directly exposed to flue gas, where HCl concentration is higher, react faster than particle in the deeper layers, which are exposed to lower acid gas concentrations. This profile in sorbent consumption originates different values of Damköhler number (*Da*) in the bed of particles, which affects the source term of Eq. 6.12.

According to the analysis of the initial transient (Section 6.3.2), the accumulation term $\partial y/\partial t$ was neglected in the following resolution because the characteristic time t_c (defined as the time of passage of the gas through the fixed bed of particles) is much lower than the time of the entire process (which depends on solid sorbent conversion). In steady state conditions, the general governing differential equation for one-dimensional convection and axial dispersion (Eq. 6.12) can be rewritten as:

$$\frac{dy}{dx} = \frac{d}{dx}\left(\frac{1}{Pe}\cdot\frac{dy}{dx}\right) - Da\cdot y \qquad 6.20$$

$$y(x\to-\infty) = 1 \qquad 6.21$$

$$\left.\frac{dy}{dx}\right|_{x=1} = 0 \qquad 6.22$$

where

- $y = \frac{C-C_{eq}}{C_{in}-C_{eq}}$ is the remaining fraction of gaseous reactant
- $x = \frac{z}{L}$ is the dimensionless distance in the axial direction (varying between 0 and 1)
- $Pe = \frac{u_0\cdot L}{\varepsilon\cdot D_z}$ is the Peclet group
- $Da = k_{glob}\cdot\frac{L}{u_0}$ is the Damköhler group for a first-order reaction [19]
- *L* is a length term that characterizes the system, here taken for convenience as the bed length

The left-hand boundary condition was set at *x* = -∞ in order to obtain a generic model that permits to model systems where the reaction takes place also in the fore section. Further details about the boundary conditions are provided in Appendix K.

In this formulation, both *Pe* and *Da* values are functions of the axial position *x*.

The *finite-volume method* was selected to solve the present problem[20]. The application of the *control volume formulation* to model the convective-diffusive steady mass transfer over the 1-D finite domain is described in the following paragraphs.

[19] The source term (reaction rate per unit volume) is given by $Da\cdot y$.

[20] Matlab ODE tools were not used because the function *y* and its derivative are defined respectively at *x* = 0 and *x* = 1.

Control-volume discretization

The control-volume formulation (Patankar, 1980) consists in dividing the calculation domain into a number of non-overlapping control volumes, each one surrounding a grid point (as shown in Figure 6.6) and integrating the differential equation over each control volume.

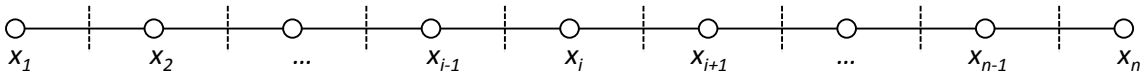

Figure 6.6 - Calculation domain along the axial direction *x*; white dots represent grid points, while dashed lines define control volumes.

The variation of the variable *y* between the grid points is expressed by piecewise profiles, which are used to evaluate the required integrals. The aim is to obtain a discretization equation containing the values of *y* for each grid point. As the discretization equation is obtained integrating the mass balance equation[21] over each control volume, it expresses the conservation principle for *y* for the finite control volume. The resulting solution would imply the integral conservation of mass over the whole calculation domain (Patankar, 1980).

Discretization equation

To derive the discretization equation, the grid-point cluster shown in Figure 6.7 is adopted. Focusing on the grid point x_i, its adjacent grid points (neighbors) are x_{i-1} and x_{i+1}. The corresponding control volume is included between *e* and *w*, which are the control volume faces between x_i and x_{i+1} and between x_{i-1} and x_i respectively. It is assumed that *e* is located midway between x_i and x_{i+1}, and *w* midway between x_{i-1} and x_i.

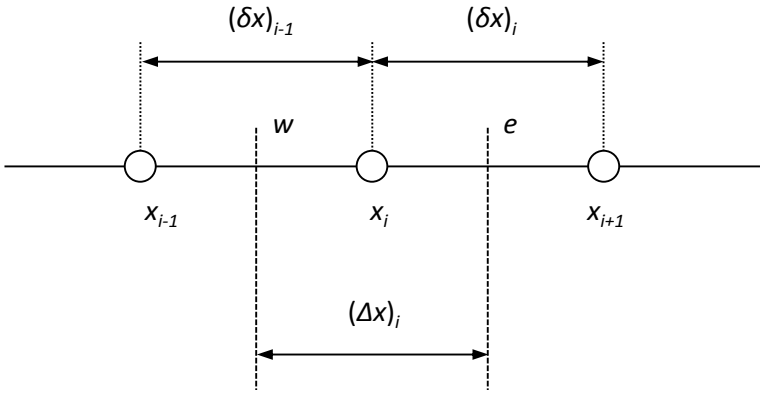

Figure 6.7 - Grid-point cluster for the one-dimension problem: $(\Delta x)_i$ represents the *x*-direction width of the control volume and δx_i is the distance between the grid points x_i and the adjacent point x_{i+1} (adapted from Patankar, 1980).

Integration of Eq. 6.20 over the control volume shown in Figure 6.7 leads to:

$$y_e - y_w = \left(\frac{1}{Pe}\cdot\frac{dy}{dx}\right)_e - \left(\frac{1}{Pe}\cdot\frac{dy}{dx}\right)_w - \int_w^e (Da\cdot y)dx \qquad 6.23$$

[21] The differential equation expresses the conservation principle for *y* for an infinitesimal control volume.

The piecewise-linear profile, shown in Figure 6.8, is the simplest profile assumption that enabled to evaluate the slope *dy*/*dx* at the control-volume faces (i.e., at *w* and *e*). Therefore, linear interpolation functions were used between the grid points.

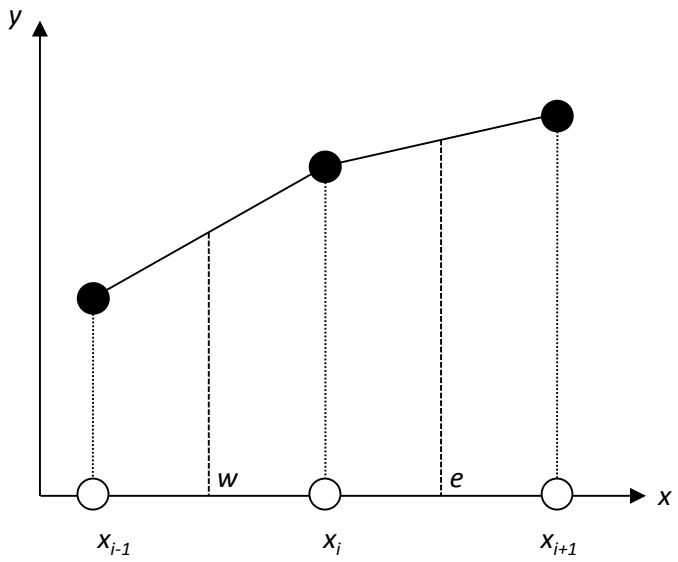

Figure 6.8 - Piecewise-linear profile assumption (adapted from Patankar, 1980).

The discretization equation is obtained calculating the values of *y* and its derivatives *dy*/*dx* from the piecewise-linear profile. The resulting equation is:

$$\frac{y_{i+1}+y_i}{2}-\frac{y_i+y_{i-1}}{2}=\left(\frac{y_{i+1}-y_i}{Pe_i\cdot(\delta x)_i}-\frac{y_i-y_{i-1}}{Pe_{i-1}\cdot(\delta x)_{i-1}}\right)-Da_i\cdot y_i\cdot \Delta x_i \qquad 6.24$$

where $Da_i \cdot y_i$ approximates the average value of the source term over the control volume and a stepwise profile for the *Pe* value was assumed[22]. According to the discretization shown in Figure 6.7, the width of the control volume along the axial direction is:

$$\Delta x_i=\frac{(\delta x)_i}{2}+\frac{(\delta x)_{i-1}}{2} \qquad 6.25$$

It is useful to cast the discretization equation 6.24 into the following form:

$$a_i\cdot y_i=a_{i+1}\cdot y_{i+1}+a_{i-1}\cdot y_{i-1}+b_i \qquad 6.26$$

where the coefficients a_i, a_{i+1}, a_{i-1}, and b_i resulted from the comparison between Eqs. 6.24 and 6.26:

[22] According to Patankar (1980), it is not necessary to use the same profile for all quantities. For example, *Da* (or *Pe*) needs not to be calculated from a linear variation of *Da* (or *Pe*) between the grid points.

$$a_{i+1} = \frac{1}{Pe_i \cdot (\delta x)_i} - \frac{1}{2} \quad 6.27$$

$$a_{i-1} = \frac{1}{Pe_{i-1} \cdot (\delta x)_{i-1}} + \frac{1}{2} \quad 6.28$$

$$a_i = a_{i+1} + a_{i-1} + Da_i \cdot \Delta x_i \quad 6.29$$

$$b_i = 0 \quad 6.30$$

It should be noticed that Eq. 6.20 was written such that the all coefficients a_{i-1}, a_i, and a_{i-1} are positive. This is related to the physical evidence that an increase in the value at one grid point should leads to an increase in the value at the neighboring grid point when other conditions do not change (Patankar, 1980).

The coefficient b_i is zero because of the assumption of first order reaction and constant value of C_{eq}. Indeed, if C_{eq} is not constant, y should be defined as $y = \frac{C}{C_{in}}$ (accordingly, $y_{eq} = \frac{C_{eq}}{C_{in}}$) and the mass balance differential equation becomes:

$$\frac{dy}{dx} = \frac{d}{dx}\left(\frac{1}{Pe} \cdot \frac{dy}{dx}\right) - Da \cdot \left(y - y_{eq}\right) \quad 6.31$$

In this case, the coefficient b_i of Eq. 6.26 would be:

$$b_i = Da_i \cdot y_{eq,i} \cdot \Delta x_i \quad 6.32$$

Boundary conditions

A discretization equation in the form of Eq. 6.24 can be written for each control volume surrounding an internal grid point x_i and solved for the respective unknown solution y_i. The two necessary boundary conditions are given by the discretization equations written for the control volumes involving grid points x_1 and x_n (shown in Figure 6.6), whose coefficients have to be determined according to Eqs. 6.21 and 6.22.

Focusing on the left-hand boundary point (x_1 in Figure 6.6), the boundary condition can be written as

$$y_1 = 1 \quad 6.33$$

The corresponding discretization equation expressed in the form of Eq. 6.26 is:

$$a_1 \cdot y_1 = a_2 \cdot y_2 + b_1 \quad 6.34$$

where the coefficients are:

$$a_1 = 1 \quad 6.35$$

$$a_2 = 0 \quad 6.36$$

$$b_1 = 1 \quad 6.37$$

On the right-hand boundary point (x_n in Figure 6.6), which is adjacent to the last internal point x_{n-1}, Eq. 6.22 gives the flux:

$$\left(\frac{dy}{dx}\right)_n = 0 \tag{6.38}$$

Integration over the half control volume $(\Delta x)_n$, represented in Figure 6.9, leads to:

$$y_n - y_w = \left(\frac{1}{Pe} \cdot \frac{dy}{dx}\right)_n - \left(\frac{1}{Pe} \cdot \frac{dy}{dx}\right)_w - \int_w^n (Da \cdot y)dx \tag{6.39}$$

Hence

$$y_n - \frac{y_{n-1} + y_n}{2} = \left(0 - \frac{y_n - y_{n-1}}{Pe_{n-1} \cdot (\delta x)_{n-1}}\right) - Da_n \cdot y_n \cdot \Delta x_n = 0 \tag{6.40}$$

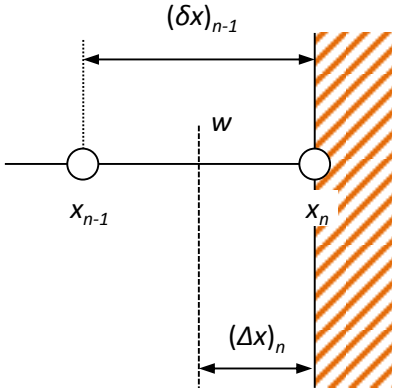

Figure 6.9 - Half control volume near the right-hand boundary (adapted from Patankar, 1980).

The discretization equation 6.40 can be written in the form of Eq. 6.26, leading to:

$$a_n \cdot y_n = a_{n-1} \cdot y_{n-1} + b_n \tag{6.41}$$

To satisfy the boundary condition (Eq. 6.38), the coefficients were defined as follows:

$$a_{n-1} = \frac{1}{Pe_{n-1} \cdot (\delta x)_{n-1}} + \frac{1}{2} \tag{6.42}$$

$$a_n = a_{n-1} + Da_n \cdot \Delta x_n \tag{6.43}$$

$$b_n = 0 \tag{6.44}$$

where Δx_n is the width of the half control volume represented in Figure 6.9:

$$\Delta x_n = \frac{(\delta x)_{n-1}}{2} \tag{6.45}$$

In the last half control volume, a stepwise profile for the source term constant *Da* was assumed. Otherwise, *Da* could be calculated from a linear variation between the grid points:

$$\int_w^n (Da \cdot y)dx \rightarrow \frac{(Da_{n-1} \cdot y_{n-1}) + 3 \cdot (Da_n \cdot y_n)}{4} \cdot \Delta x_n \tag{6.46}$$

The discretization equations were implemented in Matlab, as described in Appendix J. The software permitted to solve the system for the solutions in the n grid points of the space domain, which were expressed in the form of a vector containing the solutions $y_1 – y_n$.

6.3.4 Analysis of model results

In order to clarify how dimensionless groups affect the concentration profile and the boundary conditions, some asymptotic and intermediate regimes were simulated. This permitted to verify the stability of the numerical method in solving the considered mass balance equation. For each case, the spatial domain considered was the filter cake (i.e. reaction section, for x between 0 and 1) and the fore section ($x < 0$). Indeed, even though in the fore section there is no reaction (i.e. $Da = 0$), the concentration profile is affected by axial dispersion.

Case 1: the same value of *Pe* number in the filter cake as in the fore section

For each grid point i, the values of Da and Pe were set according to the following rules:

- if $x(i) < 0$ → $Da(i) = 0$, $Pe(i) = 1$
- if $0 \leq x(i) \leq 1$ → $Da(i) = 1$, $Pe(i) = 1$

The solution calculated through the application of the finite-volume method in fore and reaction sections is shown in Figure 6.10. The concentration profile between $x = 0$ and $x = 1$ corresponds to the analytical solution of the steady state mass balance (found in Appendix J) and with the solution of the partial differential equation at $\tau = 1$ (illustrated in Figure 6.5).

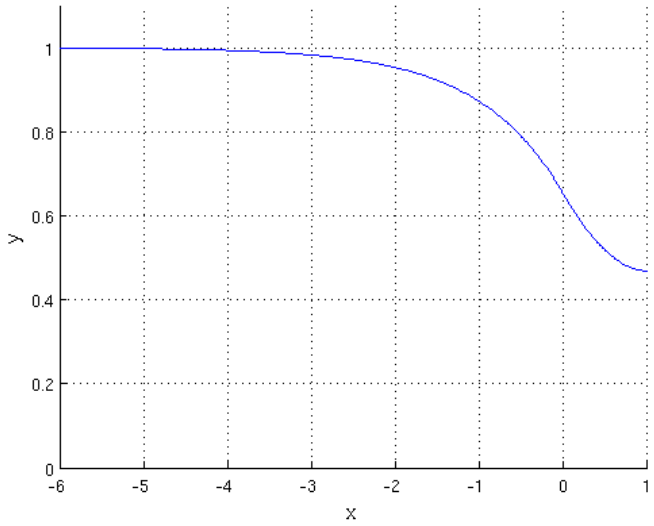

Figure 6.10 - Solution of the mass balance equation in fore section ($x < 0$, with $Da = 0$ and $Pe = 1$) and in reaction section ($0 \leq x \leq 1$, with $Da = 1$ and $Pe = 1$).

The solution was calculated setting the left-hand boundary condition at $x \rightarrow -\infty$. However, the value of the solution in $x = 0$ should correspond with the value of y_0 calculated through Eq. 11.13:

$$y_0(Da = 1, Pe = 1) = 0.653 \qquad 6.47$$

Indeed, the values computed at the two sides of the reaction section entrance were:

- $y(x=-0.001) = 0.656$
- $y(x=0.010) = 0.652$

In this case, the values of the Peclet groups in the two sections ($x < 0$ and $x \geq 0$) were set equal; thus, the slope at the entering section has to be continuous for the consideration reported in Appendix K. Indeed:

- $dy(-0.001)/dx = -0.346$
- $dy(0.010)/dx = -0.343$

It was also verified that the slope at system entrance was null:

- $dy(x=-6)/dx = -0.000$

This ensures that the spatial domain of the fore section is long enough to not be affected by the reaction zone.

Case 2: reaction section as fully stirred reactor, CSTR ($D_z \gg 1 \rightarrow Pe \ll 1$)

For each grid point i, the values of Da and Pe were set according to the following rules:

- if $x(i) < 0$ → $Da(i) = 0$, $Pe(i) = 1$
- if $0 \leq x(i) \leq 1$ → $Da(i) = 1$, $Pe(i) = 0.001$

The resulting solution is illustrated in Figure 6.11. As expected, a uniform concentration profile is obtained in the reaction section, where the mass transport is governed by axial dispersion. There is a variation of the concentration only in the fore section, where convective and diffusive mass transports have the same order of magnitude (i.e. $Pe = 1$). It should be noticed that the uniform profile in the reaction section corresponds with the solution calculated analytically in Appendix J. In this case, in the entering section of the layer of particles ($x = 0$) there is a discontinuity of the derivative of the concentration because of the variation of the Pe number in that point. A detailed discussion of this behavior is presented in Appendix K.

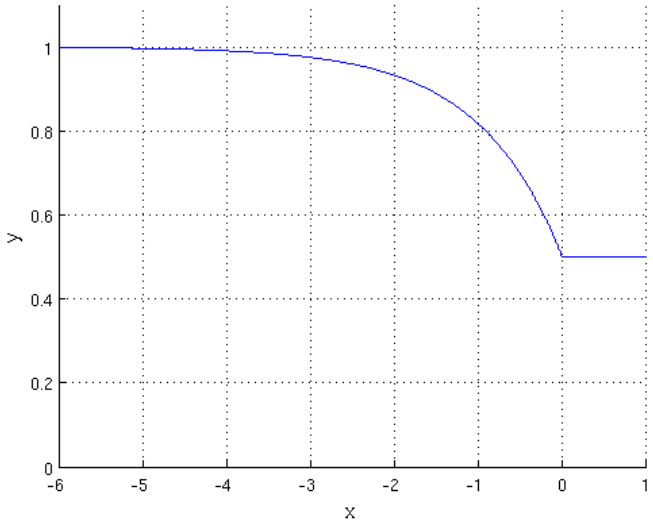

Figure 6.11 - Solution of the mass balance equation in fore section ($x < 0$, with $Da = 0$ and $Pe = 1$) and in reaction section ($0 \leq x \leq 1$, with $Da = 1$ and $Pe = 0.001$).

Case 3: reaction section as plug flow reactor (PFR) without axial dispersion (D_z=0 → *Pe*≫1)

For each grid point *i*, the values of *Da* and *Pe* were set according to the following rules:

- if $x(i) < 0$ → $Da(i) = 0$, $Pe(i) = 1$
- if $0 \leq x(i) \leq 1$ → $Da(i) = 1$, $Pe(i) = 1000$

The solution is shown in Figure 6.12. In this case, the concentration profile between $x = 0$ and $x = 1$ corresponds with the analytical solution found in Appendix J for mass transport governed by convection. As axial dispersion in negligible, there is variation of the concentration only in the reaction section, i.e. $y(x=0) \approx 1$.

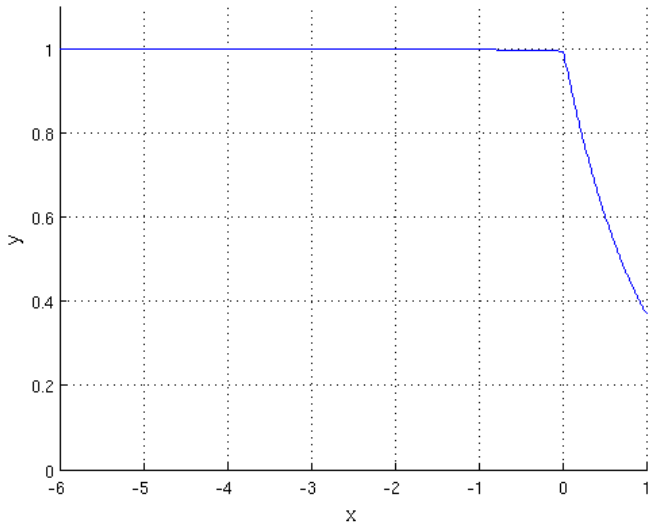

Figure 6.12 - Solution of the mass balance equation in fore section ($x < 0$, with *Da* = 0 and *Pe* = 1) and in reaction section ($0 \leq x \leq 1$, with *Da* = 1 and *Pe* = 1000).

Case 4: fore section with only convection (D_z≪1 → *Pe*≫1) and axial dispersion in the reaction section

For each grid point *i*, the values of *Da* and *Pe* were set according to the following rules:

- if $x(i) < 0$ → $Da(i) = 0$, $Pe(i) = 1000$
- if $0 \leq x(i) \leq 1$ → $Da(j) = 1$, $Pe(i) = 1$

The resulting solution is reported in Figure 6.13. According to Eq. 11.24, when *Pe* in the fore section assumes very large values, approaching the condition of zero diffusivity, the profile in $x = 0$ approaches a step function. However, the value of the solution at $x = 0$ has to be the same of *Case 1* ($y_0 = 0.653$). Indeed, according to Eq. 11.13, the value of y_0 depends only on the value of *Pe* and *Da* in the reaction section, which correspond to the values set in *Case 1*. Thus, also the concentration profile in the reaction section corresponds with the solution calculated in *Case 1*, verifying that the value of *Pe* number in the fore section affects only the concentration profile in that zone.

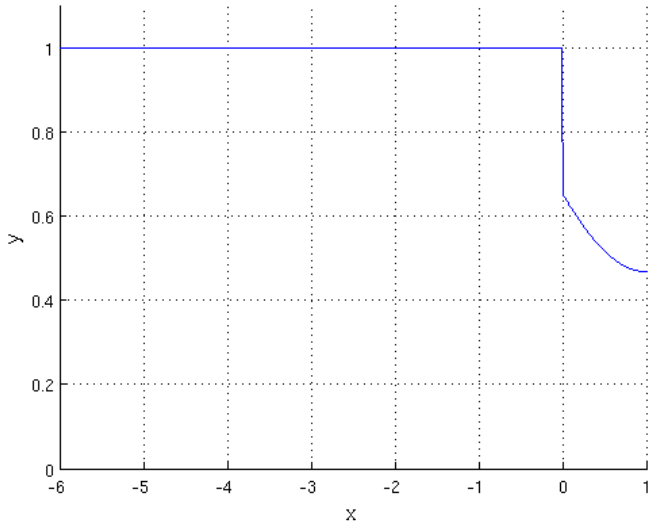

Figure 6.13 - Solution of the mass balance equation in fore section ($x < 0$, with $Da = 0$ and $Pe = 1000$) and in reaction section ($0 \leq x \leq 1$, with $Da = 1$ and $Pe = 1$).

Notes about the space domain discretization

In the initial stages of the process, the bed of particles is formed only by unreacted particles and the *Da* is uniform in the reaction section. Therefore, it is possible to calculate the analytical solution for the concentration profile (as shown in Appendix J), which can be compared with the numerical solution computed through the *finite-volume method*. This comparison, illustrated in Figure 6.14, permits to identify easily if the space domain has been discretized conveniently or if a denser mesh is required. This validation can be immediately obtained calculating the solution at the exit section ($x = 1$) through Eq. 6.20 and verifying that the same value is computed by the numerical method.

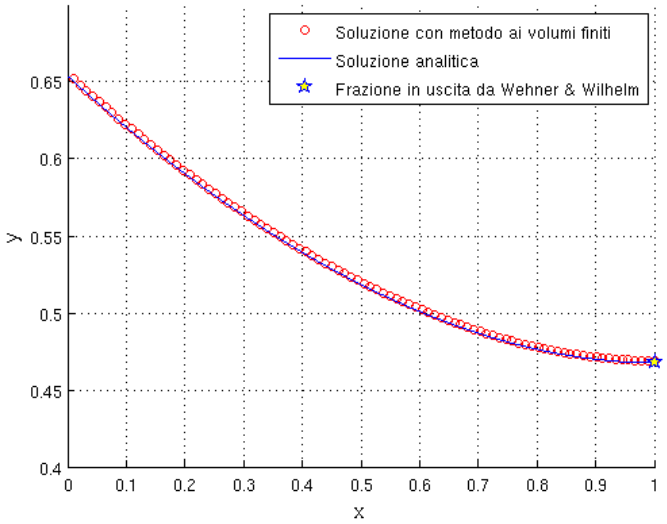

Figure 6.14 - Solutions of the differential mass balance equation calculated analytically (blue line) and through the finite-volume method (red circles); the yellow star at $x = 1$ represents the value of the concentration at the exit section calculated with Eq. 11.16.

Variation of the concentration profile with time

As previously stated, the accumulation term was neglected in the differential mass balance equation. However, the *Da* number depends on sorbent conversion, which changes during the process. Hence, concentration profile changes accordingly.

Indicating with $\bar{y}(j)$ the vector with the values of the solution in each grid point at time *j*, a model describing sorbent particle reaction is required to determine how corresponding *Da* values changes in the time interval between *j* and *j*+1. The grain model was adopted to find this correlation and its implementation and integration in the present model are discussed in Section 6.4.

6.4 Modelling of a porous particle

6.4.1 Particle description

Porous sorbent particles were described through the grain model (described by Szekely et al., 1976), sketched in Figure 6.15. Each particle is assumed to be made up of individual spherical grains, which react according to a shrinking core model (a complete description of the grain model is reported in Section 3.3.3).

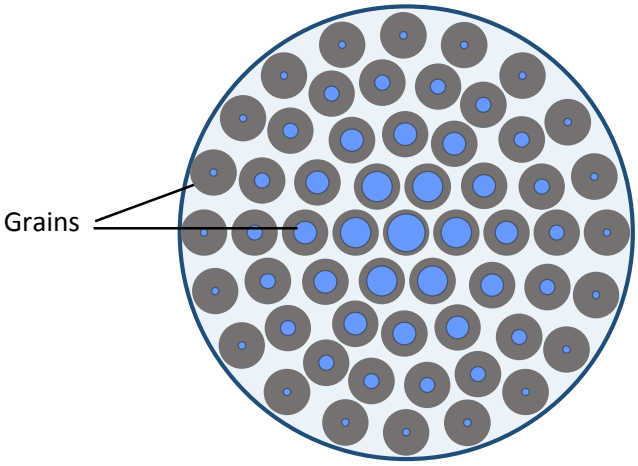

Figure 6.15 - Representation of a porous sorbent particle according to the grain model. The particle is made up of individual grains, which react by a shrinking core process. Thus, every grain is formed by a core of unreacted sorbent (in blue) and a shell of solid product (in gray).

According to this model, the acid gas flows from the bulk of the fluid phase to the external surface of the sorbent. Then, it diffuses inside the particle pores, where different types of diffusion mechanisms are involved (i.e. molecular, Knudsen and surface diffusions). Once acid gas reaches the grain surface, mass transfer is governed by solid-state diffusion through the product layer (illustrated in Figure 6.16). Finally, the reaction takes place on the unreacted core surface.

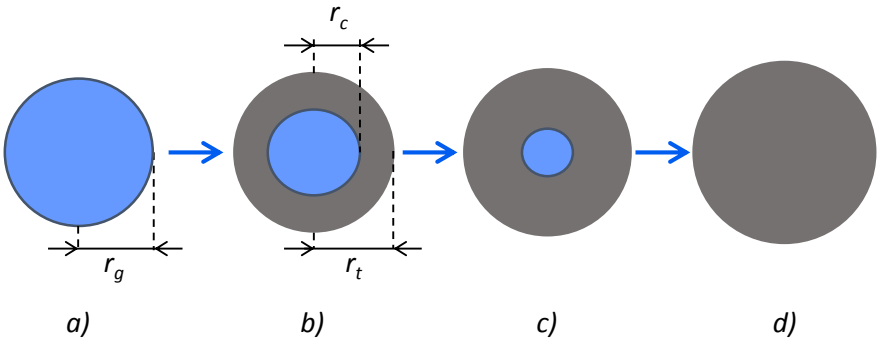

Figure 6.16 - Representation of a grain at different time step. *a*) Initially, the grain has a radius r_g and it is formed only by sorbent (in blue). *b*) and *c*) When reaction begins, a shell of solid product (in gray) is formed; the radius of the unreacted core r_c progressively decreases, while the total radius of the grain can increase or decrease according to the ratio of solid sorbent to product molar volumes. *d*) Completely converted grain.

In this schematization, three independent variables are present: the time *t*, the radial position in a particle *R*, and the radial position in a grain *r*.

Main lengths in this model are:

- R_p, the particle radius, which is constant during the process, as particles were assumed of constant size (according to the grain model presented in Section 3.3.3);
- r_g, the initial grain radius;
- r_c, the current radius of the unreacted core of a grain;
- r_t, the total radius of a grain.

The initial value of the grain radius, r_g, was calculated setting that the sum of the surface of the grains in a particle corresponds to the surface area of the particle:

$$4 \cdot \pi \cdot {r_g}^2 \cdot n_g = \frac{4}{3} \cdot \pi \cdot {R_p}^3 \cdot (1 - \varepsilon_p) \cdot \rho_s \cdot S_p \qquad 6.48$$

where

- ε_p is the initial porosity of sorbent particle;
- ρ_s is the true density of sorbent;
- S_p is the specific surface area of the particle;
- n_g is the number of grains in the particle:

$$n_g = \frac{\frac{4}{3} \cdot \pi \cdot {R_p}^3 \cdot (1 - \varepsilon_p)}{\frac{4}{3} \cdot \pi \cdot r_g^3} \qquad 6.49$$

Hence:

$$r_g = \frac{3}{\rho_s \cdot S_p} \qquad 6.50$$

The total radius of a grain can be expressed by a function of the initial grain and unreacted core radii:

$$\frac{4}{3}\pi r_t^3 = \frac{4}{3}\pi r_c^3 + \frac{4}{3}\pi\left(r_g^3 - r_c^3\right)\frac{V_{mp}}{V_{mb}} \qquad 6.51$$

where V_{mb} and V_{mp} are the molar volumes of solid sorbent and product respectively. Defining the ratio of product to sorbent molar volumes as

$$\alpha \stackrel{\text{def}}{=} \frac{V_{mp}}{V_{mb}} \qquad 6.52$$

the total radius of a grain can be expressed by:

$$r_t = \left[r_c^3 + \alpha \cdot \left(r_g^3 - r_c^3\right)\right]^{1/3} \qquad 6.53$$

Even though the particle radius R_p is constant, the porosity of the reacting particle (ε_x) changes during the process because of the difference between the solid sorbent and solid product molar volumes. The porosity ε_x can be expressed as a function of the local conversion X through the relation:

$$\varepsilon_x = \varepsilon_p + \left(1 - \varepsilon_p\right)(1 - \alpha) \cdot X \qquad 6.54$$

The local conversion of the sorbent corresponds to the conversion of a grain at that position:

$$X = 1 - \frac{r_c^3}{r_g^3} \qquad 6.55$$

It should be noticed that when the molar volume of solid product (V_{mp}) is higher than the molar volume of the sorbent (V_{mb}), i.e. $\alpha > 1$, a maximum conversion could be given by the complete filling of intraparticle voids:

$$X_{max} = \frac{\varepsilon_p}{\left(1 - \varepsilon_p\right)(\alpha - 1)} \qquad 6.56$$

However, if

$$\alpha < \frac{1}{1 - \varepsilon_p} \qquad 6.57$$

this phenomenon does not limit the process because a fraction of voids is still present when the sorbent is completely converted, i.e. $\varepsilon_x(X{=}1) > 0$.

6.4.2 Reaction rate

The variation of the unreacted core r_c (and hence of the local conversion X) can be calculated through a mass balance at the unreacted core:

$$\frac{\partial n_c}{\partial t} = r_A'' \cdot S_c \cdot b \tag{6.58}$$

where

- n_c is the number of sorbent moles contained in the unreacted core of the grain

$$n_c = \frac{4}{3} \cdot \pi \cdot r_c^3 \tag{6.59}$$

- r_A'' is the reaction rate per unit area introduced in Section 6.2

$$r_A'' = k_s \cdot \left(C_c - C_{eq}\right) \tag{6.60}$$

- S_c is the interfacial area of the unreacted core

$$S_c = 4 \cdot \pi \cdot r_c^2 \tag{6.61}$$

- b the stoichiometric coefficient of Eq. 6.2.

Substituting Eqs. 6.59 - 6.61 in Eq. 6.58, the rate of variation of the unreacted core radius can be expressed by:

$$\frac{\partial r_c}{\partial t} = -\frac{b \cdot M_s}{\rho_s} \cdot k_s \cdot \left(C_c - C_{eq}\right) \tag{6.62}$$

This equation has to be solved with the initial condition:

$$r_c(R, z, 0) = r_g \tag{6.63}$$

The gas concentration at the unreacted core surface, C_c, depends on the concentration in the interparticle voids of the filter cake, C, which is related to the axial position in the bed z and to time t through the mass balance solved in Section 6.3. However, C_c depends also on the profiles within the particle pores and within the product shell.

Concentration in particle pores is generally uniform in the gas-solid reaction considered in the present study. This fact was experimentally verified by Weinell et al. (1992), and its results are shown in Section 7.1.2. Thus, in the following section the concentration in particle pores $C_1(R,z,t)$ is assumed equal to the concentration in the interparticle voids of the filter cake:

$$C_1(R, z, t) = C(z, t) \tag{6.64}$$

However, in order to verify this assumption, the solution of the mass balance equation at a porous particle is presented Appendix M.

On the other hand, the mass balances at product shell must to be solved and incorporated in the mass balance equation at the filter cake, as shown in Section 6.4.3.

6.4.3 Mass balance equation at product shell

In order to determine the gas concentration at the surface of the unreacted core of a grain, C_c, a mass balance was written at the product shell (i.e. between $r = r_t$ and $r = r_c$). Defining C_2 as the gas concentration in the product layer, the mass balance and its initial and boundary condition are:

$$\frac{\partial C_2}{\partial t} - \frac{1}{r^2}\frac{\partial}{\partial r}\left(r^2 D_s \frac{\partial C_2}{\partial r}\right) = 0 \tag{6.65}$$

$$C_2(r, R, z, 0) = 0 \tag{6.66}$$

$$C_2(r_t, R, z, t) = C_1(R, z, t) \tag{6.67}$$

$$D_s\left(\frac{\partial C_2}{\partial r}\right)_{r=r_c} = k_s \cdot \left[C_c(R, z, t) - C_{eq}\right] \tag{6.68}$$

where

- D_s is the coefficient of solid-state diffusion through the product layer;
- C_1 is the gas concentration in the intraparticle pores.

The source term in Eq. 6.65 is null because the reaction does not occur in the product layer. However, the reaction rate appears in the system as boundary condition (Eq. 6.68).

According to Duo et al. (1993), the accumulation term of Eq. 6.65 can be neglected. The application of a pseudo steady state approximation to the differential mass balance equation with respect to the gas concentration permits to rewrite the system as:

$$\frac{1}{r^2}\frac{d}{dr}\left(r^2 D_s \frac{dC_2}{dr}\right) = 0 \tag{6.69}$$

$$C_2(r_t, R, z, t) = C_1(R, z, t) \tag{6.70}$$

$$D_s\left(\frac{dC_2}{dr}\right)_{r=r_c} = k_s \cdot \left[C_c(R, z, t) - C_{eq}\right] \tag{6.71}$$

It can be analytically solved leading to the following expression for the difference between gas concentration at the unreacted core surface and equilibrium concentration:

$$C_c - C_{eq} = \frac{D_s}{D_s + k_s \cdot r_c \cdot \left(1 - {}^{r_c}/_{r_t}\right)} \cdot \left(C_1 - C_{eq}\right) \tag{6.72}$$

This correlation permits to express the concentration at the reaction surface as a function of the concentration in the considered radius of the particle and the conversion of the grain in the same point. Indeed, both parameters D_s and k_s are constants for a given reaction.

6.4.4 Integration in the source term of the mass balance equation of the filter cake

Reaction rate per unit volume of sorbent particles

According to the grain model, the reaction takes place at the surface of the unreacted cores of the grains. Thus, the reaction rate per unit volume of the particle, at a given radial position *R*, can be written as:

$$r_{vp} = k_s \cdot \left(C_c - C_{eq}\right) \cdot {S_c}''' \tag{6.73}$$

where

- k_s is the reaction rate constant per unit area of reaction interface, introduced in Section 6.2;
- C_c is the gas concentration at the unreacted core of a grain (r_c);
- C_{eq} is the equilibrium concentration of the reactant gas (see Section 6.2);
- ${S_c}'''$ is the interfacial area of the unreacted cores of grains in a given radial position *R* per unit volume of sorbent particle[23]:

$${S_c}''' = 3 \cdot \left(1 - \varepsilon_p\right) \cdot \frac{r_c^2}{r_g^3} \tag{6.74}$$

Substitution of Eqs. 6.72 and 6.74 into Eq. 6.73 leads to:

$$r_{vp} = k_{part} \cdot \left(C_1 - C_{eq}\right) \tag{6.75}$$

where k_{part} is the overall reaction rate constant of the particle (expressed in s^{-1}), which takes into account the solid state diffusion through product layer and the reaction rate constant:

$$k_{part} = \frac{3 \cdot \left(1 - \varepsilon_p\right) \cdot r_c^2}{r_g^3} \cdot \frac{D_s \cdot k_s}{D_s + k_s \cdot r_c \cdot \left(1 - {r_c}/{r_t}\right)} \tag{6.76}$$

Reaction rate per unit volume of bed

The source term of the mass balance equation at the filter cake (r_{vb} in Eq. 6.7) can be expressed as the averaged values of the reaction rate per unit volume of sorbent particles r_{vp}, according to the following relation:

$${r_{vb}} = {n_p}''' \cdot \int_{V_p} r_{vp} \cdot dV \tag{6.77}$$

where

- V_p is the particle volume

[23] It results from the ratio of the surface area of unreacted core of a grain

$$4 \cdot \pi \cdot r_c^2$$

to the volume occupied by a grain in the particle

$$\frac{\frac{4}{3} \cdot \pi \cdot r_g^3}{1 - \varepsilon_p}$$

- n_p''' is the number of sorbent particles per unit volume of the filter cake.

Indicating with ε the interparticle void fraction of the filter cake and with F_i the inert fraction in filter cake[24], the number of sorbent particles per unit volume of the filter cake can be expressed by:

$$n_p''' = \frac{(1-\varepsilon)\cdot(1-F_i)}{V_p} = \frac{(1-\varepsilon)\cdot(1-F_i)}{\frac{4}{3}\cdot\pi\cdot R_p^3} \qquad 6.78$$

Hence, the reaction rate per unit volume of filter cake becomes:

$$r_{vb} = \frac{9\cdot(1-\varepsilon)\cdot(1-F_i)\cdot\left(1-\varepsilon_p\right)\cdot k_s}{\left(r_g\cdot R_p\right)^3}\cdot\int_0^{R_p}\left(C_c - C_{eq}\right)\cdot r_c^2\cdot R^2\cdot dR \qquad 6.79$$

If the pseudo steady-state approximation is applied to the mass balance within the product layer, C_c - C_{eq} can be expressed by Eq. 6.72, leading to:

$$r_{vb} = \frac{9\cdot(1-\varepsilon)\cdot(1-F_i)\cdot\left(1-\varepsilon_p\right)\cdot D_s\cdot k_s}{\left(r_g\cdot R_p\right)^3}\cdot\int_0^{R_p}\frac{\left(C_1 - C_{eq}\right)\cdot r_c^2\cdot R^2}{D_s + k_s\cdot r_c\cdot\left(1-{}^{r_c}/_{r_t}\right)}\cdot dR \qquad 6.80$$

When the concentration within the particle pores is uniform, i.e. $C_1(R,z,t) = C_1(z,t)$, and equal to the value in the interparticle void fraction of the filter cake (C), Eq. 6.80 can be written in the form of Eq. 6.11:

$$r_{vb} = k_{glob}\cdot\left(C - C_{eq}\right) \qquad 6.81$$

where the parameter k_{glob} is the overall reaction rate constant introduced in Section 6.3. It does not depend on gas concentration but only on kinetic parameters (i.e. k_s and D_s) and to particle conversion through the following relation:

$$k_{glob} = \frac{3\cdot(1-\varepsilon)\cdot(1-F_i)\cdot\left(1-\varepsilon_p\right)\cdot {r_c}^2}{r_g^3}\cdot\frac{D_s\cdot k_s}{D_s + k_s\cdot r_c\cdot\left(1-{}^{r_c}/_{r_t}\right)} \qquad 6.82$$

The assumption that $C_1(R,z,t) = C(z,t)$ has to be verified solving the governing equation in the particle (as shown in Appendix M), otherwise k_{glob} has to be expressed as a function of $C(z,t)$ according to Eq. 6.80 and to the mass balance equation at the particle pores.

[24] The fraction of inert material is given by fly ash, activated carbon and recycled Ca-salts, which do not participate in the HCl neutralization.

6.5 Parameters in the model

This section presents the correlations used to estimate the main model parameters reported in the previously mass balance equations (i.e. molecular diffusivity D_m, axial dispersion coefficient D_z, effective diffusivity in particle pores D_{ef}, and external mass transfer coefficient k_g). On the other hand, solid-state diffusivity D_s and reaction rate constant k_s, which are the kinetically most important parameters for gas-solid reactions at the typical conditions of dry flue-gas treatment systems (Duo et al., 1993), were estimated applying the present model to reproduce experimental data reported in literature and calculating D_s and k_s as fitting parameters. This procedure is presented in Section 7.

6.5.1 Molecular diffusivity

One of the simplest correlation to estimate the diffusivity of a generic compound *A* in *B* is the Fuller-Schettler-Giddings equation:

$$D_m = \frac{0.001 \cdot T^{1.75} \left(\frac{1}{M_A} + \frac{1}{M_B}\right)^{\frac{1}{2}}}{P\left[(\sum v_i)_A^{\frac{1}{3}} + (\sum v_i)_B^{\frac{1}{3}}\right]^2} \qquad 6.83$$

According to Green and Perry (2007), this correlation is suitable for gaseous binary mixtures of nonpolar components at low pressure[25]. These authors report the values of the correlation parameters for several compounds, which were determined by regression analysis of experimental diffusion coefficient values. Table 6.1 and Table 6.2 show respectively atomic and molecular diffusion volumes for estimating the molecular diffusivity by means of Eq. 6.83.

Table 6.1 - Atomic diffusion-volume increments of some common elements present in flue gases (extracted from Green and Perry, 2007).

Atom	v_i cm^3/mol
C	16.5
H	1.98
O	5.48
N	5.69
Cl	19.5
S	17

[25] In these conditions, the magnitude of D_m is approximately of 10^{-5} m^2/s.

Table 6.2 - Diffusion volumes for some simple compounds contained in flue gases (extracted from Green and Perry, 2007).

Molecule	Σv_i cm³/mol
N_2	17.9
O_2	16.6
Air	20.1
CO	18.9
CO_2	26.9
H_2O	12.7
Cl_2	37.7
SO_2	41.1

6.5.2 Axial dispersion in a packed bed

In the analyzed cases (see Section 5.1), the Reynolds number is usually lower than one. In this condition, according to Harker et al. (2002), longitudinal dispersion (i.e. the term $D_z \cdot \frac{\partial^2 C}{\partial z^2}$ in Eq. 6.7) may become important and the axial dispersion coefficient D_z has to be estimated.

Harker et al. (2002) present the results obtained by a number of workers, which show that for gases, at low Reynolds numbers (<1), the Peclet number increases linearly with Reynolds number:

$$Pe_p = K \cdot Re_p \tag{6.84}$$

where

- Pe_p is the Peclet number based on the superficial velocity through the bed u_0[26], the particle diameter d_p and the interparticle void fraction of the particles bed ε:

$$Pe_p = \frac{u_0 \cdot d_p}{\varepsilon \cdot D_z} \tag{6.85}$$

- Re_p is the corresponding Reynolds number:

$$Re_p = \frac{d_P \cdot u_0 \cdot \rho}{\mu} \tag{6.86}$$

Eq. 6.84 can be rewritten as:

$$\frac{u_0 \cdot d_p}{\varepsilon \cdot D_z} = \frac{K}{Sc} \cdot \frac{d_P \cdot u_0}{D_m} \tag{6.87}$$

where Sc is the Schmidt number

$$Sc = \frac{\mu}{\rho \cdot D_m} \tag{6.88}$$

Since Sc is approximately constant for gases and the void fraction of a randomly packed bed is usually about 0.4, the correlation between the axial dispersion coefficient and molecular diffusivity becomes:

[26] u_0 is the average fluid velocity based on cross-sectional area A of empty column.

$$\frac{D_z}{D_m} = 0.7 \tag{6.89}$$

where the factor 0.7 is related to the tortuous path that the gas must negotiate because of the presence of the particles in the fixed bed. This result confirms that at low Reynolds numbers, molecular diffusion predominates, according to Harker et al. (2002).

The values of D_z may be calculated also from published correlations of Peclet number. For gases, Harker et al. (2002) proposed the Edwards and Richardson correlation:

$$\frac{1}{Pe_p} = \frac{0.73 \cdot \varepsilon}{Re_p \cdot Sc} + \frac{1}{2 \cdot \left(1 + \frac{9.5 \cdot \varepsilon}{Re_p \cdot Sc}\right)} \tag{6.90}$$

In the considered cases *Re* < 1, so the second term on the right-hand side is negligible and the equation becomes:

$$\frac{1}{Pe_p} = \frac{0.73 \cdot \varepsilon}{Re_p \cdot Sc} \tag{6.91}$$

Substitution of Eqs. 6.85, 6.86 and 6.88 into Eq. 6.91 leads to:

$$\frac{D_z}{D_m} = 0.73 \tag{6.92}$$

in agreement with Eq. 6.89.

6.5.3 External mass transfer

The external mass transfer coefficient k_g can be estimated by means of correlations based on dimensionless groups for mass transfer in fixed beds. For these cases, Green and Perry (2007) proposed the use of the Ranz and Marshall correlation:

$$Sh = 2.0 + 0.6 \cdot Sc^{1/3} \cdot {Re_p}^{1/2} \tag{6.93}$$

where *Sh* is the Sherwood number

$$Sh = \frac{k_g \cdot d_p}{D_m} \tag{6.94}$$

However, the same authors state that the correlation, when applied to packed beds, has a low prediction compared to experimental data, and at low Re_p the limit of 2.0 is too high. Moreover, the correlation is not corrected for axial dispersion.

Other correlations assume that axial dispersion in the bed has been allowed, e.g. Wakao and Funazkri correlation:

$$Sh = 2.0 + 1.1 \cdot Sc^{1/3} \cdot {Re_p}^{0.6} \tag{6.95}$$

However, according to Harker et al. (2002), its applicability is limited to the range $3 < Re < 10^4$ (indeed, at lower *Re* number, *Sh* tends to 2, showing the same limitation as Ranz and Marshall correlation).

6.5.4 Diffusion within particle pores

The diffusive term of the mass balance equation at the particle pores (Appendix M) is governed by the effective diffusion coefficient D_{ef}. It depends on particle tortuosity τ_p, on reacting particle porosity ε_x, and on the superimposition of different types of diffusion mechanisms: molecular, Knudsen and surface diffusions. According to Duo et al. (1993), main contribution is given by molecular diffusion D_m and Knudsen diffusion D_k:

$$D_{ef} = \frac{\varepsilon_x}{\tau_p}\left(\frac{1}{D_m} + \frac{1}{D_k}\right)^{-1} \tag{6.96}$$

D_m can be estimated by means of Eq. 6.83, while for the Knudsen diffusion the dusty gas model can be adopted to express the coefficient D_k as a function of the sorbent particle properties:

$$D_k = \frac{4}{3} \cdot \left(\frac{8 \cdot R_{gas} \cdot T}{\pi \cdot M_A}\right)^{1/2} \cdot K_0 \tag{6.97}$$

where

$$K_0 = \left[\frac{128}{9} \cdot {n_g}''' \cdot {r_t}^2 \cdot \left(1 + \frac{\pi}{8}\right)\right]^{-1} \tag{6.98}$$

The parameter ${n_g}'''$ represents the number of grain per unit volume of particle:

$${n_g}''' = \frac{1 - \varepsilon_p}{\frac{4}{3} \cdot \pi \cdot r_g^3} \tag{6.99}$$

Eqs. 6.96- 6.99 permit to relate the effective diffusion coefficient to the local sorbent conversion. Therefore, if the concentration is not uniform within the particle, also D_{ef} is a function of the radial position within the particle.

7 Validation of the fundamental model

7.1 Description of HCl removal with $Ca(OH)_2$

7.1.1 Literature data

The fundamental model was implemented and tuned to reproduce literature data in order to validate its capability of describing HCl removal in a fixed bed of calcium hydroxide particles. In this validation, reaction rate constant k_s and solid-state diffusivity D_s were treated as fitting parameters, while other model parameters were calculated applying the correlations reported in Section 6.5 to the modelled experimental conditions.

Weinell et al. (1992) investigated HCl binding with Ca-based sorbents in a wide range of temperatures (60 – 1000 °C) using a quartz glass reactor where the solid reagent was placed on a porous support. The reaction section was described as a fixed bed, as illustrated in Figure 7.1. In this schematization, the radial variation of the properties was neglected, so the mass balance equation at the fixed bed depends only on time and on the axial coordinate along the bed thickness. Under this assumption, the fundamental model described in Section 6 can be applied to describe the neutralization process that took place in the experimental runs.

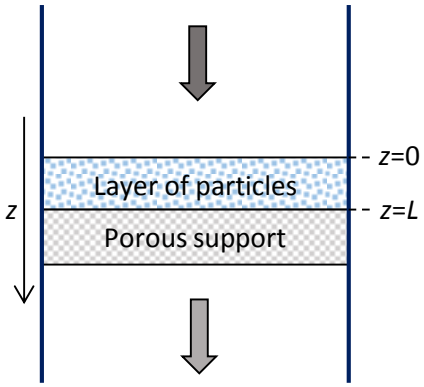

Figure 7.1 - Schematization of the reactor used by Weinell et al. (1992). Solid sorbent particles are placed on a porous support and the gas flows through the stationary phase. Axial coordinate along the bed thickness is indicated with z, where z = 0 is the entrance section of the fixed bed and L is the thickness of the layer of particles.

Weinell et al. (1992) carried out runs in several experimental conditions and with different sorbents. The curves representing HCl removal by calcium hydroxide particles obtained by the authors at three different temperatures (100, 140, and 200 °C) are reported in Figure 7.2.

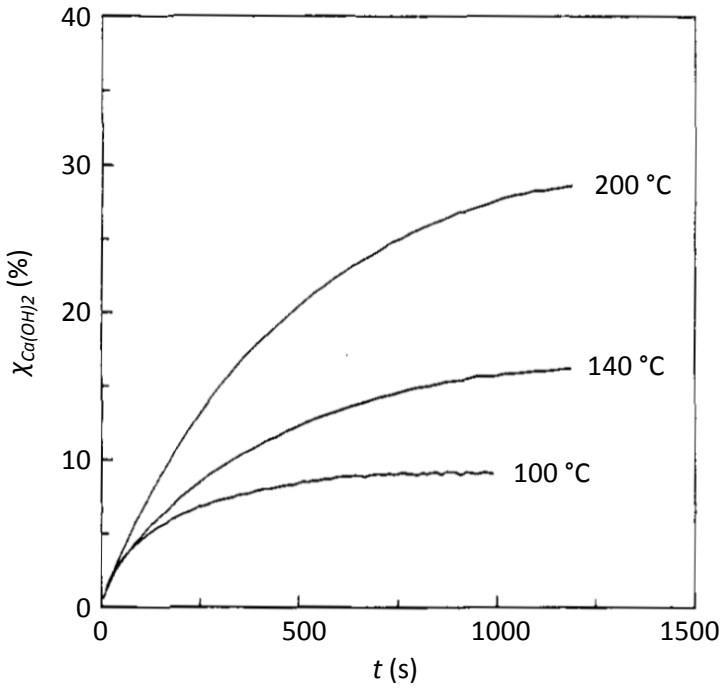

Figure 7.2 - Sorbent conversion vs. time obtained by Weinell et al. (1992) with runs at different temperatures.

The model was applied to describe the HCl removal with calcium hydroxide in the conditions reported in Table 7.1, which were the most similar to the operating conditions of the analyzed treatment system.

Table 7.1 – Experimental conditions data provided by Weinell et al., 1992.

T	200	°C	temperature
P	101325	Pa	pressure
Q_{25}	$1 \cdot 10^{-3}/60$	m^3/s	volumetric flow rate at 25°C
C_{in}	1000	ppm	inlet HCl concentration
y_{H2O}	0	-	fraction of water vapor
m_{bed}	$25 \cdot 10^{-6}$	kg	mass of the bed of particles

The inlet concentration of HCl in the reactant gas corresponds to

$$C_{in} = 1000 \cdot 10^{-6} \cdot \frac{P_{NC} \cdot M_{HCl}}{R \cdot T_{NC}} = 1.627 \cdot 10^{-3} \ \frac{kg}{Nm^3} = 1627 \ \frac{mg}{Nm^3}$$

and to

$$C_{in} = 1000 \cdot 10^{-6} \cdot \frac{P}{R \cdot T} = 2.58 \cdot 10^{-2} \frac{mol}{m^3}$$

In these conditions, the neutralization of HCl with calcium hydroxide, written in the form of Eq. 6.2, is:

$$HCl + \frac{1}{2}\,Ca(OH)_2 \rightarrow \frac{1}{2}\,(CaCl_2 \cdot 2H_2O) \qquad 7.1$$

Calcium chloride dihydrate was considered as the solid product, as reported by Weinell et al. (1992) and confirmed by other authors (e.g. Duo et al., 1995; Fonseca et al., 1998).

The corresponding properties of both gaseous and solid compounds are reported in Table 7.2.

Table 7.2 – Properties of reagents and products in the simulated conditions[27].

α	2.4	-	ratio of solid product to sorbent molar volumes
b	0.5	-	stoichiometric coefficient of sorbent (Eq. 7.1)
M_{HCl}	$36.5 \cdot 10^{-3}$	kg/mol	molar mass of HCl
M_{N2}	$28.0 \cdot 10^{-3}$	kg/mol	molar mass of N_2
M_p	$147.0 \cdot 10^{-3}$	kg/mol	molar mass of product ($CaCl_2 \cdot 2H_2O$)
M_s	$74.1 \cdot 10^{-3}$	kg/mol	molar mass of sorbent
μ_{gas}	$2.42 \cdot 10^{-5}$	Pa·s	gas viscosity
ρ_{gas}	0.734	kg/m^3	gas density
ρ_p	1835	kg/m^3	true density of product ($CaCl_2 \cdot 2H_2O$)
ρ_s	2240	kg/m^3	true density of sorbent

With regard to the solid sorbent, the authors tested different kind of commercially available particles of calcium hydroxide. However, the fundamental model was applied to describe only the experiments subsequently modelled by Duo et al. (1993). This choice was related to the fact that Duo et al. (1993) provided additional data about solid particles (listed in Table 7.3) that were not given in the original work of Weinell et al. (1992).

Table 7.3 – Sorbent properties provided by Duo et al. (1993).

S_{BET}	$1.97 \cdot 10^4$	m^2/kg	BET surface area
R_p	$1.23 \cdot 10^{-6}$	m	mean particle radius
ε	0.6	-	interparticle void fraction of the particle bed
ε_p	0.519	-	initial porosity of sorbent particles
τ_p	3.0	-	particle tortuosity

According to the particle description given by the grain model (Section 6.4), the initial radius of the grains that form a sorbent particle, is:

$$r_g = \frac{3}{\rho_s \cdot S_{BET}} = 6.8 \cdot 10^{-8}\ m$$

In the experiments performed by Weinell et al. (1992), sorbent particles were placed on a porous support in an even, thin layer. This method permitted to reduce the pressure drop of the gas flowing through the bed of particles and to consider the gas in the reaction section ideally mixed due to the effect of axial dispersion.

[27] Viscosity and density of the gaseous mixture were calculated by means of the simulation software Aspen Hysys taking into account the actual composition of the gas phase.

Indeed, the authors carried out the experimental runs in conditions such that the axial Peclet number was:

$$Pe_W = \frac{u \cdot L}{D_m} \cong 0.2 \qquad 7.2$$

where L is the thickness of the particle bed, u is the linear gas velocity, and D_m is the molecular diffusivity of HCl in air[28]. As the mean particle diameter was in the range of 2-5 µm, the corresponding Reynold number was much less than 1. In these conditions ($Re_p < 1$), according to the correlations for dispersion in fixed beds reported in Section 6.5.2, the axial dispersion is governed by molecular diffusion.

Molecular diffusivity of HCl in N_2 was estimated through the correlation proposed by Fuller-Schettler-Giddings:

$$D_m = \frac{0.001 \cdot T^{1.75} \left(\frac{1}{M_{HCl}} + \frac{1}{M_{N2}}\right)^{\frac{1}{2}}}{P\left[(\sum v_i)_{HCl}^{\frac{1}{3}} + (\sum v_i)_{N2}^{\frac{1}{3}}\right]^2} \qquad 7.3$$

Molecular diffusion volume of hydrogen chloride, $(\sum v_i)_{HCl}$, was calculated with the data provided in Table 6.1, while $(\sum v_i)_{N2}$ is given in Table 6.2. Thus, for a gas mixture of HCl in N_2 at 200 °C and 101.3 kPa, previous correlation gives:

$$D_m = 4.14 \cdot 10^{-05} \ \frac{m^2}{s}$$

To take into account the tortuous path that the gas must negotiate between the particles, the axial dispersion coefficient was estimated according to Eq. 6.89:

$$D_z = 0.7 \cdot D_m = 2.90 \cdot 10^{-05} \ \frac{m^2}{s}$$

The thickness of the fixed bed of sorbent L and the gas superficial velocity u_0 were not explicitly provided by Weinell et al. (1992). Thus, they were calculated from the values of Peclet number and the volume of the solid sorbent bed:

$$\begin{cases} Pe_W = \dfrac{u_0 \cdot L}{\varepsilon \cdot D_m} \\ V_{bed} = L \cdot \dfrac{Q}{u_0} \end{cases} \qquad 7.4$$

where

- $Pe_W = 0.2$ is the Peclet number (with D_m)
- $Q = Q_{25} \cdot \frac{T}{273.15+25} = 2.64 \cdot 10^{-5} \ m^3/s$ is the volumetric flow rate of the gas (at 200 °C)
- $\rho_{bed} = \rho_s \cdot (1 - \varepsilon_p) \cdot (1 - \varepsilon) = 431 \ kg/m^3$ is the bulk density of the layer of particles
- $V_{bed} = \frac{m_{bed}}{\rho_{bed}} = 5.80 \cdot 10^{-8} \ m^3$ is the volume of the layer of particles

[28] Weinell et al. (1992) defined the Peclet number using molecular diffusivity instead of axial dispersion coefficient. For disambiguation with the definition provided in previous sections, the dimensionless group defined by Weinell et al. (1992) is indicated with Pe_W.

Thus, the system expressed by Eq. 7.4 was solved for u_0 and L:

$$L = \sqrt{\frac{Pe_W \cdot \varepsilon \cdot D_m \cdot V_{bed}}{Q}} = 1.04 \cdot 10^{-4}\ m$$

$$u_0 = \sqrt{\frac{Pe_W \cdot \varepsilon \cdot D_m \cdot Q}{V_{bed}}} = 4.76 \cdot 10^{-2}\ \frac{m}{s}$$

The calculated superficial velocity is in agreement with the value provided by Duo et al. (1993), which reported a value of $5 \cdot 10^{-2}$ m/s at 500 K, corresponding to $4.73 \cdot 10^{-2}$ m/s at 473 K. The little difference could be due to the uncertainty about the Pe_W. However, the result confirms the right approach used to estimate the bed thickness.

Accordingly, the Reynolds number referred to a particle, for a mean particle radius R_p of 1.23 µm, results:

$$Re_p = \frac{\rho_{gas} \cdot u_0 \cdot d_p}{\mu_{gas}} = 3.55 \cdot 10^{-3}$$

As stated in Section 6, some mass transfer phenomena are usually negligible in the description acid gas removal in typical conditions of dry treatment systems. Therefore, mass transfer resistance in particle porosity and the accumulation term in mass balance equation at the fixed bed were evaluated in the analyzed experimental conditions and the results are shown in the following sections.

7.1.2 Concentration profile within the particle

Weinell et al. (1992) studied the radial distribution of chloride in a reacted particle by means of Energy-Dispersive X-Ray (EDAX) analysis. The result, illustrated in Figure 7.3, shows that a uniform distribution of chlorine was found along the radial coordinate of a reacted particle.

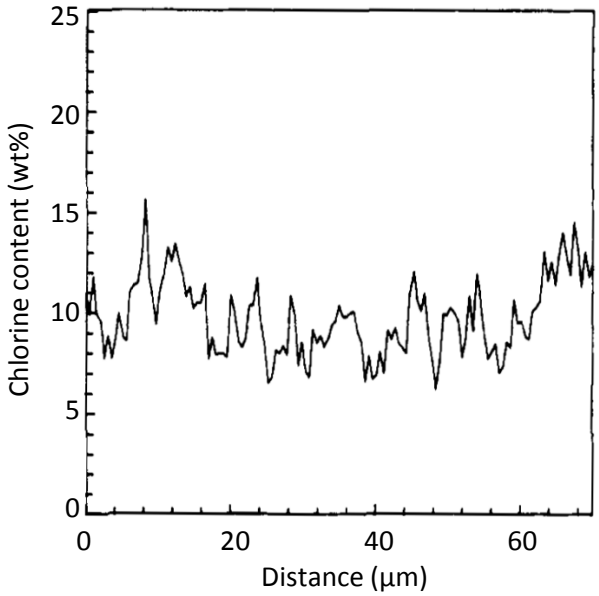

Figure 7.3 – Chloride ion distribution along a fracture surface of a reacted particle of calcium hydroxide measured by means of an Energy-Dispersive X-ray (EDAX) analysis by Weinell et al., 1992.

This experimental evidence suggests that an even profile for HCl within the pores is present during the process. However, in order to verify this assumption, the governing equation of mass transport within particle pores was solved for the initial stages of the process, according to the general resolution presented in Appendix M. The parameters concerning the mass transport and reaction kinetics within the sorbent particle considered in the simulations are listed in Table 7.4.

Table 7.4 – Parameters used in the calculation of the concentration profile within particle porosity.

ε_p	0.519	-	initial particle porosity
τ_p	3.0	-	particle tortuosity
D_k	$3.40 \cdot 10^{-5}$	m^2/s	Knudsen diffusion coefficient
D_m	$4.14 \cdot 10^{-5}$	m^2/s	molecular diffusion coefficient of HCl in N_2
r_g	$6.8 \cdot 10^{-8}$	m	initial grain radius
k_s	$4.75 \cdot 10^{-4}$	m/s	reaction rate constant
R_p	$1.23 \cdot 10^{-6}$	m	mean particle radius

The effective diffusion coefficient within particle pores at the beginning of the process, $D_{ef,0}$, was estimated taking into account molecular diffusion (calculated in Section 7.1.1) and Knudsen diffusion coefficient, which was calculated according to Eq. 6.97. Hence:

$$D_{ef,0} = \frac{\varepsilon_p}{\tau_p}\left(\frac{1}{D_m} + \frac{1}{D_k}\right)^{-1} = 3.23 \cdot 10^{-6}\ \frac{m^2}{s}$$

The overall reaction rate constant of the particle, given by Eq. 6.76, when grains are formed only by sorbent (i.e. r_c=r_g) results:

$$k_{part,0} = \frac{3 \cdot (1 - \varepsilon_p) \cdot k_s}{r_g} = 1.0 \cdot 10^4 \; s^{-1}$$

where the reaction rate constant was set equal to the value proposed by Duo et al. (1993) in similar conditions (i.e. 500 K):

$$k_s = 4.75 \cdot 10^{-4} \; \frac{m}{s}$$

The dimensionless groups required to solve the mass balance equation at the particle pores are Thiele and Biot numbers. According to the definition given in Appendix M, their values at the beginning of the process were:

$$Th_{p,0} = R_p \cdot \sqrt{\frac{k_{part,0}}{D_{ef,0}}} = 0.0684$$

$$Bi_0 = \frac{k_g \cdot R_p}{D_{ef,0}} = 13.0$$

where the mass transfer coefficient in the boundary film (k_g) was estimated through the Ranz and Marshall correlation (reported in Section 6.5.3). Hence, the partial differential equation can be solved for the HCl fraction within the particle porosity y_1, which was defined as:

$$y_1 = \frac{C_1 - C_{eq}}{C - C_{eq}}$$

where C_1 is the concentration within particle pores and C is the concentration in the interparticle voids of the filter cake. The resulting solution at τ_1 = 1 is shown in Figure 7.4, which clearly evidences that mass transfer resistance within the pores is negligible in the first stages of the process[29]. Indeed, at τ_1 = 1 the difference between the concentration at the particle center and at its surface is lower than 0.1 %.

[29] The mass balance equation was solved assuming that Th_p, Bi and ε_x values were constant during the transient between τ_1 = 0 and τ_1 = 1. This assumption was justified by the very low characteristic time of the process:

$$t_{c,part} = \left(k_{part}\right)^{-1} = 1.0 \cdot 10^{-04} \; s$$

Thus, the variation of the unreacted core radius r_c during this interval was negligible (< 10^{-5} %) and hence also other parameters could be considered constant.

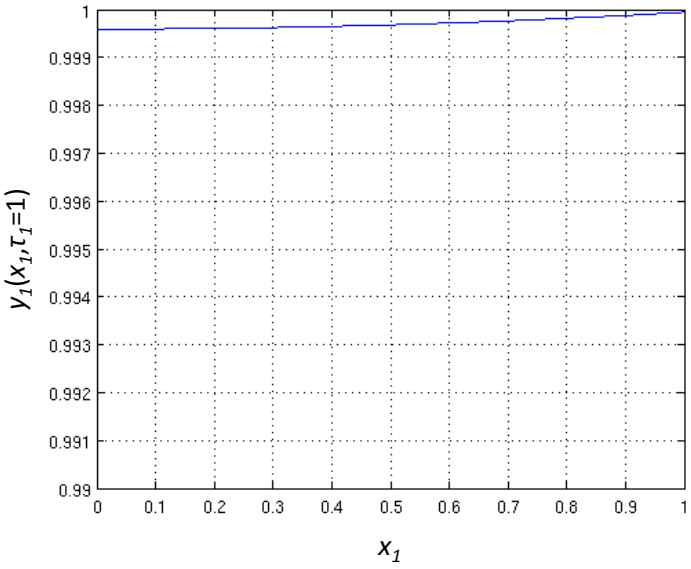

Figure 7.4 - Profile of the HCl fraction (y_1) within the calcium hydroxide particle at τ_1 = 1 as a function of dimensionless radial position (x_1).

This profile is in agreement with experimental results shown in Figure 7.3. Accordingly, the mass balance equation at the particle pores was substituted in the fundamental model by the equality

$$C_1(R,z,t) = C(z,t) \qquad 7.5$$

Therefore, in the solution of the mass balance equation at the fixed bed, the HCl concentration within particle pores was assumed uniform and equal to the value in the interparticle voids.

7.1.3 Initial transient analysis

As shown in Figure 7.2, the time required to obtain a significant conversion of the sorbent in the experimental conditions tested by Weinell et al. (1992) is much longer than the characteristic time of the governing equation in the sorbent bed (Eq. 6.7), which was defined as the residence time of the gas in the particle bed:

$$t_c = \frac{L}{u_0} = 2.19 \cdot 10^{-3}\ s$$

Therefore, the accumulation term $\frac{\partial C}{\partial t}$ of the mass balance equation should be negligible, permitting the resolution of the system as a sequence of pseudo steady states (i.e. the dependence on time is given only by the decrease of the overall reaction rate due to the sorbent consumption).

In order to verify if the system reached a steady state at $\tau = 1$ (i.e. at $t = t_c$), the partial differential equation was solved for the initial transient taking into account the accumulation term and assuming constant properties in the bed[30]. The values of reaction rate constant k_s and solid-state diffusivity D_s were set equal to the values reported by Duo et al. (1993) at 500 K[31], which were:

$$k_s(T = 500\ K) = 4.75 \cdot 10^{-4}\ \frac{m}{s}$$

$$D_s(T = 500\ K) = 2.05 \cdot 10^{-13}\ \frac{m^2}{s}$$

The PDE has been solved as described in Section 6.3.2. The resulting profile of the HCl fraction in the bed, expressed through the variable $y = (C - C_{eq})/(C_{in} - C_{eq})$, is shown in Figure 7.5.

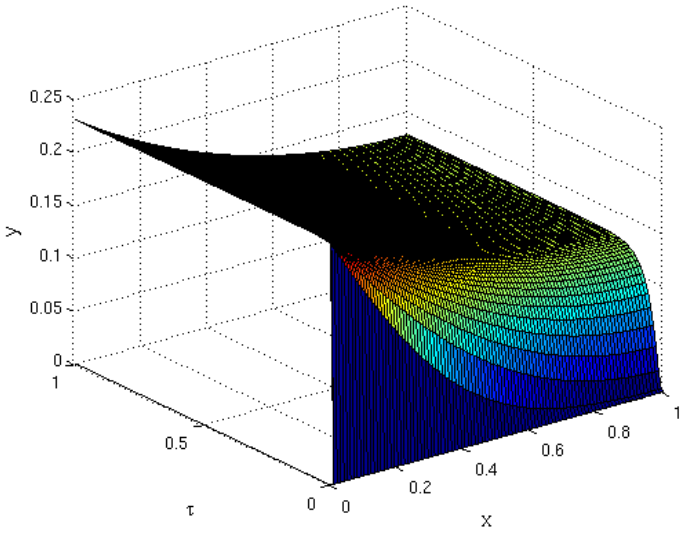

Figure 7.5 – HCl fraction $y(\tau,x)$ in the bed of particles during the initial transient ($\tau \in 0 \div 1$) as a function of τ and axial coordinate x (x=0 represents the entrance section of the fixed bed and x=1 the exit section).

[30] Even though the characteristic time of this process is longer than the characteristic time referred to the mass transfer within a particle, the variation of r_c in the time interval between the beginning of the process and t_c is negligible (< 10^{-4} %). However, the *Da* value is very sensitive to r_c variation, especially in the first stages of the process, when the controlling resistance changes from chemical kinetics to solid state diffusion through the product layer. Despite that, even assuming the maximum value of k_{glob}, the variation of *Da* value is lower than 0.1 %.

[31] The corresponding value of the superficial velocity $u_0 = 5.0 \cdot 10^{-2}$ m/s

This profile confirmed that the initial transient was concluded at $\tau = 1$ even at the exit section of the fixed bed, as evidenced by Figure 7.6. Thus, the pseudo steady state assumption was adopted in the following simulations.

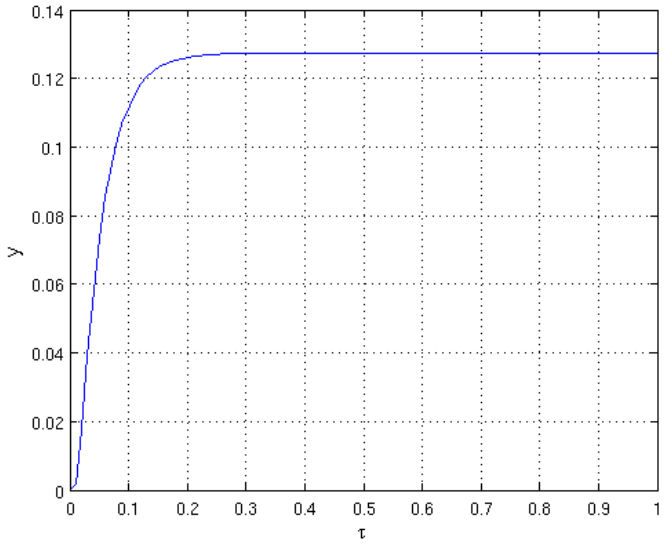

Figure 7.6 – Profile of the HCl fraction at the exit section of the fixed bed ($x = 1$) as a function of the dimensionless time τ.

7.1.4 Verification of the model implementation

In the present section, the implementation of the model according to the control volume formulation was verified through the comparison with the analytical solution (when available) and by means of the comparison of the overall conversion of HCl and $Ca(OH)_2$ during the entire process.

The first step regarded the analysis of the grid chosen to describe the spatial domain. Indeed, to avoid heavy calculations, a non-uniform grid was created, which was denser near the entrance section of the reaction section (i.e. at $x = 0$). The solution of the mass balance equation at the fixed bed is illustrated in Figure 7.7 for the initial condition (which corresponds to the end of the initial transient, i.e. at $\tau = 1$). This profile was calculated setting $Da = 5.14$ and $Pe = 0.27$, which resulted from the k_s and D_s values proposed by Duo et al. (1993) at 500 K (reported in Section 7.1.3), but the shape of the curve is the same also for the simulation of the other experimental conditions.

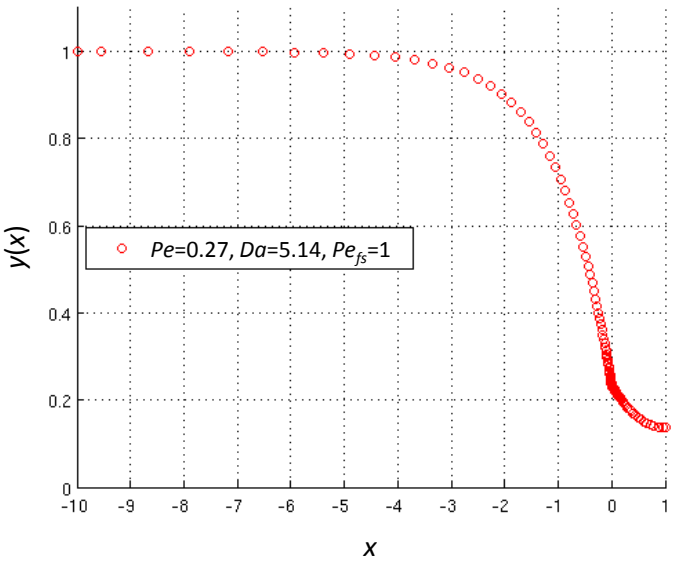

Figure 7.7 - Solution of the mass balance equation at the beginning of the process ($\tau = 1$) in fore section ($x < 0$, with $Da = 0$ and $Pe = 1$) and in reaction section ($0 \leq x \leq 1$, with $Da = 5.14$ and $Pe = 0.27$).

As properties were still uniform in the layer of particles at $\tau = 1$, the analytical solution of the initial pseudo steady state could be calculated according to Appendix J. The corresponding concentration profile, represented by the blue line in Figure 7.8, was compared with the numerical solution calculated applying the control volume formulation (red dots in the same figure), verifying that the spatial grid was created properly.

As long as the properties of the particle bed are uniform, the HCl fraction at the exit section can be calculated through Eq. 11.16, leading to $y_1 = 0.136$ (represented by the yellow star in Figure 7.8). This value corresponded to the value of the numerical solution at $x = 1$:

$$y(1.000) = 0.136$$

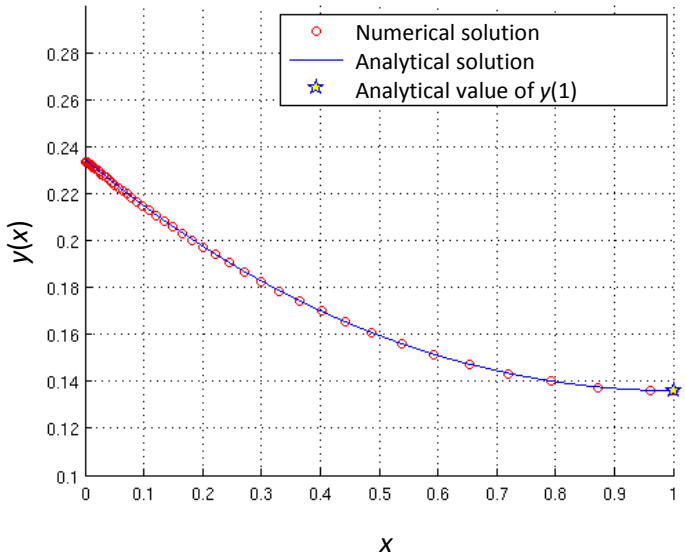

Figure 7.8 – Comparison between the analytical solution for the initial pseudo steady state (blue line) and the numerical solution (calculated in the grid points identified by red circles); the yellow star at $x = 1$ represents the value of the concentration at the exit section calculated through Eq. 11.16. All the solutions were calculated setting $Pe = 0.27$ and $Da = 5.14$.

Accordingly, the solution at $x = 0$ should correspond to the value calculated through Eq. 11.13, which led to $y_0 = 0.234$. Indeed, HCl fraction computed at the two sides of the reaction section entrance were:

$$y(0.000) = 0.234$$

$$y(-0.001) = 0.223$$

Conversely, as the values of the Peclet groups in the two sections ($x < 0$ and $x \geq 0$) were different, the slope at the entering section was discontinuous (according to Eq. 11.24 reported in Appendix K):

$$dy(0.000)/dx = -0.210$$

$$dy(-0.001)/dx = -0.766$$

Finally, to verify that the spatial domain of the fore section was long enough, the slope at system entrance was calculated:

$$\left.\frac{dy}{dx}\right|_{x=-10} = -0.000$$

As it was null, the grid point at $x = -10$ was not affected by the reaction zone, as required by the left-hand boundary condition (which should be imposed at $x = -\infty$).

Once verified that the spatial domain was properly described by the chosen grid, it was possible to calculate the variation of the concentration profile in time by means of Eq. 6.62[32], which permitted to estimate the variation of the unreacted core radius (r_c) in each point of the spatial grid and hence the corresponding *Da*

[32] Eq. 6.62 was solved expressing the gas concentration at the unreacted core surface (C_c) by means of Eq. 6.72 and the concentration in particle pores $C_1(R,z,t)$ according to Eq. 7.5.

values. Thus, for every time step the new concentration profile was estimated making use of the updated *Da* values. The resulting HCl fraction in the fixed bed during the entire process is shown in Figure 7.9.

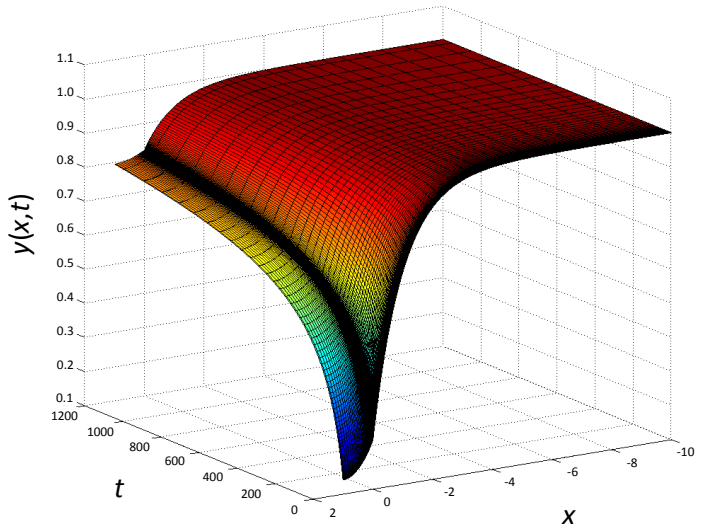

Figure 7.9 – HCl fraction in the fixed bed as a function of the dimensionless position *x* during the time interval of the experimental run carried out by Weinell et al. (1992).

HCl profile shown in Figure 7.9 was verified through the comparison of the two terms of the mass balance expressed by Eq. 11.56. At the beginning of the process, the two terms resulted:

$$y(-\infty) - y(+\infty) = 0.864$$

$$\int_0^1 Da \cdot y \cdot dx = 0.863$$

The mass balance was verified also at the end of the process:

$$y(-\infty) - y(+\infty) = 0.102$$

$$\int_0^1 Da \cdot y \cdot dx = 0.102$$

These results confirmed that the spatial domain was properly discretized.

The validation of the time domain discretization was made by means of the comparison of the HCl and $Ca(OH)_2$ conversions during the entire process. The average HCl conversion during the entire simulation, calculated by means of Eq. 11.58, resulted 18.23 %. The corresponding sorbent conversion, given by Eq. 11.62, was:

$$\chi_{Ca(OH)_2}{}^* = \frac{\chi_{HCl}{}^* \cdot \dot{n}_{HCl,in} \cdot \Delta t}{2 \cdot n_{Ca(OH)_2,0}} = 22.08\ \%$$

which corresponded to the value calculated through Eq. 11.61:

$$\chi_{Ca(OH)_2}{}^* = 22.11\ \%$$

7.1.5 Reproduction of literature data

The fundamental model presented in Section 6 was applied, according to the assumptions described in the previous sections, to reproduce the experimental results obtained by Weinell et al. (1992). Their data of solid sorbent conversion ($\chi_{Ca(OH)2}$) vs. time (t) at 473 and 523 K are shown in Figure 7.10.

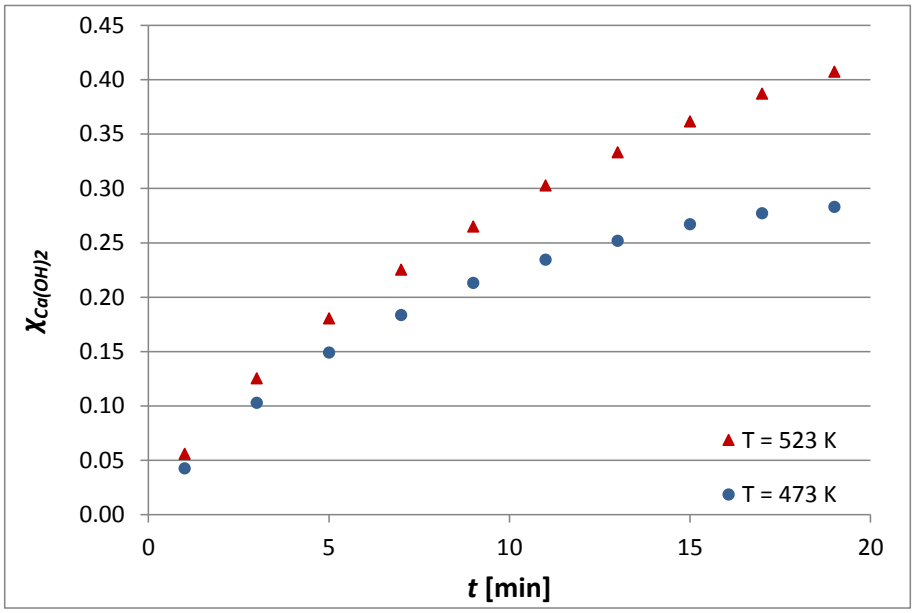

Figure 7.10 - Sorbent conversion vs. time points obtained by Weinell et al. (1992) at 473 K and 523 K (adapted from Duo et al., 1993).

In order to reproduce these data, the value of the dimensionless groups governing the neutralization process were required. Peclet group was calculated at 473 K and 523 K according to the data shown in Table 7.5. The superficial velocity of the gas u_0 depends on temperature, being the volumetric flow rate at 25°C set to 1 L/min in both runs (as reported in Table 7.1), while the dependence of molecular diffusivity on temperature was taken into account through the Fuller-Schettler-Giddings correlation (Eq. 7.3).

Table 7.5 – Values of the model parameters at experimental conditions adopted by Weinell et al. (1992) in their runs at 473 K and 523 K.

T	K	473	523
u_0	m/s	0.0476	0.0526
L	m	$1.04 \cdot 10^{-04}$	$1.04 \cdot 10^{-04}$
D_m	m^2/s	$4.14 \cdot 10^{-05}$	$4.94 \cdot 10^{-05}$
D_z	m^2/s	$2.90 \cdot 10^{-05}$	$3.45 \cdot 10^{-05}$
ε	-	0.6	0.6
Pe	-	0.286	0.265

The Damköhler number was not directly calculated with the provided data, because it depended on the values of k_s and D_s, which were treated as fitting parameters. However, according to the values calculated by Duo et al. (1993) and portrayed in Figure 3.11, the reaction rate constant is almost constant in this range of temperatures, so it was assumed equal to the value proposed by the same authors at 500 K:

$$k_s = 4.75 \cdot 10^{-4} \frac{m}{s}$$

The overall reaction rate constant, given by Eq. 6.82, at the beginning of the process (i.e. when there was no product layer on the grains) depends only on k_s, so it had the same values for both cases:

$$k_{glob,0} = \frac{3 \cdot (1-\varepsilon) \cdot (1-F_i) \cdot \left(1-\varepsilon_p\right)}{{r_g}^3} \cdot k_s = 2.48 \cdot 10^3 \; s^{-1}$$

However, as gas velocity depended on temperature, the initial values of Damköhler group[33] were different:

$$Da_0(T = 473\ K) = 5.43$$

$$Da_0(T = 523\ K) = 4.91$$

Therefore, the mass balance equation at the fixed bed could be solved at the beginning of the process, as both *Pe* and *Da* values were known. However, when the reaction proceeds the resistance given by solid-state diffusion through the product layer has to be taken into account. In fact, the variation of *Da* in each point of the fixed bed depends on D_s through Eqs. 6.18 and 6.82. Therefore, the solid-state diffusivity D_s affected the variation of the overall reaction rate in time and could be estimated fitting the sorbent conversion vs. time points illustrated in Figure 7.10, which are reported also in Figure 7.11.

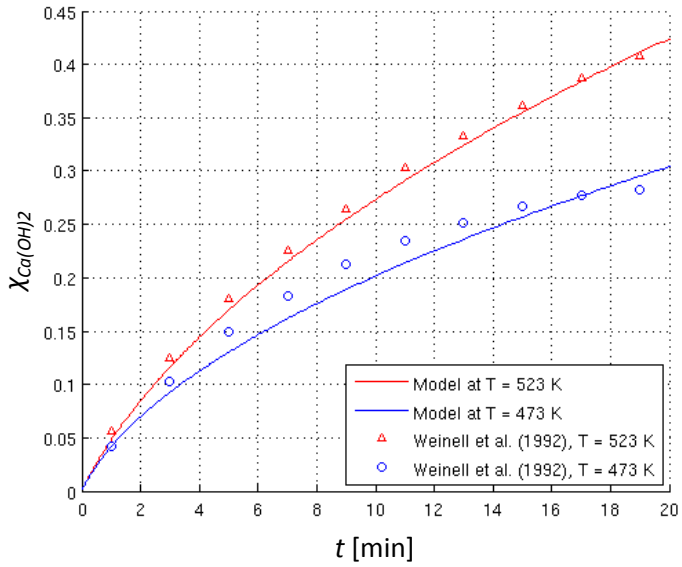

Figure 7.11 – Experimental points of sorbent conversion vs. time obtained by Weinell et al. (1992) and curves calculated by the proposed model at 473 K and 523 K.

The sorbent conversion curves reported in Figure 7.11 were obtained solving the mass balance equations at the fixed bed with the following values of the solid-state diffusion coefficient through the product layer:

$$D_s(T = 473\ K) = 4.0 \cdot 10^{-13}\ \frac{m^2}{s}$$

$$D_s(T = 523\ K) = 1.0 \cdot 10^{-12}\ \frac{m^2}{s}$$

[33] According to the definition adopted in the present work, the Damköhler number is: $Da = k_{glob} \cdot \frac{L}{u_0}$

The magnitude of D_s was in the range expected for gas diffusion in solids and both values were in line with that expected by literature data illustrated Section 3.4.

The curve representing the sorbent conversion at 523 K showed a very good agreement with experimental points and the shape of the curve at 473 K reproduced quite well the conversion of the sorbent during the process. However, Weinell et al. (1992) observed that after 15-20 minutes the variation of the HCl concentration in the gas when passing through the reactor was negligible, concluding that this behavior was caused by a maximum conversion of the sorbent. This phenomenon is not considered in the proposed model. Nevertheless, as evidenced by Chisholm and Rochelle (1999) and Chin et al. (2005), the presence of a maximum conversion strongly depends on temperature and humidity and in the operating conditions of practical interest for acid gas removal, this limit is present at definitely higher sorbent conversions, as reported in Section 4.4. Thus, the present model could be adopted in the analyzed case (described in Section 5.1) without any correction. Nevertheless, some dedicated laboratory tests (illustrated in Section 9) have been planned to better understand this phenomenon and to apply the model also in conditions near to the maximum conversion of the sorbent.

As the sorbent capacity of the system can be estimated through the value of Damköhler number, its average value in the bed, indicated by Da^*, is shown in Figure 7.12. Even though the initial value of Da was lower in the simulation at 523 K (due to the higher gas velocity, u_0), when reaction proceeded the higher value of D_s determined a slower decrease of the average value $Da*$ (according to Eq. 6.82).

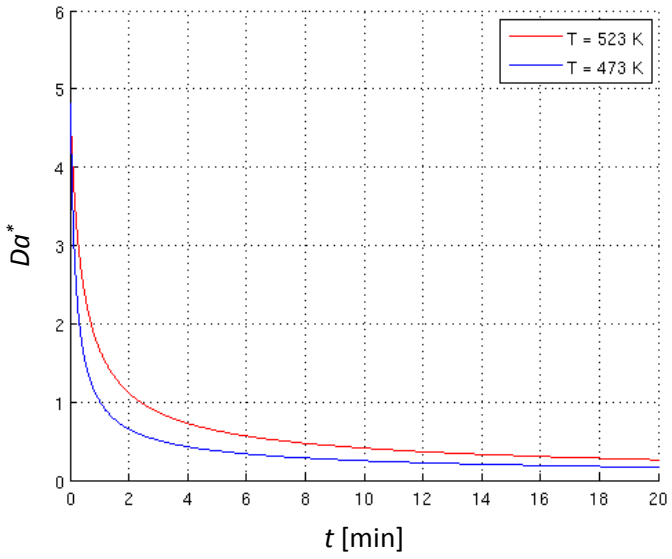

Figure 7.12 – Average values of Damköhler number (Da^*) in the fixed bed at 473 K (with a corresponding initial value of Da_0 = 5.43) and at 523 K (with Da_0 = 4.91).

7.2 Description of HCl removal with $NaHCO_3$

7.2.1 Literature data

Following the procedure described in Section 7.1, the fundamental model was adapted to describe the sorption of HCl by thermally decomposed sodium bicarbonate ($NaHCO_3$). Indeed, in the typical conditions of the dry treatment systems, when sodium bicarbonate is injected in the hot flue gases, it decomposes almost instantaneously and completely to Na_2CO_3, which has a greater pore volume:

$$2NaHCO_3 \rightarrow Na_2CO_3 + CO_2 + H_2O \qquad 7.6$$

Fellows and Pilat (1990) used a fixed-bed reactor where sorbent particles of decomposed $NaHCO_3$[34] and spherical glass beads[35] were placed on a porous support, schematized as shown in Figure 7.13.

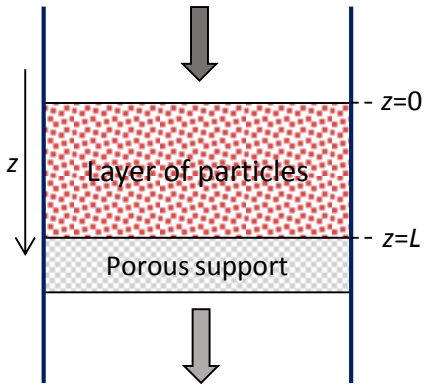

Figure 7.13 - Schematization of the reactor used by Fellows and Pilat (1990). The particle bed is formed by Na_2CO_3 (produced by decomposition of $NaHCO_3$) dispersed in spherical glass beads. *z* represents the axial coordinate along the fixed bed and *L* is the thickness of the layer of particles.

They studied the HCl neutralization process in different experimental conditions (gas flow rate, particle diameter, temperature, superficial gas velocity and inlet HCl concentration). The sorbent conversion curves obtained through runs at 107, 135, 191, 235 and 288 °C are reported in Figure 7.14.

[34] Fellows and Pilat (1990) used particle of $NaHCO_3$ with a reference diameter of 45 µm and a BET surface area of 0.11 m^2/g; after decomposition, the Na_2CO_3 produced had a BET surface area of 2.60 m^2/g.
[35] The glass beads had an average diameter of 150 µm and a bulk density of $1.5 \cdot 10^3$ kg/m^3.

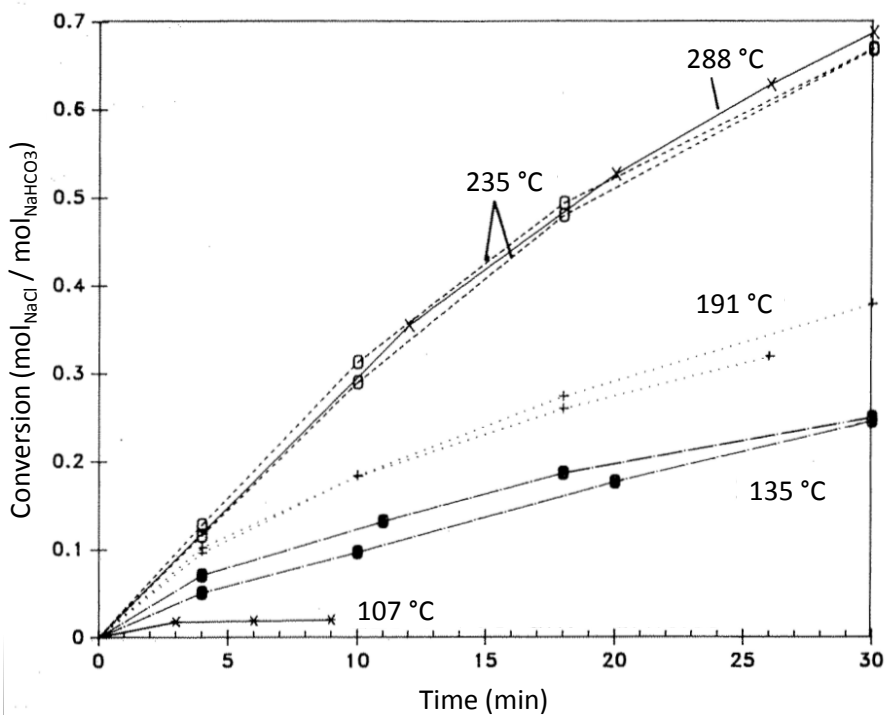

Figure 7.14 – Conversion of particles of $NaHCO_3$ to NaCl at different temperatures (adapted from Fellows and Pilat, 1990); the sorbent had a reference diameter of 45 µm in all experiments but the run at 107 °C, which was obtained with $NaHCO_3$ of 10 µm.

In order to assess the main model parameters (i.e. k_s and D_s) in conditions as similar as possible to the operating conditions on the flue-gas treatment system of the analyzed plant, the model was tuned using the results obtained by flowing 1.1 L/min[36] of a gas mixture with 760 ppm of HCl in N_2 at 191 °C[37]. Thus, the HCl concentration at the reactor entrance is:

$$C_{in} = 760 \cdot 10^{-6} \cdot \frac{P}{R \cdot T} = 2.00 \cdot 10^{-2} \frac{mol}{m^3}$$

Other experimental parameters are reported in Table 7.6.

[36] Referred at 20 °C and 1 atm.

[37] Corresponding HCl concentration in normal conditions is:

$$C_{in} = 760 \cdot 10^{-6} \cdot \frac{P_{NC} \cdot M_{HCl}}{R \cdot T_{NC}} = 1.236 \cdot 10^{-3} \frac{kg}{Nm^3} = 1236 \frac{mg}{Nm^3}$$

Table 7.6 – Experimental conditions used by Fellows and Pilat (1990).

T	464	K	temperature
P	101325	Pa	pressure
Q_{20}	$1.1 \cdot 10^{-3}/60$	m^3/s	volumetric flow rate at 20°C
t_{fin}	1800	s	duration of the run
C_{in}	760	ppm	inlet HCl concentration
m_{NaHCO3}	$9 \cdot 10^{-5}$	kg	mass of the $NaHCO_3$ prior to decomposing
m_s	$5.68 \cdot 10^{-5}$	kg	mass of the sorbent (Na_2CO_3)
m_i	$5 \cdot 10^{-3}$	kg	mass of the inert particles

The authors provided the cross-sectional area of the reactor (5.1 cm^2), hence superficial velocity results:

$$u_0 = 5.72 \cdot 10^{-2} \frac{m}{s}$$

while particle bed thickness was:

$$L = 6.65 \cdot 10^{-3}\ m$$

Sodium bicarbonate can be assumed completely decomposed in these conditions and the properties of the resulting sodium carbonate are reported in Table 7.7.

Table 7.7 –Properties of Na_2CO_3 formed by the decomposition of $NaHCO_3$ (from: Fellows and Pilat, 1990; Verdone and De Filippis, 2006).

S_{BET}	$2.60 \cdot 10^3$	m^2/kg	BET surface area
R_p	$22.5 \cdot 10^{-6}$	m	mean particle radius
ε	0.39	-	interparticle void fraction of the particle bed[38]
ε_p	0.45	-	initial porosity of sorbent particles
τ_p	3.0	-	particle tortuosity

Thus, the HCl sorption, written in the form of Eq. 6.2, results:

$$HCl + \frac{1}{2}\, Na_2CO_3 \rightarrow \frac{1}{2}\, CO_2 + \frac{1}{2}\, H_2O + NaCl \qquad 7.7$$

The properties of gaseous and solid compounds in the experimental conditions of Table 7.6 are reported in Table 7.8.

[38] Estimated from the bulk density.

Table 7.8 – Properties of reagents and products in the simulated conditions.

α	1.29	-	ratio of solid product to sorbent molar volumes[39]
b	0.5	-	stoichiometric coefficient of sorbent (Eq. 4.6)
M_{HCl}	$36.46 \cdot 10^{-3}$	kg/mol	molar mass of HCl
M_{N2}	$28 \cdot 10^{-3}$	kg/mol	molar mass of N_2
M_p	$58.44 \cdot 10^{-3}$	kg/mol	molar mass of product (NaCl)
M_s	$106.0 \cdot 10^{-3}$	kg/mol	molar weight of sorbent (Na_2CO_3)
μ_{gas}	$2.42 \cdot 10^{-5}$	Pa·s	gas viscosity
ρ_{gas}	0.734	kg/m^3	gas density
ρ_p	2165	kg/m^3	true density of product (NaCl)
ρ_s	2540	kg/m^3	true density of sorbent (Na_2CO_3)

The sorbent particles were described according to the grain model, defining the initial radius of the grains as:

$$r_g = \frac{3}{\rho_s \cdot S_{BET}} = 0.45\ \mu m = 4.54 \cdot 10^{-7}\ m$$

For a mean particle radius R_p of 22.5 µm, the Reynolds number referred to the particle resulted:

$$Re_p = \frac{\rho_{gas} \cdot u_0 \cdot d_p}{\mu_{gas}} = 7.82 \cdot 10^{-2}$$

Therefore, the axial dispersion was governed by molecular diffusion. Molecular diffusivity was assessed for a gas mixture of HCl in N_2 at 464 K and 1 atm through the correlation proposed by Fuller-Schettler-Giddings:

$$D_m = \frac{0.001 \cdot T^{1.75} \left(\frac{1}{M_{HCl}} + \frac{1}{M_{N2}}\right)^{\frac{1}{2}}}{P \left[(\sum v_i)_{HCl}^{\frac{1}{3}} + (\sum v_i)_{N2}^{\frac{1}{3}}\right]^2} = 4.00 \cdot 10^{-05}\ \frac{m^2}{s}$$

The axial dispersion coefficient, which takes into account the bed tortuosity, resulted:

$$D_z = 0.7 \cdot D_m = 2.80 \cdot 10^{-05}\ \frac{m^2}{s}$$

The values of these parameters were used in the description of the experimental results presented in the following sections.

[39] Stoichiometric coefficients of Eq. 4.5 were taken into account.

7.2.2 Concentration profile within the particle

In this section, the governing equation of mass transport within particle pores was solved for the initial stages of the process, when model parameters were constant (corresponding values are reported in Table 7.9). The solution, obtained setting k_s according to typical literature values[40], was calculated in order to verify if the resistance to mass transfer in particle pores was negligible also for HCl removal with $NaHCO_3$ decomposed particles.

Table 7.9 – Parameters used in the calculation of the concentration profile within particle porosity.

ε_p	0.45	-	initial particle porosity
τ_p	3.0	-	particle tortuosity
D_k	$1.21 \cdot 10^{-4}$	m^2/s	Knudsen diffusion coefficient
D_m	$4.00 \cdot 10^{-5}$	m^2/s	molecular diffusion coefficient of HCl in N_2
r_g	$4.54 \cdot 10^{-7}$	m	initial grain radius
k_s	$1.66 \cdot 10^{-5}$	m/s	reaction rate constant
R_p	$2.25 \cdot 10^{-5}$	m	mean particle radius

Accordingly, the initial value of the effective diffusion coefficient within particles pores results:

$$D_{ef,0} = \frac{\varepsilon_p}{\tau_p}\left(\frac{1}{D_m} + \frac{1}{D_k}\right)^{-1} = 4.51 \cdot 10^{-6}\ \frac{m^2}{s}$$

while the overall reaction rate constant of the particle is:

$$k_{part,0} = \frac{3 \cdot (1 - \varepsilon_p) \cdot k_s}{r_g} = 60.3\ s^{-1}$$

Hence, the initial values of Thiele and Biot numbers can calculated:

$$Th_{p,0} = R_p \cdot \sqrt{\frac{k_{part,0}}{D_{ef,0}}} = 0.0823$$

$$Bi_0 = \frac{k_g \cdot R_p}{D_{ef,0}} = 9.57$$

where the mass transfer coefficient in the boundary film, estimated through the Ranz and Marshall correlation, resulted

[40] The reaction rate constant per unit area of reaction interface was estimated through the correlation proposed by Verdone and De Filippis (2006):

$$k_s = 169.9 \cdot \exp\left(-\frac{62281}{R \cdot T}\right)$$

At 464 K, the reaction rate constant resulted:

$$k_s(T = 464\ K) = 1.66 \cdot 10^{-5}\ \frac{m}{s}$$

$$k_g = 1.92\ \frac{m}{s}$$

Hence, the partial differential governing equation in the particle pores can be solved as shown in Appendix M, leading to the HCl fraction within the particle porosity illustrated in Figure 7.15.

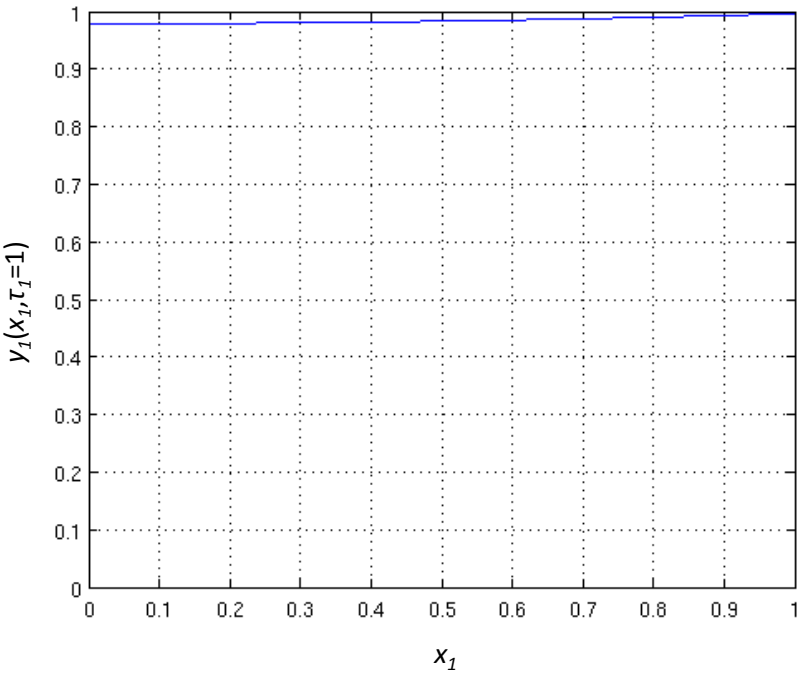

Figure 7.15 - Profile of the HCl fraction (y_1) within the Na_2CO_3 particle at $\tau_1 = 1$ as a function of dimensionless radial position (x_1).

This profile indicates that at the beginning of the process the overall reaction rate is governed by the reaction kinetics and that the resistance given by diffusion in particle porosity can be neglected.

7.2.3 Reproduction of literature data

The capability of the model of describing HCl removal by decomposed $NaHCO_3$ was verified fitting the experimental results of Fellows and Pilat (1990). They reported the conversion of the $NaHCO_3$ vs. time for several temperatures (shown in Figure 7.14).

The fundamental model was implemented to describe the experimental data at 191 °C, which were reported in Figure 7.16 (red stars). The resulting profile, shown in the same figure, was obtained setting the values of the solid-state diffusivity through the product layer to

$$D_s(464\ K) = 5.5 \cdot 10^{-12}\ \frac{m^2}{s}$$

and reaction rate constant to

$$k_s(464\ K) = 2.6 \cdot 10^{-4}\ \frac{m}{s}$$

The verification of the implementation of the fundamental model when tuned with these parameters is reported in Appendix O.

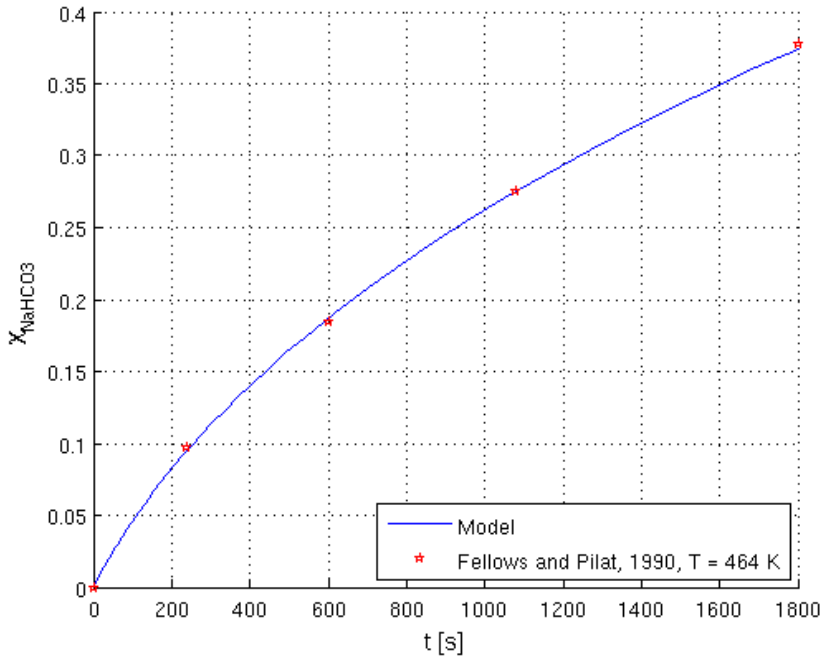

Figure 7.16 - Sorbent conversion vs. time; red stars represent the experimental results obtained by Fellows and Pilat (1990) at 191 °C, while the blue line describe the profile calculated by the proposed model.

The figure shows a very good agreement between the experimental points and the curve of $NaHCO_3$ conversion calculated by means of the proposed model. Therefore, the values of the model parameters found fitting the data obtained by Fellows and Pilat (1990) were adopted for the application of the fundamental model to the operating conditions of the analyzed case-study (as reported in Section 8).

8 Application of the fundamental model to plant design data

The fundamental model described in Section 6 was applied to describe hydrogen chloride removal in the flue-gas treatment system of the analyzed plant (illustrated in Section 5.1). The implementation was made considering the design conditions of the plant (provided in Section 5.1.2). Accordingly, the main kinetic parameters (i.e. reaction rate constant k_s and solid-state diffusivity D_s) were estimated in these conditions taking as a reference the values found from the reproduction of literature data reported in Section 7.

In the first stage of the acid gas treatment system, the HCl removal is achieved through the injection of calcium hydroxide. One of the main differences with respect to the experimental runs modeled in Section 7.1 is the presence in the flue gas of fly ash and partially reacted particles (coming from the recycle). Therefore, the model was adapted to consider the different composition of the particulate cake on the filtering surface.

In the second stage, where acid gas removal is achieved through the injection of sodium bicarbonate, additional data on filter cleaning were provided by plant designer. Therefore, the description of the cleaning cycles was included in the simulations, modeling the growing of the particulate cake on the filter bags. Another variation with respect to the case modeled in Section 7.2 is the presence of SO_2. Indeed, even though SO_2 is usually much less than HCl in flue gases produced from waste incineration, the former is only slightly removed by calcium hydroxide in the first stage. Therefore, the relative amount of SO_2 in the second stage is not negligible when compared to HCl, and its effect on sorbent consumption was taken into account.

8.1 First stage

8.1.1 Description of the system

The fundamental model was applied to describe the first stage of the system illustrated in Section 5.1. Calcium hydroxide particles (Stream 13 in Figure 8.1) are injected upstream the fabric filter together with recycled particles (Stream 11).

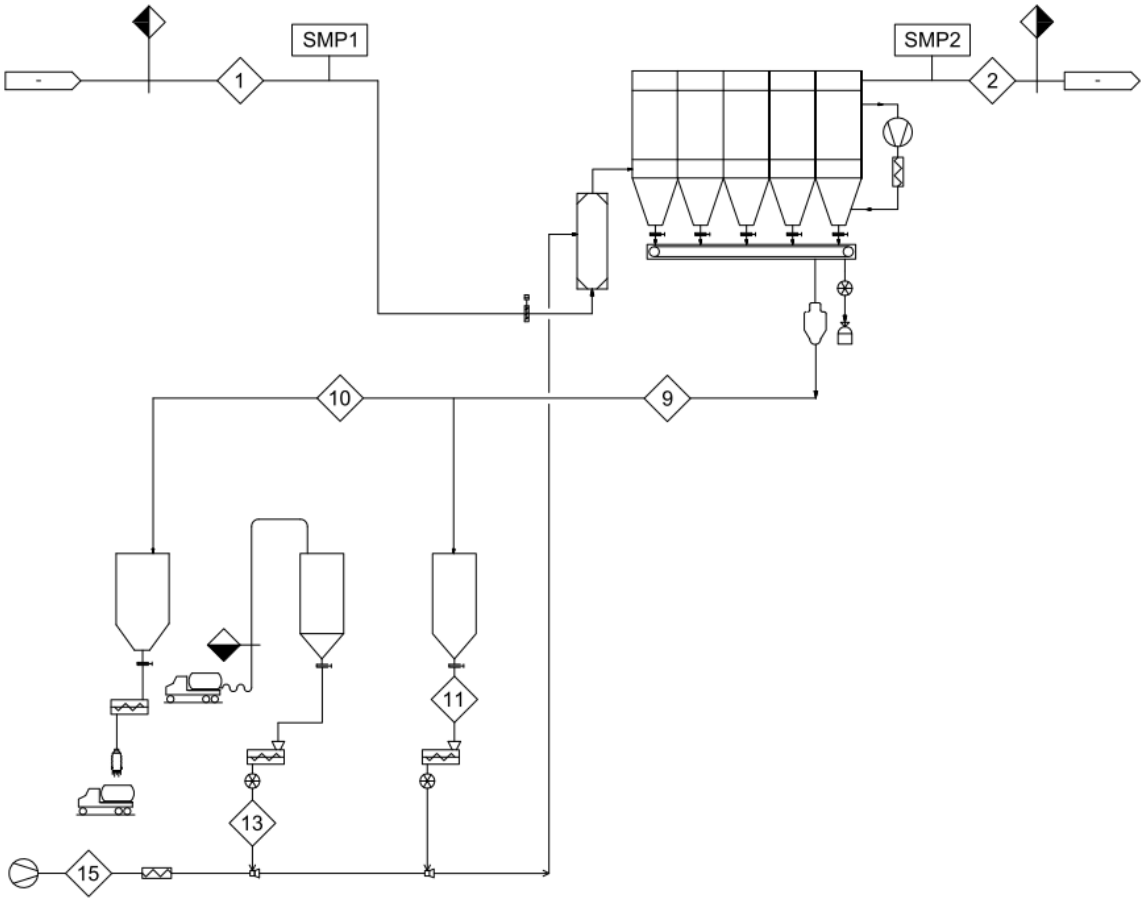

Figure 8.1 - Process flow diagram of the first stage of the acid gas removal section.

According to Duo et al. (1993), most of the acid gas neutralization takes place in the cake deposited on the bags of the fabric filter. Therefore, the model was applied to describe the reaction in this section. However, the presence of inert material (mainly fly ash) and recirculated sorbent particles have to be taken into account. Accordingly, the particulate cake was represented as shown in Figure 8.2.

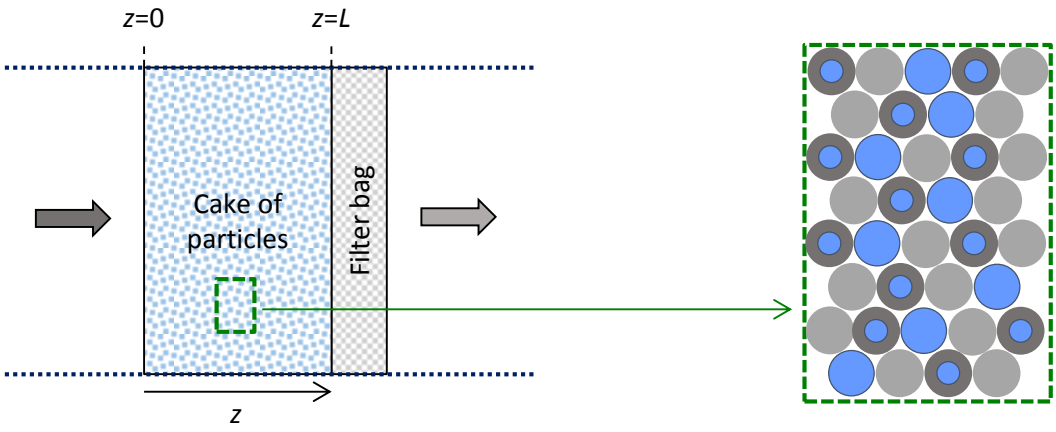

Figure 8.2 - Cake of particles deposited on the bag of the first fabric filter; the light-grey spheres represent inert particles (mainly fly ash), the blue ones represent the fresh calcium hydroxide particles, and the grey and blue spheres are the partially converted sorbent particles coming from the recycle.

The model was applied assuming that the particulate cake has a fixed thickness, which was assumed equal to the average value provided in design data[41]:

$$L = 2 \cdot 10^{-3}\ m$$

The design conditions of the inlet flue gas stream (Stream 1 in Figure 8.1) considered in the implementation of the model are reported in Table 8.1.

Table 8.1 - Design conditions of the flue gas entering the first stage of the analyzed treatment system.

Q_{NC}	110,000	Nm^3/h	Volumetric flow rate in normal conditions
Q	50.69	m^3/s	Volumetric flow rate
T	453.15	K	Temperature
P	101,325	Pa	Pressure
y_{H2O}	12 %	-	H_2O fraction (%vol)
y_{CO2}	8.5 %	-	CO_2 fraction (%vol)
$C_{HCl,in}$	800	mg/m^3	HCl concentration
$C_{SO2,in}$	200	mg/m^3	SO_2 concentration
$\dot{m}_{FA}$	343	kg/h	Mass flow rate of fly ash

As discussed in Section 5.1, HCl is the main acid gas in these conditions. Therefore, only its neutralization was considered in the implementation of the model, neglecting the effect of competitive reactions. The inlet concentration of HCl in the reactant gas corresponds to

$$C_{in} = 800\ \frac{mg}{Nm^3} \cdot \frac{10^{-6}}{M_{HCl}} \cdot \frac{T_{NC}}{T} \cdot \frac{P}{P_{NC}} = 1.323 \cdot 10^{-2}\ \frac{mol}{m^3}$$

and its equilibrium concentration results

$$C_{eq} = 6.87 \cdot 10^{-7}\ \frac{mol}{m^3}$$

[41] This situation is verified at the start-up of the plant, when the sorbent is injected in the treatment system while air is flowing. Therefore, the cake accumulated on the filtering surface is made only of fresh sorbent, and it is then exposed to the flue gas.

In these conditions, the neutralization reaction of HCl with calcium hydroxide can be written in the form:

$$HCl + \frac{1}{2}\, Ca(OH)_2 \rightarrow \frac{1}{2}\, (CaCl_2 \cdot 2H_2O) \qquad 8.1$$

The fresh sorbent, which can be approximated as 100 % $Ca(OH)_2$, is represented in Figure 8.1 by Stream 13. According to design data, its mass flow rate is

$$\dot{m}_{Ca(OH)_2,fr} = 313\ \frac{kg}{h}$$

Hence, the fraction of inert material injected into the system (given by fly ash, reported in Table 8.1) resulted:

$$F_i = \frac{343}{343 + 313} = 52.3\ \%$$

Therefore, the same fraction of inert particles was considered in the filter cake.

The properties of fresh sorbent particles are reported in Table 8.2. The BET surface area was provided by the operating company and the initial grain radius was calculated accordingly. As this sorbent is very similar to calcium hydroxide used by Weinell et al. (1992), other properties needed for model application and not available for the material were assumed equal to those presented in Table 7.3.

Table 8.2 – Properties of calcium hydroxide particles.

S_{BET}	$2.0 \cdot 10^4$	m^2/kg	BET surface area
r_g	$6.7 \cdot 10^{-8}$	m	initial grain radius
R_p	$1.23 \cdot 10^{-6}$	m	mean particle radius
ε	0.6	-	interparticle void fraction of the cake of particles
ε_p	0.519	-	initial porosity of sorbent particles
τ_p	3.0	-	particle tortuosity
ρ_s	2240	kg/m^3	true density of sorbent

According to design data, the total mass flow rate of the recycled particles (Stream 11) is

$$\dot{m}_{rec} = 2571\ \frac{kg}{h}$$

and the corresponding fraction of calcium hydroxide in recycled solids is

$$\omega_{Ca(OH)_2,rec} = 15.0\ \%$$

Taking into account the fraction of inert particles in the recycled stream and assuming that the sorbent particles are uniformly reacted, their conversion resulted:

$$\chi_{Ca(OH)_2,rec} = 68.5\ \%$$

According to the grain model, the unreacted core radius was estimated through Eq. 6.55:

$$r_c = \sqrt[3]{\left(1 - \chi_{Ca(OH)_2,rec}\right) \cdot {r_g}^3} = 4.56 \cdot 10^{-8}\ m$$

The most important geometrical size of the system is the total filtration area:

$$A = 3460\ m^2$$

Accordingly, the face velocity of flue gas to filter resulted

$$u_0 = \frac{110000}{3460} \cdot \frac{T}{273.15} \cdot \frac{1}{3600} = 0.0147\ \frac{m}{s}$$

As stated above, the cake thickness was assumed constant and equal to the design value. Therefore, the value of 2 mm represents the average thickness of the cake on all the bags in the filter (which have a different amount of particle on their surface depending on the time interval from the last cleaning). Accordingly, the simulated duration of a cleaning cycle, defined as the interval between two cleanings of the same bags, was assumed

$$t_{cycle} = 2\ h = 7200\ s$$

Indeed, the particles accumulated on the filtering surface in 2 h form a cake of 4 mm[42], which is in agreement with the an average thickness during the entire cycle of 2 mm.

[42] This value was calculated taking into account the flow rates of fresh sorbent, recycled particles and fly ash. For the latter, the interparticle void fraction was assumed equal to the value of sorbent particles.

8.1.2 Model parameters

Model parameters were estimated according to correlations presented in Section 6.5. Molecular diffusivity of HCl in N_2 was estimated by means of Fuller-Schettler-Giddings correlation at 180 °C and 101.3 kPa. Thus, according to the data provided in Table 6.1 and in Table 6.2, the molecular diffusivity resulted:

$$D_m = \frac{0.001 \cdot T^{1.75} \left(\frac{1}{M_{HCl}} + \frac{1}{M_{N2}}\right)^{\frac{1}{2}}}{P\left[(\sum v_i)_{HCl}^{\frac{1}{3}} + (\sum v_i)_{N2}^{\frac{1}{3}}\right]^2} = 3.84 \cdot 10^{-5}\ \frac{m^2}{s}$$

while corresponding axial dispersion coefficient was:

$$D_z = 0.7 \cdot D_m = \ 2.69 \cdot 10^{-5}\ \frac{m^2}{s}$$

According to the results shown in Section 7.1, the mass balance equation at the particle pores was substituted as follows in the fundamental model

$$C_1(R, z, t) = C(z, t)$$

Therefore, the HCl concentration in the particle pores was assumed uniform and equal to the value in the interparticle voids.

The characteristic time of the governing equation in the sorbent bed (Eq. 6.7), which was defined as the residence time of the gas in the filter cake, resulted:

$$t_c = \frac{L}{u_0} = 0.137\ s$$

which was much lower than both the time of a cycle and the time to obtain a significant conversion of the sorbent. Therefore, the accumulation term $\frac{\partial C}{\partial t}$ of the mass balance equation was neglected and the system was solved through a sequence of pseudo steady state equations (according to the procedure discussed in Section 6.3.3).

The governing differential equation for one-dimensional mass transfer in steady state conditions (Eq. 6.20) was rewritten taking into account the two sorbent populations (i.e. fresh and recycled particles):

$$\frac{dy}{dx} = \frac{d}{dx}\left(\frac{1}{Pe} \cdot \frac{dy}{dx}\right) - \left(Da_{fr} + Da_{rec}\right) \cdot y \qquad 8.2$$

Defining x_{fr} and x_{rec} as the fractions of sorbent fresh and recycled particles respectively, they resulted:

$$x_{new} = \frac{\dot{m}_{Ca(OH)_2,fr}}{\dot{m}_{Ca(OH)_2,fr} + \dot{m}_{rec} \cdot (1 - F_i)} = 20.3\ \%$$

$$x_{rec} = 1 - x_{fr} = 79.7\ \%$$

The overall reaction rate constants related to the two populations were expressed by:

$$k_{glob,fr} = \frac{3 \cdot (1-\varepsilon) \cdot (1-F_i) \cdot x_{fr} \cdot \left(1-\varepsilon_p\right) \cdot {r_{c,fr}}^2}{{r_g}^3} \cdot \frac{D_s \cdot k_s}{D_s + k_s \cdot r_{c,fr} \cdot \left(1 - {r_{c,fr}}/{r_{t,fr}}\right)}$$

and

$$k_{glob,rec} = \frac{3 \cdot (1-\varepsilon) \cdot (1-F_i) \cdot x_{rec} \cdot \left(1-\varepsilon_p\right) \cdot {r_{c,rec}}^2}{{r_g}^3} \cdot \frac{D_s \cdot k_s}{D_s + k_s \cdot r_{c,rec} \cdot \left(1 - {r_{c,rec}}/{r_{t,rec}}\right)}$$

which depend on the reaction rate constant k_s and the solid-state diffusion coefficient through the product D_s. The reaction rate constant was assumed equal to the value proposed by Duo et al. (1993):

$$k_s = 4.75 \cdot 10^{-4} \ \frac{m}{s}$$

The solid-state diffusion coefficient was estimated according to the values reported by the same authors. Assuming an Arrhenius temperature dependence, at 180 °C the solid-state diffusivity resulted:

$$D_s(T = 180\,°C) = 8.33 \cdot 10^{-14} \ \frac{m^2}{s}$$

The corresponding initial Damköhler number for fresh particles resulted:

$$Da_{fr,0}(T = 180\,°C) = \frac{k_{glob,0,fr} \cdot L}{u_0} = 54.1$$

The initial value of Damköhler number for recycled particles depends on D_s, as they are partially converted and a product layer is already present at the beginning of the cycle. It resulted:

$$Da_{rec,0}(T = 180\,°C) = \frac{k_{glob,0,rec} \cdot L}{u_0} = 0.82$$

As the superficial gas velocity u_0 and the cake thickness L were assumed constant during the entire cycle, the Pe number did not change during the process:

$$Pe = \frac{u_0 \cdot L}{\varepsilon \cdot D_z} = 1.82$$

8.1.3 Results

The mass balance differential equation at the filter cake was solved making use of the control volume formulation, taking into account the fraction of inert material and the two populations of sorbent particles. The resulting profiles of sorbent and HCl conversions are reported in Figure 8.3 and Figure 8.4 respectively. The former shows the evolution of the sorbent conversion for both populations vs. the coordinate along the axial direction of the cake (represented according to Figure 8.2) at different times. At the beginning of the process, i.e. when the sorbent was exposed to the flue gas, the particulate cake was formed by two homogeneous populations, which had conversions equal to:

$$\chi_{Ca(OH)_2,fr,0} = 0\ \%$$

and

$$\chi_{Ca(OH)_2,rec,0} = 68.5\ \%$$

When the reaction proceeded, the fresh particles reacted faster, due to the lower mass transfer resistance related to the diffusion through the product layer.

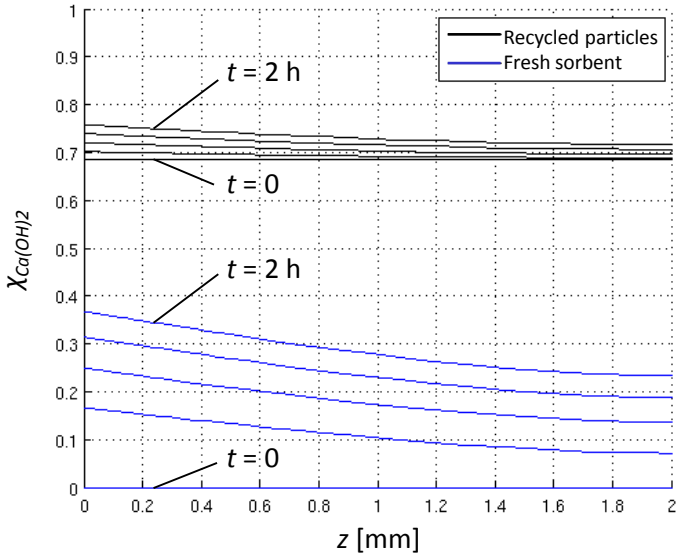

Figure 8.3 - Conversion of the two populations of sorbent particles (fresh particles in blue, recycled particles in black) between t = 0 and t = 2 h. Coordinate z represents the length along the flue gas direction.

The final conversions (at t = 2 h) of the two populations averaged on the cake length resulted 28.5 % and 73.1 %, with a corresponding global average equal to 64.1 %. This value is in agreement with the expected conversion; however, the assumption of homogeneous conversion of the recycled particles should be revised due to the difference between the two populations at the end of the process. Furthermore, a more correct profile estimation should take into account the growth of the cake.

The corresponding HCl conversion is shown in Figure 8.4. It evidences that during the initial reaction stages of the process the acid gas removal took place mainly in the layer of particles exposed to the raw flue gas. Conversely, when the reaction further proceeded, the entire cake was involved (due to the higher consumption of the sorbent at the entrance section and to the effect of the axial dispersion).

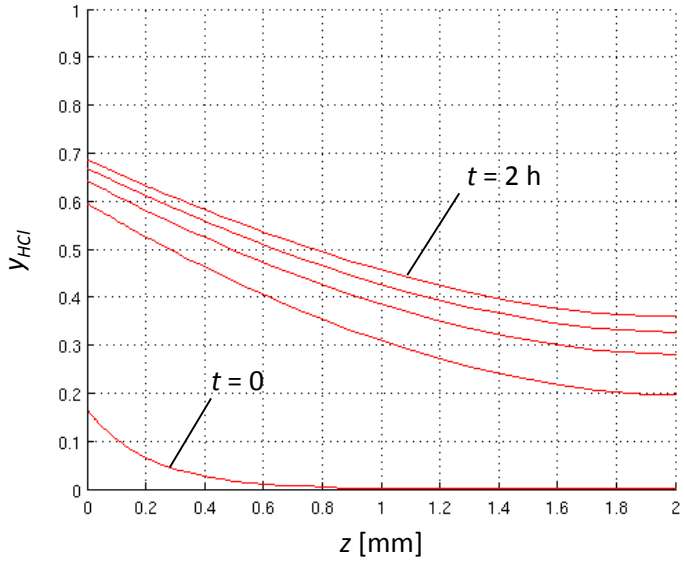

Figure 8.4 - HCl concentration in the filter cake between t = 0 and t = 2 h. Coordinate *z* represents the length along the flue gas direction.

The figure shows that the HCl removal was almost complete at the beginning of the process, while at *t* = 2 h the conversion was equal to 64 %. The corresponding average conversion during the entire cycle resulted 75.1 %, which is slightly higher than the design value (according to the data reported in Table 5.1, the HCl conversion in the first stage was 70 %). This difference is in agreement with the results proposed by Duo et al. (1993), which demonstrated that the injection of all the sorbent immediately following the filter cleaning (i.e. the simulated case) provides an enhanced removal efficiency with respect to continuous feeding. Moreover, the presence of the competitive reactions of SO_2 and CO_2 with the sorbent could determine a lower value of the HCl conversion with respect to the simulated case.

8.2 Second stage

8.2.1 Description of the system

The system modeled in this section is the second stage of the system (shown in Figure 8.5), where the solid sorbent is sodium bicarbonate (Stream 14). The more important design data regarding the fabric filter are reported in Table 8.3.

As described in Section 3.2, the decomposition of bicarbonate to carbonate can be assumed instantaneous, therefore the HCl neutralization reaction is:

$$HCl + \frac{1}{2}\, Na_2CO_3 \rightarrow \frac{1}{2}\, CO_2 + \frac{1}{2}\, H_2O + NaCl$$

Carbonate conversion is higher than that of calcium hydroxide, so recirculation of solid residues was not required.

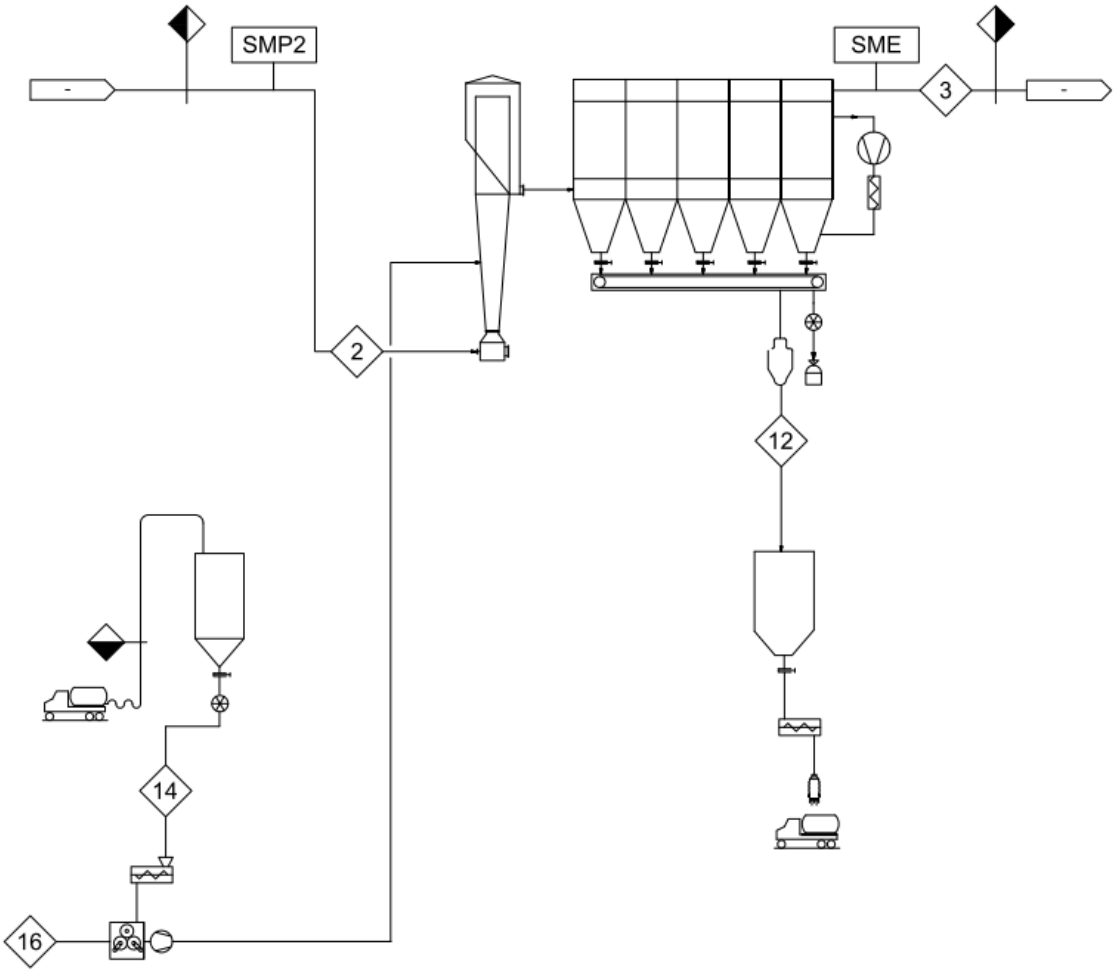

Figure 8.5 - Process flow diagram of the second stage of the acid gas removal section.

Table 8.3 - Design data of the fabric filter in the second stage of the treatment system.

A	3460	m^2	Total filtration area
ΔP_{des}	900	Pa	Design value of pressure drop in the filter
V_{react}	100	m^3	Reactor volume
V_{filter}	455	m^3	Fabric filter volume

The model was applied to describe the design conditions of the system, and main parameters of the flue gas entering the system are reported in Table 8.4.

Table 8.4 - Design conditions of the flue gas entering the second stage of the analyzed treatment system.

Q_{NC}	111,750	Nm^3/h	Volumetric flow rate in normal conditions
Q	51.27	m^3/s	Volumetric flow rate
T	178.0	°C	Temperature
P	101,325	Pa	Pressure
$C_{HCl,in}$	240	mg/Nm^3	Inlet HCl concentration
$C_{SO2,in}$	140	mg/Nm^3	Inlet SO_2 concentration
y_{H2O}	11.8 %	-	H_2O fraction (%vol)
y_{CO2}	8.4 %	-	CO_2 fraction (%vol)

The HCl concentration expressed in mol/m^3 results:

$$C_{HCl,in} = 240\ \frac{mg}{Nm^3} \cdot \frac{10^{-6}}{M_{HCl}} \cdot \frac{T_{NC}}{T} \cdot \frac{P}{P_{NC}} = 4.0 \cdot 10^{-3}\ \frac{mol}{m^3}$$

which corresponds to

$$C_{HCl,in} = 148\ ppm$$

The design value of the sodium bicarbonate mass flow rate (Stream 14) is

$$\dot{m}_{NaHCO_3} = 142\ \frac{kg}{h}$$

As illustrated in Figure 8.5, bicarbonate particles are broken into smaller particles by means of a grinder before the injection into the contact reactor. A typical diameter distribution of the ground particles is shown in Figure 3.4.

When sodium bicarbonate is exposed to hot flue gases (which are at 178 °C) it undergoes thermal activation according to the following reaction:

$$2NaHCO_3\ (s) \rightarrow Na_2CO_3\ (s) + CO_2\ (g) + H_2O\ (g)$$

Accordingly, the sorbent mass flow rate results:

$$\dot{m}_{Na_2CO_3} = \dot{m}_{NaHCO_3} \cdot \frac{M_{Na_2CO_3}}{2 \cdot M_{NaHCO_3}} = 89.6\ \frac{kg}{h}$$

8.2.2 Competitive reactions

As shown in Table 8.4, the ratio of HCl to SO_2 concentration is higher than in the first stage (reported in Table 8.1) because of the more effective reaction of calcium hydroxide with HCl than with SO_2. Therefore, the fraction of bicarbonate available for the HCl removal has to be estimated taking into account the presence of SO_2. In typical operating conditions, its neutralization reaction is:

$$Na_2CO_3 + SO_2 + ½O_2 \rightarrow Na_2SO_4 + CO_2$$

According to the definitions given in Appendix I, the fraction of Na_2CO_3 available for the HCl removal is:

$$\phi_{HCl,Na_2CO_3} \stackrel{\text{def}}{=} \frac{\dot{n}_{Na_2CO_3-HCl,in}}{\dot{n}_{Na_2CO_3,in}}$$

It can be estimated making use of the correlation proposed in Section 4.2 for HCl conversion:

$$\chi_{HCl,Na_2CO_3} = \frac{{rs_{HCl,Na_2CO_3}}^{a_{HCl,Na_2CO_3}} - rs_{HCl,Na_2CO_3}}{{rs_{HCl,Na_2CO_3}}^{a_{HCl,Na_2CO_3}} - 1}$$

where the ratio between the actual feed rate of solid reactant and its stoichiometric flow rate is

$$rs_{HCl,Na_2CO_3} \stackrel{\text{def}}{=} \frac{\dot{n}_{Na_2CO_3-HCl,in}}{\dot{n}_{Na_2CO_3-HCl,st}}$$

The stoichiometric molar flow rate was calculated according to acid gas flow rates. The parameter a_{HCl,Na_2CO_3} was estimated from Neutrec data (Figure 4.1):

$$a_{HCl,Na_2CO_3} = 16.6$$

while the HCl conversion in the second stage was calculated through design data:

$$\chi_{HCl,PFD} = 1 - \frac{1.23}{148} = 0.9917$$

Hence:

$$\phi_{HCl,Na_2CO_3} = 0.873$$

Therefore, the effect of the competitive reaction of SO_2 was taken into account assuming that only 87.3 % of the injected sorbent is available for HCl neutralization. The sorbent flow rate considered in the implementation of the model was only the fraction available for HCl neutralization:

$$\dot{m}_{Na_2CO_3} = 89.6 \cdot \phi_{HCl,Na_2CO_3} = 78.2 \ \frac{kg}{h}$$

while the rest was assumed as inert material (since not available for the reaction with HCl):

$$\dot{m}_i = 89.6 \cdot \left(1 - \phi_{HCl,Na_2CO_3}\right) = 11.4 \ \frac{kg}{h}$$

Obviously this is a clear oversimplifying assumption, that was introduced in order to obtain only a rough but representative assessment of the role of SO2 competitive reactions in the second stage.

8.2.3 Filtration process

The implementation of the fundamental model to the first stage of the treatment system has highlighted the need for describing the variation of the cake thickness during the process. The information regarding the management of the cleaning system were provided by the fabric filter designer, therefore the modeling of HCl removal with sodium bicarbonate was carried out describing the filtration process. It involves a multi-cycle process of deposition of particles on filter bags followed by filter cake removal. The pulse-jet system, adopted to clean the bags in the analyzed case, causes a complete detachment of the cake from the surface of the filter. Therefore, the modeling can take into account a single cycle.

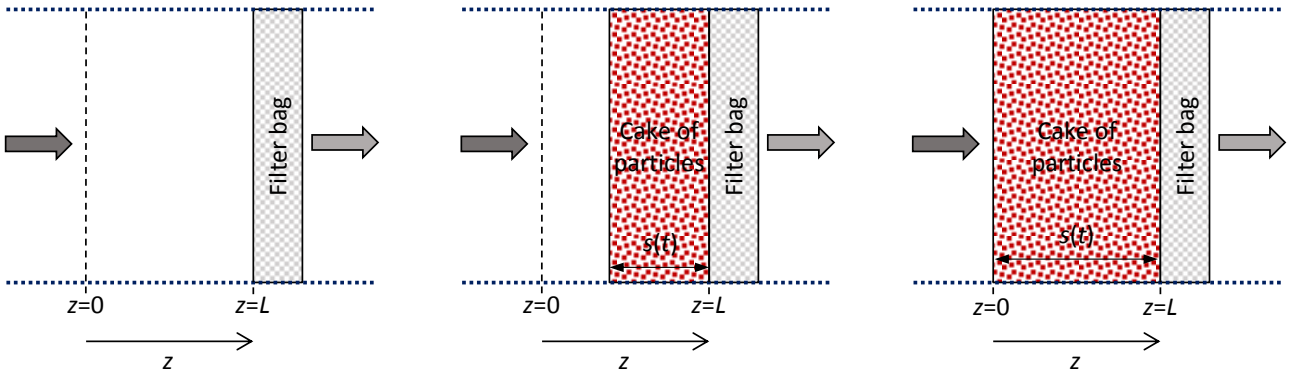

Figure 8.6 - Representation of a filtration cycle. The image on the left represents the system at t = 0, i.e. immediately following filter cleaning. During filtration process dust are collected on the filter bags. When the cake thickness s reaches the maximum allowable value L (right-hand image), the filter is cleaned and the process starts again.

To describe how the sorbent cake builds up in time, its thickness was expressed as a function of the pressure drop in the filter and flue gas velocity. According to Green and Perry (2007), when superficial face velocities used in fabric filters is in the range of 0.3 to 3 m/min, gas pressure drops conform to Darcy's law for streamline flow in porous media. Thus, the pressure drop across the fabric and the collected dust layer is directly proportional to the flow rate and may be expressed as follows

$$\Delta P = k_1 \cdot u_0 + k_2 \cdot s \cdot u_0 \qquad 8.3$$

where

- u_0 is the superficial velocity
- s is the thickness of the dust layer on the filter bags
- k_1 is the resistance coefficient for the conditioned fabric
- k_2 is the resistance coefficient for the dust layer

The specific resistance coefficient for the dust layer k_2 can be estimated using the Ergun correlation:

$$\frac{\Delta P}{s} = 150 \cdot \frac{(1-\varepsilon)^2}{\varepsilon^3} \cdot \frac{\mu_{gas} \cdot u}{{d_p}^2} + 1.75 \cdot \frac{(1-\varepsilon)}{\varepsilon^3} \cdot \frac{\mu_{gas} \cdot u^2}{d_p} \qquad 8.4$$

where d_p is the particle diameter, which can be estimated from the particle size distribution shown in Figure 3.4:

$$d_p = 12.5\ \mu m$$

In the design conditions, the Reynolds number referred to particles results

$$Re_p = \frac{d_p \cdot u_0 \cdot \rho_{gas}}{\mu_{gas}} = 5.6 \cdot 10^{-3}$$

Therefore, the second term on the right-hand side of Eq. 8.4 is negligible and the comparison with Eq. 8.3 leads to the following expression:

$$k_2 = 150 \cdot \frac{\mu_{gas}}{{d_p}^2} \cdot \frac{(1-\varepsilon)^2}{\varepsilon^3} = 3.7 \cdot 10^7 \frac{kg}{m^3 \cdot s}$$

The contribution of the resistance coefficient for the conditioned fabric (k_1) is usually negligible during the filtration process. However, it is crucial to calculate the gas velocity immediately after filter cleaning. Its value was estimated from the pressure drop through the fabric in design conditions provided by filter designer:

$$k_1 = \frac{\Delta P_{fabric}}{u_0} = \frac{70\ Pa}{0.0148\ \frac{m}{s}} = 4.73 \cdot 10^3 \frac{kg}{m^2 \cdot s}$$

The analyzed fabric filter is cleaned through a pulse-jet system, which is based on the injection of blasts of short duration of high pressure air in the bags. The system starts the cleaning when the pressure drop in the whole filter exceeds a desired value. Each blow pipe is dedicated to the cleaning of a row of bags. In the analyzed system, 55 rows are present. Thus, during a filtration cycle, which is defined as the interval between two cleaning of the same bag, there are 54 cleaning phases. Therefore, the cake thickness on a bag was assumed to grow at a constant pressure drop, neglecting the variation due to the particle removal from other bags. This assumption is confirmed by the pressure drops in the two filters during 8 h of operation. Indeed, the variations shown in Figure 8.7 seem to be related to variation in the total flow rate (which is almost the same in the two stage) rather than cleaning phases (which are independent in the two stages).

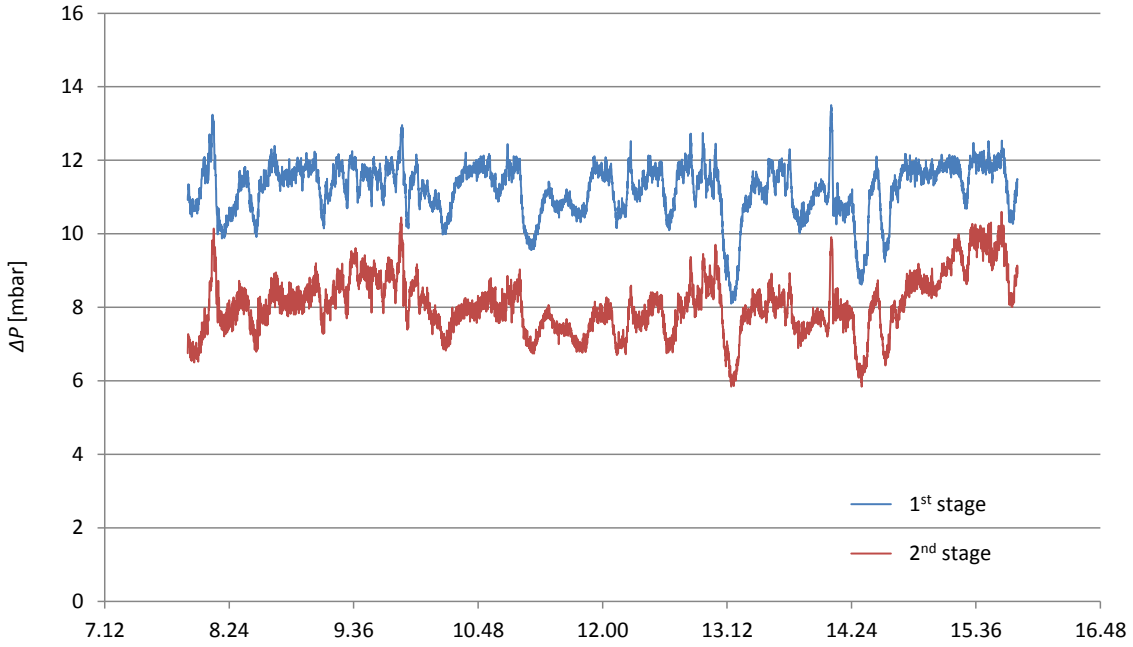

Figure 8.7 - Pressure drops in the first and second stages of the treatment system during an operating period of 8 h.

Therefore, the pressure drop was assumed equal to the design value[43]:

$$\Delta P_{des} = 900\ Pa$$

Under this assumption, the cake thickness *s* can be expressed as a function of time *t* through the equation obtained in Appendix P:

$$s(t) = \sqrt{2 \cdot \frac{c_s}{\rho_b} \cdot \frac{\Delta P}{k_2} \cdot t + \left(\frac{k_1}{k_2}\right)^2} - \frac{k_1}{k_2}$$

while the corresponding filtration velocity results:

$$u(t) = \frac{\Delta P}{\sqrt{2 \cdot \frac{c_s}{\rho_b} \cdot k_2 \cdot \Delta P \cdot t + {k_1}^2}}$$

The profile of the cake thickness in the analyzed case is shown in Figure 8.8.

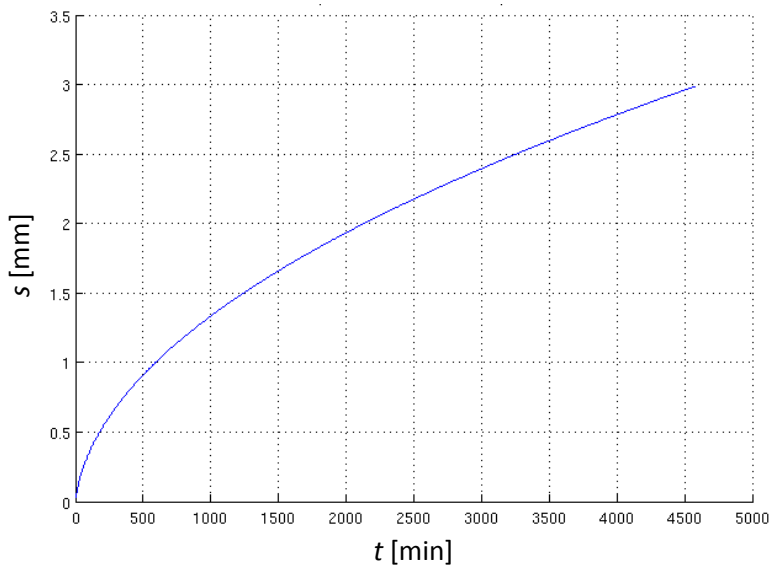

Figure 8.8 - Cake thickness *s* as a function of time *t*.

[43] The cake thickness in design conditions results:

$$s_{des} \cong \frac{\Delta P_{des}}{k_2 \cdot u_0} = 1.6\ mm$$

This thickness is in agreement with information provided by filter producer (at 1500-1800 Pa correspond a cake of 2-3 mm). Therefore, it is reasonable that at 900 Pa the cake thickness is 1.6 mm.

8.2.4 Results

The fundamental model was implemented making use of the parameters estimated according to the correlation proposed in Section 6.5. The solid-state diffusivity through the product layer and reaction rate constant were assumed equal to the values found reproducing the experimental data obtained by Fellows and Pilat (1990) reported in Section 7.2.3:

$$D_s = 5.5 \cdot 10^{-12} \frac{m^2}{s}$$

$$k_s = 2.6 \cdot 10^{-4} \frac{m}{s}$$

With these values, the governing dimensionless group for mass transfer within the particle porosity were estimated:

$$Th_p = 0.175$$

$$Bi = 12.49$$

According to the solutions illustrated in Appendix M, it is possible to neglect the mass transfer resistance in the boundary layer surrounding the particle and within its porosity, assuming a uniform value of the gas concentration.

As both cake thickness and flue gas velocity change during the process, also the Damköhler value is a function of time:

$$Da = \frac{s(t) \cdot k_{glob}(r_c)}{u(t)}$$

The resulting profile of its average value in the cake is portrayed in Figure 8.9.

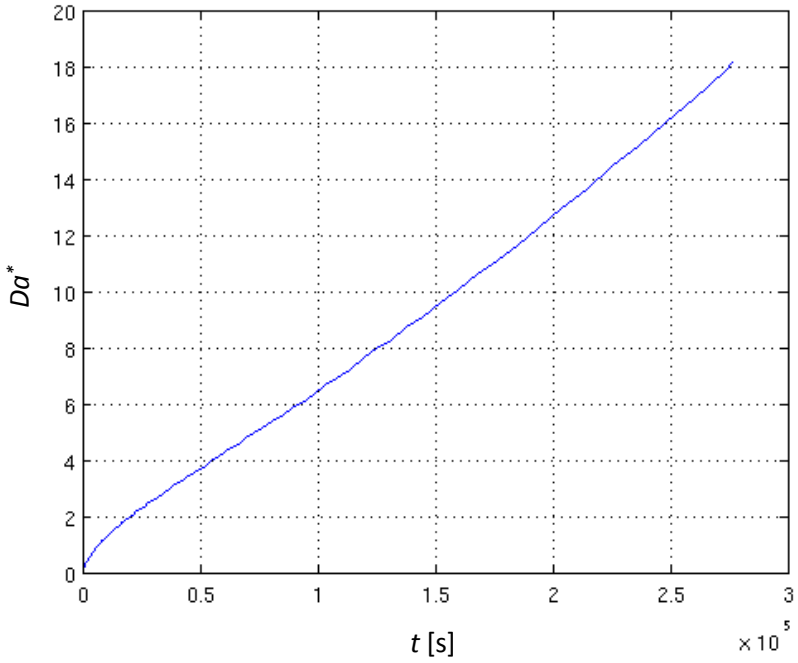

Figure 8.9 - Average value of *Da* number in the bed.

Initially Damköhler value is equal to zero because of the complete detachment of the cake from the surface of the bags. Then there is an increase of the average value related to the accumulation of the sorbent on the filter surface. However, the variation of *Da* with time is not proportional to time because of the variation of the average kinetic term for the consumption of the sorbent.

Also the Peclet group is a function of time:

$$Pe = \frac{u(t) \cdot s(t)}{\varepsilon \cdot D_z}$$

However, after an initial transient, the product $u(t) \cdot s(t)$ is constant (see Appendix P) and the Pe number results:

$$Pe = \frac{\Delta P}{k_2 \cdot \varepsilon \cdot D_z}$$

The resulting conversion of the solid sorbent is illustrated in Figure 8.10 as average conversion in the cake:

$$\chi_{NaHCO_3}{}^{*}(t) = \frac{1}{s(t)} \cdot \int_0^{s(t)} \left(1 - \frac{r_c{}^3}{r_g{}^3}\right) dz$$

The figure shows an initial increase of the conversion, while after a certain time the value decrease for the accumulation of unreacted sorbent.

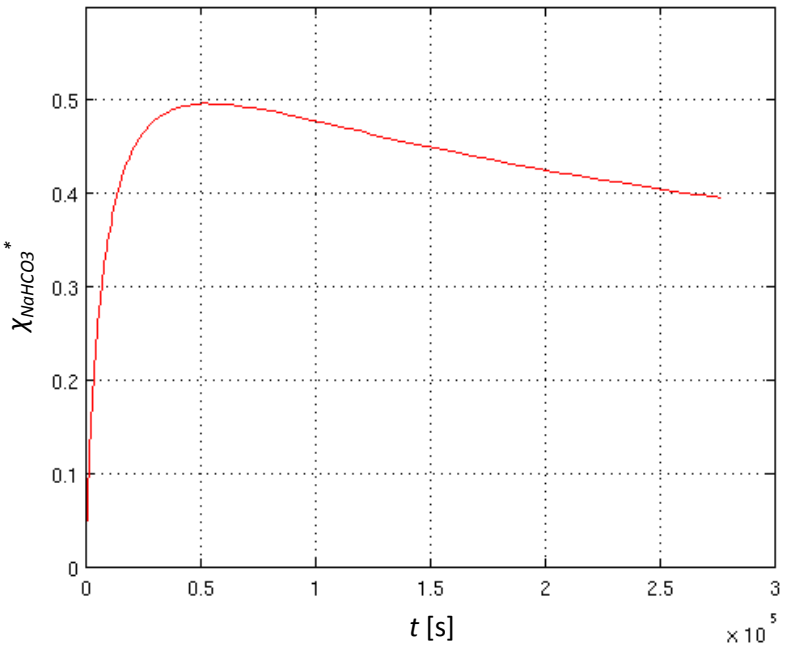

Figure 8.10 – Average conversion of the sorbent in the cake as a function of time.

This behavior is confirmed by the profile of HCl conversion shown in Figure 8.11, which initially is null and then increase reaching 100 %.

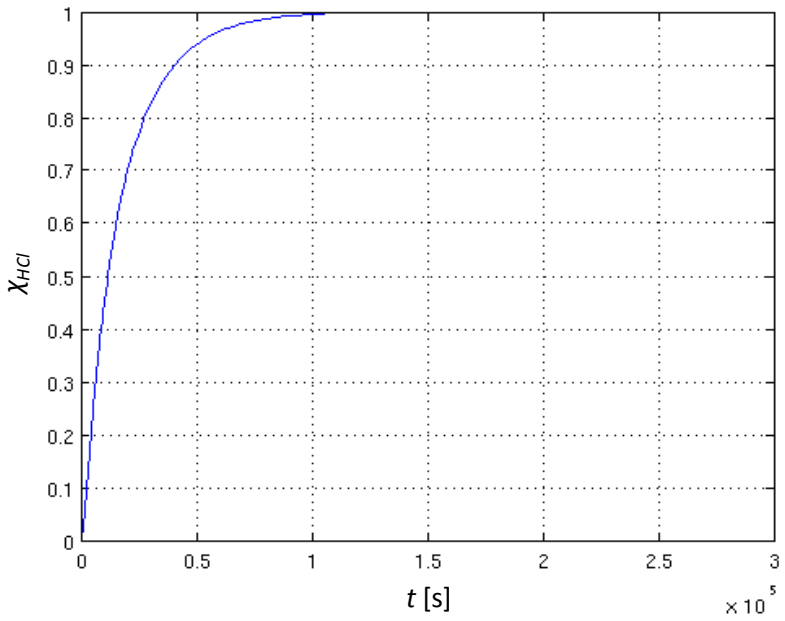

Figure 8.11 – HCl conversion through the filter cake as a function of time.

The average values of the HCl conversion during a filtration cycle are slightly lower than the design value. Nevertheless, these results show that the HCl neutralization is underestimated during the first stages of the process (i.e. immediately following the filter cleaning). This is due to the assumption that the removal takes place only in the filter cake, while the contribution of the reactor should be included in the model. This approach is illustrated in Appendix Q, where the solution of the mass balance equation in the reactor is presented. However, the application of this solution requires a better estimation of the kinetic parameter in the very first instants of the process. Indeed, the parameters used in the model implementation were estimated fitting experimental results obtained through runs of thirty minutes, while the contact time in the reactor is of about 2 seconds. Therefore, dedicated tests should be carried out to investigate the kinetic behavior also on this time interval. The description of an experimental device designed to estimate the model parameters is discussed in Section 9.

9 Planning of experimental runs for kinetic data calculation

9.1 Introduction

A fundamental model based on the description of gas-solid reaction kinetics and mass transport phenomena was described in Section 6. However, how process conditions affect these transport and reaction phenomena, and in turn the removal efficiency, is not well defined and several parameters are required (e.g. particle diameter and porosity, temperature, flue-gas composition). Moreover, the values of some model parameters are affected by relevant uncertainties. Indeed, values reported in literature can differ of orders of magnitude, as evidenced for the reaction between hydrogen chloride and calcium hydroxide by Duo et al. (1993). Therefore, an experimental activity was designed and started up in order to calculate the main parameters of the fundamental model in typical conditions of the analyzed case-study (described in 5.1) and other flue gas treatment processes.

The experimental plant was designed to study the effect of temperature, humidity, competitive reactions (carbonation and SO_2 neutralization), and the characteristics of the sorbent (particle size and specific surface area). This activity is aimed to assess correlations that link the main model parameters, i.e. coefficient of solid-state diffusion through product layer (D_S) and reaction rate constant (k_s), to process parameters. These correlations could then be extended to typical conditions of other processes, for example treatment of flue gas produced by the combustion of biomass and biogas, which are characterized by higher humidity, lower concentrations of pollutants and SO_2 as most critical acid gas. Thus, an experimental apparatus was designed to be adapted for the simulation of also these conditions.

The following sections describe the layout of the laboratory apparatus and main equipment used in the experimental activity. Next, the procedures proposed to reproduce operational conditions of flue-gas treatment systems of a waste-to-energy plant are reported.

9.2 Design of the experimental apparatus

9.2.1 Description of the layout

The designed experimental apparatus consists of a reactor filled with a solid sorbent where a synthetic flue gas is fluxed. The experimental configuration is illustrated schematically in Figure 9.1. A gas stream containing HCl is created to simulate a flue gas. The gaseous stream flows through a fixed bed of solid sorbent particles mixed with quartz beads and kept at constant temperature, which is controlled placing the reactor in an oven supplied with temperature controller. The effluent gas from the reactor is continuously analyzed by means of a Fourier transform infrared (FTIR) spectrometer, which measures the evolution of gaseous products formed in the neutralization process.

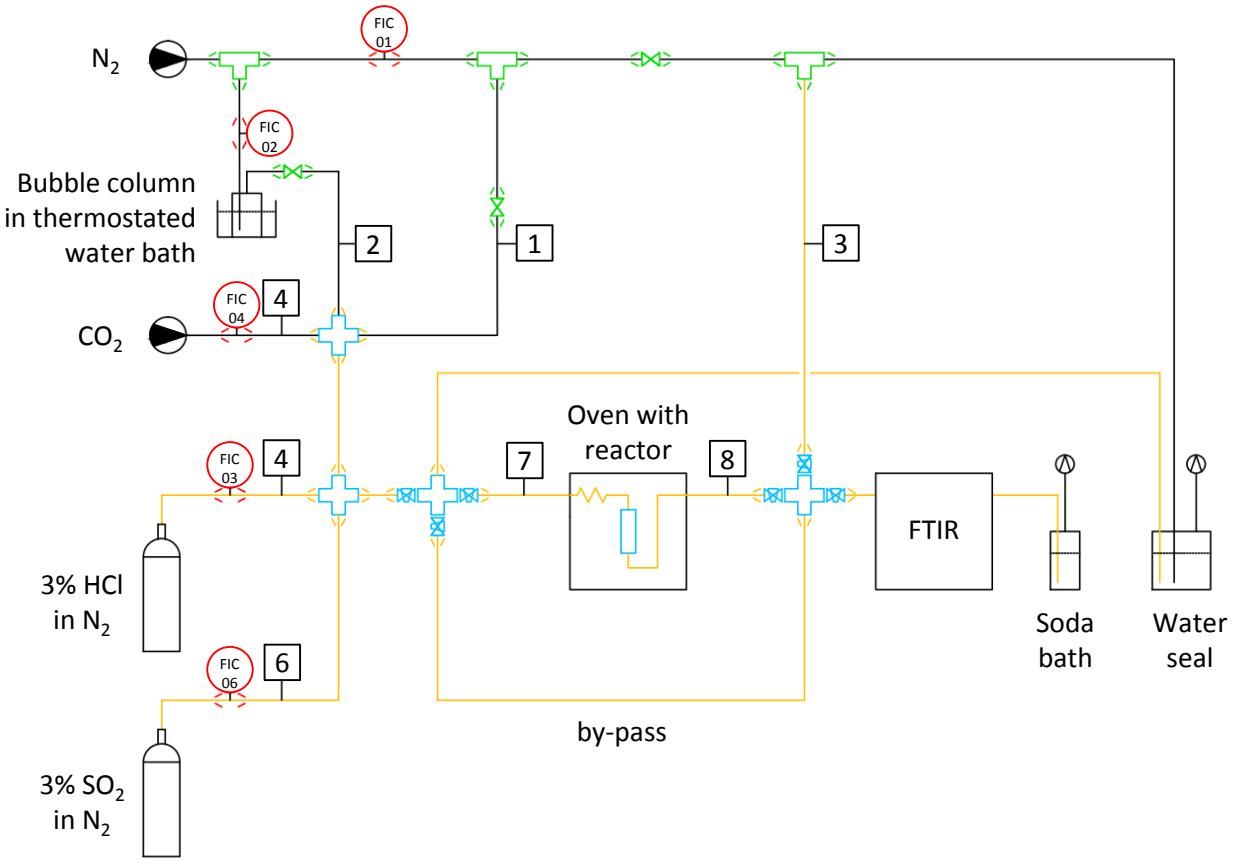

Figure 9.1 – Configuration of the experimental apparatus; nitrogen and carbon dioxide are fed by gas supply lines, while mixtures of HCl and SO_2 in N_2 are provided by cylinders; volumetric flow rates are measured by rotameters (FIC) and gas composition is analyzed by means of an FTIR spectrometer.

The main streams of the experimental system, numbered according to the labels in Figure 9.1, are:

1. Dry nitrogen from laboratory supply line
2. Humidified nitrogen
3. Nitrogen for FTIR purge
4. CO_2 from supply line
5. HCl/N_2 mixture from cylinder
6. SO_2/N_2 mixture from cylinder
7. Reagent gas
8. Effluent gas

Different gas mixtures can be prepared blending N_2, CO_2, H_2O, HCl and SO_2 streams at different flow rates. Two cylinders containing HCl and SO_2, each at 3 % in nitrogen[44], were provided by SIAD, while N_2 and CO_2 (99 % guaranteed purity) are available from supply lines already present in the laboratory. A humidified stream of N_2 can be obtained by means of the passage of the gaseous stream through a bubbling column filled with distilled water and placed inside a thermostatic water bath. Thus, humidity can be controlled through the temperature of the bath, which are related by the Antoine correlation:

$$ln(P^*) = A_{ANT} - \frac{B_{ANT}}{T + C_{ANT}} \qquad 9.1$$

where P^* is vapor pressure, T is the temperature, and A_{ANT}, B_{ANT}, and C_{ANT} are the Antoine vapor-pressure-equation coefficients[45].

The nitrogen streams (no. 1 and 2 in Figure 9.1) are regulated by ASA flowmeters (flow scale: 1-10 NL/h), while CO_2, N_2/HCl, N_2/SO_2 streams are fed through RAGK rotameters by Rota-Yokogawa (flow scales: 4-34 NmL/min for CO_2, 3-30 mL/min for N_2 mixtures). These rotameters are specifically designed for the measurement of low flows and needle valves are integrated for the adjustment of the flow.

The reagent gas, before entering into of the reactor, flows in a section of tube placed inside the oven that is aimed to bring the gas to the design temperature. When the gas reaches the reactors, it flows through a fixed bed of sorbent particles, where neutralization reactions of acid gases take place.

A Fourier transform infrared (FTIR) spectrometer is used to characterize quantitatively the gaseous products of the neutralization process. All the tubing from the humidification section to the inlet of the oven and from the outlet of the oven to the FTIR cell are thermally insulated by wrapping them with silicone heating tape to prevent any condensation. A by-pass permits to flux the reagent gas directly to the FTIR, both before starting the sorption process and at the end of the neutralization process in order to verify the actual composition of the reagent gas.

The section of the apparatus exposed to acid gases (i.e. HCl and SO_2) is composed of tubing and tube fittings made of PTFE[46] (yellow lines in Figure 9.1) and of 3-way stopcocks and cross connectors made of glass (in blue in the figure). The rest of the system is composed of polyamide-11 tubing (black lines) and stainless steel tube fittings (in green).

Finally, the outgoing gas from the FTIR cell flows through a soda bath, which operates as absorption system, while a cylinder with water is used as liquid seal.

[44] Vendor certified a concentration of 3.04 % for HCl and 2.99 % for SO_2.

[45] The values for water are provided by Reid et al. (1977):

- A_{ANT} = 18.3036
- B_{ANT} = 3816.44
- C_{ANT} = -46.13

These values refer to a vapor pressure expressed in millimeters of mercury and a temperature in kelvins; the temperature range of validity is between 284 K (10.85 °C) and 441 K (167.85 °C).

[46] PTFE resists in a temperature range between -200 °C and 260 °C and offers almost universal chemical resistance.

9.2.2 Reactor and oven

The reactor was designed to simulate the conditions of the cake of particles deposited on the filter bags of the system described in Section 5.1. Inner diameter was designed to obtain a superficial velocity of the flue gas of 0.0147 m/s at 180 °C, which corresponds to the design value (according to plant data shown in 8.1.1)[47]. Accordingly, the reactor vessel is a cylinder 150 mm long by 15 mm of ID, as shown in Figure 9.2. The vessel contains a sintered glass frit disk settled at a 20 mm from the outlet section, on which the sorbent is placed. The choice of the materials was made taking into account the gas composition (containing corrosive compounds) and typical working temperature (design value of the analyzed flue-gas treatment plant is 180 °C). Thus, the body of the reactor is made of borosilicate glass, while screw joints and tubing are made of PTFE.

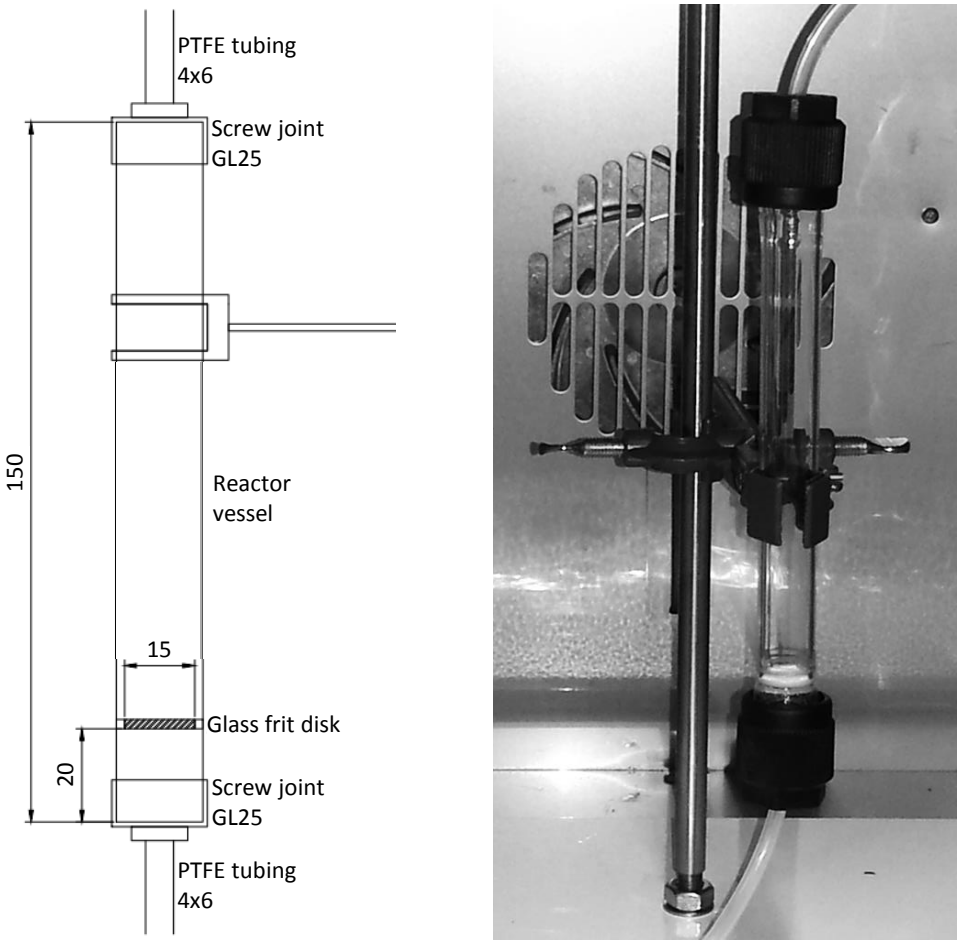

Figure 9.2 – a) Schematization of the designed quartz glass reactor; dimensions are expressed in mm. b) Picture of the reactor placed in the oven.

In order to operate at a constant temperature, the reactor is placed in an oven and a K-type thermocouple is kept in contact with the tubular reactor. The oven is the Binder APT.line™ FD-53 (illustrated in Figure 9.3).

[47] A volumetric flow rate of 150 mL/min was considered in the calculation. This value was set to meet the constraints given by flowmeters ranges and by residence time in the FTIR gas cell. The latter takes into account the instrument scan time. Indeed, since the cell volume is 8.7 mL, a 150 mL/min gas stream has a permanence time of 3.4 s, similar to the 3.7 s that are needed by the instrument to elaborate a spectrum. The pipe entering the FTIR had a diameter of 2 mm, therefore an optimal velocity lower than 1 m/s was achieved.

Figure 9.3 – Binder APT.line™ FD-53 oven (binder-world.com).

This heating oven has mechanical convection and provides a temperature range from 5 °C above ambient temperature to 300 °C (other temperature data are reported in Table 9.1).

Table 9.1 - Temperature and electrical data of the Binder APT.line™ FD-53 oven.

Temperature range		Temperature variation			Heating up time		
min	max	at 70 °C	at 150 °C	at 300 °C	at 70 °C	at 150 °C	at 300 °C
°C	°C	°C	°C	°C	min	min	min
5 °C above ambient temperature	300	0.8	2	3.7	7	24	60

According to producer's website (binder-world.com), the oven present the following performance characteristics:

- Electronically controlled APT.line™ preheating chamber assuring temperature accuracy and reproducible results
- DS control with integrated timer 0 to 99,59 hrs
- Digital temperature setting with an accuracy of one degree
- Independent adjustable temperature safety device class 2 (DIN 12880), with visual temperature alarm
- Adjustable front ventilation flap slide and rear exhaust Ø 50 mm (1.97 inch)

Dimension data of the oven are listed in Table 9.2.

Table 9.2 - Dimension data of the Binder APT.line™ FD-53 oven.

Exterior dimensions			Interior dimensions				Permitted total load	Weight (empty)
Width	Height	Depth	Width	Height	Depth	Volume		
mm	mm	mm	mm	mm	mm	l	kg	kg
635	620	575	400	400	340	53	40	44

9.2.3 FTIR spectrometer

The FTIR spectrometer is a Bruker TENSOR 27 equipped with external gas cell (shown in Figure 9.4). This instrument allows an online measurement of the flue gas composition by recording infrared energy absorbance spectra over time. The reactor was connected to the FTIR spectrometer using a transfer line with a 2 mm internal diameter Teflon tube, heated at a constant temperature of 180 °C to avoid the condensation of acid solutions.

Figure 9.4 – FTIR spectrometer Bruker TENSOR 27 equipped with external gas cell.

FTIR measurements are carried out with a MCT detector in a low volume gas cell (8.7 ml) with a 123 mm pathlength, shown in Figure 9.5. The FTIR scans from 8000 to 400 cm^{-1} with a resolution of 4 cm^{-1} and a frequency of 40 kHz. Every spectrum shown is obtained as average of 16 consecutive scans, giving an absorbance versus wavelength plot every 3.7 s.

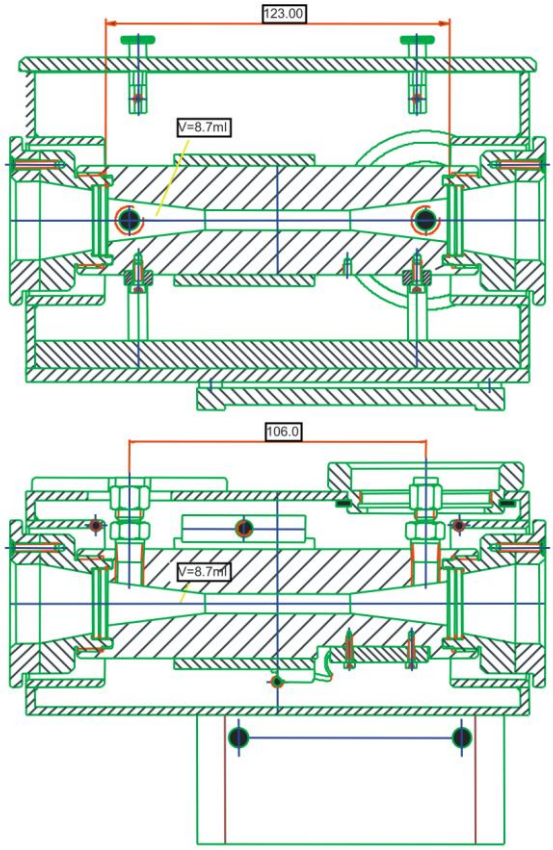

Figure 9.5 – Design of the FTIR gas cell, which has a volume of 8.7 ml and a pathlength of 123 mm.

As FTIR spectrometry was used to characterize quantitatively the gaseous products, thus a calibration is required. This process has to take into account the concurrent presence of a wide number of gaseous compounds[48] (i.e. HCl, SO_2, H_2O, CO_2), which may complicate the interpretation of FTIR data.

[48] Homodinuclear molecules (e.g. oxygen, nitrogen, and chlorine) are transparent to infrared radiation, thus they are detected.

9.3 Design of the experimental conditions and procedure

The first aim of the experiments was the reproduction of the design conditions of the analyzed case-study (described in Section 5.1.2) in order to estimate the corresponding values of the fundamental model parameters (Section 6). Thus, a first series of experiments was planned to simulate acid gas removal with calcium hydroxide, which is the solid sorbent used in the first treatment stage of the analyzed plant.

For the experiments, calcium hydroxide powder supplied by Sigma-Aldrich (> 96% guaranteed purity) was selected. In order to prepare samples with defined diameter distribution, sorbent particles were sieved to five fractions:

1. < 36 µm,
2. 36-45 µm,
3. 45-64 µm,
4. 64-120 µm,
5. > 120 µm.

The fixed bed is prepared with approximately 150-200 mg of calcium hydroxide mixed with the same amount of quartz sand (size: 36-45 µm), which are placed in the reactor on the glass frit support. The mass of sorbent was chosen to obtain a thickness of the particle layer of the same size of the filter cake usually deposited on filter bags[49]. Quartz sand is used as inert material to prevent solids agglomeration and gas channeling through the sorbent bed, according to the experimental results of Fellows and Pilat (1990). The reactor is then inserted into the oven and brought to the design temperature (usually 180 °C).

Table 9.3 – Calculation for bed thickness.

2-hour experiment: quantity of HCl fluxed (1)	mol	$2.47 \cdot 10^{-3}$
Stoichiometric quantity of $Ca(OH)_2$	mol	$1.23 \cdot 10^{-3}$
Stoichiometric excess	-	100 %
Resulting mass of $Ca(OH)_2$	g	0.183
Mass of quartz sand (2)	g	0.183
Bulk density of $Ca(OH)_2$	kg/m^3	550
Bulk density of quartz sand	kg/m^3	1500
Resulting bed thickness	mm	2.57
Notes: (1) referred to typical experimental conditions (reported in Table 9.4 and Table 9.5) (2) required fraction of inert material: 50 %		

Tubing, reactor and spectrometer are purged with nitrogen as long as FTIR spectrometer detects compounds other than N_2. Control valves are then adjusted so that the gas stream is directed around the reactor through the bypass line (see Figure 9.1). Thus, the desired gas composition can be synthesized and reach a steady state. This procedure provides the measure of the reagent gas composition for the following run. The gas is then fluxed through the reactor, where the acid gases react with the sorbent. At the end of the removal

[49] The mass of sorbent chosen for the experiments is related to the amount of acid gases which are flowed during the entire run. As 2-hour experiments were planned, a bed thickness of 2.6 mm was obtained according to the calculations reported in Table 9.3.

process, the gas flow is switched again to the bypass to verify the final gas composition by FTIR analysis, keeping the reactor isolated.

The volumetric flow rate of the reagent gas (stream 7 in Figure 9.1) is initially set so as the velocity in the particle layer corresponds with the flue gas velocity in the filter cake of the first stage of the analyzed treatment system (i.e. 0.0147 m/s at 180 °C). Thus, the volumetric flow rate has to be set to 93.6 mL/min [50], as shown in the last column of Table 9.4. Flow rates of feed streams (no. 1, 2, 4, 5, and 6 in Figure 9.1) are set in order to obtain the composition reported in design data of the analyzed system (Section 5.1.2). However, some variations are required for experimental restrictions. The most important regarded the HCl and SO_2 concentrations, which are initially set to 10 times the concentrations in design conditions to ensure that the FTIR could detect the acid gases.
Another adjustment regards humidity. Indeed, the first set of experiments was designed in dry conditions to avoid the possible interference of water vapor in FTIR analysis. The corresponding volumetric flow rates and compositions of streams 1-7 are reported in Table 9.4.

Table 9.4 – Volumetric flow rates and compositions of the streams in the case without humidity (stream numbers are given according to the layout shown in Figure 9.1).

Stream		1	2	4	5	6	7
Description		Dry nitrogen	Humidified nitrogen	CO_2 from supply liny	N_2/HCl from cylinder	N_2/SO_2 from cylinder	Reagent gas
Volumetric flow rate [(a)]	mL/min	48.2	0.0	8.0	15.6	21.8	93.6
Temperature	°C	20	-	20	20	20	20
N_2	vol%	100	-	-	97.0	97.0	90.3
H_2O	vol%	-	-	-	-	-	-
CO_2	vol%	-	-	100	-	-	8.50
HCl	vol%	-	-	-	3.0	-	0.5
SO_2	vol%	-	-	-	-	3.0	0.7
[(a)] Volumetric flow rate values are referred to 0 °C and 1 atm.							

Once determined the IR spectrum without humidity, following runs can be carried out introducing water vapor into the reagent gas. The design value of water fraction is achievable adjusting the volumetric flow rate and the temperature of stream 2, which is a nitrogen stream at 60 °C saturated with water. Volumetric flow rates and compositions for this case are reported in Table 9.5.

[50] This value is referred to standard conditions, i.e. 0 °C and 1 atm.

Table 9.5 – Volumetric flow rates and compositions of the streams in the case with humidity (stream numbers are given according to the layout shown in Figure 9.1).

Stream		1	2	4	5	6	7
Description		Dry nitrogen	Humidified nitrogen	CO_2 from supply liny	N_2/HCl from cylinder	N_2/SO_2 from cylinder	Reagent gas
Volumetric flow rate [(a)]	mL/min	29.5	18.7	8.0	15.6	21.8	93.6
Temperature	°C	20	60	20	20	20	20
N_2	vol%	100	80	-	97.0	97.0	86.3
H_2O	vol%	-	20 [(b)]	-	-	-	4.0
CO_2	vol%	-	-	100	-	-	8.5
HCl	vol%	-	-	-	3.0	-	0.5
SO_2	vol%	-	-	-	-	3.0	0.7

[(a)] Volumetric flow rate values are referred to 0 °C and 1 atm.
[(b)] Water vapor fraction was calculated through Eq. 4.12.

The effluent gas coming from the reactor (stream 8) enters the gas cell operating with an FTIR spectrometer. The concentration of the acid gases during the experiment can be assessed from the area under the characteristic peaks of the each compound. According to Chisholm and Rochelle (1999), for HCl the peak located from 2828 to 2814 cm^{-1} can be used, while for SO_2 the wavelength range to analyze is located between 1360 and 1340 cm^{-1}.

In this process, the importance of CO_2 and H_2O in the gas was demonstrated by several authors (e.g. Weinell et al, 1992; Chisholm and Rochelle, 1999; Chin et al., 2005). However, the influence of these compounds on HCl and SO_2 removal efficiencies is not well defined. Thus, other simulations were scheduled to analyze systematically how process parameters affect the acid gas removal, varying selectively humidity, CO_2 concentration and the ratio of HCl to SO_2.

Other experiments that can be carried out with the experimental apparatus consist in using sodium bicarbonate as solid sorbent. These runs were planned to reproduce the data reported in literature (e.g. Fellows and Pilat, 1990; Duo et al., 1996; Verdone and De Filippis, 2006) and to extend these results to the operating conditions of the second stage of the analyzed plant, in order to assess fundamental model parameters also for this process.

10 Conclusions

The first part of this study was dedicated to the description of the waste management issue, focusing on the European situation. This analysis highlighted the important role of thermal treatments with energy recovery among the available technological options for waste management. Indeed, energy recovery from municipal solid waste (MSW) incineration has continuously increased in Europe in the last ten years and a continuously increasing role of incineration should be expected in the future due to increasing concern over waste in landfills and increased energy cost.

Even though substantial improvements were already achieved in reducing emissions to air from Waste-to-Energy plants, the potential environmental impacts given by the increased use of W-t-E processes in last years has pointed out the need for more efficient treatment systems. Particular attention has to be paid to air pollutant emissions from incineration facilities, which have become a subject of public concern and of demanding regulations. Among air contaminants, the removal of acid gases (mostly hydrogen chloride, HCl) is of particular interest because they are directly related to the combustion process of waste. Moreover, flue-gas treatment systems are required to reduce not only air emissions, but also waterborne emissions and residue disposal. The two-stage dry treatment system emerged as one of the most promising techniques for acid gas removal. The use of two sorbents, powdered calcium hydroxide and sodium bicarbonate, showed a very high performance. However, due to the relatively scarce industrial experience present on this two-stage technology, there is still a lack of knowledge about the efficiency and yields of flue-gas treatment stages. Consequently, there is a strong need to analyze the relationships between the quantity and characteristics of air pollutant emissions and the operating conditions and design of air-pollution-control (APC) devices. Therefore, the acid gas removal process was modelled in order to optimize the use of solid reactants and to reduce the unreacted solids in dry systems.

In the second part of the study, an operational model was derived from the analysis of literature data and was proposed to describe the removal efficiency of acid gases (HCl, HF and SO_2) in the flue gas treatment of a MSW incineration plant. The model was developed considering the ratio of actual solid reactants feed rates to stoichiometric values. The model was implemented and calibrated to describe the removal efficiency of acid gases in the flue gas treatment section of an existing waste to energy plant, where the acid gas cleaning system is constituted by a two-stage dry treatment system. In this process, solid sorbents are calcium hydroxide in the first stage and sodium bicarbonate in the second stage. The implementation of the model within the Aspen Hysys software allowed the reproduction of the average process conditions of the case-study analyzed, calculated using operational data measured over a period of 13 days. Although process data were rather scattered, the results showed that the model could be applied to describe the operating conditions of the plant, even though further calibration (e.g. based on specific test-runs) could be required to properly describe the removal process in different conditions. The analysis of process operating costs based on reactant and solid disposal costs and the identification of an economic optimum were possible by the application of the model. Simulations were carried out to find optimal operating conditions for three selected days of operation. For each considered condition, a minimum in overall costs was always present. These conditions correspond to an HCl conversion in the first stage between 60% and 65%, depending mostly on the concentration of HCl in the flue gas. However, for simulated conditions with higher HCl content in raw flue gas, the range of sorbent feed rate that optimizes the operation is narrower, indicating that a more accurate management of the system is required when operating in such conditions. Simulations showed that the optimization of sorbent feed rates would permit to save between 3% and 8% on the cost of the solid reagents and of their disposal with respect to the actual operating conditions adopted in the analyzed period.

The model was then applied in order to simulate alternative configurations for the analyzed flue-gas cleaning system. Simulation results showed that if calcium hydroxide was used in both stages, operating costs would be higher. Conversely, a two-stage system with sodium bicarbonate would allow a slight reduction of operating costs, especially when the HCl concentration in the flue gas is higher. However, the difference with the current configuration is not significant, thus the advantage of using bicarbonate in both stages should be confirmed calculating the model parameters with operational data covering the entire simulated range.

The third section of the present document was aimed at the description of the development of a fundamental model based on rigorous mass transfer and kinetic equations. This approach was adopted to predict the acid gas removal in different operating conditions making use of fundamental parameters obtained from literature or experimental data. The sorbent particles were described according to the grain model, which considers spherical particles made up of smaller spherical grains of equal size. This representation allowed including into the model some physical properties of the reacting solid (i.e. particle diameter, specific surface area, porosity and tortuosity). The model was implemented to solve differential mass balance equations describing the mass transport phenomena governing the gas-solid reaction involved in the acid gas removal process. The model has been validated reproducing literature data obtained in typical operating conditions of dry treatment systems. In these conditions, hydrogen chloride removal process resulted to be controlled by chemical reaction in the first stages of the process and by solid-state diffusion through the product layer when the reaction further proceeds. Therefore, the values of the reaction rate constant and of solid-state diffusivity were estimated for HCl neutralization with both calcium hydroxide and sodium bicarbonate at different temperatures.

The fundamental model was then applied to describe HCl removal in the flue-gas treatment system of the analyzed plant. The parameters were estimated from design conditions, taking into account temperature, composition and flow rate of the flue gas, chemical and physical properties of the solid sorbent and fabric filter design. The adaptation of the model to the first stage of the analyzed system, where the HCl removal is achieved through the injection of calcium hydroxide, took into account the presence in the flue gas of fly ash and partially reacted particles (coming from the recycle of separated solids). The simulations permitted to estimate accurately enough the consumption of the solid sorbent. However, the acid gas conversion resulted overestimated, especially in the first stages of the process. The difference with respect to design data is probably due to the effect of CO_2, which consumes part of the sorbent. Another simplifying assumption was the instantaneous formation of the sorbent cake after filter cleaning. Indeed, a proper description of the transient require the modeling of the cake growing. Therefore, the filtration process was implemented in the simulation of the second stage, where the variation of the cake thickness was considered. In this stage, also the sorbent consumption due to SO_2 neutralization was taken in to account. Indeed, the relative amount of SO_2 in the second stage is higher than in the first stage for the low removal efficiency of calcium hydroxide for this pollutant. The results obtained for a cleaning cycle, defined as the interval between two cleanings of the same filter bag, permitted to analyze the sorbent consumption and the acid gas conversion. In this case, the HCl neutralization efficiency resulted underestimated after cake removal because a not negligible conversion is achieved also in the reactor upstream to the fabric filter. However, a more accurate estimation of the model parameters in these conditions is required, due to the different time scales of the two processes (reaction in the reactor and within the filter cake).

Finally, a specific activity was dedicated to the design and start-up of an experimental apparatus. This activity aimed to determine the main model parameters (i.e. reaction rate constant and solid-state diffusivity through the product layer) in typical operating conditions of flue-gas treatment systems, where humidity, competitive reactions (e.g. carbonation and SO_2 neutralization), and heterogeneous characteristics of the sorbent

(particle size and specific surface area) affect the overall removal efficiencies. The experimental apparatus was designed to simulate the composition of flue-gas produced by the combustion of waste, biogas and biomass. Therefore, the system may be fed with N_2, H_2O, CO_2, HCl and SO_2 which can mixed up to different concentrations to simulate different flue-gases. Materials were selected to guarantee an operability up to 200 °C, while different contact times permit to study the sorbent conversion in the operating conditions of fabric filters and other technologies (e.g. cyclones, electrostatic precipitators). The evolution of gaseous products is analyzed by means of a Fourier transform infrared (FTIR) spectrometer.

References

10.1 Articles and books

- Antonioni, G., Sarno, F., Guglielmi, D., Morra, P., Cozzani, V., 2011. Simulation of a two-stage dry process for the removal of acid gases in a MSWI. Chem. Eng. Trans. 24, 1063–1068, http://dx.doi.org/10.3303/CET1124178
- Antonioni, G., Guglielmi, D., Stramigioli, C., Cozzani, V., 2012. MSWI flue gas two-stage dry treatment: modeling and simulation. Chem. Eng. Trans. 26, http://dx.doi.org/10.3303/CET1226036
- Antonioni, G., Guglielmi, D., Cozzani, V., Stramigioli, C., Corrente, D., 2013. Modelling and simulation of an existing MSWI flue gas two-stage dry treatment. Process Safety and Environmental Protection, http://dx.doi.org/10.1016/j.psep.2013.02.005
- Aspen HYSYS 7.1, 2009. User's Guide, Aspen Technology Inc., Burlington, MA, USA.
- Astrup, T., 2008. Management of APC residues from W-t-E Plants - An overview of management options and treatment methods, Report of ISWA Working Group on Thermal Treatment of Waste, Second edition.
- Baukal Jr., C.E., 2003. Industrial Combustion Pollution and Control, 1st edition, CRC Press
- Bodénan, F., Deniard, P. (2003). Characterization of flue gas cleaning residues from European solid waste incinerators: assessment of various Ca-based sorbent processes. Chemosphere, 51(5), 335-347.
- Brivio, S., 2007. Depurazione dei fumi e valorizzazione dei prodotti (Flue gas cleaning and by-products valorisation). Power Technol. 4, 42–44 (in Italian).
- Chin, T., Yan, R., Liang, D.T., Tay, J.H., 2005. Hydrated lime reaction with HCl under simulated flue gas conditions. Ind. Eng. Chem. Res. 44 (10), 3742–3748.
- Chisholm, P.N., Rochelle, G.T., 1999. Dry absorption of HCl and SO_2 with hydrated lime from humidified flue gas. Ind. Eng. Chem. Res. 38 (10), 4068–4080.
- Cooper, C.D., Alley, F.C., 2004. Air Pollution, in: Dorf, R.C., The Engineering Handbook, Second Edition, Chapter 89.
- Cooper, C.D., Alley, F.C., 2010. Air Pollution Control: A Design Approach, fourth ed. Waveland Pr Inc., Long Grove, IL.
- Duo, W., Seville, J.P.K., Kirkby, N.F., Clift, R., 1993. Prediction of Dry Scrubbing Process Performance, in: Clift, R., Seville, J.P.K., Gas Cleaning at High Temperatures, Springer Netherlands, 644-662.
- Duo, W., Kirkby, N.F., Seville, J.P.K., Clift, R., 1995. Alteration with reaction progress of the rate limiting step for solid-gas reactions of Ca-compounds with HCl. Chemical Engineering Science, 50(13), 2017-2027.
- Duo, W., Kirkby, N.F., Seville, J.P.K., Kiel, J.H.A., Bos, A., Den Uil, H., 1996. Kinetics of HCl reactions with calcium and sodium sorbents for IGCC fuel gas cleaning, Chemical Engineering Science, 51(11), 2541-2546
- Fellows, K.T., Pilat, M.J., 1990. HCl Sorption by Dry NaHCO3 for Incinerator Emissions Control, Journal of the Air & Waste Management Association, 40(6), 887-893.
- Fogler, S., 2006. Elements of Chemical Reaction Engineering, 4th edition, Prentice Hall Professional Technical Reference
- Fonseca, A.M., Órfão, J.J., Salcedo, R.L., 1998. Kinetic modeling of the reaction of HCl and solid lime at low temperatures. Industrial & engineering chemistry research, 37(12), 4570-4576.
- Green, D., Perry, R., 2007. Perry's Chemical Engineers' Handbook, McGraw-Hill Professional, 8 edition

- Guiochon, G., Felinger, A., Shirazi, D.G., Katti, A.M., 2006. Fundamentals of Preparative and Nonlinear Chromatography, Academic Press, Second Edition
- Jannelli, E., Minutillo, M., 2007. Simulation of the flue gas cleaning system of an RDF incineration power plant. Waste Manage. 27 (5), 684–690.
- Karlsson, H.T., Klingspor, J., Bjerle, I. (1981). Adsorption of hydrochloric acid on solid slaked lime for flue gas clean up. Journal of the Air Pollution Control Association, 31(11), 1177-1180.
- Harker, J.H., Backhurst, J.R., Richardson, J.F., 2002. Coulson and Richardson's Chemical Engineering Volume 2 - Particle Technology and Separation Processes, Butterworth-Heinemann, 5th edition
- Levenspiel, O., 1998. Chemical Reaction Engineering, 3rd ed. John Wiley & Sons
- Mura G., Lallai A., 1994. Reaction kinetics of gas hydrogen chloride and limestone, Chemical Engineering Science, 49 (24 A), 4491-4500
- Niessen, W.R., 2010. Combustion and Incineration Processes: Applications in Environmental Engineering, Fourth edition, CRC Press
- Patankar, S., 1980. Numerical heat transfer and fluid flow, Taylor & Francis, ISBN-10: 0891165223, ISBN-13: 978-0891165224
- Reid, R. C., Prausnitz, J.M., Sherwood, T.K., 1977. The properties of gases and liquids, McGraw-Hill, 3rd edition
- Rémond, S., Pimienta, P., Bentz, D.P., 2002. Effects of the incorporation of Municipal Solid Waste Incineration fly ash in cement pastes and mortars: I. Experimental study, Cement and Concrete Research, Volume 32, Issue 2, Pages 303-311, ISSN 0008-8846, http://dx.doi.org/10.1016/S0008-8846(01)00674-3.
- Szekely, J., Evans, J.W., Sohn, H.Y., 1976. Gas-Solid Reactions, Academic Press
- Verdone, N., De Filippis, P., 2004. Thermodynamic behaviour of sodium and calcium based sorbents in the emission control of waste incinerators. Chemosphere 54 (7), 975–985.
- Verdone, N., De Filippis, P., 2006. Reaction kinetics of hydrogen chloride with sodium carbonate, Chemical Engineering Science 61, 7487 – 7496
- Villani, B., Cavazzuti, C., Peronace, M.C., Costantino, R., Bonazzi, E., Gironi, P., 2011. Annuario regionale dei dati ambientali 2010–Cap. 5. Arpa Emilia-Romagna (in Italian).
- Wehner, J. F., Wilhelm, R. H., 1956. Boundary conditions of flow reactor, Chem. Eng. Sci. 6, 89–93
- Weinell C.E., Jensen P.I., Dam-Johansen K., Livbjerg H., 1992. Hydrogen chloride reaction with lime and limestone: kinetics and sorption capacity, Ind. Eng. Chem. Res., 31 (1), 164–171
- Yassin, L., Lettieri, P., Simons, S.J.R., Germanà, A., 2007. Study of the process design and flue gas treatment of an industrial-scale energy-from-waste combustion plant. Ind. Eng. Chem. Res. 46, 2648–2656.

10.2 Web references

- Air Liquide, 2011. Hydrogen chloride material safety data sheets, accessed: 20/12/2013, from <http://www.us.airliquide.com/en/sds.html>
- binder-world.com, from <http://www.binder-world.com/en/heating-oven-heating-chamber/fd-series/fd-53/>
- Eurostat, 2013. Energy, transport and environment indicators, Publications Office of the European Union, Luxembourg, ISBN 978-92-79-33105-3, ISSN 1725-4566, doi:10.2785/4663, accessed: 02/02/2014, from <http://epp.eurostat.ec.europa.eu>

- Gruppo Hera, 2010. Il termovalorizzatore del territorio di Forlì, accessed: 20/12/2013, from <http://www.gruppohera.it>
- LCP BREF, 2006. Reference Document on Best Available Techniques for Large Combustion Plants, European Commission, July 2006, from <eippcb.jrc.ec.europa.eu/reference/>
- LCP BREF, 2013. Best Available Techniques Reference Document for the Large Combustion Plants, European IPPC Bureau – Joint Research Centre, Draft 1, June 2013, from <eippcb.jrc.ec.europa.eu/reference/>
- Solvay, 2005. Flue gas cleaning with sodium bicarbonate and recycling of residual sodium chemicals, accessed: 20/12/2013, from <http://didattica.dma.unifi.it/WebWrite/pub/Trash/PaginaPrincipale/NEUTRECESOLVAL.pdf>
- Solvay, 2012. Clean Air - Sustainable Recycling, , accessed: 20/12/2013, from http://www.solvairsolutions.com/EN/Literature/Literature.aspx
- WI BREF, 2006. Reference Document on the Best Available Techniques for Waste Incineration, European Commission, August 2006, from <eippcb.jrc.ec.europa.eu/reference/>

10.3 Legislation

- D.Lgs. 11-5-2005 n. 133, Attuazione della direttiva 2000/76/CE, in materia di incenerimento dei rifiuti, Gazz. Uff. 15 luglio 2005, n. 163, S.O. (in Italian).
- Directive, 2010/75/UE of the European Parliament and of the Council of 24 November 2010 on industrial emissions (Integrated Pollution Prevention and Control)
- D.Lgs. 3-12-2010 n. 205, Disposizioni di attuazione della direttiva 2008/98/CE del Parlamento europeo e del Consiglio del 19 novembre 2008 relativa ai rifiuti e che abroga alcune direttive, Pubblicato nella Gazz. Uff. 10 dicembre 2010, n. 288, S.O
- L. 6-8-2013 n. 96, Delega al Governo per il recepimento delle direttive europee e l'attuazione di altri atti dell'Unione europea - Legge di delegazione europea 2013, Pubblicata nella Gazz. Uff. 20 agosto 2013, n. 194.

11 Appendices

Appendix A Waste generation and management in Europe

The report "Energy, transport and environment indicators" produced by Eurostat (Eurostat, 2013) presents an overview of the growing global political importance of issues such as climate change and energy security, where energy, transport and environment sectors have become increasingly interconnected. The present appendix shows main statistic data regarding waste generation and management in Europe extracted from the Eurostat's report.

Waste generation in EU-28

According to statistical data reported in Eurostat 2013, 2404 million tonnes of non-hazardous waste were generated in the EU-28 in 2010, registering almost the same value of 2008, while hazardous waste production was 101 million tonnes (+ 4 % with respect to 2008).

An analysis of waste generation by economic activity and households is illustrated Figure 11.1. The activities that generated higher levels of waste were construction (with 860 million tonnes, corresponding to 34 % of the total waste production), and mining and quarrying (672 million tonnes, 27 %). Other important activities were manufacturing (accounted for an 11 % share) and households (9 %).

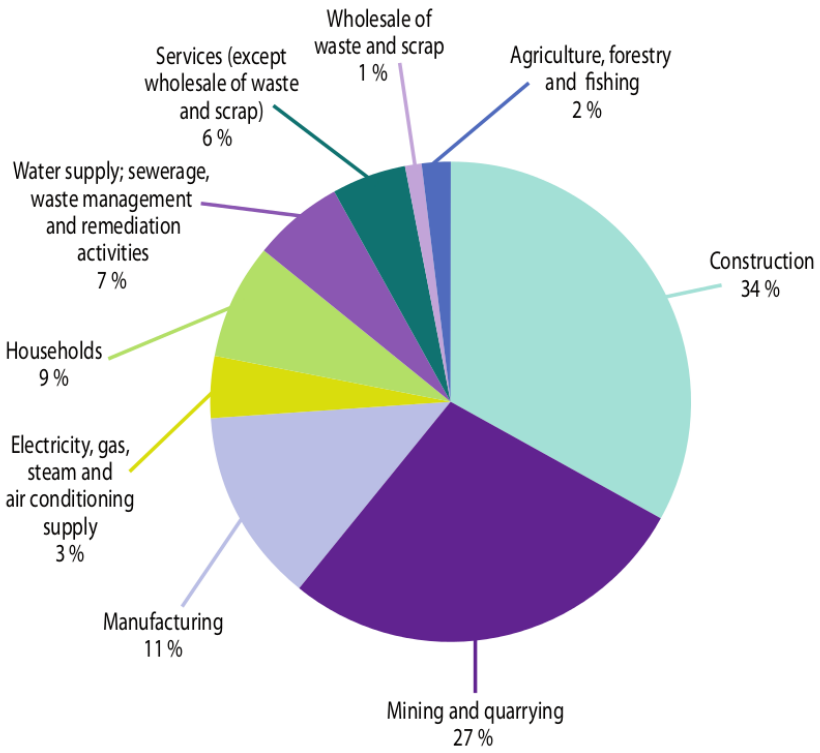

Figure 11.1 - Waste generation by economic activity and households in EU-28 in 2010 (Eurostat, 2013).

Municipal waste

Table 11.1 presents the amount of municipal waste generated per inhabitant in the period 2001-2011. Municipal waste consists mainly of waste generated by households, but also includes similar wastes generated by small businesses and public institutions; this part depends on the local waste management system. For areas not covered by a municipal waste collection scheme, the amount of waste generated is estimated.

Table 11.1 - MSW generated in the period 2001-2011; values are expressed in kg per inhabitant per year (Eurostat, 2013).

	2001	2005	2008	2009	2010	2011	Change 2001-2011 (%)
EU-28 (1)	:	:	518	508	504	499	-3.7
BE	470	479	489	489	465	464	-1.3
BG	499	475	474	470	410	375	-24.8
CZ	273	289	305	316	317	320	17.2
DK	606	662	741	693	673	719	18.6
DE	632	565	589	592	602	597	-5.5
EE (2)	373	436	391	337	303	298	-20.1
IE	699	731	729	662	636	623	-10.9
EL (3)	416	437	452	457	521	496	19.2
ES	654	592	556	547	516	498	-23.9
FR	526	530	541	535	533	527	0.2
HR (4)	:	326	403	393	369	373	14.4
IT	516	540	543	533	537	535	3.7
CY	650	670	722	736	689	658	1.2
LV	303	311	332	334	304	350	15.5
LT	377	377	408	361	381	442	17.2
LU	646	672	697	679	679	687	6.3
HU	452	461	454	430	403	382	-15.5
MT	540	623	670	647	598	583	8.0
NL (3)	613	624	624	612	593	596	-2.8
AT	576	616	599	588	558	552	-4.2
PL	290	319	320	316	315	315	8.6
PT	471	450	515	517	513	487	3.4
RO	341	378	392	362	365	365	7.0
SI	478	494	542	524	490	411	-14.0
SK	239	289	328	322	333	327	36.8
FI	465	478	521	480	470	505	8.6
SE	442	481	513	482	465	460	4.1
UK	591	583	544	526	521	518	-12.4
IS	467	516	551	556	572	571	22.3
NO (5)	361	426	487	470	469	483	33.8
CH	660	661	736	702	708	689	4.4
MK (1)	:	:	349	354	351	357	2.3
RS (1)	:	:	350	360	360	361	3.1
TR	454	435	400	419	407	395	-13.0

(1) No data for 2001; Change 2008-2011.
(2) Break in series in 2001 and 2010.
(3) Break in series in 2010.
(4) No data for 2001; Change 2005-2011.
(5) Break in series in 2001.

Waste management

Data regarding the waste management in EU-28 are reported in Table 11.2 for 2010. Recovery (other than energy recovery) accounts for 49 % of the waste treated in the EU-28, while 45 % was subject to disposal operations other than incineration (mostly landfilling, but also disposal in mining sites and discharge into water bodies). Waste incinerated with energy recovery accounts for a 4 % of the total waste treated in EU-28, while incineration without energy recovery represents a 2 %.

Table 11.2 - Waste management in EU-28 Member States in 2010; values are expressed in thousand tonnes (Eurostat, 2013).

	Recovery	Energy Recovery	Incineration	Disposal
EU-28	1145110	89650	42280	1061680
BE	20414	4797	1975	3172
BG	1819	144	2	157886
CZ	13220	767	55	4204
DK	6767	2749	0	1828
DE	241563	28423	12646	66932
EE	5956	336	0	11661
IE	3356	168	43	5854
EL	11722	126	21	58520
ES	80289	2523	412	49464
FR	200677	14241	7809	113294
HR	403	110	24	2048
IT	93037	2373	6092	25655
CY	1381	7	7	976
LV	312	63	0	630
LT	1062	111	2	3371
LU	6286	32	124	6105
HU	5125	859	82	7357
MT	129	0	7	1065
NL	57563	5835	3552	46691
AT	14982	1364	1649	11756
PL	109695	3804	369	32712
PT	7583	2343	419	9771
RO	16561	1507	75	194716
SI	3885	282	35	1436
SK	3559	255	66	3812
FI	31999	9847	389	63395
SE	16587	6261	87	87541
UK	189183	316	6343	89832
IS	340	19	0	167
NO	2566	1280	276	2170
MK	331	0	1	1775
RS	565	26	1	32466
TR	197216	126	27	580102

Landfilling

In 2010, excluding major mineral wastes, 930 million tonnes of waste were generated in the EU-28. This value, expressed relatively to population, corresponds to an average of 1839 kg per inhabitant in the EU-28. Even though landfilling should be minimized, 23 % of the total generation of waste (excluding major mineral wastes) was landfilled in 2010, as shown in Figure 11.2.

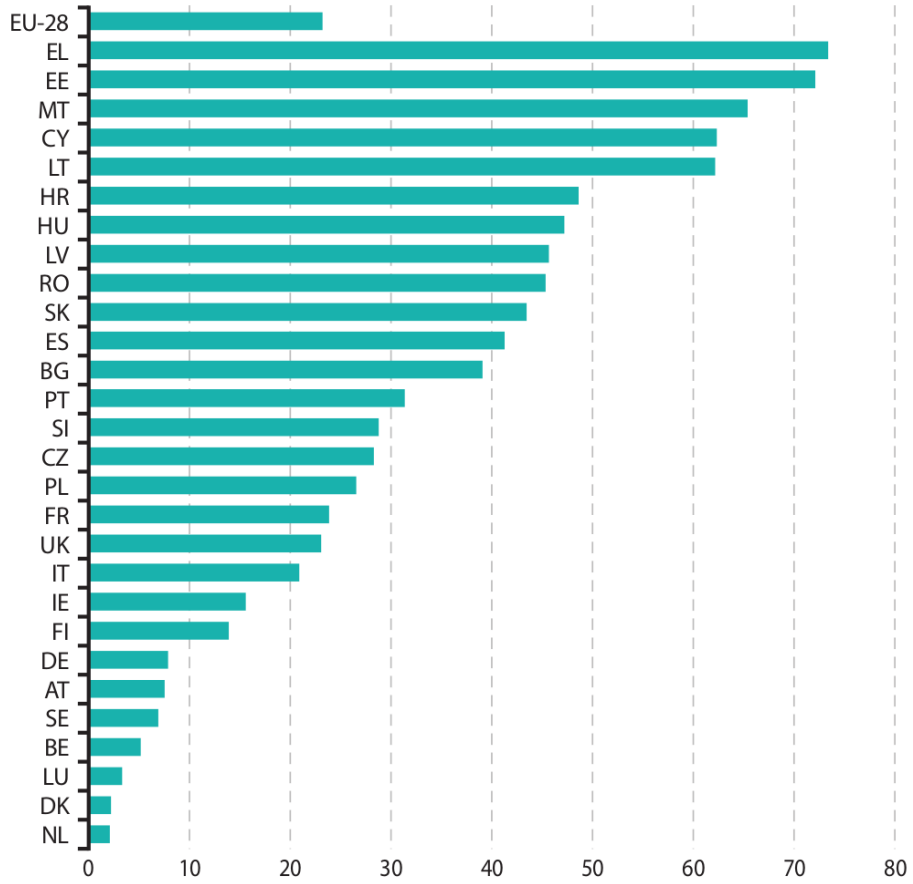

Figure 11.2 - Share (in %) of landfilled waste for Member States of EU-28 in 2010; major mineral wastes were excluded (Eurostat, 2013).

With regard to municipal waste, Figure 11.3 illustrates the treatment processes adopted in EU-27 (in the period 1995-2011) and EU-28 (from 2007 to 2011). It shows that total amount of municipal waste produced is almost the same in the last decade in EU-27. Nevertheless, landfilling has continuously decreased in the same period, while all of the other treatment processes (i.e. composting and digestion, material recycling and incineration) increased.

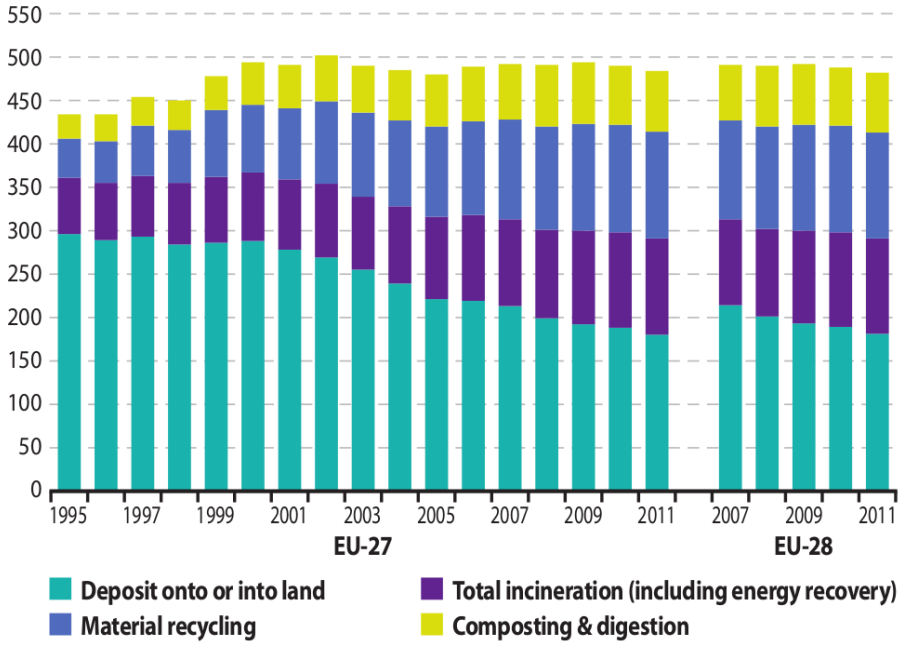

Figure 11.3 - Municipal waste treatment, EU-27 and EU-28; values are expressed in kg per inhabitant per year (Eurostat, 2013).

Energy production from municipal waste incineration

Energy production from municipal waste incineration in the EU-28 rapidly increased in the last ten years and in 2011 reached 16354 thousand tonnes of oil equivalent (more than the double of 2001, when 7973 toe were produced). According to the data reported in Eurostat (2013), at an annual basis, energy production from waste incineration has continuously grown in EU-28 with the exception of 2008-09 (when it declined by 2 %). However, between 2009 and 2011 it recorded an increase of 13 %.

As shown by Figure 11.4, Germany accounted for 29 % of total EU-28 production in 2011, followed by France (15 %), Italy and the Netherlands (10 % each). Between 2001 and 2011, all Member States recorded increases in their energy production from municipal waste incineration and Italy presented a fourfold increase.

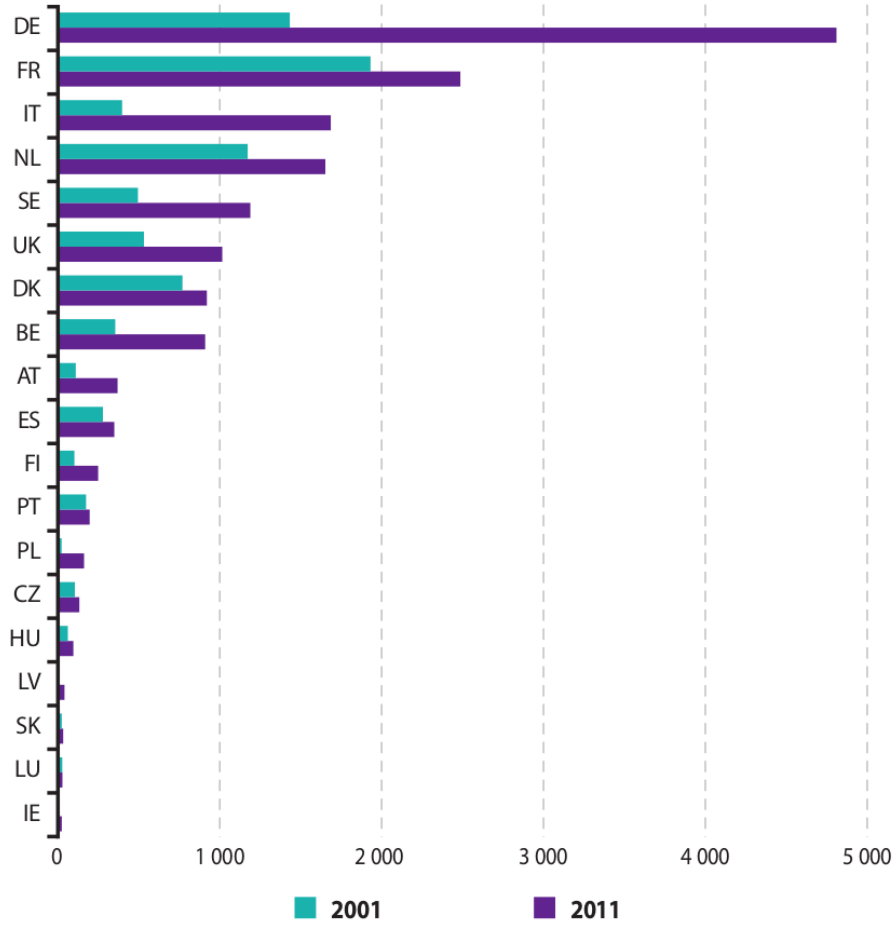

Figure 11.4 - Energy production from municipal waste incineration; values are expressed in thousand tonnes oil equivalent (Eurostat, 2013).

Appendix B Typical waste composition

Table 11.3 provides data concerning the content of waste arising in Germany (WI BREF, 2006). *Hazardous waste* refers to those wastes classified as hazardous under Directive 91/689/EC[51], while *Sewage sludge* includes sludge from the wastewater treatment plants. The following Table 11.4 reports main sources of organic chlorine in wastes.

Table 11.3 - Typical composition of waste in Germany (WI BREF, 2006).

Parameter	Municipal waste	Hazardous waste	Sewage sludge
Calorific value (upper) (MJ/kg)	7 – 15	1 – 42	2 – 14
Water (%)	15 – 40	0 – 100	3 – 97
Ash	20 – 35	0 – 100	1 – 60
Carbon (% d.s.)	18 – 40	5 – 99	30 – 35
Hydrogen (% d.s.)	1 – 5	1 – 20	2 – 5
Nitrogen (% d.s.)	0.2 – 1.5	0 – 15	1 – 4
Oxygen (% d.s.)	15 – 22	not supplied	10 – 25
Sulfur (% d.s.)	0.1 – 0.5	not supplied	0.2 – 1.5
Fluorine (% d.s.)	0.01 – 0.035	0 – 50	0.1 – 1
Chlorine (% d.s.)	0.1 – 1	0 – 80	0.05 – 4
Bromine (% d.s.)	not supplied	0 – 80	not supplied
Iodine (% d.s.)	not supplied	0 – 50	not supplied
Lead (mg/kg d.s.)	100 – 2,000	0 – 200,000	4 – 1000
Cadmium (mg/kg d.s.)	1 – 15	0 – 10,000	0.1 – 50
Copper (mg/kg d.s.)	200 – 700	not supplied	10 – 1,800
Zinc (mg/kg d.s.)	400 – 1,400	not supplied	10 – 5,700
Mercury (mg/kg d.s.)	1 – 5	0 – 40,000	0.05 – 10
Thallium (mg/kg d.s.)	< 0.1	not supplied	0.1 – 5
Manganese (mg/kg d.s.)	250	not supplied	300 – 1,800
Vanadium (mg/kg d.s.)	4 – 11	not supplied	10 – 150
Nickel (mg/kg d.s.)	30 – 50	not supplied	3 – 500
Cobalt (mg/kg d.s.)	3 – 10	not supplied	8 – 35
Arsenic (mg/kg d.s.)	2 – 5	not supplied	1 – 35
Chrome (mg/kg d.s.)	40 – 200	not supplied	1 – 800
Selenium (mg/kg d.s.)	0.21 – 15	not supplied	0.1 – 8
PCB (mg/kg d.s.)	0.2 – 0.4	Fino al 60%	0.01 – 0.13
PCDD/PCDF (ng I-TE/kg)	50 – 250	10 – 10,000	8.5 – 73

Notes:
- *% d.s.* means *percentage dry solids*
- The calorific value for sewage sludge relates to raw sludge of > 97 % d.s.
- Sub-fractions of hazardous waste can show variations outside these ranges
- I-TE represents the International Toxic Equivalents for dioxins and furans

[51] Council Directive 91/689/EEC of 12 December 1991 on hazardous waste, which was repealed with effect from 12 December 2010 by Article 41 of Directive 2008/98/EC on waste (illustrated in Appendix C).

Table 11.4 - Organic chlorine content of some plastic materials (Niessen, 2010).

Compound	Chlorine (wt. %)	Uses
Polyvinyl chloride	59.0 [a]	Bottles, film, furniture
Polyvinylidene chloride	73.2 [a]	Film
Methylene chloride	82.6	Solvent
Chloroform	88.2	Anesthetic
DDT	50	Insecticide
Chlordane	59	Insecticide
[a] Pure resin.		

Appendix C Regulation

Directive 2008/98/EC on waste

Directive 2008/98/EC on waste (Waste Framework Directive)[52] sets the basic concepts and definitions related to waste management. This Directive establishes a legal framework for the treatment of waste within the European Community. It aims at protecting the environment and human health through the prevention of the harmful effects of waste generation and waste management.

The Directive, in **Article 13**, lays down some basic waste management principles for protection of human health and the environment:

> Member States shall take the necessary measures to ensure that waste management is carried out without endangering human health, without harming the environment and, in particular
>
> (a) without risk to water, air, soil, plants or animals;
> (b) without causing a nuisance through noise or odours; and
> (c) without adversely affecting the countryside or places of special interest.

Article 4 sets the following waste hierarchy, which shall apply as a priority order in waste prevention and management legislation and policy:

(a) prevention;
(b) preparing for re-use;
(c) recycling;
(d) other recovery, e.g. energy recovery; and
(e) disposal.

The meaning of this action, with other important definitions, are given in **Article 3**:

1 "waste" means any substance or object which the holder discards or intends or is required to discard;

2 "hazardous waste" means waste which displays one or more of the hazardous properties listed in Annex III;

9 "waste management" means the collection, transport, recovery and disposal of waste, including the supervision of such operations and the after-care of disposal sites, and including actions taken as a dealer or broker;

10 "collection" means the gathering of waste, including the preliminary sorting and preliminary storage of waste for the purposes of transport to a waste treatment facility;

[52] The Directive has been transposed into Italian legislation on 3 December 2010 by Legislative Decree No. 205.

11 “separate collection” means the collection where a waste stream is kept separately by type and nature so as to facilitate a specific treatment;

12 “prevention” means measures taken before a substance, material or product has become waste, that reduce:

(a) the quantity of waste, including through the re-use of products or the extension of the life span of products;

(b) the adverse impacts of the generated waste on the environment and human health; or

(c) the content of harmful substances in materials and products;

13 “re-use” means any operation by which products or components that are not waste are used again for the same purpose for which they were conceived;

14 “treatment” means recovery or disposal operations, including preparation prior to recovery or disposal;

15 “recovery” means any operation the principal result of which is waste serving a useful purpose by replacing other materials which would otherwise have been used to fulfil a particular function, or waste being prepared to fulfil that function, in the plant or in the wider economy. Annex II sets out a non-exhaustive list of recovery operations;

16 “preparing for re-use” means checking, cleaning or repairing recovery operations, by which products or components of products that have become waste are prepared so that they can be re-used without any other pre-processing;

17 “recycling” means any recovery operation by which waste materials are reprocessed into products, materials or substances whether for the original or other purposes. It includes the reprocessing of organic material but does not include energy recovery and the reprocessing into materials that are to be used as fuels or for backfilling operations;

19 “disposal” means any operation which is not recovery even where the operation has as a secondary consequence the reclamation of substances or energy. Annex I sets out a non-exhaustive list of disposal operations;

Directive 2010/75/EU on industrial emissions

Directive 2010/75/EU on industrial emissions[53] (integrated pollution prevention and control) lays down the obligations for industrial activities with a major pollution potential. The Directive establishes a permit procedure and environmental requirements, in particular with regard to discharges, to avoid or minimize polluting emissions in the atmosphere, water and soil. The Directive brings together Directive 2008/1/EC (the "IPPC Directive") and six other directives, including Directive 2000/76/EC on waste incineration[54], in a single directive on industrial emissions.

Main sectors of activity defined in the Directive are energy industries, production and processing of metals, mineral industry, chemical industry, waste management, and rearing of animals. Special provisions are given for combustion plants (≥ 50 MW), waste incineration or co-incineration plants, certain installations and activities using organic solvents and installations producing titanium dioxide. These industrial installations must meet some environmental requirements:

- preventive measures are taken against pollution;
- the best available techniques (BAT) are applied;
- no significant pollution is caused;
- waste is reduced, recycled or disposed of in the manner which creates least pollution;
- energy efficiency is maximised;
- accidents are prevented and their impact limited;
- sites are remediated when the activities come to an end.

Instead, the Directive shall not apply to research activities, development activities or the testing of new products and processes.

In the following part, some extracts of Articles and Annexes concerning waste incineration plants of the Industrial Emissions Directive are presented.

[53] Directive 2010/75/EU of the European Parliament and of the Council of 24 November 2010 on industrial emissions (integrated pollution prevention and control); the Directive has been transposed into Italian legislation on 6 August 2013 by Law No. 96.

[54] Directive 2010/75/EU replaces definitively, with effect from 7 January 2014, Directive 2000/76/EC on waste incineration.

Chapter I – Common provisions

Article 3 - Definitions

For the purposes of this Directive the following definitions shall apply:

(4) "emission" means the direct or indirect release of substances, vibrations, heat or noise from individual or diffuse sources in the installation into air, water or land;

(10) "best available techniques" means the most effective and advanced stage in the development of activities and their methods of operation which indicates the practical suitability of particular techniques for providing the basis for emission limit values and other permit conditions designed to prevent and, where that is not practicable, to reduce emissions and the impact on the environment as a whole;

(a) "techniques" includes both the technology used and the way in which the installation is designed, built, maintained, operated and decommissioned;

(b) "available techniques" means those developed on a scale which allows implementation in the relevant industrial sector, under economically and technically viable conditions, taking into consideration the costs and advantages, whether or not the techniques are used or produced inside the Member State in question, as long as they are reasonably accessible to the operator;

(c) "best" means most effective in achieving a high general level of protection of the environment as a whole;

(11) "BAT reference document" means a document, resulting from the exchange of information organised pursuant to Article 13, drawn up for defined activities and describing, in particular, applied techniques, present emissions and consumption levels, techniques considered for the determination of best available techniques as well as BAT conclusions and any emerging techniques, giving special consideration to the criteria listed in Annex III;

(13) "emission levels associated with the best available techniques" means the range of emission levels obtained under normal operating conditions using a best available technique or a combination of best available techniques, as described in BAT conclusions, expressed as an average over a given period of time, under specified reference conditions;

(37) "waste" means waste as defined in point 1 of Article 3 of Directive 2008/98/EC of the European Parliament and of the Council of 19 November 2008 on waste[55];

(38) "hazardous waste" means hazardous waste as defined in point 2 of Article 3 of Directive 2008/98/EC[56];

(40) "waste incineration plant" means any stationary or mobile technical unit and equipment dedicated to the thermal treatment of waste, with or without recovery of the combustion heat generated, through the incineration by oxidation of waste as well as other thermal treatment processes, such as pyrolysis, gasification or plasma process, if the substances resulting from the treatment are subsequently incinerated;

[55] Reported previously in this Appendix
[56] Reported previously in this Appendix

(41) “waste co-incineration plant” means any stationary or mobile technical unit whose main purpose is the generation of energy or production of material products and which uses waste as a regular or additional fuel or in which waste is thermally treated for the purpose of disposal through the incineration by oxidation of waste as well as other thermal treatment processes, such as pyrolysis, gasification or plasma process, if the substances resulting from the treatment are subsequently incinerated;

Chapter IV – Special provisions for waste incineration plants and waste co-incineration plants

Article 49 - Compliance with emission limit values

The emission limit values for air and water shall be regarded as being complied with if the conditions described in Part 8 of Annex VI are fulfilled.

Article 50 - Operating conditions

1. Waste incineration plants shall be operated in such a way as to achieve a level of incineration such that the total organic carbon content of slag and bottom ashes is less than 3 % or their loss on ignition is less than 5 % of the dry weight of the material. If necessary, waste pre-treatment techniques shall be used.

2. Waste incineration plants shall be designed, equipped, built and operated in such a way that the gas resulting from the incineration of waste is raised, after the last injection of combustion air, in a controlled and homogeneous fashion and even under the most unfavourable conditions, to a temperature of at least 850 °C for at least two seconds.

   Waste co-incineration plants shall be designed, equipped, built and operated in such a way that the gas resulting from the co-incineration of waste is raised in a controlled and homogeneous fashion and even under the most unfavourable conditions, to a temperature of at least 850 °C for at least two seconds.

   If hazardous waste with a content of more than 1 % of halogenated organic substances, expressed as chlorine, is incinerated or co-incinerated, the temperature required to comply with the first and second subparagraphs shall be at least 1100 °C.

   In waste incineration plants, the temperatures set out in the first and third subparagraphs shall be measured near the inner wall of the combustion chamber. The competent authority may authorise the measurements at another representative point of the combustion chamber.

3. Each combustion chamber of a waste incineration plant shall be equipped with at least one auxiliary burner. This burner shall be switched on automatically when the temperature of the combustion gases after the last injection of combustion air falls below the temperatures set out in paragraph 2. It shall also be used during plant start-up and shut-down operations in order to ensure that those temperatures are maintained at all times during these operations and as long as unburned waste is in the combustion chamber.

   The auxiliary burner shall not be fed with fuels which can cause higher emissions than those resulting from the burning of gas oil as defined in Article 2(2) of Council Directive 1999/32/EC of 26 April 1999 relating to a reduction in the sulfur content of certain liquid fuels [36], liquefied gas or natural gas.

4. Waste incineration plants and waste co-incineration plants shall operate an automatic system to prevent waste feed in the following situations:

   (a) at start-up, until the temperature set out in paragraph 2 of this Article or the temperature specified in accordance with Article 51(1) has been reached;

(b) whenever the temperature set out in paragraph 2 of this Article or the temperature specified in accordance with Article 51(1) is not maintained;

(c) whenever the continuous measurements show that any emission limit value is exceeded due to disturbances or failures of the waste gas cleaning devices.

5. Any heat generated by waste incineration plants or waste co-incineration plants shall be recovered as far as practicable.

6. Infectious clinical waste shall be placed straight in the furnace, without first being mixed with other categories of waste and without direct handling.

7. Member States shall ensure that the waste incineration plant or waste co-incineration plant is operated and controlled by a natural person who is competent to manage the plant.

ANNEX VI - Technical provisions relating to waste incineration plants and waste co-incineration plants

PART 3 - Air emission limit values for waste incineration plants

1. All emission limit values shall be calculated at a temperature of 273.15 K, a pressure of 101.3 kPa and after correcting for the water vapour content of the waste gases.

   They are standardised at 11 % oxygen in waste gas except in case of incineration of mineral waste oil as defined in point 3 of Article 3 of Directive 2008/98/EC[57], when they are standardised at 3 % oxygen, and in the cases referred to in Point 2.7 of Part 6.

   1.1. Daily average emission limit values for the following polluting substances (mg/Nm^3)

Total dust	10
Gaseous and vaporous organic substances, expressed as total organic carbon (TOC)	10
Hydrogen chloride (HCl)	10
Hydrogen fluoride (HF)	1
Sulfur dioxide (SO_2)	50
Nitrogen monoxide (NO) and nitrogen dioxide (NO_2), expressed as NO_2 for existing waste incineration plants with a nominal capacity exceeding 6 tonnes per hour or new waste incineration plants	200
Nitrogen monoxide (NO) and nitrogen dioxide (NO_2), expressed as NO_2 for existing waste incineration plants with a nominal capacity of 6 tonnes per hour or less	400

   1.2. Half-hourly average emission limit values for the following polluting substances (mg/Nm^3)

	(100 %) A	(97 %) B
Total dust	30	10
Gaseous and vaporous organic substances, expressed as total organic carbon (TOC)	20	10
Hydrogen chloride (HCl)	60	10
Hydrogen fluoride (HF)	4	2
Sulfur dioxide (SO_2)	200	50
Nitrogen monoxide (NO) and nitrogen dioxide (NO_2), expressed as NO_2 for existing waste incineration plants with a nominal capacity exceeding 6 tonnes per hour or new waste incineration plants	400	200

   1.3. Average emission limit values (mg/Nm^3) for the following heavy metals over a sampling period of a minimum of 30 minutes and a maximum of 8 hours

[57] Reported previously in this Appendix

Cadmium and its compounds, expressed as cadmium (Cd)	Total: 0.05
Thallium and its compounds, expressed as thallium (Tl)	
Mercury and its compounds, expressed as mercury (Hg)	0.05
Antimony and its compounds, expressed as antimony (Sb)	Total: 0.5
Arsenic and its compounds, expressed as arsenic (As)	
Lead and its compounds, expressed as lead (Pb)	
Chromium and its compounds, expressed as chromium (Cr)	
Cobalt and its compounds, expressed as cobalt (Co)	
Copper and its compounds, expressed as copper (Cu)	
Manganese and its compounds, expressed as manganese (Mn)	
Nickel and its compounds, expressed as nickel (Ni)	
Vanadium and its compounds, expressed as vanadium (V)	

These average values cover also the gaseous and the vapour forms of the relevant heavy metal emissions as well as their compounds.

1.4. Average emission limit value (ng/Nm^3) for dioxins and furans over a sampling period of a minimum of 6 hours and a maximum of 8 hours. The emission limit value refers to the total concentration of dioxins and furans calculated in accordance with Part 2.

Dioxins and furans	0.1

1.5. Emission limit values (mg/Nm^3) for carbon monoxide (CO) in the waste gases:

(a) 50 as daily average value;
(b) 100 as half-hourly average value;
(c) 150 as 10-minute average value.

The competent authority may authorise exemptions from the emission limit values set out in this point for waste incineration plants using fluidised bed technology, provided that the permit sets an emission limit value for carbon monoxide (CO) of not more than 100 mg/Nm^3 as an hourly average value.

2. Emission limit values applicable in the circumstances described in Article 46(6) and Article 47.

The total dust concentration in the emissions into the air of a waste incineration plant shall under no circumstances exceed 150 mg/Nm^3 expressed as a half-hourly average. The air emission limit values for TOC and CO set out in points 1.2 and 1.5(b) shall not be exceeded.

3. Member States may lay down rules governing the exemptions provided for in this Part.

PART 4 - Determination of air emission limit values for the co-incineration of waste

This Part is not reported in the present thesis because it does not apply to the reference plant analyzed.

PART 7 - Formula to calculate the emission concentration at the standard percentage oxygen concentration

$$E = \frac{21 - O_S}{21 - O_M} \cdot E_M$$

E_S = calculated emission concentration at the standard percentage oxygen concentration

E_M = measured emission concentration

O_S = standard oxygen concentration

O_M = measured oxygen concentration

PART 8 - Assessment of compliance with emission limit values

1. Air emission limit values

1.1. The emission limit values for air shall be regarded as being complied with if:

(a) none of the daily average values exceeds any of the emission limit values set out in point 1.1 of Part 3 or in Part 4 or calculated in accordance with Part 4;
(b) either none of the half-hourly average values exceeds any of the emission limit values set out in column A of the table under point 1.2 of Part 3 or, where relevant, 97 % of the half-hourly average values over the year do not exceed any of the emission limit values set out in column B of the table under point 1.2 of Part 3;
(c) none of the average values over the sampling period set out for heavy metals and dioxins and furans exceeds the emission limit values set out in points 1.3 and 1.4 of Part 3 or in Part 4 or calculated in accordance with Part 4;
(d) for carbon monoxide (CO):

(i) in case of waste incineration plants:

- at least 97 % of the daily average values over the year do not exceed the emission limit value set out in point 1.5(a) of Part 3; and,
- at least 95 % of all 10-minute average values taken in any 24-hour period or all of the half-hourly average values taken in the same period do not exceed the emission limit values set out in points 1.5(b) and (c) of Part 3; in case of waste incineration plants in which the gas resulting from the incineration process is raised to a temperature of at least 1100 °C for at least two seconds, Member States may apply an evaluation period of 7 days for the 10-minute average values;

(ii) in case of waste co-incineration plants: the provisions of Part 4 are met.

1.2. The half-hourly average values and the 10-minute averages shall be determined within the effective operating time (excluding the start-up and shut-down periods if no waste is being incinerated) from the measured values after having subtracted the value of the confidence interval specified in point 1.3 of Part 6. The daily average values shall be determined from those validated average values.

To obtain a valid daily average value no more than five half-hourly average values in any day shall be discarded due to malfunction or maintenance of the continuous measurement system. No more than ten daily average values per year shall be discarded due to malfunction or maintenance of the continuous measurement system.

1.3. The average values over the sampling period and the average values in the case of periodical measurements of HF, HCl and SO_2 shall be determined in accordance with the requirements of Articles 45(1)(e), 48(3) and point 1 of Part 6.

2. Water emission limit values

The emission limit values for water shall be regarded as being complied with if:

(a) for total suspended solids 95 % and 100 % of the measured values do not exceed the respective emission limit values as set out in Part 5;
(b) for heavy metals (Hg, Cd, TI, As, Pb, Cr, Cu, Ni and Zn) no more than one measurement per year exceeds the emission limit values set out in Part 5; or, if the Member State provides for more than 20 samples per year, no more than 5 % of these samples exceed the emission limit values set out in Part 5;
(c) for dioxins and furans, the measurement results do not exceed the emission limit value set out in Part 5.

Appendix D Properties of the compounds

In this appendix, the properties of the compounds required by the simulation software Aspen Hysys are listed. Specific heat capacity is required in the following form:

$$c_p(T) = A + B \cdot T + C \cdot T^2 + D \cdot T^3 + E \cdot T^4$$

where *A*, *B*, *C*, *D* and *E* are coefficients which have to be set for each compound, *T* is the absolute temperature (in K), and the specific heat capacity is expressed in kJ g^{-1} K^{-1}. The values of these coefficients were calculated from the data reported in the NIST (National Institute Standard and Technology) Chemistry WebBook.

$Ca(OH)_2$

- Molecular weight, mw = 74.1 kg/kmol;
- Density, ρ = 2240 kg/m^3;
- Heat of Formation at 25 °C, $\Delta H_f°$ = -985,200 kJ/kmol;
- Specific heat capacity coefficients:
    - A = $1.76791 \cdot 10^{-3}$;
    - B = $-1.11746 \cdot 10^{-6}$;
    - C = $1.65904 \cdot 10^{-9}$;
    - D = $-6.80974 \cdot 10^{-13}$;
    - E = 0.

$CaCl_2$

- Molecular weight, mw = 111.1 kg/kmol;
- Density, ρ = 2150 kg/m^3;
- Heat of Formation at 25 °C, $\Delta H_f°$ = -795,400 kJ/kmol;
- Specific heat capacity coefficients:
    - A = $7.86499 \cdot 10^{-4}$;
    - B = $-3.16000 \cdot 10^{-7}$;
    - C = $3.97548 \cdot 10^{-10}$;
    - D = $-8.87251 \cdot 10^{-14}$;
    - E = 0.

Na_2CO_3

- Molecular weight, mw = 106 kg/kmol;
- Density, ρ = 2530 kg/m^3;
- Heat of Formation at 25 °C, $\Delta H_f°$ = -1,130,700 kJ/kmol;
- Specific heat capacity coefficients:
    - A = $1.65284 \cdot 10^{-3}$;
    - B = $-3.28357 \cdot 10^{-6}$;

- C = $7.01011 \cdot 10^{-9}$;
- D = $-2.288256 \cdot 10^{-12}$;
- E = 0.

NaCl

- Molecular weight, mw = 58.44 kg/kmol;
- Density, ρ = 2160 kg/m^3;
- Heat of Formation at 25 °C, $\Delta H_f°$ = -411,200 kJ/kmol;
- Specific heat capacity coefficients:
  - A = $0.86792 \cdot 10^{-3}$;
  - B = $0.1141670 \cdot 10^{-6}$;
  - C = $-0.43070 \cdot 10^{-10}$;
  - D = $0.173833 \cdot 10^{-12}$;
  - E = 0.

Na_2SO_4

- Molecular weight, mw = 142 kg/kmol;
- Density, ρ = 2698 kg/m^3;
- Heat of Formation at 25 °C, $\Delta H_f°$ = -1,383,500 kJ/kmol;
- Specific heat capacity coefficients:
  - A = $1.08547 \cdot 10^{-3}$;
  - B = $8.62650 \cdot 10^{-8}$;
  - C = $3.4784 \cdot 10^{-10}$;
  - D = $-1.08630 \cdot 10^{-13}$;
  - E = 0.

Ca_2SO_4

- Molecular weight, mw = 136.14 kg/kmol;
- Density, ρ = 2660 kg/m^3;
- Heat of Formation at 25 °C, $\Delta H_f°$ = -1,434,500 kJ/kmol;
- Specific heat capacity coefficients:
  - A = $5.69549 \cdot 10^{-4}$;
  - B = $6.75647 \cdot 10^{-10}$;
  - C = 0;
  - D = 0;
  - E = 0.

Appendix E Emission limits and BAT

The BAT (Best Available Techniques) used in waste incineration sector are reported in the corresponding reference document (WI BREF, 2006), which was compiled to according to the IPPC Directive. Table 11.5 reports the emission levels associated with the use of the principal BAT for flue gas treatment. Even though they are not legally binding emission limit values (ELVs), the ranges of emission levels given in the BREFs are significant because shall be the reference for setting the permit conditions to installations covered by the Industrial Emissions Directive (see Appendix C).

Table 11.6 reports the range emissions levels registered in some European MSWI plants, while the ranges of concentration of various pollutants in the flue gas before flue-gas cleaning in waste incineration plants of various types are shown in Table 11.7.

Table 11.5 - Operational emission level ranges associated with the use of BAT for releases to air from waste incinerators; values are expressed in mg/Nm^3, or as stated, and standardized at 11 % oxygen, dry gas, 273 K and 101.3 kPa (adapted from WI BREF, 2006).

Substance(s)	Non-continuous samples(1)	½ hour average	24 hour average	Comments
Total dust		1 – 20	1 – 5	In general, the use of fabric filters gives the lower levels within these emission ranges. Effective maintenance of dust control systems is very important. Energy use can increase as lower emission averages are sought. Controlling dust levels generally reduces metal emissions too.
Hydrogen chloride (HCl)		1 – 50	1 – 8	Waste control, blending and mixing can reduce fluctuations in raw gas concentrations that can lead to elevated short-term emissions. Wet FGT systems generally have the highest absorption capacity and deliver the lowest emission levels for these substances, but are generally more expensive.
Hydrogen fluoride (HF)		<2	<1	
Sulfur dioxide (SO_2)		1 – 150	1 – 40	
Nitrogen monoxide (NO) and nitrogen dioxide (NO_2), expressed as nitrogen dioxide for installations using SCR		40 – 300	40 – 100	Waste and combustion control techniques coupled with SCR generally result in operation within these emission ranges. The use of SCR imposes an additional energy demand and costs. In general, at larger installations the use of SCR results in less significant additional cost per tonne of waste treated. High N waste may result in increased raw gas NO_X concentrations.
Nitrogen monoxide (NO) and nitrogen dioxide (NO_2) expressed as nitrogen dioxide for installations not using SCR		30 – 350	120 – 180	Waste and combustion control techniques with SNCR generally result in operation within these emission ranges. 24 hour averages below this range generally require SCR, although levels below 70 mg/Nm^3 have been achieved using SNCR (e.g. where raw NO_X is low and/or at high reagent dose rates) Where high SNCR reagent dosing rates are used, the resulting NH_3 slip can be controlled using wet FGT with appropriate measures to deal with the resultant ammoniacal waste water. High N waste may result in increased raw gas NO_X concentrations.
Gaseous and vaporous organic substances, expressed as TOC		1 – 20	1 – 10	Techniques that improve combustion conditions reduce emissions of these substances. Emission concentrations are generally not influenced greatly by FGT. CO levels may be higher during start-up and

Carbon monoxide (CO)		5 – 100	5 – 30	shut down, and with new boilers that have not yet established their normal operational fouling level
Mercury and its compounds (as Hg)	<0.05	0.001 – 0.03	0.001 – 0.02	Adsorption using carbon-based reagents is generally required to achieve these emission levels with many wastes - as metallic Hg is more difficult to control than ionic Hg. The precise abatement performance and technique required will depend on the levels and distribution of Hg in the waste. Some waste streams have very highly variable Hg concentrations – waste pretreatment may be required in such cases to prevent peak overloading of FGC system capacity. Continuous monitoring of Hg is not required by Directive 2000/76/EC but has been carried out in some Member States
Total cadmium and thallium (and their compounds expressed as the metals)	0.005 - 0.05			See comments for Hg. The lower volatility of these metals than Hg means that dust and other metal control methods are more effective at controlling these substances than Hg.
∑ other metals [(2)]	0.005 - 0.5			Techniques that control dust levels generally also control these metals
Dioxins and furans[(3)] (ng_{TEQ}/Nm^3)	0.01 – 0.1			Combustion techniques destroy PCDD/F in the waste. Specific design and temperature controls reduce *de-novo* synthesis. In addition to such measures, abatement techniques using carbon-based absorbents reduce final emissions to within this emission range. Increased dosing rates for carbon absorbent may give emissions to air as low as 0.001 but result in increased consumption and residues.
Substances not included in Directive 2000/76/EC on waste incineration:				
Ammonia (NH_3)	<10	1 – 10	<10 [(4)]	Effective control of NO_X abatement systems, including reagent dosing contributes to reducing NH_3 emissions. Wet scrubbers absorb NH_3 and transfer it to the wastewater stream.

NOTES:

[(1)] Non-continuous measurements are averaged over a sampling period of between 30 minutes and 8 hours. Sampling periods are generally in the order of 4 – 8 hours for such measurements.

[(2)] ∑ other metals = sum of Sb, As, Pb, Cr, Co, Cu, Mn, Ni, V and their compounds expressed as the metals

[(3)] Dioxin and furans are calculated using the equivalence factors as in EC/2000/76

[(4)] A few Member States and the Environmental NGO expressed that the 24 hour NH_3 emission range associated with the use of BAT should be <5 mg/Nm3 (in the place of <10 mg/ Nm^3).

Table 11.6 - Range of clean gas operation emissions levels reported from some European MSWI plants; data standardized at 11 % oxygen, dry gas, 273 K and 101.3 kPa (adapted from WI BREF, 2006).

Parameter	Type of measurement (1)	Daily averages (where continuous measurement used) in mg/m³		Half hour averages (where continuous measurement used) in mg/m³		Annual averages in mg/m³
		Limits(2)	Range of values	Limits(2)	Range of values	Range of values
Dust	C	10	0.1 - 10	20	< 0.05 - 15	0.1 - 4
HCl	C	10	0.1 - 10	60	< 0.1 - 80	0.1 - 6
HF	C/N	1	0.1 - 1	4	< 0.02 - 1	0.01 - 0.1
SO_2	C	50	0.5 - 50	200	0.1 - 250	0.2 - 20
NO_x (3)	C	200	30 - 200	400	20 - 450	20 - 180
NH_3	C	n.a.	< 0.1 - 3		0.55 - 3.55	
N_2O		n.a.				
COV	C	10	0.1 - 10	20	0.1 - 25	0.1 - 5
CO	C	50	1 - 100	100	1 - 150	2 - 45
Hg	C/N	0.05	0.0005 - 0.05	n.a.	0.0014 - 0.036	0.0002 - 0.05
Cd	N	n.a.	0.0003 - 0.003	n.a.		
As	N	n.a.	< 0.0001 - 0.001	n.a.		
Pb	N	n.a.	< 0.002 - 0.044	n.a.		
Cr	N	n.a.	0.0004 - 0.002	n.a.		
Co	N	n.a.	< 0.002	n.a.		
Ni	N	n.a.	0.0003 - 0.002	n.a.		
Cd and Tl	N	0.05		n.a.		0.0002 - 0.03
Σ other metals (4)	N	0.5		n.a.		0.0002 - 0.05
Σ other metals (5)	N	n.a.	0.01 - 0.1	n.a.		
Benz(a)pyrene	N	n.a.		n.a.		< 0.001
Σ PCB	N	n.a.		n.a.		< 0.005
Σ PAH	N	n.a.		n.a.		< 0.01
PCDD/F (ng_{TEQ}/m^3)	N	0.1		n.a.		0.0002 - 0.08

Notes:

(1) C = continuous measurements, N = non-continuous measurements (sampling periods are generally in the order of 4 – 8 hours for such measurements)

(2) Limits in Directive 2000/76/EC; n.a. = not available

(3) In some cases, there are no emission limit values in force for NOX. For such installations, a typical range of values is 250 - 550 mg/Nm3 (discontinuous measurement).

(4) Sb, As, Pb, Cr, Co, Cu, Mn, Ni, V

(5) Sb, Pb, Cr, Cu, Mn, V, Co, Ni, Se and Te

Table 11.7 – Raw flue-gas concentrations (i.e. after the boiler) at various German waste incineration plants; values are standardized at 11 % oxygen (adapted from WI BREF, 2006).

Components	Units	Incineration plants for		
		Municipal waste	Hazardous waste	Industrial sewage sludge
Dust	mg/Nm³	1,000 – 5,000	1,000 – 10,000	30,000 – 200,000
Carbon monoxide (CO)	mg/Nm³	5 – 50	< 30	5 – 50
TOC	mg/Nm³	1 – 10	1 – 10	1 – 10
PCDD/PCDF	ng_{TEQ}/Nm³	0.5 – 10	0.5 – 10	0.1 – 10
Mercury	mg/Nm³	0.05 – 0.5	0.05 – 3	0.2
Cadmium + thallium	mg/Nm³	< 3	< 5	2.5
Other heavy metals (Pb, Sb, As, Cr, Co, Cu, Mn, Ni, V, Sn)	mg/Nm³	< 50	< 100	800
Inorganic chlorine compounds (as HCl)	mg/Nm³	500 – 2,000	3,000 – 100,000	
Inorganic fluorine compounds (as HF)	mg/Nm²	5 – 20	50 – 550	
Sulfur compounds, total of SO_2/SO_3, counted as SO_2	mg/Nm³	200 – 1,000	1,500 – 50,000	
Nitrogen oxides, counted as NO_2	mg/Nm³	250 – 500	1,00 – 1,500	< 200
Nitrous oxide	mg/Nm³	< 40	< 20	10 – 150
CO_2	%	5 – 10	5 – 8	
Water steam (H_2O)	%	10 – 20	6 – 20	

Notes:
1. Sewage sludge plants are those for the incineration of industrial sewage sludge
2. Hazardous waste values refer to mixed hazardous waste merchant plants rather than dedicated stream plants.

Appendix F Techniques for particulate emission control

The main techniques for reducing particulate emissions are (WI BREF, 2006):

- Electrostatic precipitators
- Wet electrostatic precipitators
- Condensation electrostatic precipitators
- Ionization wet scrubbers
- Fabric filters
- Cyclones and multi-cyclones

However, as shown in Table 11.8, cyclones are applicable only for the removal of the particles with a diameter higher than 5 µm, permitting their use only as first de-dusting system.

Table 11.8 – Typical performance of particulate control devices (adapted from LCP BREF, 2013).

Technology	**Removal efficiency %**				**Other performance parameters**	
	<1 µm	2 µm	5 µm	>10 µm	Parameter	Value
Electrostatic precipitator (ESP)	>96.5	>98.3	>99.95	>99.95	Operating temperature	80 – 220 °C (cold ESP) 300 – 450 °C (hot ESP)
					Energy consumption as % of electric capacity	0.1 – 1.8 %
					Pressure drop	0.15 – 0.3 kPa
					Residue	Fly ash
					Off-gas flow rate	>200,000 m^3/h
					Applicability	Solid and liquid fuels
					Market share	90 %
Fabric filter	>99.6	>99.6	>99.9	>99.95	Operating temperature	150 °C (polyester) 260 °C (fibreglass)
					Energy consumption as % of electric capacity	0.2 – 3 %
					Pressure drop	0.5 – 2 kPa
					Residue	Fly ash
					Off-gas flow rate	<1,100,000 m^3/h
					Applicability	Solid and liquid fuels
					Market share	10 %
Cyclone	85 – 90 %. The smallest diameter of the dust trapped is 5 to 10 µm					
Wet scrubber (high energy Venturi)	98.5	99.5	99.9	>99.9	Energy consumption as % of electric capacity	Up to 3 % (5 – 15 kWh/1000 m^3)
					Liquid to gas ratio	0.8 – 2.0 L/m^3
					Pressure drop	3 – 20 kPa
					Residue	Fly ash sludge/slurry

The most common systems adopted in large combustion plants are electrostatic precipitators (LCP BREF, 2006). This is due to the very high efficiency of ESPs, even for smaller particles (see Table 11.8), which can be achieved with low operating costs (except at very high removal rates). Thanks to the low pressure drops, ESP can treat very large gas flow rate. However, once installed, these systems are not very flexible to change operating conditions. Another drawback is given by particulates with very high electrical resistivity, which might show low removal efficiencies.

Another widely used system for particle control, especially in smaller combustion plants, is given by fabric filters (or baghouses). In a fabric filter, portrayed in Figure 11.5, the air passes through the cloth, leaving the dust behind and providing a clean air stream. The dust builds up as a cake on the cloth until removed. Therefore, fabric filters have been used together with the dry scrubbing-injection of powdered or slurried sorbents to simultaneously control both acid gases and fly ash emissions (LCP BREF, 2013).

Figure 11.5 - Representation of a fabric filter (from: BREF WI, 2006)

According to the cleaning method, there are three main types of fabric filters (Cooper and Alley, 2004):

- shaker,
- reverse-air,
- pulse-jet.

The first two types need parallel compartments to permit the cleaning, which is performed taking the compartment off-line. Conversely, the pulse-jet system permits to clean the bags in sequence by blasts of high-pressure air while filtration occurs. As shown in Table 11.8, the efficiency of a fabric filter system is extremely high. Moreover, the particulate cake that builds up on the cloth permits to collect with also smaller particles with a high efficiency. However, as the thickness of the dust cake increases, so does the pressure drops (as described in Appendix P). The main drawbacks of fabric filter are the inability to treat highly humid gases and the high capital costs, which are related quantitatively to the fabric area (Cooper and Alley, 2004).

Appendix G General description of the reference plant

The MSWI, located in northern Italy, consists in a single line for incineration of municipal solid wastes and non-hazardous industrial wastes. Electric energy production is obtained through a Rankine cycle. The actual nominal feed rate can reach up to 384 tons/day (about 120,000 tons/year assuming 7,500 operating hours per year). Assuming an upper heating value of the waste equal to 2500 kcal/kg (company standard), the nominal power of the plant at the nominal feed rate is of about 46.5 MWt (corresponding to 10.8 MWe). The plant general layout is shown in Figure 11.6, where six main sections can be identified:

1. Waste collection and storage: the wastes delivered to the plant are collected and stored in a reinforced concrete pit. Waste handling and loading kilns are operated by buckets connected to two hydraulic cranes located at the top of the pit.
2. Combustion: On the grate, kiln solids are burnt under controlled conditions using primary and secondary air fans. In the post-combustion chamber, a solution of ammonia is injected for a preliminary SNCR treatment for nitrogen oxides reduction (50-70 %).
3. Steam generator: the hot gases, produced during the combustion, pass through heat exchangers and a boiler to produce super-heated steam.
4. Flue gas cleaning: the line is provided with a flue gas cleaning system that will be described in the following.
5. Electrical power generation: superheated steam (produced in section 3 of the Figure 11.6) is expanded in the steam turbine in order to generate electric power.
6. District heating: the residual heat is used for district heating when required (on seasonal basis).

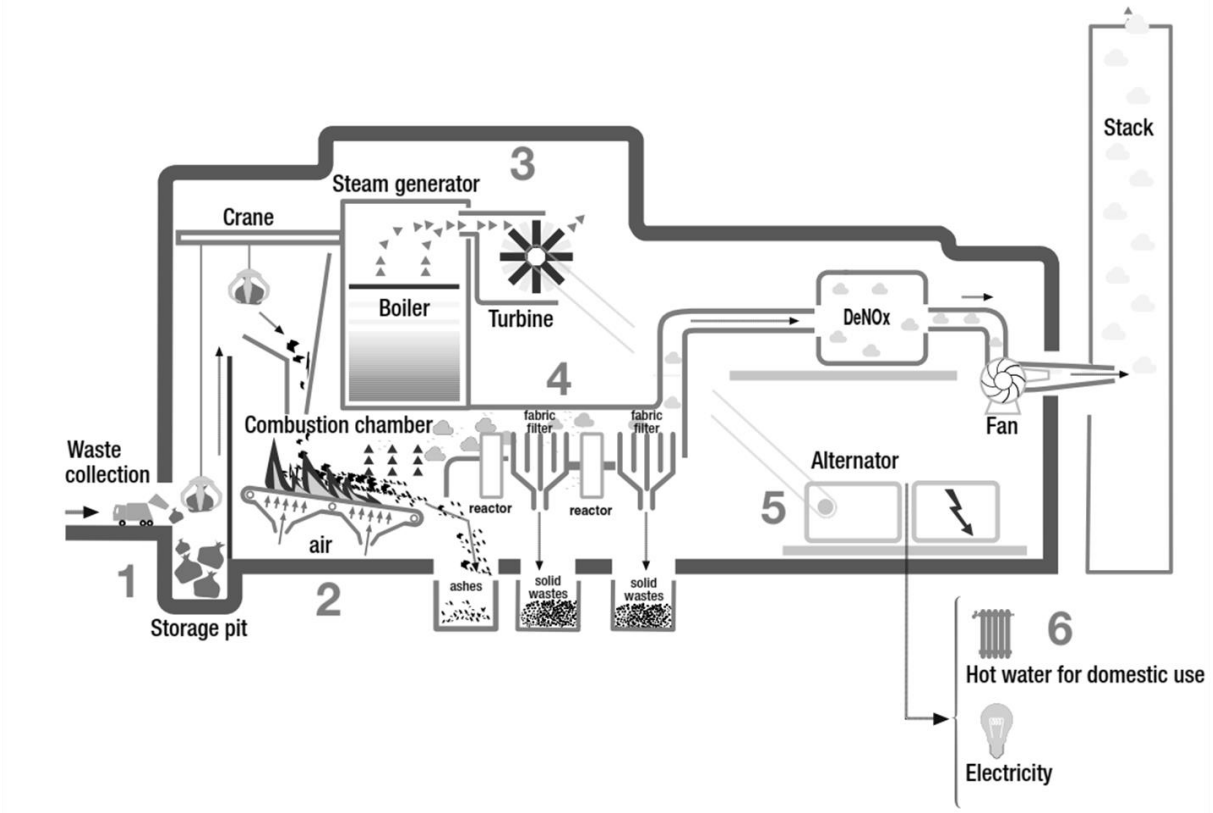

Figure 11.6 - Overall plant layout and main process sections (adapted from Gruppo Hera, 2010).

Appendix H Daily average operational data of the reference plant

In the present appendix, operational data measured during a month of regular operation are reported as registered at the DCS (Distributed Control System) of the analyzed plant (described in Appendix G).

In the following table, the values of flue gas composition with its temperature and volumetric flow rate (at standard conditions) are reported as measured the first sampling point (i.e. at first stage entrance).

	HCl	SO_2	HF	CO_2	CO	O_2	H_2O	T	Flow rate
	mg/Nm^3	mg/Nm^3	mg/Nm^3	%	mg/Nm^3	%	%	°C	Nm^3/h
1-Apr	1062.0	129.5	6.2	9.1	6.9	7.1	16.4	180.9	101270
2-Apr	1121.2	78.3	10.2	8.8	4.2	7.5	14.9	181.7	103697
3-Apr	1291.5	192.4	16.9	8.7	12.6	7.7	13.4	181.3	102868
4-Apr	1705.5	95.4	30.6	8.5	2.8	8.0	13.0	182.7	105462
5-Apr	1590.0	122.7	21.8	8.4	1.1	8.1	13.2	183.1	106435
6-Apr	1285.5	78.6	11.7	8.7	4.7	7.6	15.3	183.3	102051
7-Apr	739.1	45.7	5.4	7.2	2.1	8.9	14.4	182.2	97310
8-Apr	1042.6	67.2	6.7	8.6	4.2	7.6	15.8	181.3	105665
9-Apr	931.1	47.4	6.5	8.6	35.2	7.5	16.1	182.8	102616
10-Apr	1348.2	72.4	7.7	8.5	2.3	7.8	14.2	183.6	105836
11-Apr	1227.9	41.9	10.5	7.8	19.6	8.3	14.7	183.7	100758
12-Apr	1443.0	166.8	12.8	8.3	11.2	8.2	13.4	184.7	103562
13-Apr	1508.3	130.5	15.1	8.5	2.5	7.8	14.5	187.5	108230
14-Apr	1249.4	174.0	9.0	7.9	4.4	7.9	15.8	184.7	100266
15-Apr	743.6	56.4	5.5	7.4	36.9	8.3	15.8	181.9	89559
16-Apr	1280.7	70.4	6.7	8.4	5.5	7.6	16.0	184.4	103833
17-Apr	1177.3	53.2	7.4	8.4	25.2	7.8	15.0	184.8	103488
18-Apr	1486.2	58.8	8.2	8.3	10.3	7.8	15.0	185.3	103126
19-Apr	1904.7	89.4	14.3	8.6	4.1	7.8	13.6	185.6	105044
20-Apr	1634.2	45.1	10.4	8.8	11.8	7.4	15.3	184.6	100635
21-Apr	1226.7	98.6	9.2	8.0	3.0	7.8	15.4	182.1	92156
22-Apr	823.7	32.3	4.8	8.2	3.5	7.7	17.0	185.0	99206
23-Apr	1132.2	49.2	6.0	8.5	2.8	7.6	16.1	183.8	94129
24-Apr	1448.0	123.0	8.7	9.0	42.5	7.1	14.9	185.4	99170
25-Apr	1344.9	108.7	8.7	8.7	90.7	7.4	15.5	190.3	104060
26-Apr	1322.9	53.0	10.3	8.7	4.6	7.5	15.4	192.5	105573
27-Apr	1265.9	50.6	8.9	8.7	3.1	7.6	14.8	189.4	100367
28-Apr	1160.2	73.6	8.8	8.5	6.1	7.9	15.3	188.9	97339
29-Apr	688.5	24.9	4.3	7.8	7.7	8.1	16.4	186.1	90805
30-Apr	976.0	32.6	5.3	7.7	4.1	8.5	14.8	188.9	96633

In the following table, the values of flue gas composition with its temperature and volumetric flow rate (at standard conditions) are reported as measured the second sampling point (i.e. at first stage exit).

	HCl	SO_2	HF	CO_2	CO	O_2	H_2O	T	Flow rate
	mg/Nm^3	mg/Nm^3	mg/Nm^3	%	mg/Nm^3	%	%	°C	Nm^3/h
1-Apr	324.2	90.4	0.8	7.7	7.3	8.5	14.0	169.7	112529
2-Apr	186.9	50.4	0.8	7.5	5.6	8.8	12.9	170.8	114634
3-Apr	348.9	155.9	1.0	7.5	10.1	8.9	11.7	170.9	112632
4-Apr	406.2	79.8	1.0	7.2	4.1	9.2	11.4	172.8	116025
5-Apr	343.8	101.6	1.3	7.2	2.8	9.2	11.5	173.1	117070
6-Apr	286.7	61.7	0.8	7.4	5.3	8.9	13.2	172.7	112848
7-Apr	168.9	27.8	0.8	6.1	3.4	10.0	12.4	171.1	107589
8-Apr	204.2	45.0	1.4	7.2	5.2	9.0	13.4	171.0	118353
9-Apr	229.8	31.0	0.9	7.3	33.0	8.9	13.7	171.7	114510
10-Apr	277.2	57.4	1.0	7.2	3.8	9.2	12.1	173.0	117643
11-Apr	216.8	32.3	1.0	6.7	12.2	9.5	12.8	173.0	111546
12-Apr	328.3	136.2	1.1	7.0	12.1	9.4	11.6	174.1	114259
13-Apr	402.0	103.7	1.0	7.3	4.3	9.1	12.6	176.9	120026
14-Apr	303.2	117.2	1.5	6.7	5.6	9.2	13.7	173.9	111610
15-Apr	162.9	34.8	0.8	6.3	40.2	9.4	13.8	170.0	97884
16-Apr	273.1	51.3	1.3	7.2	5.4	8.9	13.8	174.2	114815
17-Apr	251.2	37.1	1.4	7.2	22.1	9.0	12.9	174.2	113490
18-Apr	321.5	46.5	1.4	6.9	9.9	9.1	12.6	173.5	114673
19-Apr	463.4	70.9	1.3	6.9	5.6	9.3	11.2	172.6	119123
20-Apr	410.6	34.6	0.7	7.1	8.6	8.9	12.5	171.5	113662
21-Apr	288.0	73.5	0.6	6.4	3.9	9.4	12.6	167.6	104693
22-Apr	256.9	17.8	0.7	6.7	5.0	9.3	14.0	170.8	112742
23-Apr	312.3	31.7	3.7	7.0	5.4	9.0	13.4	170.6	104947
24-Apr	355.4	91.2	1.9	7.5	27.3	8.4	12.4	174.1	109450
25-Apr	370.3	74.3	1.2	7.4	88.8	8.7	13.1	179.6	114290
26-Apr	426.9	33.9	1.2	7.4	5.6	8.8	13.0	181.7	116559
27-Apr	386.8	38.1	1.0	7.5	4.1	8.7	12.6	178.5	109420
28-Apr	341.2	54.2	1.0	7.2	7.6	9.0	13.1	178.2	106324
29-Apr	157.2	14.5	1.0	6.6	7.0	9.3	13.9	174.9	99692
30-Apr	249.8	24.7	1.0	6.4	3.5	9.6	12.5	178.5	106587

In the following table, the values of flue gas composition with its temperature and volumetric flow rate (at standard conditions) are reported as measured the emission stack.

	HCl	SO_2	HF	CO_2	CO	O_2	H_2O	T	Flow rate
	mg/Nm^3	mg/Nm^3	mg/Nm^3	%	mg/Nm^3	%	%	°C	Nm^3/h
1-Apr	2.0	2.6	0.0	8.2	6.2	8.2	15.6	186.3	110728
2-Apr	1.4	1.2	0.0	8.0	5.4	8.6	14.3	186.6	112987
3-Apr	2.3	3.6	0.0	7.9	8.0	8.8	13.0	186.9	111829
4-Apr	2.3	0.8	0.0	7.6	3.3	9.2	12.5	187.4	115374
5-Apr	2.8	2.1	0.0	7.7	1.7	9.1	12.7	187.6	115450
6-Apr	2.2	0.6	0.0	7.8	3.6	8.7	14.5	187.0	111430
7-Apr	0.7	0.0	0.0	6.6	2.4	10.0	13.8	186.1	106727
8-Apr	1.6	0.4	0.0	7.8	3.3	8.8	15.0	187.0	115743
9-Apr	1.5	0.3	0.0	7.9	5.7	8.8	15.3	186.3	113045
10-Apr	2.0	0.4	0.0	7.8	4.6	9.1	13.6	187.5	116146
11-Apr	1.1	0.1	0.0	7.2	5.4	9.4	14.0	186.1	110038
12-Apr	1.4	1.5	0.0	7.7	10.8	9.3	13.0	187.1	113267
13-Apr	1.9	1.1	0.0	7.8	2.6	8.9	14.0	187.7	117194
14-Apr	1.2	2.2	0.0	7.3	5.5	9.1	15.2	186.3	110362
15-Apr	0.7	0.2	0.0	6.9	14.9	9.4	15.1	184.1	98679
16-Apr	2.0	1.1	0.0	7.8	5.6	8.8	15.5	186.8	112813
17-Apr	1.9	0.7	0.0	8.0	8.3	9.0	14.8	187.0	112433
18-Apr	2.2	0.3	0.0	7.9	7.2	8.9	14.6	187.1	112603
19-Apr	4.2	0.9	0.0	8.2	4.5	8.9	13.1	187.9	116448
20-Apr	3.6	0.0	0.0	8.2	6.5	8.6	14.6	186.8	111331
21-Apr	2.3	1.0	0.0	7.5	3.4	9.3	14.4	185.3	103661
22-Apr	1.9	0.0	0.0	7.7	6.0	9.1	16.3	186.7	110122
23-Apr	2.6	0.2	0.0	8.0	8.9	8.8	15.6	186.3	103170
24-Apr	2.7	1.4	0.0	8.5	9.7	8.2	14.6	187.2	106556
25-Apr	3.1	3.0	0.0	8.3	7.6	8.3	15.1	188.2	110735
26-Apr	3.8	0.4	0.0	8.2	4.9	8.5	15.0	188.8	113064
27-Apr	3.5	0.1	0.0	8.4	7.8	8.4	14.8	187.7	106888
28-Apr	2.6	0.4	0.0	8.1	12.1	8.7	15.2	187.2	103936
29-Apr	0.8	0.0	0.0	7.4	5.3	9.1	16.0	186.1	98469
30-Apr	2.0	0.0	0.0	7.5	3.3	9.4	14.6	187.4	104693

The following table shows the feed rates of conveying screws that extract solid powders of calcium hydroxide, sodium bicarbonate, activated carbons (AC) and calcium solid waste (CSW) from respective silos. The weights of the silos are also reported.

Weight of silos				Screw feed rates								
$Ca(OH)_2$	$NaHCO_3$	AC	CSW	$Ca(OH)_2$ - A	$Ca(OH)_2$ - B	$NaHCO_3$ - A	$NaHCO_3$ - B	AC – 2nd stage	AC – 1st stage - A	AC – 1st stage - B	Recycle - A	Recycle - A
t	t	t	t	%	%	%	%	%	%	%	%	%
28.7	31.1	8.6	1.1	20.5	0.0	3.6	28.5	23.3	23.3	0.0	0.0	0.0
40.9	28.5	8.1	1.2	4.4	15.2	0.0	18.8	23.7	7.8	15.9	0.0	0.0
43.4	25.0	7.9	1.2	16.9	6.8	0.0	38.0	23.7	15.2	8.5	0.0	0.0
32.7	36.8	7.6	1.2	42.2	0.1	8.7	38.2	24.3	24.3	0.3	0.0	0.0
23.5	40.9	7.3	1.3	38.0	0.0	1.4	33.2	24.4	24.4	0.0	0.0	0.0
39.1	37.6	7.1	1.3	31.0	0.0	0.0	22.6	23.6	23.6	0.0	0.0	0.0
51.1	35.6	6.8	1.3	15.3	0.0	0.0	13.1	22.5	22.5	0.0	0.0	0.0
46.7	33.7	6.5	1.2	21.9	0.0	0.0	16.4	24.3	24.3	0.0	0.0	0.0
41.4	31.5	6.3	1.2	19.4	0.0	0.0	16.7	23.7	23.7	0.0	0.0	0.0
35.9	45.5	6.0	1.2	34.4	0.0	0.0	20.5	24.3	24.3	0.0	0.0	0.0
27.2	51.9	5.7	1.2	28.7	0.0	0.0	15.3	23.2	23.2	0.0	0.0	0.0
19.4	49.4	5.4	1.3	38.5	0.6	5.7	33.1	23.8	23.8	0.8	0.0	0.0
22.8	43.3	5.1	1.3	37.7	0.0	11.1	33.1	24.8	24.8	0.0	0.0	0.0
22.7	38.8	4.8	1.2	22.8	0.0	8.0	28.4	23.0	23.0	0.0	0.0	0.0
19.1	36.4	4.7	1.2	12.6	0.0	0.0	13.0	21.2	21.2	0.0	0.0	0.0
24.8	34.6	4.5	1.3	25.3	0.0	0.0	23.2	22.6	23.9	0.0	0.0	0.0
31.5	41.4	4.3	1.3	22.7	0.0	0.0	17.6	23.8	23.8	0.0	0.0	0.0
17.3	53.6	4.1	1.0	26.0	0.0	18.3	12.5	23.9	23.9	0.0	16.4	0.0
21.6	49.2	3.9	0.9	36.6	0.0	44.6	0.0	24.1	24.1	0.0	33.4	0.0
40.0	45.4	3.6	1.0	34.1	0.0	34.5	0.0	23.3	23.0	0.0	26.9	0.0
38.9	41.4	3.5	0.9	25.1	0.0	27.5	0.0	22.0	22.0	0.0	31.6	0.0
34.5	39.3	3.3	0.9	14.6	0.0	20.3	0.0	22.9	22.9	0.0	22.4	0.0
29.6	36.8	6.1	0.6	22.3	0.0	27.3	0.0	22.0	22.0	0.0	28.7	0.0
38.5	32.6	8.6	0.5	29.2	0.0	39.8	0.0	22.8	22.8	0.0	32.8	0.0
35.7	28.9	8.4	0.8	29.2	0.0	36.3	0.0	24.1	24.1	0.0	33.2	0.0
25.4	24.7	8.2	0.3	29.7	0.0	40.9	0.0	24.2	24.2	0.0	33.5	0.0
36.0	33.7	7.9	0.8	26.6	0.0	33.3	0.0	21.5	23.2	0.0	31.2	0.0
40.9	41.5	7.7	0.8	20.7	0.0	30.6	0.0	0.3	22.7	0.0	27.4	0.0
36.8	39.5	7.6	0.9	11.8	0.0	11.7	0.0	15.9	21.4	0.0	20.3	0.0
50.9	37.8	7.4	1.0	16.6	0.0	21.9	0.0	22.6	22.6	0.0	22.4	0.0

Pressure drops measured across the two fabric filters are reported in the following table.

	Δp 1st stage	Δp 2nd stage
	mbar	mbar
1-Apr	11.3	8.8
2-Apr	11.5	8.9
3-Apr	11.2	9.1
4-Apr	11.5	9.2
5-Apr	11.7	9.5
6-Apr	11.3	9.0
7-Apr	10.6	8.6
8-Apr	12.0	9.1
9-Apr	11.7	8.8
10-Apr	12.2	9.3
11-Apr	11.2	8.5
12-Apr	11.6	9.0
13-Apr	12.5	9.5
14-Apr	11.4	8.7
15-Apr	9.7	8.5
16-Apr	11.6	8.9
17-Apr	11.4	9.0
18-Apr	11.1	9.0
19-Apr	11.4	9.4
20-Apr	10.7	9.0
21-Apr	9.7	8.4
22-Apr	10.9	8.7
23-Apr	10.3	8.9
24-Apr	10.9	9.1
25-Apr	11.9	9.0
26-Apr	12.7	9.3
27-Apr	11.6	9.1
28-Apr	11.3	9.0
29-Apr	10.5	8.5
30-Apr	11.7	7.8

Appendix I Ratio to stoichiometric flow rate

Considering a single reaction between a gaseous compound *i* and a solid sorbent *s*, the generic form is:

$$\nu_i i + \nu_s s \rightarrow \nu_p p + \nu_q q \tag{11.1}$$

where ν_x represents the stoichiometric coefficient of the *x*th compound.

Parameter $rs_{i,s}$ of the conversion function proposed in Section 4.2 is defined as the ratio between the actual feed rate of solid reactant $\dot{n}_{s,in}$ and its stoichiometric flow rate $\dot{n}_{s-i,st}$:

$$rs_{i,s} = \frac{\dot{n}_{s,in}}{\dot{n}_{s-i,st}} \tag{11.2}$$

where the stoichiometric flow rate is the sorbent required to consume all of the gaseous compound *i* assuming that the reaction proceeds to completion:

$$\dot{n}_{s-i,st} = \dot{n}_{i,in} \cdot \frac{\nu_s}{\nu_i} \tag{11.3}$$

When more than one acid gas can react with the same solid sorbent (e.g. reactions in Table 4.1), the definition of $rs_{i,s}$ can be adapted as follows:

$$rs_{i,s} = \frac{\dot{n}_{s-i,in}}{\dot{n}_{s-i,st}} \tag{11.4}$$

where the $\dot{n}_{s-i,in}$ is the flow rate of sorbent *s* available for the reaction with the *i*th acid gas. To relate $\dot{n}_{s-i,in}$ to the molar flow rate injected into the system $\dot{n}_{s,in}$, a distribution coefficient $\phi_{i,s}$ was introduced:

$$\dot{n}_{s-i,in} = \phi_{i,s} \cdot \dot{n}_{s,in} \tag{11.5}$$

where $\sum_j \phi_{j,s}$ is equal to 1 (the sum of the sorbent amounts available for all the reactions is the overall amount of sorbent available for the system). The distribution coefficient was defined according to the stoichiometry of the involved reactions:

$$\phi_{i,s} = \frac{\dot{n}_{s-i,st}}{\sum_j \dot{n}_{s-j,st}} \tag{11.6}$$

Combining Eqs. 11.4, 11.5 and 11.6, the generic expression for $rs_{i,s}$ is obtained:

$$rs_{i,s} = \frac{\dot{n}_{s,in}}{\dot{n}_{s,st}} \tag{11.7}$$

where the stoichiometric flow rate is the sorbent required to completely convert all of the gaseous compounds:

$$\dot{n}_{s,st} = \sum_j \left(\dot{n}_{j,in} \cdot \frac{\nu_s}{\nu_j} \right) \tag{11.8}$$

With the assumption described by Eq. 11.6, $rs_{i,s}$ is the same for all the gaseous compounds *i*: $rs_{i,s} = rs_s$.

An alternative approach consists in defining the distribution coefficient $\phi_{i,s}$ according to solid product fractions. In this case, $\phi_{i,s}$ corresponds to the selectivity coefficient of *s* against *q*:

$$\phi_{i,s} = \frac{\frac{\dot{n}_{q,out}}{\nu_q}}{\sum_t \frac{\dot{n}_{t,out}}{\nu_t}} \qquad 11.9$$

where *q* is the solid compound produced by the gaseous reactant *i*, while *t* represents a generic solid produced by the sorbent *s*. This definition, even though more rigorous, requires the knowledge of solid product composition, which was not available in operating data (shown in Section 5.1.3).

Appendix J Analytical solution of the steady-state mass balance equation at a fixed bed

Mass balance at the filter cake (expressed in dimensionless form by Eq. 6.12) refers to a first order reaction, so it can be solved analytically if *Pe* and *Da* are constant and the accumulation term can be neglected (this assumption is discussed in Section 6.3.2). As flow regime does not change during the process, *Pe* value is constant. Conversely, *Da* number depends on sorbent consumption, which intrinsically changes during the process. However, the analytical solution gives an indication of the concentration profile at the beginning of the process, i.e. as long as the sorbent conversion is negligible and hence k_{glob} and *Da* are uniform in the filter cake.

Dimensionless system defined in Section 6.3.1 in steady state condition becomes:

$$\frac{dy}{dx} - \frac{1}{Pe} \cdot \frac{d^2y}{dx^2} + Da \cdot y = 0 \tag{11.10}$$

$$y(x = 0) = y_0 \tag{11.11}$$

$$\left.\frac{dy}{dx}\right|_{x=1} = 0 \tag{11.12}$$

This expression shows that the fractional conversion of gaseous reactant (*y*) in its passage through the reactor is governed by the dimensionless groups *Pe* and *Da*. When these parameters are constant in the reaction section, the fraction of reactant at fore section boundary y_0 can be calculated through the solution obtained by Wehner and Wilhelm (1956):

$$y_0 = g_0 \cdot \left[(1 + a_w) \cdot \exp\left(\frac{a_w \cdot Pe}{2}\right) - (1 - a_w) \cdot \exp\left(-\frac{a_w \cdot Pe}{2}\right)\right] \tag{11.13}$$

where

$$a_w = \sqrt{1 + 4 \cdot \frac{Da}{Pe}} \tag{11.14}$$

$$g_0 = \frac{2}{(1 + a_w)^2 \cdot \exp\left(\frac{a_w \cdot Pe}{2}\right) - (1 - a_w)^2 \cdot \exp\left(-\frac{a_w \cdot Pe}{2}\right)} \tag{11.15}$$

According to Eq. 11.13, the value of y_0 depends upon the parameters *Pe* and *Da* in the reaction section. However, the profile in the reaction section does not depend upon *Pe* in the fore section. Wehner and Wilhelm (1956) calculated also the value of the solution at the exit section of the reactor (*x* = 1):

$$y_1 = 2 \cdot a_w \cdot g_0 \cdot \exp\left(\frac{Pe}{2}\right) \tag{11.16}$$

Analytical solution

The system given by Eqs. 11.10 - 11.12 has been analytically solved with Matlab through the following command:

```
y=simplify(dsolve('D2y=Pe*Dy+Da*Pe*y, Dy(1)=0, y(0)=y_0','x'));
```

where y_0 is the function $y_0(Pe,Da)$ written according to Eq. 11.13.

The resulting concentration profile is:

$$
\begin{aligned}
y = \\
& y_0\cdot(Pe\cdot\exp(x\cdot(Pe/2-(Pe\cdot(Pe+4\cdot Da))^{(1/2)}/2))\cdot\exp(Pe/2+(Pe\cdot(Pe+4\cdot Da))^{(1/2)}/2) \\
& -Pe\cdot\exp(x\cdot(Pe/2+(Pe\cdot(Pe+4\cdot Da))^{(1/2)}/2))\cdot\exp(Pe/2-(Pe\cdot(Pe+4\cdot Da))^{(1/2)}/2) \\
& +\exp(x\cdot(Pe/2-(Pe\cdot(Pe+4\cdot Da))^{(1/2)}/2))\cdot\exp(Pe/2+(Pe\cdot(Pe+4\cdot Da))^{(1/2)}/2)\cdot(Pe\cdot(Pe+4\cdot Da))^{(1/2)} \\
& +\exp(x\cdot(Pe/2+(Pe\cdot(Pe+4\cdot Da))^{(1/2)}/2))\cdot\exp(Pe/2- \\
& (Pe\cdot(Pe+4\cdot Da))^{(1/2)}/2)\cdot(Pe\cdot(Pe+4\cdot Da))^{(1/2)}))/(\exp(Pe/2- \\
& (Pe\cdot(Pe+4\cdot Da))^{(1/2)}/2)\cdot(Pe\cdot(Pe+4\cdot Da))^{(1/2)} \\
& +\exp(Pe/2+(Pe\cdot(Pe+4\cdot Da))^{(1/2)}/2)\cdot(Pe\cdot(Pe+4\cdot Da))^{(1/2)} \\
& -Pe\cdot\exp(Pe/2-(Pe\cdot(Pe+4\cdot Da))^{(1/2)}/2)+Pe\cdot\exp(Pe/2+(Pe\cdot(Pe+4\cdot Da))^{(1/2)}/2)
\end{aligned}
\qquad 11.17
$$

Analysis of analytical solution profiles

Figure 11.7 shows the concentration profiles given by Eq. 11.17, where both convection and axial dispersion terms were taken into account. Concentration profiles were plotted for different values of *Pe* number, while *Da* value was always set to 1.

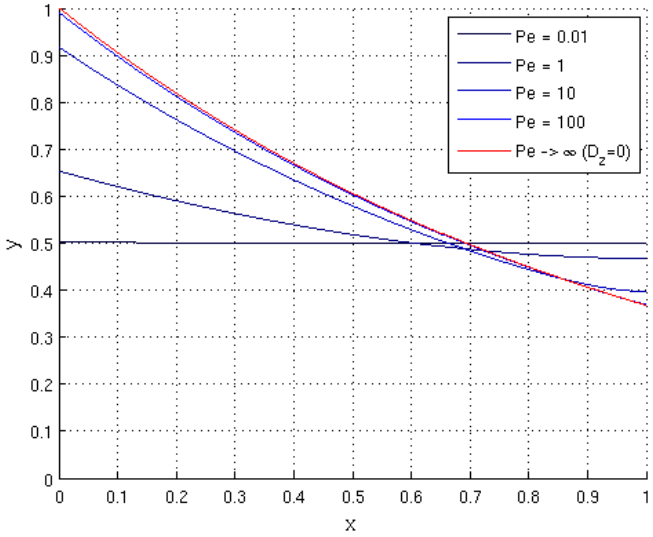

Figure 11.7 - Plot of analytical solutions for steady-state mass balance equations with convection and axial dispersion for *Da* = 1 and *Pe* between 0.01 and 100; also analytical solution of the asymptotic case with only convection is plotted (red line).

When convection mass transport is negligible compared to axial dispersion (i.e. $Pe = 0.01$), the concentration profile is almost uniform throughout the reaction section, according to a CSTR behavior. In this case, as the left-hand boundary condition has been set by Eq. 11.13, the value of the solution at $x = 0$ corresponds to the limit of y_0 for *Pe* approaching zero[58]:

[58] In Matlab: limit(y_0,Pe,0,'right')

$$\lim_{Pe\to 0} y_0\,(Pe, Da) = \frac{1}{1+Da} \qquad 11.18$$

As Da = 1, y_0 tends to 0.5, as verified by the darker line in Figure 11.7.

On the other hand, when diffusive mass transport is negligible (i.e. Pe = 100), the solution should correspond with the profile obtained solving the mass balance equation without the axial dispersion term. In order to verify this asymptotic behavior, the concentration profile for pure convection was calculated.

Analytical solution for pure convection

When mass transport is governed by convection (i.e. $Pe\to\infty$), Eq. 11.10 becomes:

$$\frac{dy}{dx} + Da \cdot y = 0 \qquad 11.19$$

The value of y_0 was determined calculating the limit for $Pe\to\infty$ of Eq. 11.13, which results:

$$\lim_{Pe\to\infty} y_0 = 1 \qquad 11.20$$

Thus, the boundary condition required to solve the mass balance is:

$$y(x=0) = 1 \qquad 11.21$$

This result confirms that when the effect of axial dispersion is negligible, the concentration of the reactant gas at the beginning of the filter cake is equal to the concentration entering the system C_{in}, i.e. $y(x{=}0){=}1$.

Thus, the solution for the dimensionless concentration profile in the reaction section is[59]:

$$y = \exp[-Da \cdot x] \qquad 11.22$$

Concentration profile given by Eq. 11.22 is shown by red line in Figure 11.7. This is almost overlapped the solution of the general mass balance equation solved with Pe = 100, except in the exit zone (i.e. for x approaching 1), because of the right-hand boundary condition imposed by Eq. 11.12.

Discussion about the assumptions on uniformity of *Pe* and *Da*

Previously solutions were found assuming that Pe and Da numbers were constant in the reaction section. When $Pe \ll 1$, concentration profile is uniform; hence, sorbent particles react with the same velocity and Da number decreases homogenously in the bed. In this case, the system can be solved as a series of pseudo steady states. Otherwise, a generic solution must be calculated through a numerical method which permits to define the Da number as a function of the dimensionless position x (this case is reported in Section 6.3.3).

The analysis of the initial transient and a discussion on the assumption of neglecting the accumulation term are reported in the Section 6.3.2.

[59] Corresponding Matlab command is:
y=simplify(dsolve('Dy+Da*y=0,y(0)=1','x'))

Appendix K Notes about boundary conditions

Left-hand boundary of the reaction section

According to Wehner and Wilhelm (1956), at the left-hand boundary of the reaction section ($x = 0$) the slopes can be discontinue because of the boundary conditions:

$$y(0^-) = y(0^+) \tag{11.23}$$

$$y(0^-) - \frac{1}{Pe_l}\frac{dy}{dx}\Big|_{x\to 0^-} = y(0^+) - \frac{1}{Pe}\frac{dy}{dx}\Big|_{x\to 0^+} \tag{11.24}$$

where Pe_l is the value of the Peclet number in the fore section, while Pe represents Peclet number in the reaction section.

Right-hand boundary condition

The right-hand boundary conditions should be set at $x \to \infty$, where y must be finite (Wehner and Wilhelm, 1956), hence:

$$\frac{dy}{dx}\Big|_{x\to\infty} = 0 \tag{11.25}$$

The differential equation for the section after the exit of the reactor ($x > 1$) is

$$\frac{1}{Pe_r}\frac{d^2y}{dx^2} - \frac{dy}{dx} = 0 \tag{11.26}$$

where Pe_r is the value of the Peclet group in the after section. The general solution of Eq. 11.26 is

$$y(x) = c_1 + c_2 \cdot \exp[Pe_r \cdot x] \tag{11.27}$$

For the boundary condition (Eq. 11.25), c_2 has to be zero. Thus, the solution yields a flat profile, so:

$$\frac{dy}{dx}\Big|_{x\to 1^+} = 0 \tag{11.28}$$

The conservation of the reactant at the exit of the reaction section ($x = 1$) can be expressed through the equivalence of the fluxes on the two sides of the right-hand boundary:

$$u(1^-) \cdot A(1^-) \cdot \left[y(1^-) - \frac{1}{Pe}\frac{dy}{dx}\Big|_{x\to 1^-}\right] = u(1^+) \cdot A(1^+) \cdot \left[y(1^+) - \frac{1}{Pe_r}\frac{dy}{dx}\Big|_{x\to 1^+}\right]$$

where u is the linear velocity and A is the cross-sectional area through which flow occurs.

Because of the continuity of the solution at the end of the reaction section:

$$y(1^-) = y(1^+)$$

and the total continuity equation states that

$$u(1^-) \cdot A(1^-) = u(1^+) \cdot A(1^+)$$

The result is that the gradient at the end of the reaction section is zero:

$$\frac{1}{Pe} \left.\frac{dy}{dx}\right|_{x \to 1^-} = \frac{1}{Pe_r} \left.\frac{dy}{dx}\right|_{x \to 1^+} = 0$$

leading to the boundary condition given in Eq. 6.22.

Appendix L Implementation in Matlab of the mass balance equation at the filter cake

The discretization equations that describe the mass balance equation at the filter cake with corresponding boundary conditions (obtained in Section 6.3.3), have to be solved together for the solution in the *n* grid points of the space domain (i.e. $y_1 - y_n$). According to the calculation domain illustrated in Figure 11.8, there are *n* grid points and *n* control volumes (*n*-2 *complete* internal control volumes and 2 *half* boundary control volumes).

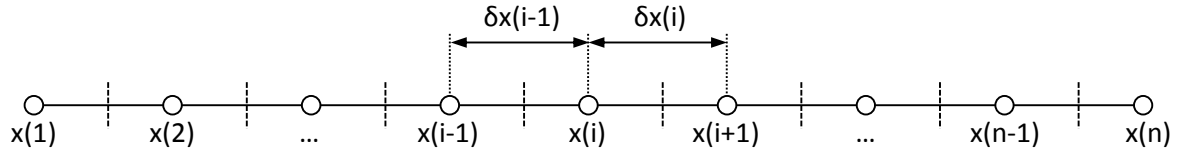

Figure 11.8 - Calculation domain implemented in Matlab; white dots x(i) represent the grid points and δx(i) the dimensionless distance between the points x(i) and x(i+1).

Once created the vector *x* representing the space domain in the axial direction (representing the dimensionless coordinate between -∞ and 1), the number of grid points *n* is the size of the vector *x*. The vector with the dimensionless distances between adjacent grid points can be evaluated through the command *δx=diff(x)*. Thus, the resulting vector *δx* contains *n*-1 elements defined by the correlation:

$$\delta x(i) = x(i+1) - x(i)$$

For each *i*th control volume (with *i* = 1, 2, …, *n*), the discretization equation can be written as:

$$a_P(i) \cdot y(i) = a_E(i) \cdot y(i+1) + a_W(i) \cdot y(i-1) + b_i(i) \qquad 11.29$$

where the coefficients $a_P(i)$, $a_E(i)$, $a_W(i)$, and $b(i)$ correspond to the coefficients of the discretization equation 6.26 according to the Table 11.9.

Table 11.9 - Correspondence between the coefficients of discretization equations 6.26 and 11.29

Coefficient in Eq. 6.26	**Coefficient in Eq. 11.29**
a_i	$a_P(i)$
a_{i-1}	$a_W(i)$
a_{i+1}	$a_E(i)$
b_i	$b(i)$

Thus, the searched value of *y*(*i*) is related to the neighboring solutions *y*(*i*+1) and *y*(*i*-1). Coefficients of Eq. 11.29 were written according to Eqs. 6.27 - 6.30 for internal control volumes, to Eqs. 6.35 - 6.37 for the first control volume (representing the left-hand boundary condition), and to Eqs. 6.42 - 6.44 for the *n*th control volume (right-hand boundary condition). Resulting vectors of the coefficients are:

$$\bar{a}_W = \begin{bmatrix} 0^* \\ \vdots \\ \dfrac{1}{Pe(i-1)\cdot\delta x(i-1)} + \dfrac{1}{2} \\ \vdots \\ \dfrac{1}{Pe(n-1)\cdot\delta x(n-1)} + \dfrac{1}{2} \end{bmatrix} \tag{11.30}$$

$$\bar{a}_E = \begin{bmatrix} 0 \\ \vdots \\ \dfrac{1}{Pe(i)\cdot\delta x(i)} - \dfrac{1}{2} \\ \vdots \\ 0^* \end{bmatrix} \tag{11.31}$$

$$\bar{a}_P = \begin{bmatrix} 1 \\ \vdots \\ a_W(i) + a_E(i) + Da(i)\cdot\dfrac{\delta x(i) + \delta x(i-1)}{2} \\ \vdots \\ a_W(n) + a_E(n) + Da(n)\cdot\dfrac{\delta x(n-1)}{2} \end{bmatrix} \tag{11.32}$$

$$\bar{b} = \begin{bmatrix} 1 \\ \vdots \\ 0 \\ \vdots \\ 0 \end{bmatrix} \tag{11.33}$$

To take into account the different form of the boundary-point equations, coefficients $a_W(1)$ and $a_E(n)$ (indicated with a *) were set to zero (they do not play any role in the calculation, so any value could be used).

The *n* discretization equations expressed in the form of Eq. 11.29 can be rewritten as:

$$\bar{\bar{A}} \cdot \bar{y} = \bar{b} \tag{11.34}$$

where $\bar{\bar{A}}$ is the tri-diagonal matrix of the coefficients $a_W(i)$, $a_P(i)$, and $a_E(i)$, with all the nonzero coefficients located along three diagonals of the matrix:

$$\bar{\bar{A}} \overset{\text{def}}{=} \begin{bmatrix} a_P(1) & -a_E(1) & 0 & 0 & 0 & 0 & 0 \\ -a_W(1) & a_P(2) & -a_E(2) & 0 & 0 & 0 & 0 \\ 0 & \ddots & \ddots & \ddots & 0 & 0 & 0 \\ 0 & 0 & -a_W(i) & a_P(i) & -a_E(i) & 0 & 0 \\ 0 & 0 & 0 & \ddots & \ddots & \ddots & 0 \\ 0 & 0 & 0 & 0 & -a_W(n-1) & a_P(n-1) & -a_E(n-1) \\ 0 & 0 & 0 & 0 & 0 & -a_W(n) & a_P(n) \end{bmatrix} \tag{11.35}$$

and $\bar{y}$ is the vector of the searched solutions:

$$\bar{y} = \begin{bmatrix} y(1) \\ y(2) \\ \vdots \\ y(i) \\ \vdots \\ y(n-1) \\ y(n) \end{bmatrix} \tag{11.36}$$

Thus, the vector of the solutions can be calculated multiplying the inverse of the square matrix $\bar{\bar{A}}$ by the vector $\bar{b}$:

$$\bar{y} = \bar{\bar{A}}^{-1} \cdot \bar{b} \tag{11.37}$$

Appendix M Mass balance equation for a porous particle

Mass balance equation

According to the grain model (described in Section 3.3.3 and implemented in Section 6.4), the governing equation in the particle pores and corresponding initial and boundary conditions are:

$$\varepsilon_x \cdot \frac{\partial C_1}{\partial t} - \frac{1}{R^2}\frac{\partial}{\partial R}\left(R^2 \cdot D_{ef} \cdot \frac{\partial C_1}{\partial R}\right) = -r_{vp} \tag{11.38}$$

$$C_1(R, z, 0) = 0 \tag{11.39}$$

$$D_{ef} \cdot \left.\frac{\partial C_1}{\partial R}\right|_{R=R_p} = k_g \cdot \left[C(z,t) - C_1(R_p, z, t)\right] \tag{11.40}$$

$$\left.\frac{\partial C_1}{\partial R}\right|_{R=0} = 0 \tag{11.41}$$

where

- C_1 is the gas concentration in the intraparticle pores;
- R is the radial coordinate in the particle, varying from 0 (center of the particle) to R_p (radius of the particle);
- ε_x is the porosity of the reacting particle;
- D_{ef} is the effective diffusion coefficient within the particles, which is a function of particle tortuosity τ_p and porosity ε_x (therefore it depends on radial position R and time through correlations reported in Section 6.5);
- r_{vp} is the reaction rate per unit volume of the particle;
- k_g is the external mass transfer coefficient.

External mass transfer

The external mass transfer affects the concentration profile through the boundary condition given by Eq. 11.40. Harker et al. (2002) model this effect through the steady-state film-theory, assuming that the difference in concentration between the bulk fluid, $C(z,t)$, and the external surface of the particle, $C_1(R_p, z, t)$, is confined to a narrow laminar boundary-layer. Assuming that the accumulation in this zone is negligible, the rate of mass transfer is governed by a mass transfer coefficient defined as the ratio of the fluid diffusivity to the thickness of boundary film:

$$k_g = \frac{D}{x_f} \tag{11.42}$$

Generally, the boundary film does not offer much resistance to mass transfer, except during the unsteady state conditions that exist when a pellet is first exposed to a fluid (Harker et al., 2002). Thus, the effect of the

boundary film on mass transfer in packed bed was estimated calculating the coefficient k_g through the Ranz and Marshall correlation (proposed in Section 6.5).

Solution of the system in dimensionless variables

The mass balance at particle pores can be rewritten making use of the following dimensionless variables:

- $x_1 = \frac{R}{R_p}$
- $y_1 = \frac{C_1 - C_{eq}}{C - C_{eq}}$
- $\tau_1 = \frac{t}{t_{c,part}}$

The characteristic time of the particle $t_{c,part}$ has been defined as:

$$t_{c,part} = \frac{1}{k_{part}} \qquad 11.43$$

where k_{part} is the overall reaction rate constant of the particle expressed according to the grain model by Eq. 6.76.

The mass balance equation in dimensionless form becomes:

$$\varepsilon_x \cdot \frac{\partial y_1}{\partial \tau_1} = \frac{1}{{x_1}^2} \cdot \frac{\partial}{\partial x_1}\left({x_1}^2 \cdot \frac{1}{{Th_p}^2} \cdot \frac{\partial y_1}{\partial x_1}\right) - y_1 \qquad 11.44$$

$$y_1(\tau_1 = 0) = 0 \qquad 11.45$$

$$\frac{1}{Bi} \cdot \frac{\partial y_1}{\partial x_1}\bigg|_{x=1} = 1 - y_1(x_1 = 1) \qquad 11.46$$

$$\frac{\partial y_1}{\partial x_1}\bigg|_{x=0} = 0 \qquad 11.47$$

Two dimensionless groups emerged from this formulation, defined as follows:

- $Th_p = R_p \cdot \sqrt{\frac{k_{part}}{D_{ef}}}$ is the Thiele number, representing the relative importance of chemical kinetics and pore diffusion;
- $Bi = \frac{k_g \cdot R_P}{D_{ef}}$ is the Biot number, which measures the relative importance of the boundary-film and intra-pellet diffusion in mass transfer (a high value of *Bi* indicates that intra-pellet diffusion is controlling the rate of transport).

This system has to be solved in order to verify the assumption made in Section 6.4 of uniform concentration profile in the considered cases. Thus, the solution was searched for the initial stages of the process, when the reaction proceed at the maximum rate and an unsteady state condition is present due to the first exposure of the particle to the flue gas. In this condition, all of the grains show the same conversion degree, as the particle is formed only by sorbent, i.e. $r_c = r_g$. Thus, also the porosity of the reacting particle (ε_x) and

the effective diffusion coefficient (D_{ef}) are homogenous within the particle. According to Eq. 6.76, the overall reaction rate constant of the particle assumes its initial (and maximum) value:

$$k_{part} = \frac{3 \cdot (1 - \varepsilon_p)}{r_g} \cdot k_s \qquad 11.48$$

Under this assumption, the partial differential equation representing the mass balance at a spherical particle was solved with the Matlab® tool *pdepe*.

As described in Section 6.3.2, the form required by the solver is:

$$c\left(x_1, \tau_1, y_1, \frac{\partial y_1}{\partial x_1}\right) \cdot \frac{\partial y_1}{\partial \tau_1} = {x_1}^{-m} \cdot \frac{\partial}{\partial x_1}\left({x_1}^{-m} \cdot f\left(x_1, \tau_1, y_1, \frac{\partial y_1}{\partial x_1}\right)\right) + s\left(x_1, \tau_1, y_1, \frac{\partial y_1}{\partial x_1}\right) \qquad 11.49$$

with the initial condition:

$$y_1(x_1, \tau_{1,0}) = y_{1,0}(x_1) \qquad 11.50$$

and the boundary conditions:

$$p(a, \tau_1, y_1(a, \tau_1)) + q(a, \tau_1) \cdot f\left(a, \tau_1, y_1(a, \tau_1), \frac{\partial y_1(a, \tau_1)}{\partial x_1}\right) = 0 \qquad 11.51$$

$$p(b, \tau_1, y_1(b, \tau_1)) + q(b, \tau_1) \cdot f\left(b, \tau_1, y_1(b, \tau_1), \frac{\partial y_1(b, \tau_1)}{\partial x_1}\right) \qquad 11.52$$

From the comparison of Eq. 11.49 and Eq. 11.44, solver parameters were set as follow:

- $a = 0$
- $b = 1$
- $m = 2$
- $c = \varepsilon_x$
- $f = \frac{1}{{Th_p}^2} \cdot \frac{\partial y_1}{\partial x_1}$
- $s = -y_1$
- $y_0(x) = 0$
- $p(a) = 0$
- $q(a) = {Th_p}^2$
- $p(b) = y_1 - 1$
- $q(b) = \frac{{Th_p}^2}{Bi}$

Analysis of model results

The mass balance equation was solved for some significant values of the dimensionless group that control the diffusion process in the particle pores. Resulting concentration profiles permitted to clarify in which cases the concentration variation with the radial coordinate of the particle can be neglected and when it has to be taken into account (and therefore incorporated into the mass balance equation at the filter cake).

Case 1: Th_p = 1, Bi = 1 and ε_p = 0.5

The dimensionless concentration $y_1(\tau_1,x_1)$ in the particle pores for Th_p = 1, Bi = 1 and ε_p = 0.5 is shown in Figure 11.9.

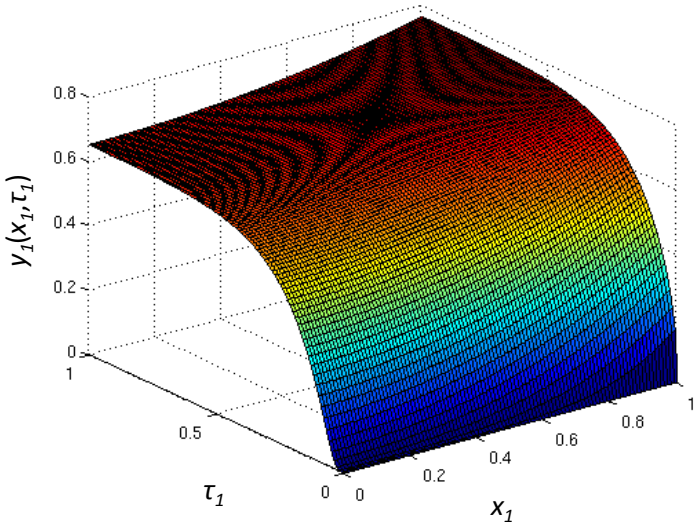

Figure 11.9 – Dimensionless concentration of gaseous reactant within the particle (y_1) as a function of dimensionless radial position (x_1) and time (τ_1); the mass balance equation was solved setting Th_p = 1, Bi = 1 and ε_p = 0.5.

This result shows that when Thiele number and Biot number are equal to one, the concentration in the particle pores is significantly lower than the value in the interparticle voids of the filter cake. However, even though the variation within the particle is not negligible, the concentration difference is due especially to the resistance in the boundary film. This aspect is more evident in the profile concentration within the porous particle at τ_1 = 1, shown in Figure 11.10.

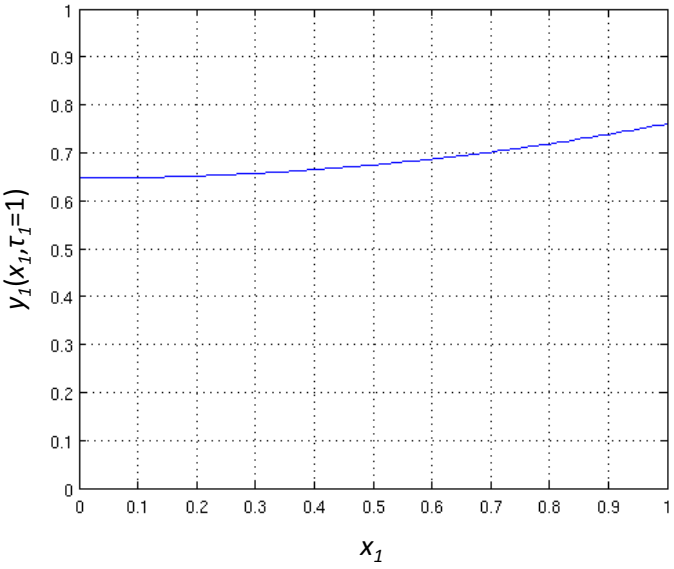

Figure 11.10 – Profile of the dimensionless concentration of gaseous reactant (y_1) within the particle as a function of dimensionless radial position (x_1); the mass balance equation was solved setting Th_p = 1, Bi = 1 and ε_p = 0.5.

Another interesting result is that the concentration variation reach a pseudo steady state very quickly both at the particle surface (as shown in Figure 11.12) and at the particle center (Figure 11.11). Indeed, at τ_1 = 1 the time is equal to $t_{c,part}$, thus inversely proportional to the grain radius (according to Eq. 11.48). In the analyzed cases (reaction of porous particle with high specific surface) this length is of the order of 10^{-7} - 10^{-8} m, hence $t_{c,part}$ results negligible compared to the typical time of the process.

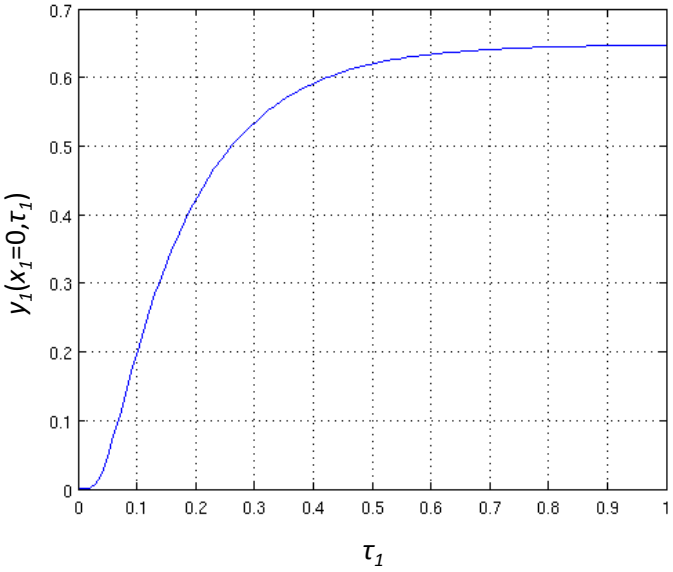

Figure 11.11 - Dimensionless concentration of gaseous reactant (y_1) at the center of the particle (x_1=0) as a function of dimensionless time (τ_1); the mass balance equation was solved setting Th_p = 1, Bi = 1 and ε_p = 0.5.

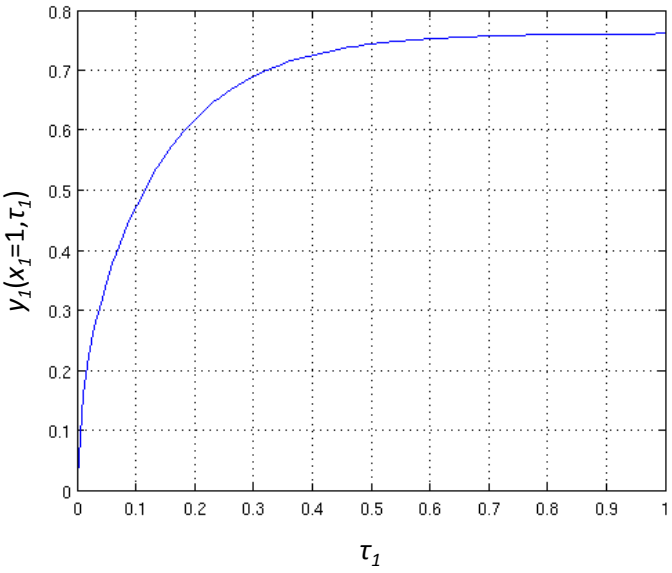

Figure 11.12 - Dimensionless concentration of gaseous reactant (y_1) at the surface of the particle (x_1=1) as a function of dimensionless time (τ_1); the mass balance equation was solved setting Th_p = 1, Bi = 1 and ε_p = 0.5.

Case 2: Th_p = 1, Bi = 10 and ε_p = 0.5

In this case, a high value of the Biot number means that the mass transfer is controlled by the diffusion inside the particle, while the film mass transfer rate is much higher. As shown in Figure 11.13, at τ_1 = 1 the dimensionless concentration at the surface is almost the same as the concentration in the bulk (i.e. $y_1(x_1=1) \approx 1$) and the variation is almost completely inside the particle.

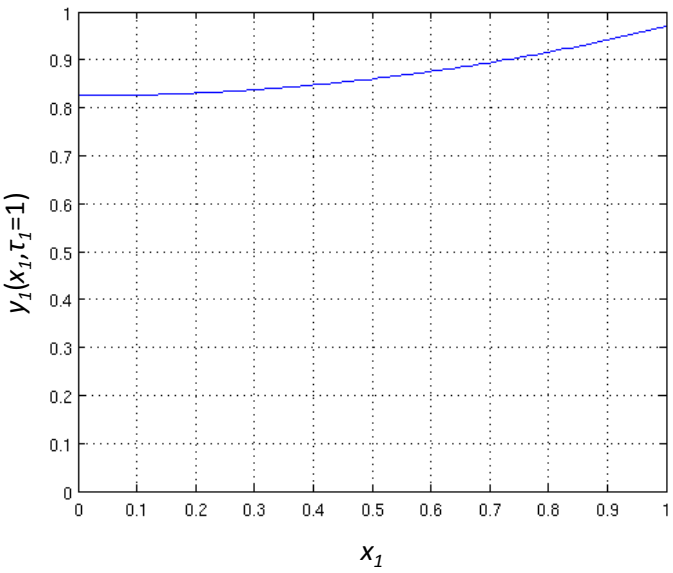

Figure 11.13 - Profile of the dimensionless concentration of gaseous reactant (y_1) within the particle as a function of dimensionless radial position (x_1) at τ_1 = 1; the mass balance equation was solved setting Th_p = 1, Bi = 10 and ε_p = 0.5.

Case 3: Th_p = 0.1, Bi = 0.01 and ε_p = 0.5

Conversely, a low value of the Biot number indicates that the controlling resistance is associated to the film mass transfer. Indeed, the concentration profile within the particle at τ_1 = 1 is almost flat and the concentration variation is only in the boundary film: $y_1(x_1=0) \approx y_1(x_1=1)$. In this case, instead of including the mass balance equation at the particle into the governing equation of the filter cake, it is possible to evaluate the ratio between $C(z,t)$ and $C_1(R_p,z,t)$, which can then be used in the reaction term.

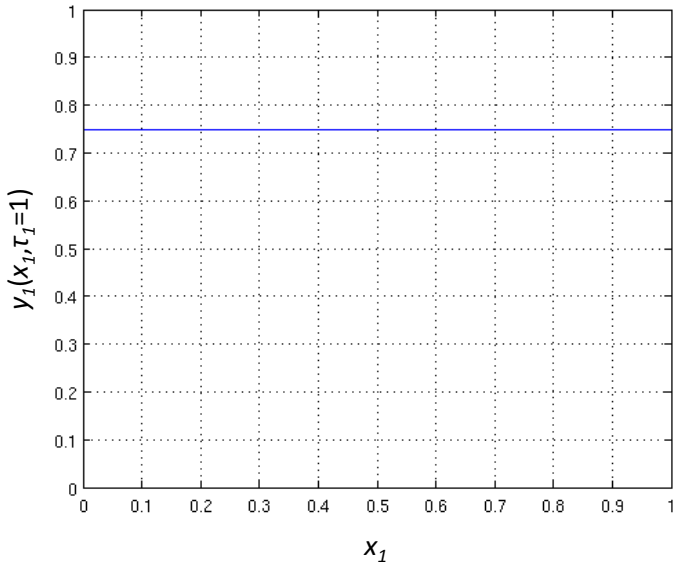

Figure 11.14 - Profile of the dimensionless concentration of gaseous reactant (y_1) within the particle as a function of dimensionless radial position (x); the mass balance equation was solved setting Th_p = 1, Bi = 0.01 and ε_p = 0.5.

Appendix N Mass balance verification

The implementation of the fundamental model was verified through overall mass balances with the aim of confirming the discretization of spatial and time domains. In this appendix, the mass balance is referred to the HCl neutralization by $Ca(OH)_2$:

$$HCl + \frac{1}{2}\, Ca(OH)_2 \rightarrow \frac{1}{2}\, (CaCl_2 \cdot 2H_2O)$$

However, the procedure is the same for other gaseous and solid reactants.

Discretization of the spatial domain

For every time step, the HCl mass balance at the entire spatial domain, i.e. $z \in (-\infty,+\infty)$, should be verified:

$$\dot{n}_{HCl,in} - \dot{n}_{HCl,out} = \int_V \dot{n}_{HCl,g}''' \cdot dV \qquad 11.53$$

Hence:

$$\dot{V} \cdot (C_{in} - C_{out}) = \int_{-\infty}^{+\infty} k_{glob} \cdot (C - C_{eq}) \cdot S_t \cdot dx \qquad 11.54$$

As the reaction term is not null only in the reaction section, i.e. $x \in [0,1]$, Eq. 11.54 becomes:

$$S_t \cdot u_0 \cdot [(C_{in} - C_{eq}) - (C_{out} - C_{eq})] = \int_0^1 k_{glob} \cdot L \cdot (C - C_{eq}) \cdot S_t \cdot dx \qquad 11.55$$

Dividing both terms by $(C_{in} - C_{eq})$ leads to the following form of the HCl mass balance:

$$1 - y_{out} = \int_0^1 Da \cdot y \cdot dx \qquad 11.56$$

where both *Da* and *y* are a function of the axial position in the bed *x*.

Discretization of the time domain

The validation of the time domain discretization was made through an overall mass balance verification, i.e. comparing the conversion of HCl and $Ca(OH)_2$ during the entire process.

The average HCl conversion during the process can be calculated as

$$\chi_{HCl}{}^{*} \overset{\text{def}}{=} \frac{\dot{n}_{HCl,in} - \dot{n}_{HCl,out}{}^{*}}{\dot{n}_{HCl,in}} = \frac{C_{HCl,in} - C_{HCl,out}{}^{*}}{C_{HCl,in}} \cong 1 - y_{out}{}^{*} \qquad 11.57$$

where the symbol * indicates the average value during the process[60], i.e. between $t = 0$ and $t = t_{fin}$. Thus:

$$\chi_{HCl}{}^{*} = 1 - \frac{1}{t_{fin}} \cdot \int_{0}^{t_{fin}} y_{out} dt = 1 - \frac{1}{t_{fin}} \cdot \sum_{t=0}^{t_{fin}-\Delta t} \left(\frac{y(t) + y(t+\Delta t)}{2} \cdot \Delta t \right) \tag{11.58}$$

The average conversion of the sorbent bed of at the end of the process ($t = t_{fin}$) is given by

$$\chi_{Ca(OH)_2}{}^{*} \stackrel{\text{def}}{=} 1 - \frac{n_{Ca(OH)_2,fin}}{n_{Ca(OH)_2,0}} \tag{11.59}$$

According to the grain model, the amount of sorbent is given by the sum of the unreacted cores of the grains. Indicating with n_g the number of grains per particle and with n_p the number of particle in the fixed bed, the average conversion can be expressed as:

$$\chi_{Ca(OH)_2}{}^{*} = 1 - \frac{\frac{4}{3} \cdot \pi \cdot r_c{}^{*3} \cdot \frac{\rho_s}{M_s} \cdot n_g \cdot n_p}{\frac{4}{3} \cdot \pi \cdot r_g{}^{3} \cdot \frac{\rho_s}{M_s} \cdot n_g \cdot n_p} = 1 - \frac{r_c{}^{*3}}{r_g{}^{3}} \tag{11.60}$$

where $r_c{}^{*3}$ is the average value of the unreacted core radii along the the axial coordinate of the sorbent bed ($x \in 0 \div 1$) at the end of the process ($t = t_{fin}$):

$$\chi_{Ca(OH)_2}{}^{*} = 1 - \frac{1}{L} \cdot \int_{0}^{L} \frac{r_c{}^{3}}{r_g{}^{3}} dz = 1 - \frac{1}{r_g{}^{3}} \cdot \sum_{x=0}^{1-\Delta x} \left(\frac{r_c(x)^3 + r_c(x+\Delta x)^3}{2} \cdot \Delta x \right) \tag{11.61}$$

According to the stoichiometry of HCl neutralization reaction, the following equivalence should be verified:

$$\chi_{Ca(OH)_2}{}^{*} \cdot n_{Ca(OH)_2,0} = \frac{1}{2} \cdot \chi_{HCl}{}^{*} \cdot \dot{n}_{HCl,in} \cdot t_{fin} \tag{11.62}$$

where

$$n_{Ca(OH)_2,0} = \frac{4}{3} \cdot \pi \cdot r_g{}^{3} \cdot \frac{\rho_s}{M_s} \cdot n_g \cdot n_p{}''' \cdot V_{bed} \tag{11.63}$$

According to Eq. 6.78, the number of sorbent particle per unit volume of fixed bed can be expresses as:

$$n_p{}''' = \frac{(1-\varepsilon) \cdot (1-F_i)}{\frac{4}{3} \cdot \pi \cdot R_p{}^{3}} \tag{11.64}$$

while the number of grains per particle is given by:

---

[60] Strictly speaking, $y_{out}{}^{*}$ is

$$y_{out}{}^{*} = \frac{C_{HCl,out}{}^{*} - C_{eq}}{C_{HCl,in} - C_{eq}}$$

However, the approximation

$$y_{out}{}^{*} = \frac{C_{HCl,out}{}^{*}}{C_{HCl,in}}$$

is justified by the great difference between the values of $C_{HCl,out}$ (or $C_{HCl,in}$) and C_{eq} during the analyzed process.

$$n_g = \frac{V_{part} \cdot (1 - \varepsilon_p)}{V_{grain}} = \frac{\frac{4}{3} \cdot \pi \cdot {R_p}^3 \cdot (1 - \varepsilon_p)}{\frac{4}{3} \cdot \pi \cdot {r_g}^3} = \frac{{R_p}^3}{{r_g}^3} \cdot (1 - \varepsilon_p) \quad 11.65$$

Hence[61]:

$$n_{Ca(OH)_2,0} = V_{bed} \cdot (1 - \varepsilon) \cdot (1 - F_i) \cdot (1 - \varepsilon_p) \cdot \frac{\rho_s}{M_s} \quad 11.66$$

[61] When the mass of the particle bed is given, it can be used to calculate the initial number of sorbent moles:

$$n_{Ca(OH)_2,0} = \frac{m_{bed}}{M_s}$$

Appendix O Verification of the model implementation in the case of HCl removal with $NaHCO_3$

The solution of the mass balance equation calculated in the experimental conditions adopted by Fellows and Pilat (1990), shown in Section 7.2, was analyzed in order to verify the correct implementation of the model.

The pseudo steady state assumption, which consists in neglecting the accumulation term of the governing equation at the fixed bed, was justified by the comparison of the experimental time (t_{fin} = 1800 s) with the characteristic time of the mass balance equation

$$t_c = \frac{L}{u_0} = 1.16 \cdot 10^{-1}\ s$$

Indeed, the variation of the unreacted core radius (and accordingly the other properties) was negligible even at the beginning of the process, i.e. when the reaction rate is maximum[62].

The dimensionless groups required to solve the equation were the Péclet number

$$Pe = \frac{u_0 \cdot L}{\varepsilon \cdot D_z} = 34.84$$

and the Damköhler number, which at the beginning of the process was equal to

$$Da_0 = \frac{k_{glob,0} \cdot L}{u_0} = 1.31$$

With the values of k_s and D_s found in Section 7.2.3, it was possible to calculate the variation of the *Da* number in time by means of Eqs. 6.62 and 6.82, leading to the HCl concentration profile illustrated in Figure 11.15.

[62] The variation of the unreacted core radius between t = 0 and $t = t_c$ was $3 \cdot 10^{-3}$ %, and the corresponding variation of Damköhler number was $8 \cdot 10^{-2}$ %.

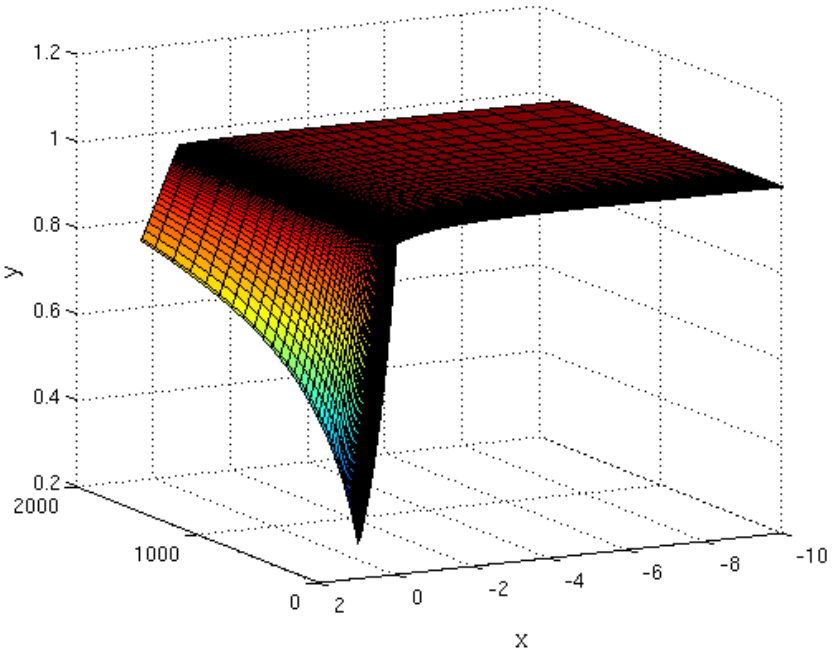

Figure 11.15 - HCl fraction in the fixed bed as a function of the dimensionless position *x* during the time interval of the experimental run carried out by Fellows and Pilat (1990).

In this case, the variation of the HCl concentration is almost entirely within the particle bed. This behavior, which is clearly illustrated in Figure 11.16 for the beginning of the process, is due to high value of the Peclet number, as discussed in Case 3 of Section 6.3.4. Indeed, the fraction of the HCl at the entrance section of the bed at the beginning of the process, calculated by means of Eq. 11.13, resulted:

$$y_0 = 0.965$$

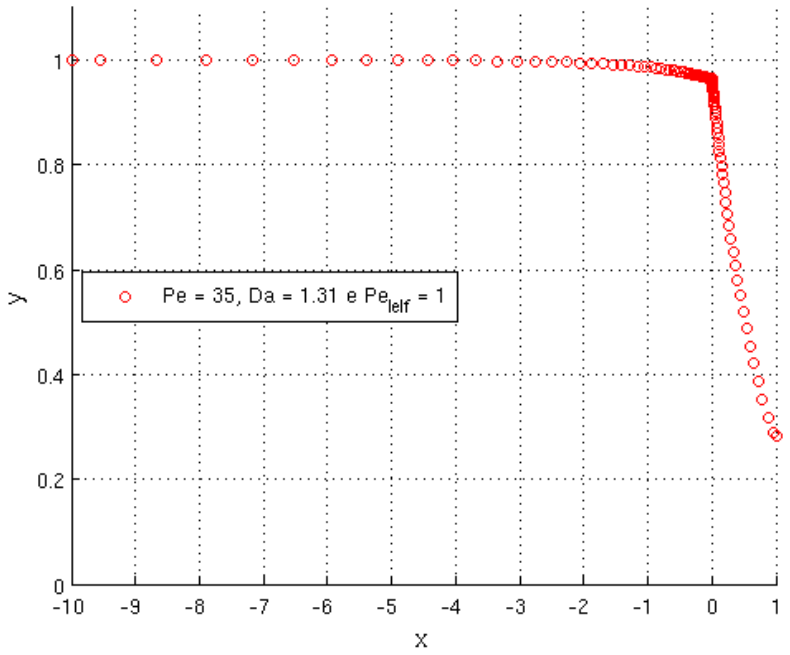

Figure 11.16 – Solution of the mass balance equation at the beginning of the process ($\tau = 1$) in fore section ($x < 0$, with $Da = 0$ and $Pe = 1$) and in reaction section ($0 \leq x \leq 1$, with $Da = 1.31$ and $Pe = 34.8$).

The spatial grid was verified through the comparison of the initial solution calculated through the finite volume method with the analytical solution obtained with the initial values of *Pe* and *Da*. The comparison is shown in Figure 11.17, where also the value of HCl fraction at the exit section calculated by means of Eq. 11.16 is reported:

$$y_1 = 0.282$$

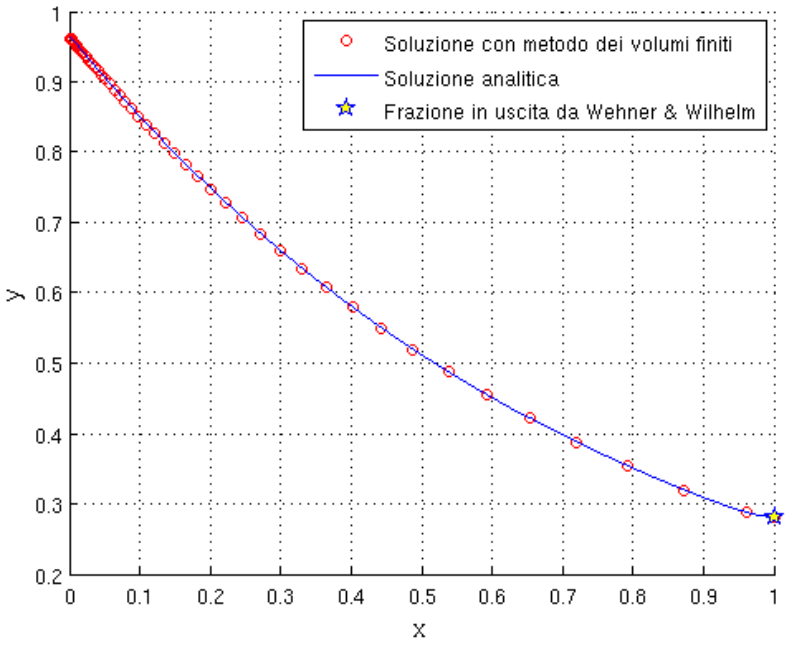

Figure 11.17 - Comparison of the numerical solution (calculated in the grid points denoted by red circles) with the analytical solution for the initial pseudo steady state (blue line); the yellow star at *x* = 1 represents the value of the concentration at the exit section calculated through Eq. 11.16. All the solutions were calculated with *Pe* = 34.8 and *Da* = 1.31.

The figure shows that the numerical method estimated correctly the value of the solution in the entire spatial domain. Indeed, HCl fraction computed at the two sides of the reaction section entrance were:

$$y(0.000) = 0.964$$

$$y(-0.001) = 0.964$$

while the numerical solution at *x* = 1 was:

$$y(1.000) = 0.282$$

The length of the fore section was verified calculating the slope at system entrance, which resulted:

$$\left.\frac{dy}{dx}\right|_{x=-10} = -0.000$$

The HCl concentration has to satisfy the mass balance, expressed by Eq. 11.56, at every time step (which corresponds to a pseudo steady state). It was verified at the beginning of the process:

$$y(-\infty) - y(+\infty) = 0.718$$

$$\int_0^1 Da \cdot y \cdot dx = 0.718$$

and at the end:

$$y(-\infty) - y(+\infty) = 0.217$$

$$\int_0^1 Da \cdot y \cdot dx = 0.217$$

Finally, the integration over time was verified by means of the overall mass balance, described in Appendix N. According to Eq. 11.57, average HCl conversion between t = 0 and at t = 1800 s is

$$\chi_{HCl}{}^{*} = 35.2\ \%$$

while the HCl conversion calculated from the sorbent conversion (given by 11.61) resulted:

$$\chi_{HCl}{}^{*} = 36.0\ \%$$

Even though a little difference is present between the two values, the time grid can be considered dense enough. Indeed, in the mass balance an error is intrinsically introduced calculating the average conversion in the bed assuming constant proprieties within each control volume.

Appendix P Filter cake thickness

In the present appendix, the growth of the cake thickness, $s(t)$, given by the accumulation of solid particles on the filtering surface of a fabric filter, is related to the pressure drops across the cake, $\Delta P(t)$, and to the flue gas velocity, $u(t)$. The problem was treated as one-dimensional, because in the analyzed case (i.e. the fabric filter of the system described in Appendix G) the maximum value of the cake thickness (≈ 4 mm, according to design data reported in Section 8.1.1) is much less than the diameter of the bags (130 mm).

The equations describing the variation of the dust layer thickness and the flue gas velocity are:

$$\frac{ds}{dt} = \frac{c_s}{\rho_s} \cdot u(t) \tag{11.67}$$

$$u(t) = \frac{\Delta P(t)}{k_1 + k_2 \cdot s(t)} \tag{11.68}$$

In these equations, s denotes the dust layer thickness (m), u is the flue gas velocity (m/s), c_s represents the dust concentration in the flue gas (kg/m^3), ρ_s density of the dust layer (kg/m^3), ΔP equals the pressure drop (Pa), and k_1 (kg/(m^2·s)) and k_2 (kg/(m^3·s)) are resistance coefficients for the "conditioned" fabric and the dust layer, respectively.

The general solution of Eq. 11.67, with the initial condition $s(0)=0$ [63], is

$$s(t) = \int_0^t \frac{u(\tilde{t}) \cdot c_s}{\rho_s} d\tilde{t} \tag{11.69}$$

Assuming that $\Delta P(t) \rightarrow \Delta P$ [64] and substituting Eq. 11.68 in Eq.11.67, one obtains

$$s(t) = \int_0^t \frac{\Delta P}{k_1 + k_2 \cdot s(\tilde{t})} \cdot \frac{c_s}{\rho_s} d\tilde{t} \tag{11.70}$$

The integration of Eq. 11.70 with respect to $\tilde{t}$ in the range [0 , t] yields

$$s(t) = \sqrt{2 \cdot \frac{c_s}{\rho_s} \cdot \frac{\Delta P}{k_2} \cdot t + \left(\frac{k_1}{k_2}\right)^2} - \frac{k_1}{k_2} \tag{11.71}$$

The velocity profile can be determined by substituting Eq. 11.71 in Eq. 11.67:

[63] According to the description of the pulse-jet cleaning system (Appendix F), the dust layer is completely removed from the surface of the fabric.

[64] In the analyzed case-study, the time of a complete cleaning cycle, t_{cycle} (defined as the time interval between two cleanings of the same row of bags), is much higher than the interval between two cleanings (of one row of bags and the following). Therefore, the variation of the pressure was neglected.

$$u(t) = \frac{\Delta P}{\sqrt{2 \cdot \frac{c_s}{\rho_s} \cdot k_2 \cdot \Delta P \cdot t + {k_1}^2}} \qquad 11.72$$

Considerations

On account of Es. 11.72, the flue gas velocity at the beginning of the cleaning cycle results:

$$u(0) = \frac{\Delta P}{k_1}$$

The characteristic time of the process can be defined as:

$$t^* = \frac{{k_1}^2 \cdot \rho_s}{2 \cdot k_2 \cdot c_s \cdot \Delta P} \qquad 11.73$$

When $t \gg t^*$ it is easily shown that

$$s = \sqrt{2 \cdot \frac{c_s}{\rho_s} \cdot \frac{\Delta P}{k_2} \cdot t} \qquad 11.74$$

$$u = \sqrt{\frac{\Delta P}{2 \cdot \frac{c_s}{\rho_s} \cdot k_2 \cdot t}} \qquad 11.75$$

so

$$s \propto \sqrt{t} \qquad 11.76$$

$$u \propto \frac{1}{\sqrt{t}} \qquad 11.77$$

Therefore, if $t_{cycle} \gg t^*$, the approximation of *s(t)* can be used during the entire cycle[65].

Accordingly, when $t \gg t^*$ the Peclet group[66] is constant:

$$Pe = \frac{\Delta P}{k_2 \cdot \varepsilon \cdot D_z}$$

[65] *u(t)* can't be approximated with Eq. 11.75 because at the beginning of the cycle it gives: $u(0) \rightarrow \infty$

[66] It was defined as:

$$Pe = \frac{u(t) \cdot s(t)}{\varepsilon \cdot D_z}$$

Conversely, the Damköhler number[67] changes with time because the cake continuously builds up and because of the sorbent consumption:

$$Da = 2 \cdot \frac{c_s}{\rho_b} \cdot t \cdot k_{glob}(r_c)$$

[67] It was defined as:

$$Da = \frac{s(t) \cdot k_{glob}(r_c)}{u(t)}$$

Appendix Q HCl removal in the reactor and in the flue gas duct

In the second stage of the analyzed case-study (described in Section 5.1), the sorbent is injected in a dedicated reactor (represented in Figure 11.18), which is designed to guarantee a minimum contact time between flue gas and solid particles of 2 s.

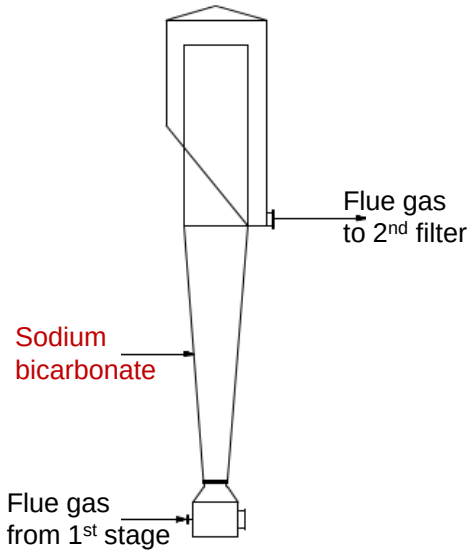

Figure 11.18 - Reactor of the second stage of the flue-gas treatment system, where ground sodium bicarbonate is injected into the flue gas.

To take into account the acid gas removal in the reactor and in the following flue gas duct, the mass balance equation was adapted and solved for this case. The governing differential equation can be expressed by:

$$\frac{\partial C}{\partial t} = -u_0 \cdot \frac{\partial C}{\partial z} + \varepsilon \cdot D_z \cdot \frac{\partial^2 C}{\partial z^2} + \dot{n}_g{}''' \qquad 11.78$$

where the source term is defined as:

$$\dot{n}_g{}''' = -r_{vr} = -n_{p,r}{}''' \cdot \int_{V_p} r_{vp}\, dV_p \qquad 11.79$$

$n_{p,r}{}'''$ is the number of particle per unit volume of the reactor. Assuming a uniform concentration profile within the particle (as shown for similar conditions in Section 7.2.2), the reaction term can be expressed according to the grain model. Substitution of Eqs. 6.75 and 6.76 in 11.79 leads to:

$$r_{vr} = \frac{\dot{m}_{Na_2CO_3}}{Q} \cdot \frac{3}{\rho_s \cdot r_g} \cdot \frac{{r_c}^2}{{r_g}^2} \cdot k_s \cdot \frac{D_s}{D_s + k_s \cdot r_c \cdot \left(1 - {r_c}/{r_t}\right)} \cdot \left(C - C_{eq}\right) \qquad 11.80$$

Eq. 11.78 can be rewritten in dimensionless form:

$$\frac{\partial y}{\partial \tau_r} = -\frac{\partial y}{\partial x_r} + \frac{1}{Pe_r} \cdot \frac{\partial^2 y}{\partial {x_r}^2} - Da_r \cdot y \qquad 11.81$$

where the governing groups are:

- $Pe_r = \frac{u_{0,r} \cdot L_r}{D_z}$
- $Da_r = \frac{r_{vr} \cdot L_r}{u_{0,r}}$
- $y = \frac{C - C_{eq}}{C_{in} - C_{eq}}$

The Damköhler number depends on the unreacted core radius, so on sorbent conversion, through the equation:

$$Da_r = \frac{L_r}{u_{0,r}} \cdot \frac{\dot{m}_{Na_2CO_3}}{Q} \cdot \frac{3}{\rho_s \cdot r_g} \cdot \frac{{r_c}^2}{{r_g}^2} \cdot k_s \cdot \frac{D_s}{D_s + k_s \cdot r_c \cdot \left(1 - {r_c}/{r_t}\right)} \quad 11.82$$

In this case, *Pe* ≫ 1. Thus, the axial dispersion term can be neglected. As the characteristic time of the process are much longer than the residence time of the gas in the reactor, also the accumulation term was neglected, leading to the system:

$$\frac{dy}{dx_r} + Da_r \cdot y = 0 \quad 11.83$$

$$y(x_r = 0) = 1 \quad 11.84$$

This system can be included in the solution found in Section 6.3.3, where the reactor length can be described as the fore section.

A first indication of the importance of the reactor in the acid gas removal process can be assessed assuming Da_r equal to its initial value. Indeed, when the product layer is not formed, i.e. $r_c = r_g$, the Damköhler number can be written as:

$$Da_{r,0} = t_{c,r} \cdot \frac{\dot{m}_{Na_2CO_3}}{Q} \cdot S_{BET} \cdot k_s \quad 11.85$$

where

- $t_{c,r} = \frac{L_r}{u_{0,r}}$
- $S_{BET} = \frac{3}{\rho_s \cdot r_g}$

As long as Da_r can be assumed as constant, the solution is:

$$y = \exp(-Da_r \cdot x_r)$$

Therefore, the HCl conversion in the reactor results:

$$\chi_{reatt} = 1 - y(x_r = 1) = 1 - \exp(-Da_r)$$